

A COMPUTATIONAL APPROACH TO FRETTING WEAR PREDICTION IN TOTAL HIP REPLACEMENTS

ARIYAN ASHKANFAR

A THESIS SUBMITTED IN PARTIAL FULFILMENT OF THE REQUIREMENTS OF
LIVERPOOL JOHN MOORES UNIVERSITY FOR THE DEGREE OF
DOCTOR OF PHILOSOPHY

AUGUST 2015

Abstract

A challenge in engineering coupling design is the understanding of performance of contact geometry for a given application. “Wear” is one of a number of mechanical failures that can occur in mechanical coupling design. “Fretting wear” occurs where surfaces in contact are subjected to oscillating load and very small relative motion over a period of time. Fretting has been observed in many mechanical interactions and is known to be a reason for failure in many designs.

Recent evidence suggests that fretting wear occurs at the taper junction of modular total hip replacements and leads to failure of the implants. Experimental testing to determine the wear behaviour that occurs in mechanical devices is time consuming, expensive and complicated. Computational wear modelling is an alternative method which is faster and cheaper than real testing and can be used in addition to testing to help improve component design and enhance wear characteristics. Developing an algorithm that can accurately predict fretting wear considering linear wear, volumetric wear and surface wear damage is the main focus of this thesis.

The thesis proposes a new computational methodology incorporating published wear laws into commercial finite element code to predict fretting wear which could occur at the taper junction of total hip replacements. The assessment of wear in this study is solely based on mechanical wear (fretting) as being the primary mechanism causing surface damage. The method is novel in that it simulates the weakening of the initial taper ‘fixation’ (created at impaction of the head onto the stem in surgery) due to the wearing process. The taper fixation is modelled using a contact analysis with overlapped meshes at the taper junction. The reduction in fixation is modelled by progressive removal of the overlap between components based on calculated wear depth and material loss.

The method has been used for three different studies to determine surface wear damage, linear and volumetric wear rates that could occur at taper junction of total hip replacements over time. The results obtained are consistent with those found from observation and measurement of retrieved prostheses. The fretting wear analysis approach has been shown to model the evolution of wear effectively; however, it has been shown that accurate, quantitative values for wear are critically

dependant on mesh refinement, wear fraction and scaling factor, wear coefficient used and knowledge of the device loading history. The numerical method presented could be used to consider the effect of design changes and clinical technique on subsequent fretting wear in modular prosthetic devices or other mechanically coupled designs.

Acknowledgments

I would have never been able to finalise this research without the help, support and contributions of the following people and organizations. I would like to take this chance to express my deepest gratitude to them.

First of all, this research would not be possible without the continued support and guidance given from my supervisors, Dr Russell English and Dr Glynn Rothwell. The supervision, support and advice given truly helped to finalise this research. They have always time for me, believe in me and encourage me with their priceless ideas on my research. They always care about me, my research and also my career. The opportunities for teaching and demonstrating they gave me during my research were invaluable indeed. No words can express how I am grateful and I may, only to mention my deepest and special gratitude to them both.

This project has been funded and supported by the School of Engineering, Technology and Maritime Operations, Liverpool John Moores University, Liverpool, UK. I wish to thank them for the support provided by the scholarship, conferences travel and experimental costs.

My special thanks also go to Professor Ian Jenkinson, for his continued support on this project. I would like to express my appreciation for the wonderful opportunities given to me.

I would like to acknowledge the contribution of Mr Viju Peter, Mr Alasdair Santini and Mr Andrew Phillipson, orthopaedic surgeons from Broadgreen Hospital, Liverpool, UK, for their invitations to surgery visits and advice, the co-operation is much indeed appreciated.

I am grateful to Professor Thomas Joyce from Newcastle University, Newcastle, UK, for his valuable information in tribology that helped to validate my results.

I would like to thank Mr Clint Davies Taylor, form Dassault Systems, Simulia Ltd, Warrington, UK, Dr Li Chenxi, from Smith and Nephew PLC, Hull, UK, Mr Jay Cunningham from Zimmer Ltd, UK, Mr Jason Steffens, from Zimmer Ltd, USA, Mr

Chris Phillips and Mr Sam Hopkins, from Taylor Hobson Ltd, Leicester, UK, for their advice.

I owe a special thanks to Dr Ramin Riyahi, for his kind advice and help on both an academic and personal level. Not forgetting to thank one of my best friends and as a colleague, Shayan, who is always willing to help and give his best suggestions. Also, I would like to thank all my friends and family, to name a few, Mohammad, Behnam, Erfan, James, uncle Jam, Sara, Charlotte, David, Moha, Peyman and Moj.

Always last but not indeed least, I wish to express my warmest thanks and love to my parents, Narges and Mostafa, my siblings, Goli and Amir, my siblings-in-laws, Masy and Farzad and my little niece and nephew, Anisa and Arya, for their unending love and support. Finally, to the eternal memory of my grandma, Papar...

*Ariyan Ashkanfar
Liverpool, 2015*

This thesis is dedicated to:

My parents, who have always stood beside me, not only throughout the duration of this PhD, but also through the whole of my life...

I am deeply indebted to you both.

My Mom has recently had implanted a total knee prosthesis. I hope this type of research could be of help for returning active life to all patients needing arthroplasty...

Contents

Abstract.....	iii
Acknowledgments	v
Table of figures.....	xiii
Table of tables.....	xvii
Table of algorithms	xviii
Nomenclature	xix
Glossary and Abbreviation	xxi
1 Introduction.....	22
1.1 Background	22
1.2 Aim and Objectives.....	25
1.3 Scope of the thesis.....	26
1.4 Outline of the thesis	27
1.5 Publications resulting from this thesis	29
2 Background - a review.....	31
2.1 Introduction.....	31
2.2 Wear and its characteristics.....	32
2.2.1 Adhesive wear.....	35
2.2.2 Abrasive wear.....	36
2.2.3 Corrosion wear	38
2.2.4 Surface fracture wear	39
2.2.5 Erosive or percussive wear	39
2.2.6 Fatigue wear	41
2.3 Fretting wear	41
2.3.1 Fretting wear characteristics	42
2.3.2 Fretting wear theories.....	43
2.4 Wear laws.....	44

2.4.1	Archard's wear law	44
2.4.2	Dissipated energy wear law	46
2.5	Hip joint	48
2.5.1	Hip joint disorders.....	49
2.6	Hip arthroplasty.....	50
2.6.1	Procedure of total hip replacements.....	54
2.6.2	Femoral head and stem assembly.....	55
2.6.3	Material and material combination of total hip replacements.....	58
2.6.4	Surface characteristics of total hip replacements.....	61
2.6.5	Failure of total hip replacements.....	64
2.7	Wear and fretting wear in total hip prosthesis	66
2.7.1	Fretting wear at taper junction of total hip replacements.....	68
2.7.2	Fretting wear of cobalt-chrome and titanium.....	69
2.7.3	Wear particles released from hip implant	71
2.8	Wear assessment	71
2.8.1	Archard and Energy wear assessment.....	72
2.8.2	Wear coefficient	72
2.8.3	Wear fraction.....	76
2.8.4	Effect of frequency on the wear rate	77
2.9	Computational wear modelling	78
2.10	Discussion and rationale	86
2.11	Conclusion	89

3 Computational method of fretting wear prediction91

3.1	Introduction.....	91
3.2	Theoretical wear calculation	92
3.2.1	Dissipated Energy wear law.....	92
3.2.2	Archard's wear law	95
3.3	Wear implementation.....	96
3.4	Finite Element implementation.....	99
3.4.1	Material properties and interaction behaviour	99
3.4.2	Wear fraction.....	100
3.4.3	Finite element models	101
3.4.4	Impaction Load	102

3.4.5	Walking load and boundary conditions.....	104
3.5	Updating the geometry.....	107
3.6	Computational framework	108
3.7	Initial assembly of components.....	110
3.8	Impaction and Overlapped analysis	112
3.9	Algorithms	115
3.9.1	Input requested from user.....	117
3.9.2	Initial coordinates of the nodes in contact.....	118
3.9.3	Extract data from input file	118
3.9.4	Nodal normal direction	119
3.9.5	Node deformed coordinate.....	119
3.9.6	Pairing nodes in contact	120
3.9.7	Wear depth calculation.....	121
3.9.8	Geometry update	123
3.9.9	Results report (*.txt format).....	123
3.9.10	Writing results in output databases of ABAQUS (*.odb format) ...	123
3.9.11	Error detection.....	124
3.9.12	Main algorithm.....	125
3.10	Computer specification and computational time.....	127
3.11	Convergence.....	127
3.11.1	Finite element mesh study.....	127
3.11.2	Mesh study for wear modelling	128
3.11.3	Scaling factor (β).....	129
3.12	Summary and Conclusion	130

4 Prediction of fretting wear damage using an axisymmetric model of a total hip replacement.....134

4.1	Introduction.....	134
4.2	Wear analysis input.....	135
4.3	Results.....	135
4.3.1	Initial contact stress and slip variation.....	136
4.3.1	Variation in contact stress, slip and wear depth.....	138
4.3.2	Linear and volumetric wear rate	142

4.4	Theoretical validation.....	143
4.5	Discussion	145
4.6	Conclusions	147
5	Fretting wear evaluation and evolution at taper junctions of total hip replacements	149
5.1	Introduction.....	149
5.2	Wear analysis input.....	150
5.3	Results and discussion	151
5.3.1	Variation in contact pressure and relative displacement during the walking cycle	151
5.3.2	Variation in taper wear over 5 year period.....	154
5.3.3	Volumetric and linear wear rate.....	156
5.4	Validation.....	157
5.5	Conclusions	162
6	Effect of different taper fixation of the head and stem on the extent of fretting wear	164
6.1	Introduction.....	164
6.2	Experimental procedure	165
6.2.1	Impaction tests	165
6.2.2	Pull-off test.....	168
6.3	Finite element modelling of the initial forces (phase 1)	169
6.4	Wear analysis input (phase 2 and 3)	171
6.5	Results.....	172
6.5.1	Transition point from phase 2 to 3 of the wear analysis	172
6.5.2	Evolution of wear pattern damage (phase 2 and 3).....	174
6.5.3	Variation of contact pressure and slip during the wear analysis (phase 2 and 3)	176
6.5.4	Volumetric wear rate for different impaction loads.....	180
6.6	Validation.....	183
6.7	Discussion	187
6.8	Conclusion	191

7	Conclusion and future work	192
7.1	Conclusion	192
7.2	Future work	195
	References	196
	Appendices	205

Table of figures

Figure 1-1: Mechanical failures	26
Figure 1-2: The thesis structure and research track	28
Figure 2-1: Different mechanisms of wear and fretting wear	33
Figure 2-2: Two (a) and three-body (b) abrasive wear	36
Figure 2-3: A human hip joint, model created in SolidWorks.....	49
Figure 2-4: A THR, a Birmingham acetabular component, a Freeman uncemented stem and a Birmingham XL head (retrieved).....	51
Figure 2-5: Different design of hip implants.....	52
Figure 2-6: Schematic of the THR in service, model created in SolidWorks, JRI implant, AEON cemented hip system.....	54
Figure 2-7: Metal-on-Plastic total hip replacement	60
Figure 2-8: An example of head taper surface topography.....	63
Figure 2-9: An example of threaded stem trunnion surface topography	64
Figure 2-10: Fracture occurred at Polyethylene cup of a total hip prosthesis.....	65
Figure 3-1: Nodal pairing and relative displacement of the paired node on axisymmetric models	96
Figure 3-2 Nodal pairing and calculation of relative displacement on 3D models....	97
Figure 3-3: Mesh assigned on (a) axisymmetric model and (b) 3D model.....	102
Figure 3-4: Drop rig to investigate impulse time and impact magnitude	103
Figure 3-5: Impaction assembly load amplitude.....	103
Figure 3-6: Boundary conditions and impaction loading assigned on (a) axisymmetric and (b) 3D model.....	104
Figure 3-7: Hip loadings during a single walking cycle	104
Figure 3-8: Hip rotations during a single walking cycle.....	105

Figure 3-9: loading and boundary condition assigned on 3D FE model.....	106
Figure 3-10: Opposite of nodal normals indicating the direction of wear evolution, (a) axisymmetric and (b) 3D model	108
Figure 3-11: Quantitative procedure to predict fretting wear.	110
Figure 3-12: Contact pressure distribution along stem trunnion surface at the end of phase 1 and at the commencement of step 2 of phase 2, (a) 3D model and (b) axisymmetric model (swept by 80°)	112
Figure 3-13: Graphical user interface of the wear algorithm, other tabs of this window are presented in the Appendix I.....	116
Figure 3-14: Mesh study	127
Figure 3-15: Wear evolution convergence. Interface distance is shown in Figure 3-12	128
Figure 3-16: Effect of different scaling factor values.....	129
Figure 4-1: Contact pressure and slip distribution throughout a walking load discretised to 10 intervals during 1.2s.....	137
Figure 4-2: Contact pressure, slip and wear pattern evolution during phase 2 of the analysis (from 1 million to 6.8 million load cycles)	139
Figure 4-3: Contact pressure, slip and wear pattern evolution during phase 3 of the wear analysis (from 7 million to 10million load cycles)	140
Figure 4-4: Wear depth along contact interface after 6.8 million load cycles (when initial overlap is removed),(contact interface shown in Figure 3-12).....	141
Figure 4-5: Wear depth along contact interface after 10 million load cycles (contact interface shown in Figure 3-12)	141
Figure 4-6: Wear depth evolution (from 1 to 10 million load cycles) along the head taper interface (contact interface shown in Figure 3-12)	142

Figure 4-7: Variation in volumetric wear rate with respect to time	143
Figure 4-8: Overlap analysis (theoretical approach)	144
Figure 4-9 A comparison between theoretical and FE results	145
Figure 4-10: Reaction forces generated by overlap analysis	146
Figure 5-1: Variation in contact pressure and relative displacement during a walking cycle	153
Figure 5-2: Evolution of contact pressure, slip and wear pattern during wear analysis, row (a) and (b) show the pattern of wear depth in mm and contact slip changes on the stem trunnion, row (c) and (d) show the contact pressure in MPa and the pattern of wear depth in mm on the head taper, results shown at the last time interval.....	155
Figure 5-3: Variation in volumetric wear rate with respect to time	157
Figure 5-4: Validation against retrieved prostheses; figures are rotated anticlockwise based on a label shown as (*).....	159
Figure 5-5: (a) wear modelling and (b ⁵) coordinate measuring analysis of the retrieved head taper	161
Figure 6-1: Total hip replacement in situ, impaction of the modular head onto the stem trunnion.....	166
Figure 6-2: Impaction experiment on single-pedestal load cell	167
Figure 6-3: hand press load (press-fit) amplitude	167
Figure 6-4: Approximate average impaction force from tests	168
Figure 6-5: Tinius Olsen, tensile testing machine.....	169
Figure 6-6: Variation of contact pressure for different assembly load (MPa)	170
Figure 6-7: Initial overlap created for phase 2 of the wear analysis based on different assembly loads	171
Figure 6-8: Transition point from phase 2 to 3 of the wear analysis	173

Figure 6-9: Evolution of wear pattern during wear analysis in mm; row (a) for hand press, (b), (c), (d) and (e) for different impaction force, results shown at the last time interval of cycle.....	175
Figure 6-10: Variation of contact pressure during wear analysis in MPa, row (a) for hand press, (b), (c) and (d) for different impaction force, results shown at the last time interval of cycle.....	177
Figure 6-11: Variation of contact slip during wear analysis in mm, row (a) for hand press, (b), (c) and (d) for different impaction force, results shown at the last time interval of cycle.....	179
Figure 6-12: Total volumetric wear rate with respect to assembly load and over the wear analysis	181
Figure 6-13: Total volume loss after 5million load cycles for different assembly forces.....	183
Figure 6-14: Comparison of fretting wear damage between FE wear model (2kN initial impaction) and a retrieved prosthesis; figures are rotated 180° based on a label shown as (*)	184
Figure 6-15: Comparison of fretting wear damage between FE wear model (6kN initial impaction) and a retrieved prosthesis; figures are rotated 180° based on a label shown as (*)	186
Figure 6-16: Comparison of fretting wear damage between FE wear model (hand press initial assembly) and a retrieved prosthesis; figures are rotated 180° based on a label shown as (*).....	186
Figure 6-17:Zero, positive and negative mismatch angle	189

Table of tables

Table 2-1: Values of wear coefficient for the same material combination of reviewed wear models	81
Table 2-2: Values of wear coefficient for the different material combination of reviewed wear models.....	83
Table 2-3: Different approach to wear prediction of reviewed wear modelling.....	84
Table 3-1: Material properties.....	100
Table 3-2: Tribological material combination	100
Table 4-1: Input data for wear analysis of this study	135
Table 4-2: Linear and volumetric wear rate of the head, stem and in total.....	143
Table 5-1: Input data for 3D wear analysis	150
Table 5-2: Average linear and volumetric wear rate on head taper and stem trunnion	157
Table 6-1: Input data for wear analysis.....	172
Table 6-2: Average of total volumetric wear rate	182

Table of algorithms

Algorithm 1: inputRequest.....	117
Algorithm 2: nodeCoordinates.....	118
Algorithm 3: dataFromInputFile.....	119
Algorithm 4: nodalNormalDirection.....	119
Algorithm 5: nodeDefCoordinate.....	120
Algorithm 6: pairNode.....	120
Algorithm 7: wearDepth.....	122
Algorithm 8: geoUpdate.....	123
Algorithm 9: resultsReport.....	124
Algorithm 10: resultsODB.....	124
Algorithm 11: errorDetection.....	125
Algorithm 12: mainAlgorithm.....	126

Nomenclature

E	Young's modulus
ν	Poisson's ratio
ρ	Density of the material
μ	Friction coefficient
W_v	Volumetric wear
V	Volume of worn material per unit distance (wear rate)
V_p	Volume of plastically deformed
L	Sliding distance
A_r	Real contact area
A_w	Worn area of contact
H	Hardness of the material
F_n	Normal applied force
Q	Tangential force
k	Dimensionless wear coefficient
k_{abr}	Dimensionless abrasive wear coefficient
k_{cut}	Dimensionless cutting wear coefficient
k_{cor}	Dimensionless corrosive wear coefficient
k_{ero}	Dimensionless erosive wear coefficient
k_{fat}	Dimensionless fatigue wear coefficient
K	Dimensional Archard's wear coefficient
α	Dimensional energy wear coefficient
s	Sliding distance or slip
s_i	Relative displacement or relative slip

ζ	Cutting wear chip
f	Under-formed wear chip thickness (feed parameter)
λ	Critical thickness of corrosion
K_c	Material fracture toughness
e_r	Erosion ratio
E_i	Energy resulting in erosive wear
E_k	Kinetic energy
E_s	Sliding energy
E	Accumulated dissipated energy
K	Archard's wear coefficient
μ	Friction coefficient
β	Wear scaling factor
W_d	Linear wear depth
W_c	Cyclic wear depth
Q	Shear traction
τ	Contact shear stress
τ_i	Surface shear stress at time interval i
s_i	Relative displacement at time interval i
F	Normal contact force
P	Contact pressure
P_i	Surface contact stress at time interval i

Glossary and Abbreviation

FE	Finite Element
THR	Total Hip Replacement
MoM	Metal-on-Metal
CoC	Ceramic-on-Ceramic
MoP	Metal-on-Plastic
CoP	Ceramic-on-plastic
Co-Cr	Cobalt-Chrome
Ti	Titanium
ASTR	Adverse Soft Tissue Reaction
MACC	Mechanical Assisted Crevice Corrosion
SEM	Scanning Electron Microscope
Taper	Female taper or head taper
Trunnion	Male taper or stem taper
Tribo-film	Over sliding contact of surfaces, a thin solid film is generated and stick fast on its worn surface which has different chemical composition, structure and tribological properties.
Metallosis	Aseptic fibrosis, local necrosis or loosening of a prosthetic device secondary to metal debris and corrosion
Tribology	Is the science of interacting surfaces in relative motion (Oxford Dictionary)
Arthroplasty	The surgical reconstruction or replacement of a joint (Oxford Dictionary)
Pathology	The science of the causes and effects of diseases (Oxford Dictionary)
UHMWPE	Ultra-High-Molecular-Weight Polyethylene
HXLPE	Highly Cross-Linked Polyethylene

Chapter 1

Introduction

1.1 Background

A complicated challenge in the design of coupled engineering components is the understanding of the performance of contact geometry within the design for a given application, including the loading and/or rotation that the mechanical design needs to undertake.

From a tribological point of view, one of the characteristic of a material is that all engineering surfaces are more or less rough and uneven. When the engineering components are subjected to load and coupling together, surfaces are in contact over a very small area. Due to this very small contact area, contact stresses generated can be relatively high.

“Wear” is one of a number of mechanical failures (see Figure 1-1) that occur due to this high contact stress at the surfaces. It is an inevitable phenomenon occurring when surfaces of mechanical components are mated together while subjected to load

and sliding or rolling. During the wear process, material is removed from the surfaces as particles. This removal of particles occurs in different ways and by varying mechanisms. In many practical situations high wear rate, and increased friction occurs, the reduction of which is the greatest aim.

The surfaces of mechanical components in contact under oscillating load and relative motion will also become contaminated over time. This contamination may appear due to the chemical reaction of the material with the environment or due to debris released from worn surfaces. There is evidence that even for perfectly clean rubbing surfaces in contact with no lubrication, there would be a considerable wear damage that contaminates the surfaces.

Considering the study of wear, both theoretical and experimental approaches are needed to answer one essential question, “how is the debris removed from the surfaces?”

Wear can be associated in two forms, “macroscopic” and “microscopic”.

- Macroscopic wear occurs when specific stress levels or the number of contact stresses (fatigue) reach the elastic limit of the material with a depth of material being removed depending on the shear stresses present.
- Microscopic form of wear is similar to macroscopic wear but it is associated with individual asperity contacts compared to the single larger region of the contact area.

“Fretting wear” is, generally, associated with very small relative movement (micromotion) of solid surfaces in contact under load. Fretting wear can be categorised by the micromotion and loading at the coupling causing adhesion of

surface asperities that are subsequently torn apart. This leads to transfer of material or the creation of metal particulate debris. This debris is then oxidised and becomes harder than the mating surfaces. If the debris remains in the contact zone abrasive wear can occur resulting in further surface damage (Archard, 1953).

Fretting is observed in many mechanical assemblies such as shrink fitted coupling, keyway-shaft couplings and the specific example which has motivated this research, the taper junction of total hip prostheses.

Currently, most joints in the human body can be replaced with mechanical artificial devices. This procedure is known as “arthroplasty” and is one of the most successful surgeries performed since 1960’s. The aim of the surgery is to accommodate an active life style for patients with joint disorders such as osteoarthritis. The fundamental principle of all arthroplasty is that the portion of affected joint is removed and replaced with an artificial one. Among all different type of arthroplasty, hip arthroplasty is the focus of this study. The procedure of hip arthroplasty is called “Total Hip Replacement” (THR) and the mechanical artificial joint is known as the “Prosthetic Device”.

Typically an implanted THR will have a 10 to 15 years life (11th Annual Report 2014, NJR for England, Wales and Northern Ireland, 2014) (Aldinger et al., 2003, Teloken et al., 2002). There is evidence that the wear and fretting wear that occurs in THRs contributes significantly to the failure of these devices (Aldinger et al., 2003, Langton et al., 2012).

1.2 Aim and Objectives

The aim of this work is to develop a computational methodology to predict “fretting wear” that could occur in THRs. The study proposes a methodology to predict the wear depth, volumetric wear loss and also the surface damage associated with wear which could occur in a hip prosthesis over time in service. The aim is to develop this method as a general tool that is independent of the model and can be used to predict fretting wear for other prosthetic designs or even other mechanical designs subjected to oscillating loads.

In order to achieve this aim, a commercial model of a hip prosthesis is used, to illustrate the wider principles of wear process and wear modelling. Then, the study develops a new fretting wear model using the programming language (Python) and finite element (FE) analysis (ABAQUS) by investigating and considering parameters in the prediction of wear. One of these parameters, for instance, is the effect of initial assembly such as impaction that provides fixation between components on fretting wear prediction. Another parameter is the wear fraction that defines the percentage of the wear that needs to be applied on the components and the effect of change in geometry during wear analysis. The method, explained in Chapter 3, includes as many of these parameters as possible to provide an accurate prediction of fretting wear.

A significant goal is to develop and generalize the algorithm with a graphical user interface for any FE analysis (axisymmetric or 3D) with the FE package (ABAQUS) as an add-in (user plug-in) in order to accurately predict linear and volumetric wear rate (material loss) in the form of contours of the wear damage occurring on the surfaces.

1.3 Scope of the thesis

Figure 1-1 illustrates a simplified “bird’s eye view” of the important aspects causing mechanical failure in engineering designs. Each type of mechanical failures produces different forms of failure surfaces. The more vital, crucial and complex the mechanical design is, the more necessary a good understanding of its failure causes, to ensure success of their operations over time. Wear as a kind of mechanical failure occurs in different scales and in different forms, such as adhesive, abrasive, corrosive, erosive, surface fracture and fatigue wear (see Figure 1-1).

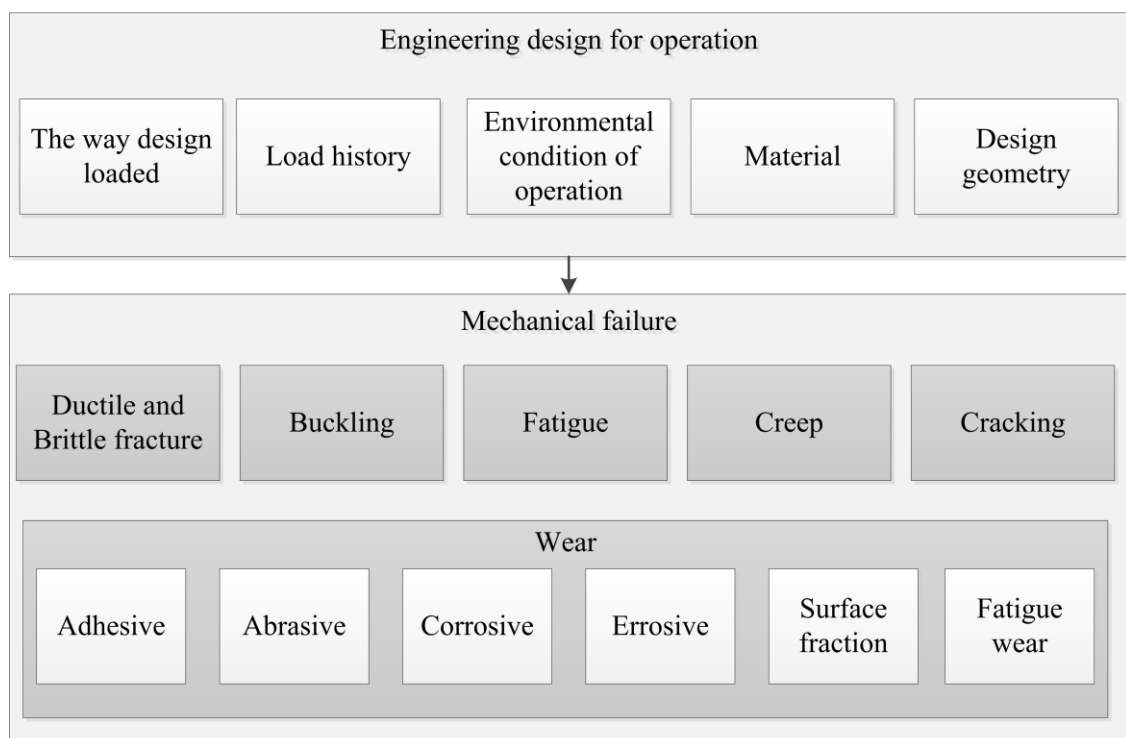


Figure 1-1: Mechanical failures

Fretting wear (and the surface damage occurring due to fretting) is known as a very complex phenomenon to investigate, measure and predict. Being able to predict the extent of wear that could occur in mechanical designs (specifically in THR which is the focus of this study) over time in service is vital in order to improve current and future designs.

The work presented here focuses solely on mechanical wear (fretting) as being the primary mechanism causing damage on contacting surfaces. The method presented has been used to predict fretting wear in the taper junction of THRs and could be used for different applications in future.

1.4 Outline of the thesis

The whole structure of this thesis is presented in Figure 1-2.

The main aim of this first chapter was to present an introduction to the thesis as a whole, the aim of the research and outline of the research. Chapter 1 also contains a brief description of the motivation of this research.

In Chapter 2, an extensive literature review was conducted to provide and establish a suitable background for the chapters which follow. This includes a suitable background on wear, wear characteristics, fretting wear, hip joint, hip arthroplasty, problems with current THRs, wear in total hip prosthesis and a review of the current wear modelling available in the literature.

The method presented in this study involves the use of FE analyses and Python scripting to perform wear modelling. Chapter 3 details the whole methodology including FE implementation, wear laws and the development of the wear algorithm. A FE model of a commercial hip prosthesis was modelled both axisymmetrically and in 3D. A developed fretting wear algorithm was then applied to the FE model to investigate the likelihood of fretting damage occurring in the taper junction of THRs.

Different studies were performed using the method illustrated in Chapter 3 and all the findings are detailed in Chapter 4, 5 and 6. The results have been discussed in separate discussion sections within these chapters.

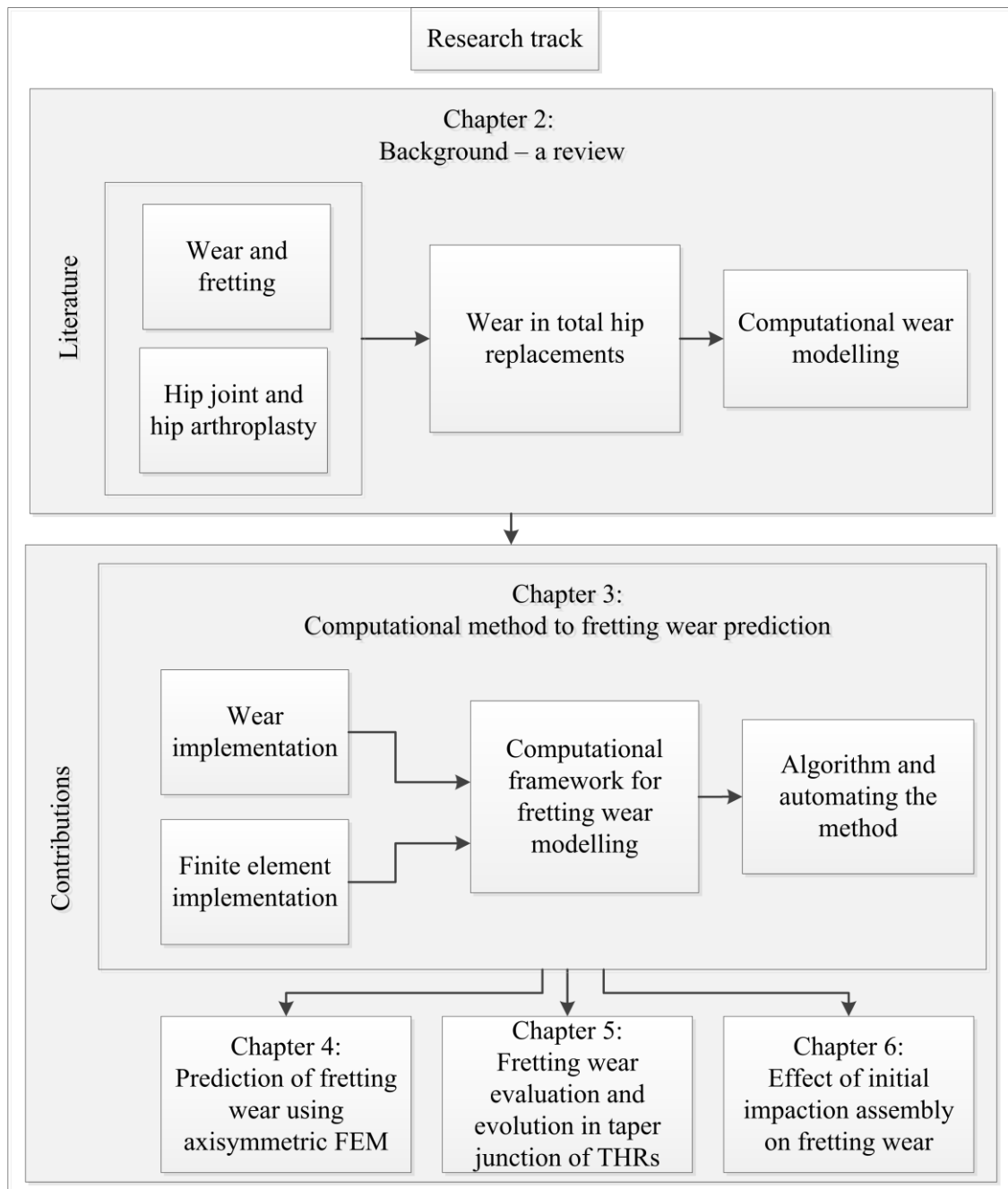


Figure 1-2: The thesis structure and research track

In Chapter 4 the axisymmetric model of the THR that has been used to develop the algorithm, and the results have been presented in detail.

A full description of the 3D results based on the realistic loading conditions from the wear analysis is depicted in Chapter 5. In this chapter the results from the wear algorithm have been validated by observation of wear patterns of retrieved

prosthesis. The linear and volumetric wear rates obtained are also in the range of the experimental measurement of the retrieved prostheses.

Chapter 6 illustrates the importance and effects of initial impact assembly on extent of fretting wear over time in service.

Lastly, a complete conclusion to this research and possible future work are provided in chapter 7.

1.5 Publications resulting from this thesis

1. “A computational approach to fretting wear prediction at the head-stem taper junction of THRs” — *Wear*, 338, 210-220, (2015) (Appendix IV)
2. “A computational assessment of taper junction fretting wear in a total hip replacement due to different assembly loads” — Submitted to *Journal of Engineering in Medicine*, August 2015
3. “Effect of impaction force at assembly on fretting wear at the taper junction of total hip prosthesis” — American Society for Testing and Materials (ASTM) International, given the option to revise for acceptance, 2015, (Appendix IV)
4. “A computational approach to fretting wear modelling in total hip replacements” – LJMU research conference, 2015, (Appendix IV)
5. “Finite Element Models for quantitative analysis of wear damage in Metal-on-Metal modular hip prosthesis” — GERI Annual Research Symposium, 2013, (Appendix IV)

In-preparation journal papers

1. “Effect of the different head sizes and taper lengths of total hip replacements on extent of fretting wear” — to be submitted to *Wear*, in August 2015 .
2. “The effect of modular neck geometry on fretting wear potential at the neck-stem taper interface of the Kinectiv total hip replacement” — to be submitted to *Tribology International* in 2015

Chapter 2

Background - a review

2.1 Introduction

The purpose of this chapter is to present a complete review of current literature and a summary of the existing fundamental knowledge on wear as a suitable background for the chapters which follow. In this Chapter, firstly, a general explanation of wear and its characteristics in tribology is provided. This will be followed by a comprehensive review of fretting wear and its theoretical laws. A comprehensive review of literature is also performed relating to the application of THR. Secondly, fretting wear and its associated damage that could occur in THRs are explained in detail and a review on the current state of the art in computational wear modelling is provided.

2.2 Wear and its characteristics

In terms of tribology, all surfaces are rough. Where engineering surfaces nominally mate together, they contact at the tips of the higher asperities and the contact area is determined by the deformation of these tip asperities under applied pressure. The real area of contact is always smaller than the total area of the surfaces and consists of a number of small surfaces. Increasing the load increases the number and size of these areas based on the resistance of the material to deformation and consequently, increases the contact area. So that, finding a relationship between force, real contact area and the depicted pressure due to them is relatively complex (Archard, 1953). The asperities at the real contact area might either fracture or plastically deform. If fracture happened at asperities, particles of material are removed from the surface and if they are plastically deformed, this may lead to transfer of the material between the contacting surfaces.

Wear is defined as the gradual removal of material from contacting surfaces under relative movement. Wear and friction are intimately linked together, wear is associated with timely and costly mechanical failure, whereas, friction results in energy loss due to shearing and ploughing.

Wear can be expected only if surfaces in contact under relative motion are not separated. Generally, lubrication is used to separate contacting surfaces from each other resulting in reduced wear and friction forces. Lubricant is a fluid that either completely separates the surfaces in contact (fluid film lubrication) or acts as boundary lubrication.

Material can be removed from surfaces in a tribological couple by different mechanisms (see Figure 2-1) such as (Archard, 1953):

- **Adhesive wear:** At the sliding asperity tips of the surfaces, material is welded and transferred to a harder state. It is then removed from the surface by fracture.
- **Abrasive wear:** Occurs due to deforming or cutting of material by a harder material or particles (sometimes harder oxide particles of material)
- **Corrosion wear:** A layer of film is formed due to environmental reaction and or lubrication which leads to material removal from the surface by sliding.
- **Surface fracture wear:** When the normal applied stress exceeds the ultimate stress of the material the particle removes from the surface by fracture.
- **Erosive or percussive wear:** Occurs due to impact of particles (solid or liquid) on a surface.
- **Fatigue wear:** When a surface is elastically worked, micro-cracks can form, grow and propagate forming wear particles.

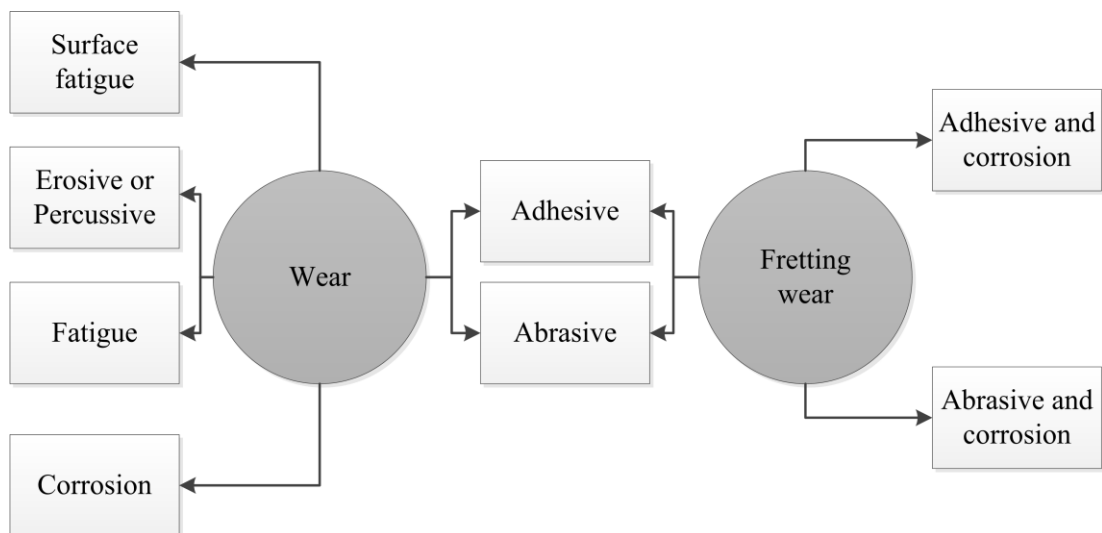


Figure 2-1: Different mechanisms of wear and fretting wear

Measurement of wear is generally performed using wear testing equipment. Tribologists measure the material loss from surfaces based on contact force, duration and extent of contact. A typical measurement of wear is the volume of worn material

per unit sliding distance over time. Therefore, “volumetric wear” is the specific volume of the material removed by wear in the specific distance over time (Archard, 1953). The volume of worn material (V) per unit sliding distance (L) can be obtained using Equation (2-1):

$$V = W_v/L \quad (2-1)$$

where W_v is the total volume of the material removed. Therefore, the volume loss per unit distance (V) has units of area and may be expressed per unit time. The real area (A_r) of contact between two mating surfaces depends on the applied load (F_n) and the hardness of the softer material (H) in the friction coupling and can be calculated using Equation (2-2):

$$A_r = F_n/H \quad (2-2)$$

The wear ratio, known as the wear coefficient (k), is the unit of volume removed per unit sliding distance over the real interface area of the surfaces in contact. This is expressed as a dimensionless coefficient and can be calculated using Equation (2-3):

$$k = \frac{V}{A_r} = \frac{W_v/L}{F_n/H} \quad (2-3)$$

Assuming the contact surfaces mate at N asperities and n of those form wear debris, the value of the wear coefficient can be considered as being the ratio of two areas, the worn area (A_w) of the n asperities and the real area (A_r) of all contact asperities. As such, the wear coefficient (k) can be obtained using Equation (2-4):

$$k = \frac{A_w}{A_r} = \frac{n}{N} \quad (2-4)$$

The interpretation of Equation (2-4), along with the finding of a very small value for k in practice, indicates that all the asperities in contact contribute to the friction phenomenon but very small numbers of them result in wear (Archard, 1953). Furthermore, some asperities are just plastically deformed on the surfaces and not removed from the component. The volume of asperities that belongs to the deformed zone (V_p) is also represented in the k value. The k value is proportional to the removed volume of the component (W_v) and to the plastically deformed volume (V_p) (Equation (2-5)).

$$k = \frac{W_v}{V_p} \quad (2-5)$$

2.2.1 Adhesive wear

In adhesive wear theory, the asperities of surfaces mate with each other to form an adhesive junction. In this wear mechanism, it is assumed that the volumetric wear results only from adhesion between asperities and material is removed from the surface. A very first model of Adhesive wear states that the volumetric wear (W_v) is proportional to the contact load (F_n) and relative slip (s). So that the wear in terms of Equation (2-3) can be represented as Equation (2-6):

$$W_v = \frac{k}{H} F_n L \quad (2-6)$$

The expression of Equation (2-6) is known as Archard's wear law. Although this form of equation was firstly proposed by Holm (1951) on electric contact, Archard (1953) used this equation for a simplified model of mechanical contact interaction.

The Archard (Adhesive) wear coefficient correlates with the friction coefficient; however, unlike friction, wear rate varies over a very large range. The experimental measurement of k indicates a frequently small value in the range of 10^{-3} to 10^{-9} for metals which depends on several aspects such as lubrication regime, load applied, relative motion and range of motion (Yang, 2005).

2.2.2 Abrasive wear

Abrasive wear is where hard asperities or third bodies (particles trapped between surfaces) rub under pressured load. If wear occurs only between two surfaces it is known as two-body abrasive wear but where oxide particles are involved in the wear process it is named three-body wear (see Figure 2-2).

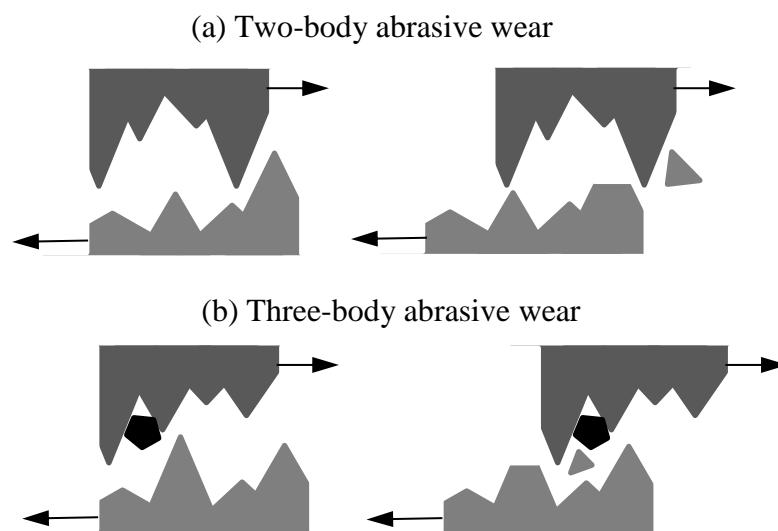


Figure 2-2: Two (a) and three-body (b) abrasive wear

There are three modes of abrasive wear, “Ploughing”, “Wedging” and “Cutting”. “Ploughing” is a ridge formed along the wear track side, “Wedging” is a short wedge

formed aside of the asperities and “Cutting” is a ribbon shaped chip formed aside of the asperities. In the all different forms of the abrasive wear, debris formed is removed from the underlying surfaces. The Adhesive wear theory seems to be useful to derive for abrasive wear as well.

In “Ploughing” abrasive wear, assuming a surface profile containing conical shaped asperities with an angle (α) that ploughs through the surfaces in contact, the volume loss W_v from the material is being removed from the ploughed groove over sliding distance and can be calculated using Equation (2-7) (Zum Gahr, 1988).

$$W_v = \frac{k'}{H} \left(\frac{2\overline{\tan(\alpha)}}{\pi} \right) F_n L = \frac{k_{abr}}{H} F_n L \quad (2-7)$$

where $\overline{\tan(\alpha)}$ is an average value of $\tan(\alpha)$ of all asperities and k_{abr} is the abrasive wear coefficient which is dependent on profilometry geometry of surfaces (k' is a constant coefficient).

In “Cutting” abrasive wear, material is removed as in a machining procedure by the forming of a chip. The chip (ζ) is based on a hard wedge asperity of width b , shear plane angle (φ) which is perpendicular to the direction of motion and rake angle (α) and can be determined from Equation (2-8) (Merchant et al., 2002),

$$\zeta = \frac{\cos(\varphi - \alpha)}{\sin(\varphi)} f \quad (2-8)$$

where, the thickness of under-formed chip f , is known as feed in machining applications. The feed parameter, f , is directly proportional to the applied normal force and inversely proportional to the hardness of the material, as Equation (2-9).

$$f = \frac{k'}{H} F_n \quad (2-9)$$

So that, the volume loss from the material by cutting is given by Equation (2-10):

$$W_v = UFbt = Lfb = \frac{k_{cut}}{H} F_n L \quad (2-10)$$

where t and U are the cutting time and cutting speed respectively.

2.2.3 Corrosion wear

Materials embedded in a corrosive environment experience chemical reactions which may result in wear. Fretting wear that occurs under oscillatory load over a small relative motion, is usually subjected to this chemical attack. When an asperity slides over and past the surface of the counter-face, material at the counter-face could rapidly be oxidized. Depending on the material, the asperity might stay in place (producing a hard oxide layer) or be removed by fracture over subsequent sliding.

A model of corrosive wear can be developed based on consideration of adhesive and abrasive wear occurring in a reactive environment. This leads to formation of a tribo-film¹ on the surfaces. In this condition, wear occurs where the tribo-film reaches a critical thickness (λ) and becomes weak enough to be removed by rubbing. Considering one single asperity covered with this film of thickness (λ) the volumetric wear loss is $\pi a^2 \lambda$, where a is the radius of a hemispherical asperity shape. Therefore

¹ Over sliding contact of surfaces, a thin solid film is generated and sticks fast on its worn surface with different tribological properties, chemical composition and structure.

the result for n identical asperities can be obtained as Equation (2-11) (Stack and Jana, 2004):

$$W_v = \frac{\lambda}{2a} n\pi a^2 L = \frac{\lambda}{2a} A_r L = \frac{k_{cor}}{H} F_n L \quad (2-11)$$

where k_{cor} is the corrosive wear coefficient. Note that the corrosive wear coefficient is directly proportional to the tribo-film thickness. This hypothesis is very dependent on aggressiveness of the environment and the temperature which increases the wear rate as both make the film grows faster.

2.2.4 Surface fracture wear

Brittle material is usually worn out under abrasive wear by subsurface lateral fracture crack propagation. The volume loss per unit distance over N asperities rubbing on a surface of fracture toughness (K_c), Young's modulus E and material constant c is given by Equation (2-12) (Ajayi and Ludema, 1988):

$$W_v = cN \left(\frac{(E/H)F_n^{9/8}}{K_c^{1/2}H^{5/8}} \right) F_n L \quad (2-12)$$

2.2.5 Erosive or percussive wear

Erosive wear is due to the repeated impact by wear particles (erosive) or hammering with a hard object (percussive), so that material is removed from the surfaces. The kinetic energy of the impaction is transformed into the plastic deformation on the asperities of the surface. Then, particles can be removed by cutting (for ductile material), fracture (for brittle material) or ploughing.

There are only a fraction of the total impacts (ζ) which result in erosive wear. The erosion ratio (e_r), over a total mass of m with impaction velocity (U), can be obtained using Equation (2-13) (ElTobgy et al., 2005),

$$e_r = \zeta \frac{\rho U^2}{2H} \quad (2-13)$$

where ρ is the density of the material. Again, similar to the adhesive wear law, the applied load (F_n) is replaced with ρU^2 and the term $F_n L$ represents a sliding energy. By considering n identical particles of mass m and velocity v , the individual kinetic energy (E_k) of the particles would be:

$$E_k = \frac{1}{2} m v^2 \quad (2-14)$$

As explained the ζ fraction of the total impacts results in wear, so that the impacting energy (E_i) resulting in wear can be calculated as Equation (2-15):

$$E_i = \zeta n E_k = \zeta n \frac{1}{2} m v^2 \quad (2-15)$$

Therefore the volumetric wear can be obtained using Equation (2-16):

$$W_v = \frac{k_{ero}}{H} E_k L \quad (2-16)$$

where k_{ero} is the erosive wear coefficient and can be interpreted as the fraction of all the impacts that results in wear.

2.2.6 Fatigue wear

If subsurface cracks occur on usually ductile material due to cyclic loading, fatigue wear may proceed on surfaces in contact. Where little adhesive and/or abrasive forms of wear occur prior to a fatigue event, extensive pitting may be observed once fatigue sets in. Again, by considering a large number of individual microscopic asperities mating in contact, where limitation of fatigue reaches at a particular asperity, a volume of material is removed from surfaces. An expression of volumetric fatigue wear can be obtained using Equation (2-17) (Karmakar et al., 1996):

$$W_v = k_{fat} A_r L = \frac{k_{fat}}{H} F_n L \quad (2-17)$$

where the fatigue wear coefficient (k_{fat}) interprets the proportion of the contacts that produces wear debris by failing. It can also be associated with the number of load cycles (or stress cycles) to failure N_f (Equation (2-18)).

$$N_f = \frac{1}{k_{fat}} \quad (2-18)$$

2.3 Fretting wear

“Fretting” is a special type of wear process. It refers to a very small relative movement of solid surfaces in contact (Hutchings, 1992). It occurs where surfaces in contact are subjected to vibration, repeated oscillating load or varying stresses in any form, and very small relative motion over a period of time. Fretting causes surface damage by leading to material removal from one or both surfaces (with equal or unequal fractions) in contact. In fact, fretting could itself contain adhesive, abrasive

and/or corrosive forms of wear (see Figure 2-1) while a small relative displacement occurs between surfaces in contact.

The mechanism of the fretting can be described based on the micromotion and loading at the coupling surfaces causing adhesion of surface asperities that are subsequently torn apart. This leads to creation of metal particulate debris. The debris is then oxidised and becomes harder than the mating surfaces. If the debris remains in the contact zone abrasive wear can occur resulting in further surface damage.

The difference between fretting wear with the other types of wear is mainly the magnitude of movement. This movement is known as “slip” which is always tangential to the surfaces in contact. Fretting and its resulting damage causes failure in many types of mechanical devices such as pressure armour layers, keyway-shaft couplings and taper junction of total hip prosthesis.

2.3.1 Fretting wear characteristics

Although fretting occurs in different forms the damage is distinctive. The result of fretting is manifested on the surfaces in contact in different characteristic ways. One of these characteristics is the wear debris from fretting and its consequent oxidization. Typically, fretting wear of steel produces a deep red oxide debris known as “cocoa” (the size of particles is usually less than $0.2\mu\text{m}$ (Varenberg et al., 2002)) while for aluminium the oxide is presented as a white powder.

Due to the condition of fretting where contact surfaces are always under high contact stresses, debris cannot usually escape from the gap between the surfaces. This leads to a third-body damage (abrasive and/or corrosive wear) which increases the wear rate with further surface damage.

Another characteristic of fretting is the scar of wear that remains on the surfaces, generally known as a “fretting scar” or “fretting wear pattern”. The scars appear at contact surfaces undergoing fretting as grey staining (matt surface due to micro pitting), undulations (in parts metallically smooth), pitting (localised piling up of particles), compaction zones (plastic indentations within the material), roughening (plastic deformation in the form of uniform corrugations) and tower like growth (built up from pasty particles at a few strengthened contact points) (Stowers and Rabinowicz, 1973).

Fretting can be assessed with three regimes, namely, “gross slip”, “partial slip” and “mixed slip”. Gross slip refers to where the displacement amplitude is higher than transition amplitude, partial slip occurs where the displacement is lower than the transition and for intermediate displacement amplitudes, the displacement may evolve from one sliding to another called mixed slip regime (Hannel et al., 2001). Vingsbo and Söderberg (1988) have shown that fretting is significantly dependent on the slip regime.

Fretting may also lead to a change of surface hardness which is another characteristic of wear. The surface hardness often (not always) increases mainly because of work hardening and oxidation.

2.3.2 Fretting wear theories

There are different theories on fretting and its process over time while all are based on similar foundations.

A strong theory of fretting, proposed by Archard (1953), is that where adhesive, corrosive and abrasive forms of the wear are all occurring, fretting takes place. Based

on this theory, fretting has three main stages. Initially, relative displacement between surfaces in contact causes adhesive wear between the asperities producing particles. Then, the released particles oxidize rapidly (because of their small size). The relatively hard oxide particles may further cause abrasive wear to the surfaces. The abrasive wear occurs because the debris has nowhere to escape from the contacting surfaces and is trapped between them. Finally, the wear progresses with further chemical reaction based on the environment causing corrosive wear.

A theory proposed by Engel and Klingele (1981) is similar to Archard's but not necessarily in the same order. Another theory stated by Wassef and Schmalzried (2013) is that, where the existing formed oxide layer on the surface is removed by physical fretting, adhesive wear due to micromotion, further oxidation and/or corrosion of the surface is possible.

2.4 Wear laws

As outlined earlier in section 2.2, the wear rate for contacting surfaces is proportional to the contact load and the relative displacement between them. Theoretical approaches to the assessment of wear are mainly based on “Archard's Wear Law” or the “Dissipated Energy Wear Law”.

2.4.1 Archard's wear law

The Archard-based wear law is the most common theory to model the wear process in tribology and is classically used in many studies. This approach relates the volumetric wear to the product of the normal load and relative sliding distance of the surfaces in contact. Then a wear coefficient is extrapolated to establish the wear resistance of the material. The dimensional Archard wear coefficient (K) from

Equation (2-3) which contains the hardness of the material ($K = k/H$) can usually be obtained using Equation (2-19).

$$K = \frac{W_v}{F_n s} \quad (2-19)$$

where s is relative sliding distance or “slip”. This wear coefficient, due to correlation of hardness, has units of Pa^{-1} . Equation (2-19) was originally proposed by Archard for unidirectional sliding wearing process but it has been widely used for fretting wear modelling as well.

The relative sliding in fretting occurs tangential to the surfaces with reciprocating action and Archard’s wear law needs a gradual approach to obtain the sliding distance. This can be represented as,

$$W_v = K \sum F_n s_i \quad (2-20)$$

where s_i is the relative slip per stroke and $\sum F_n s_i$ is the sum of $F_n s$ products over the load cycles.

Many studies have demonstrated that the Archard wear coefficient (K) for the same material combination, is strongly dependant on wear mechanism, progression of wear, contact geometry, displacement amplitude, loading condition and other parameters. For instance the K value for unidirectional sliding is completely different from reciprocating sliding (fretting for example) (Fridrici et al., 2001). Furthermore, other studies show that it is necessary for the wear rate of metals under fretting to consider the effect of elasto-plastic response of geometry (Johnson, 1995, Kapoor,

1997). The stress on the structure will be maintained within an elastic response up to the critical cyclic stress state where the material then undergoes cumulated plastic dissipation. This defines a shake-down boundary as a function of the “Hertzian” pressure. Such a theory has been confirmed with many other studies (Johnson, 1995, Van and Maitournam, 1994, Fouvry et al., 2001, Fouvry et al., 2003) and demonstrates that it is essential to integrate the change of friction coefficient for the assessment of wear rate under alternated sliding situations which is known as the greatest limitation of Archard’s wear law. Therefore, the Archard wear approach cannot accommodate the change of friction coefficient during the wearing process.

2.4.2 Dissipated energy wear law

The wear rate seems to be much more dependent on another significant parameter which is interfacial shear work (Fouvry et al., 2003, Fouvry et al., 2001, Teoh et al., 2002). The wear resistance of the material can be evaluated by an Energy wear approach that relates the wear volume to the friction energy dissipated through the interface. This method gives the wear volume proportional to dissipated energy ($\sum E$) given by,

$$W_v = \alpha \sum E \quad (2-21)$$

where α is an energy wear coefficient. The dissipated energy (E) is the product of tangential force (Q) and slip (s) given by,

$$E = Qs \quad (2-22)$$

The Energy wear law introduces the energy wear coefficient which allows rationalizing the quantification of wear and classifying the wear resistance. This method also interprets different wear mechanisms (such as abrasive, corrosive and fatigue wear) in a much more appropriate way. Similar to K (the Archard wear coefficient) in the Archard wear law, the α value (Energy wear coefficient) again depends on material combination, sliding condition and the contact geometry. In this law, a minor dissipated energy participates in plasticity with the majority part of the energy being consumed by debris flow through the interface. It can also accommodate the change of friction coefficient during the wear analysis. These advantages show the superiority of this law compared to Archard's wear law.

2.5 Hip joint

The Hip joint is fundamentally a ball and socket joint (Figure 2-3) with the large area of the ball (femur head) surrounded by the socket (acetabulum). It bears more weight with high stability but carries less range of motion in comparison with other ball-socket joints such as the shoulder. A hip joint contains the head of the femur bone, the acetabulum, cartilage, joint capsule (ligaments) and tendons.

The joint is supported with muscles, tendons and ligaments. The whole hip joint is covered by a joint capsule that helps to stabilize the motion of the hip. This capsule covers all femur head cartilages and the acetabulum. The fibrous and thick capsule contains three ligaments, “iliofemoral”, “ischiofemoral” and “pubofemoral” located beside the labrum and ligamentum teres (see Figure 2-3).

The femur or thigh bone is known as the longest, heaviest and strongest bone in the human body. Its duty is to support and carry all the body weight during human activities. There is always extreme force applied on the femur which can be stabilized with the strength of the muscles attached to it.

The acetabulum is basically a cup dented in the pelvis (the concave surface of the pelvis) shown in Figure 2-3. The femur head meets the pelvis at this concave surface to form the hip joint.

The main duty of the cartilage on the acetabulum and head of the femur bone is to lubricate the joint and provides a smooth surface in order to facilitate a nearly frictionless and smooth motion. From a mechanical point of view it acts in a similar way to lubricant in machinery. Its performance in the joint is crucial as if it is damaged due to overuse, overweight and/or any specific diseases affecting the joint,

two hard bony surfaces act upon each other causing high stresses in the joint articulation with high friction making the joint stiff and painful.

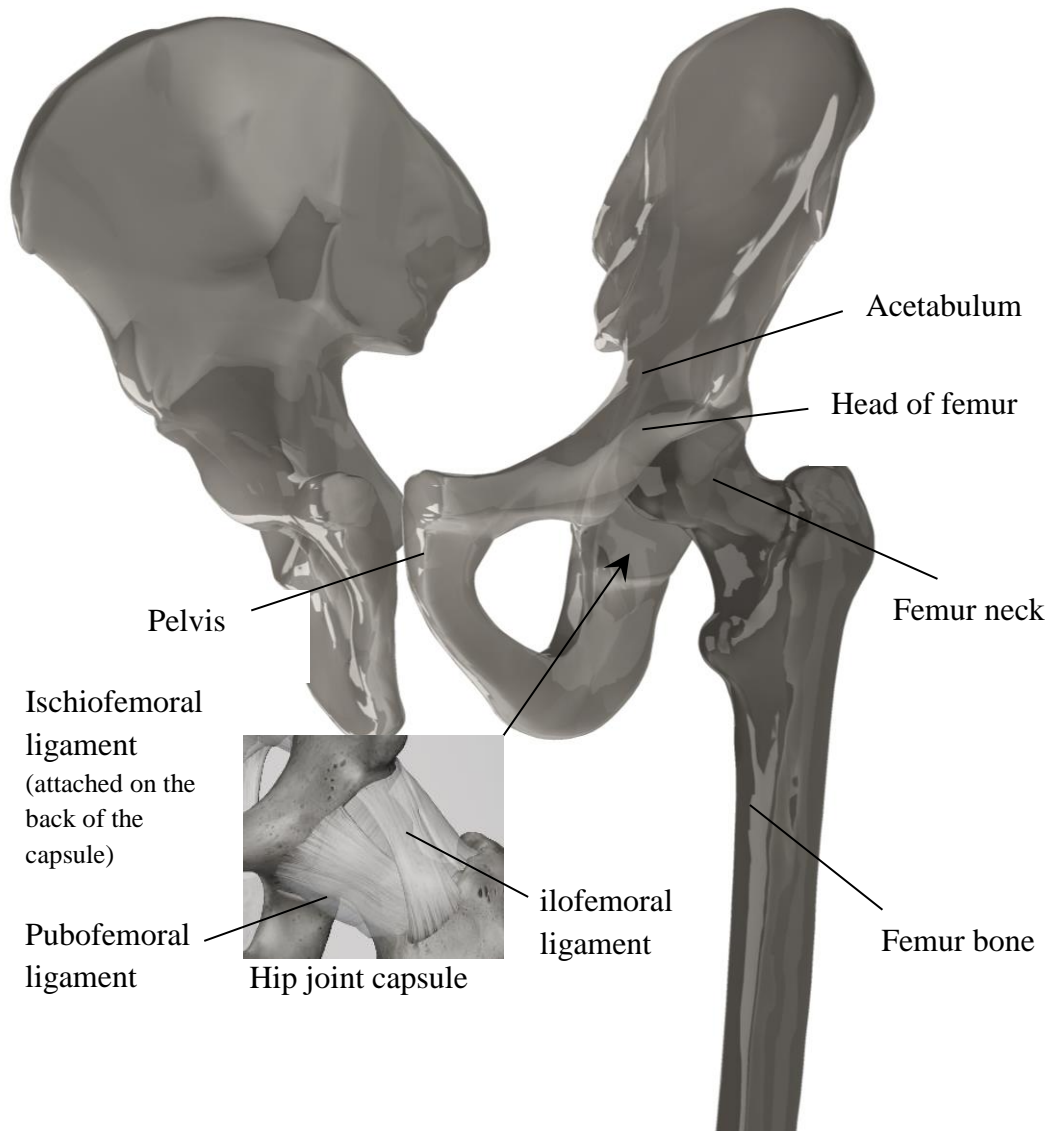


Figure 2-3: A human hip joint, model created in SolidWorks

2.5.1 Hip joint disorders

A hip joint can allow a wide range of movement and transmit high dynamic loads. Its ability to carry loads and provide this mobility is remarkable; however, it is vulnerable and can lose its functionality due to diseases such as:

- **Osteoarthritis:** When the joint cartilage is worn away, bones grind against each other causing stiffness, pain and immobility.
- **Rheumatoid arthritis:** This arthritis is a chronic disease which while progressing leads to severe damage in joint ligaments and erosion of the bone.
- **Avascular Necrosis:** This is defined as death of organ cells in the joint tissue due to lack of blood supply and mostly affects the top of the femur bone. Avascular necrosis may lead to change of the shape of the bone, joint stiffness, pain and loss of range of movement.
- **Trauma and bone fracture**
- **Others,** such as Tendonitis of the adductors of the hip, Trochantric bursitis, Snapping hip Syndrome.

Drugs and physio-therapy can help to reduce pain for patients; however, in severe cases, to eliminate the pain, the effective treatment would be replacement of the affected joint. At the final stage of severe hip pathologies², arthroplasty is a key solution for patients who wish to pursue an active lifestyle again.

2.6 Hip arthroplasty

THR is a common arthroplasty performed worldwide as a key and successful solution to improve a patient's lifestyle who is suffering from painful hip joints, hip joint diseases or joint fracture. Sir John Charnley (1911-1982) carried out the very first hip arthroplasty in November 1962. He developed a method to replace the whole

² Pathology is "The science of the causes and effects of diseases, especially the branch of medicine that deals with the laboratory examination of samples of body tissue for diagnostic or forensic purposes". Oxford Dictionary

hip joint by an artificial one and established a surgical technique for implantation. Although, implants and surgical techniques have advanced since then, the same foundation proposed by Charnley is currently being used. The main aim of the surgery is to accommodate an active lifestyle for patients.

A total hip prosthesis is a ball and socket joint normally comprising of three components, an acetabular cup, femoral head and stem (see Figure 2-4 and Figure 2-7).

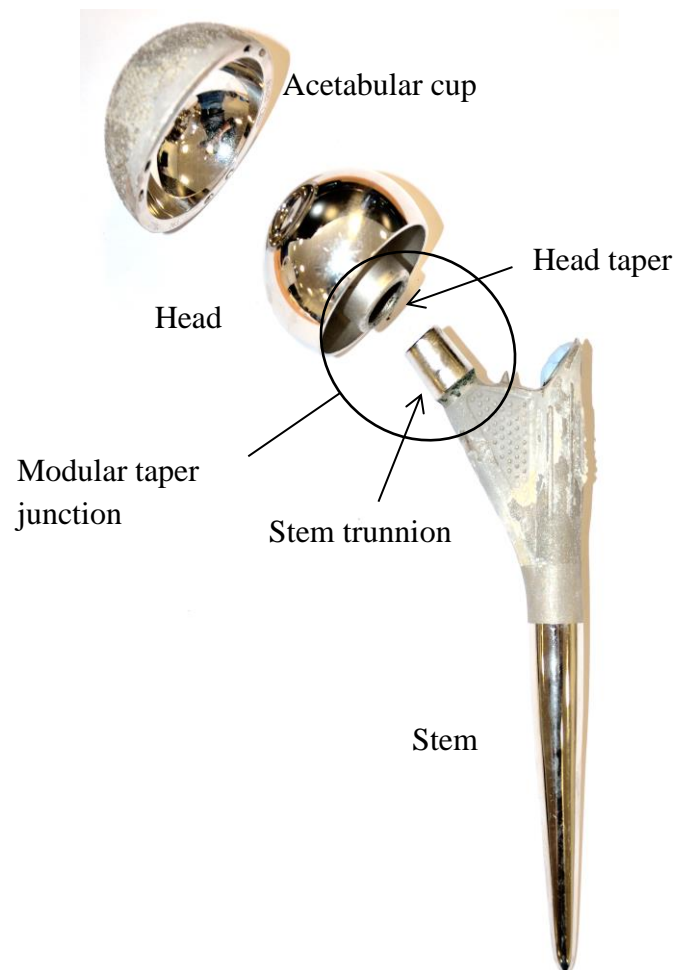


Figure 2-4: A THR, a Birmingham acetabular component, a Freeman uncemented stem and a Birmingham XL head (retrieved)

Since the very first Charnley hip prosthetic design, this implant has been developed in terms of design, material, bearing surfaces and resurfacing techniques. The

success of the design is only based on the longevity of them *in-vivo*. Although the sizes of the components are different based on the anatomy of the patients, their basic geometry is similar. Currently, a wide range of Prosthetic devices are available commercially in terms of design, type and material. The main joint replacement manufactures are DePuy, Zimmer, Smith & Nephew, Stryker, Biomet and Link. Figure 2-5 shows just some of the many different implant designs.



Figure 2-5: Different design of hip implants

In early designs of THRs, the head and stem were manufactured as a single component (monolithic prosthesis). Using two separate components (modularity) in THRs allows flexibility intra-operatively to facilitate optimum prosthetic functionality and anatomical fit for individual patients. Modular connection involves a male and female junction. Interlocking ridges are machined to a certain roughness to connect a tapered shank and socket. This allows a surgeon to choose different prosthesis components dependent on a patients' anatomy, age and level of activity

without a large inventory. The main advantages of modularity in total hip prosthesis can be listed as below:

- Custom implants that attempts to enhance fit and fill of different hip geometry.
- Better adjustment of head size, leg length offset, neck length, anteversion³
- Decrease implant inventory
- An ability to remove the femoral head at revision surgery to improve exposure or change head size without stem component removal.
- Use of different materials for components (different material combination to provide good bearing properties mainly low friction and high wear resistance)
- Self-lock with no screw

Beside all the advantages of modularity, clinical experience has witnessed significant drawbacks associated with modularity, such as:

- Introduction of one or two more interfaces which may lead to increased fretting wear
- Dissociation of implant, possible loosening of the parts
- Possible corrosion of mixed metals,
- Possible fracture below the head and neck
- Reduced range of motion

³ Anteversion is an angle between an imaginary transverse line that runs medially to laterally through the knee joint and the imaginary transverse line passing through the centre of the femoral head and neck.

- Cost of modular implants is relatively higher than a monolithic prosthesis (McCarthy et al., 1997), however, Srinivasan et al. (2012) believed that the use of modularity results in cost savings.

2.6.1 Procedure of total hip replacements

THR is a surgical procedure. The surgery involves the replacement of the hip joint with an artificial mechanical one. During the surgery the whole hip joint is removed and replaced by a prosthetic device (see Figure 2-3 and Figure 2-6).

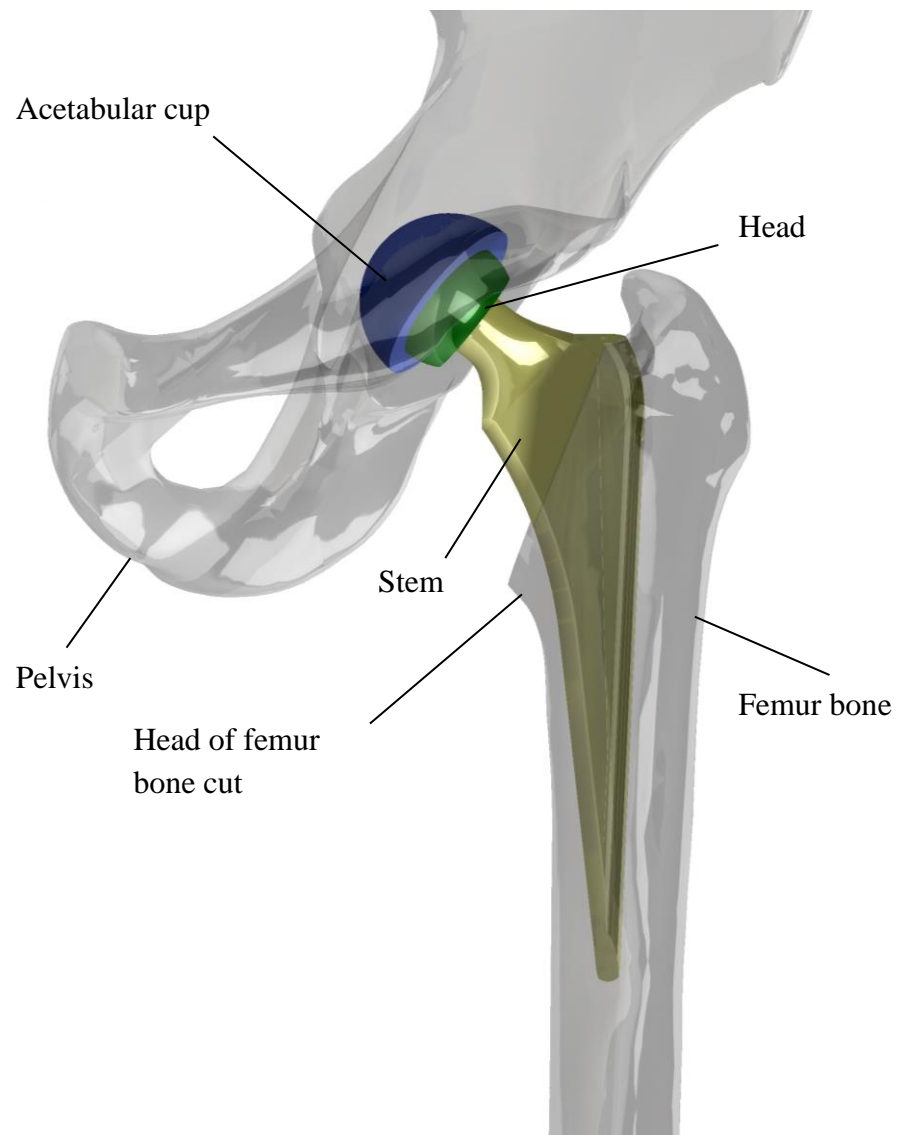


Figure 2-6: Schematic of the THR in service, model created in SolidWorks, JRI implant, AEON cemented hip system

On reaching the hip joint, the surgeon dislocates the femoral bone from the socket and cuts the head of the femur bone (the top of the thigh bone). The inside of the femur bone is cleaned (using various techniques) and the stem placed into the bone. The stem fixes into the femur canal using either a cement mantle (typically Plexiglas) or biological ingrowth that allows the bone to grow into and onto the metal stem surface coated with a porous or rough material.

Then a perfect hemispherical bone socket, matched with the external shape of the acetabular cup, is made in the pelvis acetabulum (hip socket) by a reamer and the acetabular cup is placed into that.

A trial head is placed on the top of the femoral stem in order check the size and adequacy of the hip motion. When the appropriate head size is found, the actual head is placed on the stem trunnion and usually fixed with impaction. Generally, one to three firm impactions are applied to the top of the head.

2.6.2 Femoral head and stem assembly

As discussed, the assembly of the femoral head onto the stem trunnion at surgery is achieved by impaction by the surgeon. In order to apply impaction on the head, surgeons use a polymer tipped impactor instrument and a mallet to avoid damaging the prosthesis (see Figure 6-1 in Chapter 6).

It is known that the magnitude of this impaction force affects the initial taper strength for long-term and safe fixation. The strength of fixation is obviously dependent on the impaction force, design of the taper, the condition of the taper surfaces, mismatch angle, angle of impaction, environment (dry or wet) and number of impactions (Heiney et al., 2009, Pennock et al., 2002). It has been postulated that attaining

maximum fixation is crucial in minimizing problems associated with these tapers such as corrosion, fretting, micromotion and unintended disassembly.

A number of experimental studies have investigated parameters that affect taper fixation (Heiney et al., 2009, Pennock et al., 2002, Rehmer et al., 2012, Lavernia et al., 2009) with taper “pull-off” force being used as the measure to assess taper strength. All of these studies involved (at least) the simulation of the assembly and disassembly of cobalt chrome alloy heads with a titanium alloy stem.

The magnitude of the impaction forces used were determined initially using tests in Heiney et al. (2009), Pennock et al. (2002), and Lavernia et al. (2009) where surgeons were required to apply an impact typical of that used intra-operatively to assemble the head to the stem. The average of the measured forces from the three studies were approximately 5000N (1 surgeon \times 11 impacts) (Pennock et al., 2002); 1633N, Standard Deviation 422N (8 surgeons \times 5 impacts each) (Lavernia et al., 2009); and 4409N (10 surgeons \times 1 impact) (Heiney et al., 2009). Rehmer et al. (2012) used impact forces of 2000N, 3000N and 4000N (to cover the typical range of force applied by surgeons) describing them as light, medium and firm hammer blows for seating the femoral head on to the stem. A linear relationship was found by Heiney et al. (2009), Pennock et al. (2002), and Rehmer et al. (2012) such that increased impaction resulted in increased pull-off forces (with the ratio between pull-off and impaction being around 0.4 (Pennock et al., 2002) and 0.48 (Heiney et al., 2009)). Lavernia et al. (2009) found much reduced pull-off forces where biological debris (blood, fat) existed on the taper during assembly.

Pennock et al. (2002) and Rehmer et al. (2012) stated multiple impacts did not increase taper fixing strength, whereas Heiney et al. (2009) advised two firm blows

would attain maximum fixation. Pennock et al. (2002) suggested that surgeons should apply an in-line maximum impaction but Heiney et al. (2009) and Rehmer et al. (2012) recommended a firm blow (4000N) so as not to risk damage to the femur. However, Mroczkowski et al. (2006) used an impact load of 6700N and hand assembly to represent the extremes of what may be seen “clinically” in an experimental study into the effect of impact assembly on fretting corrosion of hip tapers.

These studies highlight the non-standard nature of the surgical assembly process for the prosthetic femoral head and stem with evidence of significant variation by surgeons with regard to impaction force and technique used. This variation occurs due to a surgeon’s differing experience; the type of head (metal or ceramic); and crucially, the quality of the bone stock of the patient.

So, there is not only evidence that the magnitude of the impaction force affects taper fixation (Heiney et al., 2009, Pennock et al., 2002, Rehmer et al., 2012), but also, Mroczkowski et al. (2006) suggest that the extent of taper fixation may have an effect on corrosion, micromotion and fretting wear.

Surgeons are provided with general guidelines and training by manufacturers on how to assemble a head to a particular stem; however, manufacturers’ guidelines are vague for the assembly of the head and stem with statements such as ‘slightly’ or ‘firmly’ impacted the norm to describe the magnitude of any impaction force to be used. In reality, the magnitude of the impact used is based on a surgeons’ preference, experience, the type of prosthetic femoral head, and the quality of the patients’ bone stock.

2.6.3 Material and material combination of total hip replacements

All materials used to manufacture THR's must be biocompatible in order to reduce the risk of rejection of the implants and possible toxicity. Increases in the number of young active patients using hip prostheses has led to an amplified use of alternative bearing materials. In the highly corrosive human body environment, the material properties of different components of implants play a significant role in their longevity.

- **Acetabular cup.** The acetabular cup is fitted into the pelvis and the bearing surface is typically manufactured from Ultra-High-Molecular-Weight Polyethylene (UHMWPE) which has low friction and wear rate, high toughness, good impact resistance and good biocompatibility. In some designs it is manufactured from highly cross-linked polyethylene (HXLPE), ceramic (such as alumina or zirconia) or to a lesser extent recently a cobalt-chrome alloy (Jeffers et al., 2009).
- **Femoral head.** Prosthetic femoral heads are normally made from a cobalt-chrome alloy, but also either ceramic or high grade stainless steel. The main advantage of ceramic used for a femoral head is low friction which leads to a low wear rate and reduced wear debris; however, it is brittle. Cobalt-chrome alloy provides very good biocompatibility, corrosion resistance, high hardness, reduced inflammation and superior wear resistance for bearings especially where it is combined with itself or on a UHMWPE cup. It provides relatively successful performance and has been widely used in orthopaedic applications (Brown and Lemons, 1996).
- **Modular stem.** The stem which needs to be fitted into the medullary cavity of the femur is usually made from titanium alloy (typically Ti-6Al-4V) which has

similar elasticity as bone, good tissue tolerance, high strength to weight ratio and lighter weight than other orthopaedic alloys. It is rarely made from a cobalt-chrome alloy or stainless steel (Head et al., 1995).

The combination of different materials for the components also creates different interfacial properties. When the term “material combination” arises, it means the material of the femoral head and acetabular cup (bearing material combination). There are several different material combinations for the articulating surfaces in THRs, such as Metal-on-Plastic (MoP), Ceramic-on-Plastic (CoP), Ceramic-on-Ceramic (CoC) and Metal-on-Metal (MoM).

- **MoP and CoP.** Plastic which is usually UHMWPE or high cross-linked polyethylene (see Figure 2-7) has high wear resistance compared to other types of plastics, however, compared to metal and ceramic it has a high wear rate. It allows the use of a larger femoral head. Further, UHMWPE allows the bearing to act as a good shock absorber and this helps to possibly allow greater activity levels.
- **CoC.** This type of prosthesis reduces the possibility of scratches on the surfaces and therefore, makes the couples less vulnerable to wear. The wear rate is 10 percent less than MoM. In this type of prosthesis, it is possible to use a thinner acetabular cup (because of its strength) and therefore, it is possible to choose a bigger femoral head fitted into a smaller acetabular shell. It provides a wider range of motion and higher stability and is a good bearing for young active patients. This type of prosthesis, however, is expensive, brittle and “squeaking” has been widely reported which is unpleasant for patients (Mai et al., 2010).

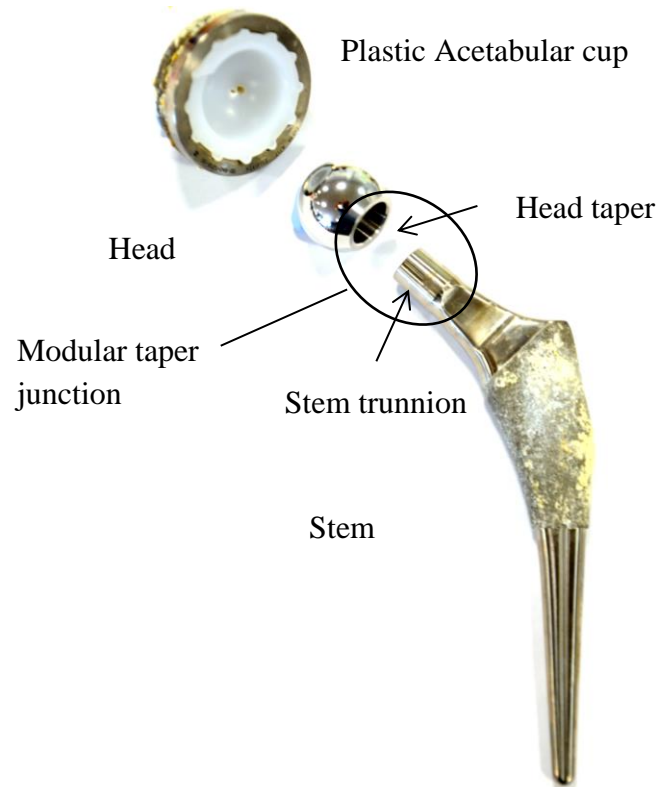


Figure 2-7: Metal-on-Plastic total hip replacement

- **MoM.** The difference in hardness is the main advantage of this kind of prosthesis. The MoM prosthesis (see Figure 2-4) is fabricated from different metallic alloys such as cobalt-chromium alloy. One of their biggest advantages to ceramic is that they are hard but not brittle. Their advantage over plastic is that they are more resistant to wear and scratching. Another advantage of this coupling is that it can be made with a bigger femoral head diameter for the same sized acetabular shell. Therefore, it provides a wider range of motion for the hip. This combination is also supposed to provide less wear, less bone resorption, fewer offset problems, less risk of dislocation and make it easy for revision surgery. The MoM hip prosthesis has been developed to help the failure rate; however, it leads to other serious problems that increase the failure rate such as metallosis (Milošev et al., 2000) and infection.

The acetabular cup and femoral head need to provide a smooth articulating bearing surface to allow necessary hip movement and to minimize wear. There is evidence that cobalt-chrome femoral head with UHMWPE acetabular cup provide a good combination for bearing surfaces. Furthermore, the advantages of titanium and cobalt-chrome alloy brought these two materials in combination as a titanium modular stem and cobalt-chrome femoral head and these combinations have been widely used in orthopaedic devices.

2.6.4 Surface characteristics of total hip replacements

- **Bearing**

British standard (BS ISO 7206-2:1987) suggested that for articulating surfaces (bearing) of implants the surface roughness finish should not exceed $70\mu m$ and $30\mu m$ in average (R_a) for metals and ceramic respectively. In fact, due to advanced manufacturing and polishing techniques, these surface finishes are much smoother than suggested. Recently, available femoral heads are manufactured from an average R_a of less than $0.03\mu m$ to $0.1\mu m$ (Hosseinzadeh et al., 2012). This has helped to reduce wear at bearing surfaces significantly (Smith et al., 2001). The material investigations and advanced manufacturing techniques on bearings have fairly well reduced the wear rate that could occur at bearings.

- **Modular stem**

The modular stem of earlier THRs was initially developed with stainless steel with a relatively smooth surface and developed further to a high degree of surface finish. This detrimentally effected fretting wear between stem and bone (Ohashi et al., 1998, DANIEL M ESTOK and Harris, 1994). In the 1970's studies tried to change the

surface finish of the modular stem from what was highly polished to a rough surface with a matt appearance in order to have better fixation between the stem and bone. Coating has commonly been used on some modular stems to encourage bone ingrowth and better fixation.

- **Taper junction**

The focus of this study, however, is the taper junction or taper interface of THRs. The taper junction contains of female taper or head taper surface namely “taper” and male taper or stem taper surface namely “trunnion” (see Figure 2-4). Although the taper and trunnion are manufactured to produce a component geometry as a specific locking mechanism, micromotion between them is inevitable. Therefore, good fixation between them is of the greatest importance to reduce micromotion and subsequently reduce the wear rate.

A change of friction coefficient at the surfaces will affect the relative micromotion which in turn affects the wear rate. Between the 1980s and 1990s, theoretical studies tried to decrease the contact pressure as a means of decreasing wear in the taper junction (Bartel et al., 1985, Fessler and Fricker, 1989, Jin et al., 1999). Subsequently, Wang et al. (2001) used a joint simulator to determine the effect of contact pressure on wear and friction coefficient. They showed that increasing the contact pressure reduces both the coefficient of friction and wear rate. They suggested that higher taper friction is a desirable condition in order to provide better fixation and reduce wear.

Water and blood only reduce the magnitude of the friction coefficient slightly (Fessler and Fricker, 1989). Water has no effect (in comparison to a dry condition) on the friction coefficient at the taper junction; however, blood reduces the friction

coefficient slightly due to the protein complexes that enhance boundary lubrication (Fessler and Fricker, 1989).

Ceramic and metal tapers are typically (but not always) manufactured relatively smooth and polished (see Figure 2-8); however, some prosthetic devices have threaded trunnion surfaces (see Figure 2-9) in order to increase friction and improve fixation of the components. Threaded tapers provide better fixation especially for a metal trunnion and ceramic taper. Hallab et al. (2004) performed an in-vitro fretting test comparing possible fretting corrosion between metal-stem/metal-head and metal-stem/ceramic-head combination. They showed approximately 11-fold greater metal debris released from metal-stem/metal-head. This is due to the hard on soft mechanical interlocking of the harder ceramic and softer metal contact interface that could reduce the potential relative micromotion.

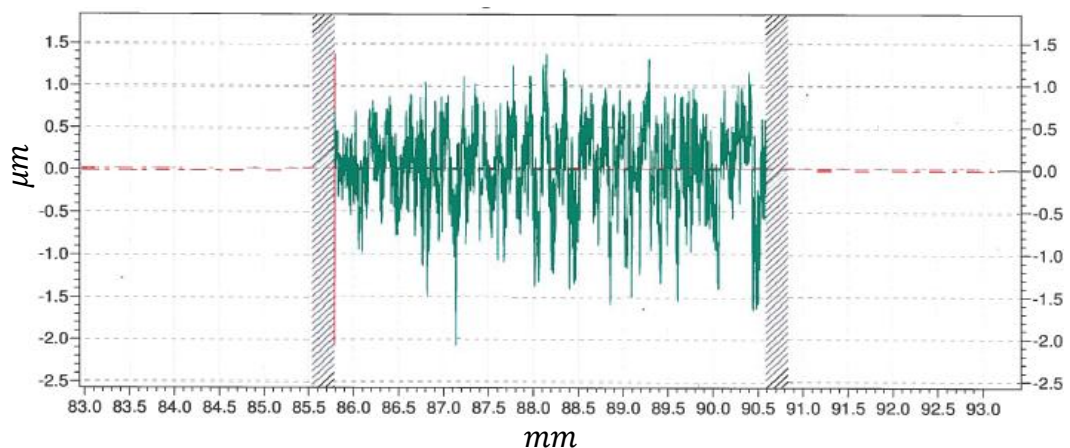


Figure 2-8: An example of head taper surface topography

Figure 2-8 and Figure 2-9 show the surface topography on a commercial head taper and stem trunnion respectively using a contact profilometer (Talysurf PGI 840, Taylor Hobson, Leicester, UK). The arithmetic mean value (R_a) of $0.4\mu\text{m}$ on the head taper surface roughness and $2.1\mu\text{m}$ on threaded stem trunnion are visually apparent.

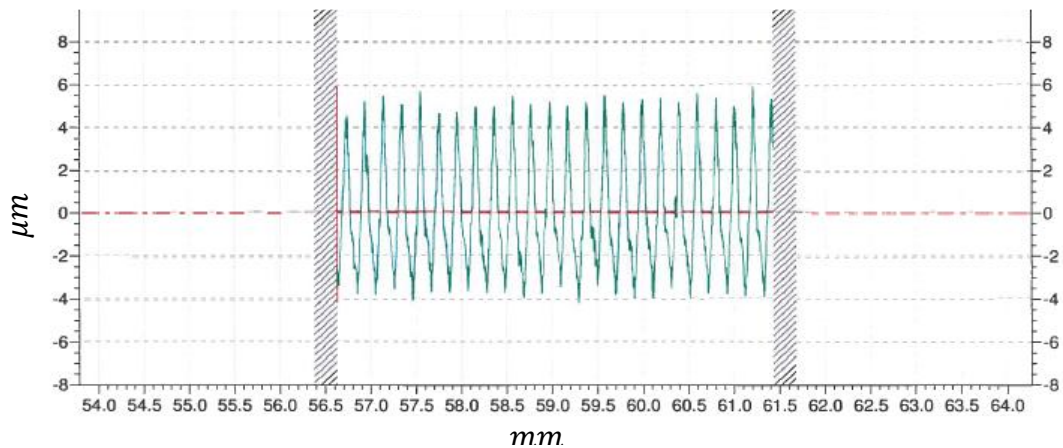


Figure 2-9: An example of threaded stem trunnion surface topography

2.6.5 Failure of total hip replacements

Modern THRs are a major clinical success with expected lifetimes of 10 to 15 years (Aldinger et al., 2003, Teloken et al., 2002). Failure after this is known as a “fair success” of the implant and any failure below that called “premature failure”.

Recent data from the National Joint Registry (NJR) indicates that around 89,000 hip operations were performed in the UK using arthroplasty in 2013 (11th Annual Report, NJR for England, Wales and Northern Ireland, 2014). The American Academy of Orthopaedic Surgeons (AAOS) has indicated that more than 285,000 THRs are performed each year in the United States (National Hospital Discharge Survey, USA, 2010) with this number expected to rise with an ageing population. The number of patients receiving THRs has increased over the past decade by 14% in the United Kingdom and 35% in the United States (Smith et al., 2012). In addition, as these devices are becoming more common place, younger patients are adopting this solution too and as such there is a need to improve existing designs further to accommodate their more active lifestyle and to extend the prostheses life.

Instances of premature failure of these implants (< 5 years) has been reported and attributed to aseptic loosening (Langton et al., 2011, Mattei et al., 2011). Aseptic loosening which is a loss of fixation of the implants is known as the main factor of failure of THRs. This loss of fixation may be a result of inadequate initial fixation, mechanical loss of fixation over time or biologic loss of fixation happening due to wearing process. It could occur at modular stem-bone (cemented or uncemented) or the head-taper interface (Abu-Amer et al., 2007). The Swedish Hip Arthroplasty Registry reported that 75% of premature mechanical failure is due to aseptic loosening and the rest is due to dislocation, infection and rarely fracture (see Figure 2-10) around the implant. Mostly, all the recalls are due to unexpected pain or pain due to Adverse Soft Tissue Reaction (ASTR) to debris released. Thus, one of the main mechanical requirements for an improved prosthetic design is to minimise wear to increase device longevity.



Figure 2-10: Fracture occurred at Polyethylene cup of a total hip prosthesis

When failure happens, revision surgery is needed to replace the failed implant. Revisions are less successful than primary due to the much more complex procedure and also the reduction of the bone quality. It is also much more costly than primary surgery with more discomfort and pain for patients.

The failure rate varies with the type, design and brand of the prosthesis. For instance, for MoM THRs, the failure rate at seven years is around 13.6%, compared with 4.9% failure rate for those made of other materials (Smith et al., 2012, Cohen, 2012). For articular surface replacement (ASR; DePuy, United Kingdom) the NJR (2014) announced more than 29% failure in 2013. In general, the registry has shown the MoM THRs have not performed satisfactorily enough as bearing surfaces. Large numbers of recalls of MoM hip prostheses are due to the ASTR in patients (Pandit et al., 2008). Metal ions released into the body may enter the blood vessels or other organs of the body and increase the iron percentage in the blood (Smith et al., 2012).

Another concern with MoM THRs is the possibility of metallic cancerous ions. Smith et al. (2012) investigated 40,576 patients with MoM and 248,995 with alternative bearings hip replacement. Based on the results, there is no evidence on the risk of cancer diagnosis in the first seven years after MoM implantation with no increase in the risk of malignant melanoma, Prostate or Renal cancer. Although all the data presented is reassuring, this kind of finding is observational with a short follow-up using hospital statistics.

Consequently, an understanding of all clinical failure (mainly wear for this research) at all interfaces is needed to reduce the number of revisions, increase longevity and provide more comfort for patients.

2.7 Wear and fretting wear in total hip prosthesis

Wear is inevitable at each interface of a total hip prosthesis due to the cyclic load. As a matter of fact, wear occurs in all different types of prosthetic devices in varying amounts. Prosthetic wear produces different types of wear particles in terms of size and shape. The wear debris produced from these devices is created at:

- **Head and acetabular cup interface.** The wear occurring at this interface has been minimised significantly with the introduction of advanced materials with low wearing rate, improvement of manufacturing and polishing techniques, and optimisation of size and geometry.
Although generation of wear at the head and acetabular cup has reduced significantly, the amount of debris released from this interface is generally inevitable and acceptable due to the nature of bearing and interaction between those components.
- **Stem and cemented stem interface.** In cemented THRs the femoral stem is secured typically using Plexiglas (Poly-Methylmethacrylate PMMA). The wear occurring between stem and the bone cement is well documented in the literature (Brown et al., 2007, Zhang et al., 2008b, Buly et al., 1992, Zhang et al., 2008a, Hailer et al., 2010, Morshed et al., 2007).
- **Head taper and stem trunnion (taper junction) interface.** The form of wear occurring at this interface is fretting wear. The main issue with fretting in arthroplasty is that the oxide debris released has no escape route, and is accumulated either on surrounding tissue within the body or trapped between contacting surfaces which has a damaging effect. It may lead to ASTR and trapped particles causing further abrasive and corrosive wear. Tissue reaction to metallic wear debris plays a major role in aseptic loosening of joint implants.

As well as the benefits associated with modularity there are inherent difficulties associated with the release of wear debris at both the acetabular cup-head articulating surface and also the head taper-stem trunnion junction which have led to ASTR in recipients (Langton et al., 2011, Mattei et al., 2011).

2.7.1 Fretting wear at taper junction of total hip replacements

Traditionally the debris released at the head stem interface has been assumed negligible compared to the wear occurring at bearing surfaces. The determination of wear in THRs up until recently has mainly focused on the articulating surfaces between the head and (plastic) acetabular cup (Fialho et al., 2007, Maxian et al., 1996a, Maxian et al., 1996b, Maxian et al., 1997, Patil et al., 2003, Raimondi et al., 2001, Teoh et al., 2002, Wu et al., 2003); however, fretting and its resulting damage at the taper junction causes failure in many types of prosthetic device. Corrosion occurs due to fretting which not only leads to implant failure but also causes serious problems such as ASTR.

As discussed, MoM prostheses incorporate a metal femoral head and cup articulation and have a much reduced wear rate in comparison to MoP. Modern large diameter MoM prostheses (Figure 2-4) were introduced around 1997 (Cohen, 2012) as an option for young active patients to provide a device with reduced wear debris and risk of dislocation, greater strength and longer life than MoP types. However, under certain circumstances, metal debris can be generated at the articulating surfaces which can damage the surrounding soft tissues leading to “aseptic lymphocyte dominated vasculitis-associated lesions” (ALDVAL) and Metallosis and cause immobility in patients (Sporer and Chalmers, 2012).

Importantly, evidence of metal wear debris has been reported in MoP (case-report level) and CoC THRs too, implicating taper wear and also neck-cup impingement (Langton et al., 2011, Mao et al., 2012). Langton et al. (2012) and Bolland et al. (2011) have shown damage at the taper junction in retrieved MoM prostheses where there is correspondingly minimal wear at the bearing surfaces but still serious soft

tissue damage. Langton et al. (2012) presented Scanning Electron Microscope (SEM) images of taper junction surface damage occurring in the femoral heads from retrieved large diameter MoM prostheses. The images show surface peaks (created by the impression of the machining grooves from the trunnion) having been sheared off leading to significant material loss, and evidence of the formation of pits with inclusions which it was hypothesised were primarily due to mechanical fretting wear. There was evidence of only small amounts of chlorides and oxides suggesting corrosion was not the primary mechanism of material loss, contrary to the opinion of Malviya et al. (2011), Goldberg et al. (2002), and Gilbert et al. (1993).

As the junctions would have been subject to oscillatory loads and small relative displacements (micromotion), the type of mechanical wear taking place is likely to have been fretting wear. There is evidence in the literature of experimental investigations relating to fretting in THRs (Hallab et al., 2004, Duisabeau et al., 2004) but only a limited number of studies on the numerical simulation of this type of wear (Zhang et al., 2013, Elkins et al., 2014). Due to this serious problem large diameter MoM prostheses are no longer used for arthroplasty.

ASTR and Metallosis have been shown to not only be an issue for MoM prostheses, there have also been reports of them due to metallic wear debris produced from the taper-trunnion interface for both MoP (Mao et al., 2012) and CoC (Milošev et al., 2000) prostheses. This indicates that damaging metal debris can also be created at the taper junction between a metal head and stem even in MoP or CoC prostheses.

2.7.2 Fretting wear of cobalt-chrome and titanium

As discussed, the advantages of titanium for the modular stem and cobalt-chrome for the femoral head brought this combination of materials in THRs together. Besides all

the material advantages of cobalt-chrome and titanium, recent studies show a different scenario for the cobalt-chrome and titanium taper junction combination of modular head and stem (Bishop et al., 2013, Bone et al., 2015, Moharrami et al., 2013). This combination seems to lead to a risk of significant enhancement of potential wear and corrosion. Significant damage on the surface of the harder cobalt-chrome has been reported (Cook et al., 1994, Mears, 1975) and a large number of failures have been reported due to the wear occurring between the cobalt-chrome head and titanium stem (Bolland et al., 2011).

Unexpectedly, the harder cobalt-chrome shows more surface damage than the softer titanium alloy. This is due to fretting wear and the tribocorrosion mechanism between these materials (Moharrami et al., 2013). Moharrami et al. (2013) undertook an investigation on the Young's Modulus and hardness of both materials considering *in-vivo* corrosive environment to determine how titanium with lower hardness can wear cobalt-chrome with higher hardness. Their investigation showed that *in-vivo* oxidation has a significant effect on the surface material properties of titanium alloy making it harder but makes no difference to the hardness of cobalt-chrome. The hardness of cobalt-chrome remains relatively constant as it is more resistant to oxidation.

Therefore in fretting between these two materials, titanium significantly abrasively wears cobalt-chrome. Experimental measurement of fretting wear for this combination showed the wear rate on the cobalt-chrome head taper was almost 10 times higher than on the titanium stem trunnion (Bone et al., 2015, Langton et al., 2012).

2.7.3 Wear particles released from hip implant

Wear particles release into the body from THRs can be found in different organs such as the blood, kidneys and bladder (Maloney et al., 1995). During revision surgery, debris accumulated around the joint and surrounding tissue has been clearly presented (Kusaba and Kuroki, 1997). The debris contains metal and plastic particles dependant on the type of prosthesis. Even for MoP THRs, analysis of the debris has showed that particles are not only from UHMWPE (which come from the acetabular cup) but also from metallic particles generated mostly from the head-stem interface (Minakawa et al., 1998, Shahgaldi et al., 1995, Young et al., 1998).

Observations of the failed implants show significant damage at the taper junction (visible with the naked eye). The metal debris released leads to serious problems and infection of the surrounding tissue. Bolland et al. (2011) has shown damage at the taper junction in retrieved prostheses. Although there is correspondingly minimal wear at the bearing surfaces, serious wear damage on the taper and trunnion surfaces was visible.

2.8 Wear assessment

As explained, theoretical and computational approaches to the assessment of wear are mainly based on ‘Archard’s Wear Law’ or the ‘Dissipated Energy Wear Law’. In both methods an experimentally determined wear coefficient is required which encompasses a variety of parameters affecting wear such as material combination and properties, geometry, surface roughness, friction coefficient, lubrication regime, temperature, and loading frequency.

2.8.1 Archard and Energy wear assessment

In the gross slip regime it can be seen that there is a relationship between Archard and the Energy wear coefficient as follows,

$$\alpha = \frac{\mu k}{H} \quad (2-23)$$

where μ is the friction coefficient. However, in the partial slip regime where the traction force (Q) is lower than the product of the friction coefficient and normal load ($Q < \mu F_n$) the Archard and Energy approaches will not provide the same results (Zhang et al., 2011).

The Energy wear approach considers the interfacial shear work as the main parameter controlling the wear modelling. This approach uses a single Energy wear coefficient that unifies prediction of wear across a wider range of stroke (from $50\mu\text{m}$ to 1.3mm) than Archard (Magaziner et al., 2008). Therefore, this approach has a greater range of application than Archard's wear law (Fouvry et al., 2001, Fouvry et al., 2003, Liskiewicz and Fouvry, 2005).

2.8.2 Wear coefficient

For engineering application the quantity of dimensional wear coefficient ($K = k/H$) is often more useful quoted by units of Pa^{-1} or MPa^{-1} . Due to a lack of a standard test method, the value of wear coefficients obtained from different investigations available in the literature vary significantly by a deviation of 1000% or more (Yang, 2005). The wear coefficient encompasses a variety of parameters affecting wear and in addition it is known to change during the wearing process.

The values of “taper-trunnion” (fretting) wear coefficients can only be obtained accurately by controlled *in-vitro* studies using hip simulators or specially designed fretting rigs, as basic techniques such as pin on disk do not provide the necessary geometries, *in-vivo* loading conditions or environment to facilitate this.

The vast majority of research into wear modelling of hip prostheses has involved the analysis of wear occurring between the cup and head articulation of MoP types (Fialho et al., 2007, Maxian et al., 1996a, Maxian et al., 1996b, Maxian et al., 1997, Patil et al., 2003, Raimondi et al., 2001, Teoh et al., 2002, Wu et al., 2003). However, there has been a limited number of *in-vitro* studies considering metallic interactions for both cup and head wear (hip simulators/pin-on-disk) and to consider taper junction wear due to fretting (by means of fretting test rigs) (Chiba et al., 2007, Fridrici et al., 2001, Liu et al., 2008, Magaziner et al., 2008, Zhang et al., 2013).

Liu et al. (2008) determined wear coefficients from wear volumes obtained from the cup and head of cobalt chrome (CoCr) MoM hip resurfacing implants after simulator tests by Leslie et al. (2008). The wear coefficients were obtained by a trial and error method using a computational wear simulation of the experimental tests and comparing the computed volumetric wear with the hip simulator values. Archard wear coefficients of $1.13 \times 10^{-11} MPa^{-1}$ and $0.12 \times 10^{-11} MPa^{-1}$ were obtained for the bedding-in (0– 1 million cycles) and steady-state (1– 15 million cycles) wear phases respectively.

Uddin and Zhang (2013) used wear coefficients of similar value to Liu et al. (2008) in a study to predict wear in hard-on-hard hip prostheses. For wear between a Co-Cr-Mo alloy cup and head, Archard coefficients of $0.5 \times 10^{-11} MPa^{-1}$ and $0.15 \times 10^{-11} MPa^{-1}$ for bedding-in (0-1million cycles) and steady state (1-3 million cycles)

were used by Uddin and Zhang (2013) following hip simulator tests undertaken by Chan et al. (1999).

Chiba et al. (2007) used a traditional pin on disk unidirectional technique with Archards wear law to determine wear coefficients for cast CoCr/CoCr and forged CoCr/CoCr alloys. The volumetric wear was calculated from gravimetric measurement of mass loss producing overall values of $K = 3.8 \times 10^{-9} MPa^{-1}$ and $2.0 \times 10^{-9} MPa^{-1}$ respectively.

Fridrici et al. (2001) investigated the effects of shot peening on the fretting wear behaviour of Ti-6Al-4V using a fretting wear rig with a cylinder on plane geometry. A number of tests were undertaken with different normal loading resulting in contact pressures of $525 MPa$ and $830 MPa$ respectively, and displacement amplitudes ($\pm 5 \mu m$ to $\pm 50 \mu m$). The tests were carried out in dry conditions at a frequency of $5 Hz$ up to a maximum of 10^6 cycles. A coefficient of friction was determined as being around 0.8 to 1 after 10^6 cycles. Profilometry was used to determine the wear volume with similar wear occurring on both the cylinder and plane. Energy wear coefficients were calculated for the different experimental conditions showing differences dependant on changes in the contact pressure or relative displacement. For a contact pressure of $830 MPa$ and a displacement amplitude of $\pm 50 \mu m$ for a test of duration 250,000 cycles, the energy wear coefficient was determined as $2.9 \times 10^{-8} MPa^{-1}$.

Magaziner et al. (2008) used a modified servo-controlled MTS testing machine with two actuators and fretting fixture to study the fretting-reciprocating sliding of titanium alloy Ti-6Al-4V on itself as cylinder on flat contact. The relative displacement range was $872 - 1381 \mu m$ and the range of test cycles $1000 - 60000$.

Profilometry determined the wear volume which was found to be nearly linearly proportional to the cumulative product of contact load and relative slip ($\Sigma F_n s$) and total dissipated energy (ΣE) producing an Archard wear coefficient $K = 3.703 \times 10^{-7} MPa^{-1}$ and an energy wear coefficient $\alpha = 7.121 \times 10^{-7} MPa^{-1}$.

Zhang et al. (2013) used pin on disk with linear reciprocating motion ($\pm 2mm$) to determine the energy wear coefficients for two head-stem material combinations (Co-28Cr-6Mo / DMLS Ti-6Al-4V and Co-28Cr-6Mo / forged Ti-6Al-4V) with the dissipated energy wear law approach for application to fretting at THR taper junctions. The authors state that with this approach α is fairly insensitive to the magnitude of the relative displacement and is constant over a comparatively wide range of motion (Liskiewicz and Fouvry, 2005, Magaziner et al., 2008). Contact stresses were generated of similar magnitude to those at a THR taper junction and the volumetric wear was measured using SEM and profilometry. For Co-28Cr-6Mo / forged Ti-6Al-4V average energy wear coefficients of $\alpha = 9.9 \times 10^{-8} MPa^{-1}$ and $1.6 \times 10^{-8} MPa^{-1}$ were determined using SEM and profilometry respectively (a difference in magnitude of 6.2 due to the measurement techniques used). For Co-28Cr-6Mo / DMLS Ti-6Al-4V the values for α were $4.16 \times 10^{-8} MPa^{-1}$ and $3.34 \times 10^{-9} MPa^{-1}$ using SEM and profilometry respectively (a difference in magnitude of 12.46).

The wear coefficient is of the fundamental importance. This value provides a valuable means of wear modelling in different systems. The wear coefficients obtained from the studies explained in this section should be treated with caution as their values are dependent on the specific test machines used, component design, test configurations and test conditions (Cawley et al., 2003). Furthermore, a direct

comparison of the wear performance of a particular material is difficult due to the reasons stated. The wear coefficients obtained in literature are summarized in Table 2-1 and Table 2-2.

2.8.3 Wear fraction

In the process of wear, material can be removed from both components in contact by different amounts. This depends on their surface material properties such as hardness, wear resistance and surface roughness. The proportion of wear that is removed from each of the contacting components in this work is specified by a “wear fraction”. Simplistically, for example, a wear fraction of (1:0) would remove all of the wear volume from one component, whereas a wear fraction of (0.5:0.5) would remove the wear equally from both components.

Typically, in studies that attempt to predict wear or fretting wear between a pair of components one part is modelled as a rigid body and wear is only considered to occur on the other. For instance, Zhang et al. (2014) in a recent study assumed that fretting wear, between titanium stem and cobalt-chrome alloy head, only occurs on the titanium stem trunnion. They stated that the cobalt-chrome head was a harder material and as such can be assumed as a rigid body. In the light of their study three main issues need to be considered. First, they have neglected the effect of geometry change during the wearing process. Second, there is a large limitation of applying accurate loading and boundary condition on an axisymmetric model. Finally and more importantly, as discussed in Section 2.7.2, recent studies show the softer titanium alloy abrasively wears the harder cobalt-chrome due to oxidation of titanium (Bishop et al., 2013, Bone et al., 2015, Langton et al., 2012, Moharrami et al., 2013).

In a 3D FE analysis of a MoM THR (femoral head-acetabular cup), Uddin and Zhang (2013) only updated the geometry of the cup stating that the femoral head surface normally wears equally to the cup surface and as such the wear analysis of the head would be repetitive. However, the change of geometry on both parts during wear modelling has a significant effect on the wear rate and the prediction of the final surface damage.

To the author's knowledge, the wear fraction is one of the main parameters in wear modelling and cannot be neglected by simplification of the model. The wear method proposed in this study permits wear to occur on one component only, both components equally or by unequal amounts.

2.8.4 Effect of frequency on the wear rate

Regarding the experimental set-up for wear analysis, using a high frequency has an effect on assessment of wear rate. For instance, a high frequency of the pin-on-disk apparatus leads to vibrate the test samples. Chowdhury et al. (2010) indicate that increasing the frequency, vibrates the pin-on-disk experimental set-up that leads to increase the wear rate.

Furthermore, accelerating the fretting wear test by using a high frequency has an effect on fretting wear tests (Schaaff et al., 2006). Schaaff et al. (2006) used a piezo-electrically driven fretting test device and determined the volume loss using radiotracer technique to assess the effect of frequency on fretting wear rate of Co-28Cr-6Mo on Ti-6Al-4V. Their results for different frequencies (1 to 8Hz) show higher wear rate for lower frequencies.

Consequently, the examples above indicate that accelerating the fretting wear tests of materials must be considered extremely carefully.

2.9 Computational wear modelling

Experimental testing to determine the wear behaviour that occurs in mechanical devices is time consuming, expensive and complicated. Computational wear modelling is an alternative method which is faster and cheaper than real testing and can be used in addition to testing, to help improve the wear characteristics of mechanical designs (Elkins et al., 2014, Elkins et al., 2011, Liu et al., 2008, Uddin and Zhang, 2013, Zhang et al., 2013).

A computational approach to wear prediction is a useful tool for use in design or improving an existing design. When validated experimentally or *in-vivo*, it could be used to assess different gait cycles, functional performance of prosthetic devices and refine critical points of a design.

There is some evidence that work has been successful in the prediction of fretting wear experimentally and computationally to assess functional aspects of new and existing designs. All methods presented in the literature have been significantly simplified due to the complexity of the prediction. Some of these considerations are summarized in Table 2-3.

Zhang et al. (2011) investigated the fretting performance of two 2D contrasting contact geometries transmitting a normal load and tangential displacement. They tried to investigate the effect of three different contact geometries on fretting to understand which geometry performs better in terms of fretting wear and fatigue. McColl et al. (2004) developed a 2D FE model to simulate fretting wear, validated

experimentally based on Archard equation. They highlighted the effect of slip amplitude on evolution of multiaxial contact stress and fretting parameters. Their work was followed by Madge et al. (Madge et al., 2007b, Madge et al., 2008) who used an Archard based wear simulation with FE based method to predict multiaxial fretting wear on fretting wear life validated experimentally with a rounded punch-on-flat fretting test rig. The effect of incremental plasticity during fretting wear analysis has been investigated by Tobi et al. (2009). On the assessment of fretting wear fatigue, Ding et al. (2004) used a combined 2D numerical and experimental approach to predict fretting fatigue life using wear scars due to gross slip, partial slip and mixed slip.

There are also some studies on the development of adhesive wear modelling. For instance, Abdelgaied et al. (2011) proposed a new computational wear model to predict wear in knee implants using the Archard wear law based on a non-dimensional wear coefficient. They used a laboratory joint simulator to validate predicted wear volume. Fialho et al. (2007) developed a computational framework to simulate the wear and heat generation between the head and acetabular cup of THRs.

Liu et al. (2008) presented a computational wear model based on the Archard wear equation and FE analysis to predict wear on MoM hip resurfacing prostheses. They performed short and long term tests using a hip simulator to investigate the wear coefficient up to 50 million load cycles. They obtained 6 to 8 μ m wear depth with no edge contact at the cup and head. This result was obtained using average linear triangular interpolation of contact stresses rather than actual incremental contact stresses.

Different theories on wear modelling have also been presented to simplify the wear prediction. For instance, Elkins et al. (2014) tried to develop an investigation on the fretting wear behaviour using a “potential wear rate”. However, in their study the effect of changing geometry due to wear evolution was ignored. They used only two parameters of the Archard based wear law, contact pressure and slip to assess potential wear rate. The study tried to parametrically compare different head diameters on potential fretting wear rate.

Donaldson et al. (2014) considered varying parameters (four hundred) to investigate a “fretting work done” on the head neck taper and trunnion junction. They defined fretting work done as $(\mu \times P \times s)$, where μ is the friction coefficient, P is contact pressure and s is micromotion. Their investigation showed that fretting work was correlated with only three parameters, which are angular mismatch, centre offset and body weight. The “fretting work done” may be considered as a “potential wear rate” using the dissipated energy wear law and assuming an energy wear coefficient as unity.

Table 2-1: Values of wear coefficient for the same material combination of reviewed wear models

Same material combination	Wear law	Wear model	Experiment	Wear measurement	Wear coefficient (MPa^{-1})	Reference
Cobalt-chrome on itself	Archard	Adhesive	Hip simulator	Computational wear simulation (trial and error)	Bedding: 1.13×10^{-11} Steady-state: 0.12×10^{-11}	(Liu et al., 2008) and (Leslie et al., 2008)
Co-Cr-Mo alloy on itself	Archard	Adhesive	Pin-on-disk	Computational wear simulation (trial and error)	Bedding: 0.5×10^{-11} Steady-state: 0.15×10^{-11}	(Chan et al., 1999) (Uddin and Zhang, 2013)
Co-Cr-Mo alloy on itself	Archard	Abrasive	Hip simulator	SEM	Varying from 0.95×10^{-6} to 1.24×10^{-6}	(Cawley et al., 2003)
Cast Cobalt-chrome on itself	Archard	Adhesive	Pin-on-disk	Gravimetric measurement of mass loss	3.8×10^{-9}	(Chiba et al., 2007)
Forged CoCr on itself	Archard	Adhesive	Pin-on-disk	Gravimetric measurement of mass loss	2.0×10^{-9}	
Ti-6Al-4V on itself	Archard	Fretting	Servo-controlled MTS testing	Profilometry	3.703×10^{-7}	(Magaziner et al., 2008)
Ti-6Al-4V on itself	Archard	Fretting	Cylinder-on-flat fretting test rig	Profilometry / SEM	Gross sliding: 8.5×10^{-9} Partial slip: 4.5×10^{-9}	(Tobi et al., 2009)

Same material combination	Wear law	Wear model	Experiment	Wear measurement	Wear coefficient (MPa^{-1})	Reference
Ti-6Al-4V on itself	Energy	Fretting	Fretting wear rig	Profilometry	2.9×10^{-8}	(Fridrici et al., 2001)
Ti-6Al-4V on itself	Energy	Fretting	Electrodynamic fretting rig	SEM	1.12×10^{-8}	(Fouvry et al., 2003)
Ti-6Al-4V on itself	Energy	Fretting	Servo-controlled MTS testing	Profilometry	7.121×10^{-7}	(Magaziner et al., 2008)
High strength steel on itself	Archard	Fretting	None	FEA	1.0×10^{-7}	(Ding et al., 2004)
High strength steel on itself	Archard	Fretting	Cylinder-on-flat fretting test rig	SURFCOM 200 scanning stylus Profilometry	185N: 2.8×10^{-8} 500N: 5.1×10^{-8} 1670N: 2.8×10^{-8}	(McColl et al., 2004)
Aluminium alloy on itself	Archard	Adhesive	Pin-on-disk	Weight loss	Varying from 0.2×10^{-5} to 25×10^{-5}	(Yang, 2003)
Metal-matric composite on itself	Archard	Adhesive	Pin-on-disk	Weight loss	Varying from 2.7×10^{-5} to 24.6×10^{-5}	(Yang, 2005)

Table 2-2: Values of wear coefficient for the different material combination of reviewed wear models

Different material combination	Wear law	Wear model	Experiment	Wear measurement	Wear coefficient (MPa^{-1})	Reference
Co-28Cr-6Mo / DMLS Ti-6Al-4V	Energy	Fretting		SEM	5.35×10^{-8} and 2.97×10^{-8}	
Co-28Cr-6Mo / forged Ti-6Al-4V	Energy	Fretting	Pin-on-disk with linear	SEM	10.6×10^{-8} and 9.18×10^{-8}	(Zhang et al., 2013)
Co-28Cr-6Mo / DMLS Ti-6Al-4V	Energy	Fretting	reciprocating motion	Profilometry	3.91×10^{-9} and 2.76×10^{-9}	
Co-28Cr-6Mo / forged Ti-6Al-4V	Energy	Fretting		Profilometry	1.31×10^{-8} and 1.88×10^{-8}	
Ti-6Al-4V on High strength steel	Archard	Fretting	From (McColl et al., 2004)	Fretting fatigue test	2.75×10^{-8}	(Madge et al., 2007a) (Madge et al., 2008) (Madge et al., 2007b)
Polyethylene / CoCr	Archard	Adhesive	Hip simulator	FEA	10.6×10^{-7}	(Fialho et al., 2007)

Table 2-3: Different approach to wear prediction of reviewed wear modelling

Auteurs	Method	Application	Loading	Consideration
Uddin and Zhang (2013)	FEA(ANSYS) / WM*: Manually Archard Adhesive	THR taper junction	LC**: 2million SF***: 200,000 WF****:1:0	Nodal position updates in constant radial direction for all updates Manually updated the geometry Wear damage pattern presented in 2D Wear coefficient from Pin-on-disk
Zhang et al. (2013) and Zhang et al. (2014)	FEA (ABAQUS) WM: Adaptive meshing Eergy Fretting	THR taper junction	LC: 1million SF: 50,000 WF: 1:0	Not applicable for 3D models with realistic loading condition Sinusoidal load rather than hip loading Press fit rather than impaction Assumption of Titanium wears only, however as discussed softer Titanium wears Cobalt-Chrome
Elkins et al. (2014)	FEA (ABAQUS) WM: Mathcad Archard Fretting	THR taper junction	LC: 1 SF: None WF:1:0	No geometry update, Wear potential Non-converged FE analysis found in their work
Fialho et al. (2007)	FEA (ANSYS) WM: None Archard Adhesive	THR head and cup	LC: 1million SF: 1million WF: 1:0	Wear damage pattern obtained based on one analysis Not applicable for MoM
(Liu et al., 2008)	FEA (ABAQUS) WM: Manually Archard Adhesive	Hip resurfacing	LC: 50million SF: 50million WF: 0.5/0.5	Just superior-inferior hip loading applied on the model Average linear triangular interpolation to obtain contact stress Updated on radial direction and not normal direction
*WM: wear modelling			***SF: Scaling Factor,	
*LC: Number of Load Cycles,			****WF, wear fraction ABAQUS	

Auteurs	Method	Application		Limitation
Abdelgaied et al. (2011)	FEA (ABAQUS) WM*: MATLAB Modified Archard Adhesive	Artificial knee joint	LC** : 5million SF*** : 500,000 WF**** : 1:0	The method allow to obtain volumetric wear only No presentation of wear damage pattern
Tobi et al. (2009)	FEA WM: Adaptive meshing Archard Fretting	Fretting test	LC: 300,000 SF: 3,000 WF:0.5:0.5	Not applicable for 3D models with realistic loading condition Need of highly refined mesh: 10 μ m element size Nodal adjustment assigned: 0.001 μ m Wear depth accuracy: 1 μ m High frequency, 20Hz Considered the last time increment only
Madge et al. (2007a) Madge et al. (2008) Madge et al. (2007b)	FEA / WM: MATLAB Adaptive meshing Archard fretting	Fretting test	LC and SF from (Ding et al., 2004)	Not applicable for 3D models with realistic loading condition Need of highly refined mesh: 16 μ m element size Missing of nodal coordinate, due to adaptive meshing procedure
McColl et al. (2004) (Ding et al., 2004)	ABAQUS/ WM: Fortran Adaptive meshing Archard Fretting	Fretting test	FWC: 18000 SF: 30 WF:0.5:0.5	Not applicable for 3D models with realistic loading condition Need of highly refined mesh: 10 μ m element size High frequency, 20Hz Assumption of displacement as a total local slip Assumption of constant nodal contact pressure and slip during the wear analysis Manually run the Fortran program after each analysis Wear depth accuracy: 5 μ m
(Zhang et al., 2011)	FEA / WM: Fortran Adaptive meshing Energy Fretting	Pressure armour layer of a marine riser	FWC: 100,000 SF: 2,000 WF:0.5:0.5	Not applicable for 3D models with realistic loading condition Wear depth accuracy: 1 μ m Need of highly refined mesh
*WM: wear programing			***SF: Scaling Factor,	
LC: Number of Load Cycles,			**WF, wear fraction ABAQUS	

2.10 Discussion and rationale

Fretting is known as one of the most significant and complicated mechanical failures that occur (see Figure 1-1). There is evidence the wear that could occur in total hip implant is still an issue in orthopaedics. The wear debris produced from these devices occurs mainly from the acetabular cup and head articulating surface and the head-stem taper connection. In the past, fretting wear occurring between the fixed parts of the modular prosthesis (head-stem) had been neglected in investigations claiming that debris released is mostly from the bearing surfaces; However, fretting wear can remove the effect of initial impaction assembly, which is used to fix these parts together and lead to aseptic loosening of the implant. Further, the fine wear debris released due to the fretting can lead to adverse side effects such as ASTR or metallosis. As demonstrated in this chapter there is evidence that more investigation is needed to determine why artificial joints are failing prematurely. Currently, fretting wear is known as one of the main reasons of failure in modular THRs.

The review presented in this Chapter reveals possible gaps in research for prediction of fretting wear in THRs and wear modelling. These gaps are:

- Long term effects of current and new design of THRs remain unknown. There is no specific statistics on the failure rate in THRs for the more recent designs as their long term behaviour *in-vivo* needs time in service before this can be established. Although experimental simulation (such as hip simulators) could provide insight into long term behaviour in service, these tests have many limitations such as applying accurate loading conditions, providing accurate corrosive environment and timing and costly procedure. Furthermore, a limited number of tests can be carried out using the

experimental simulations for a specific design and therefore it cannot be used for all the parameters that may affect the wear phenomenon.

- Success of the prosthetic devices in service depends on variable factors, such as design, initial fixation, material combination, method of manufacture, surface roughness and manufacture tolerances. All of these parameters highlight the possible differences on their long term behaviour in service. Currently there is no accurate, standard and straightforward experimental and computational approach to incorporate all these aspects together to predict the exact behaviour of the prosthetic devices.
- There is a lack of understanding and guidelines to provide adequate assembly of the prosthetic devices. For instance the effect of variability of impaction forces on fretting wear at the taper junction is still unclear (Wassef and Schmalzried, 2013). Manufacturing guidelines are vague and the THR procedure is very dependent on the surgeons' experience.
- There are a number of experimental research investigations to determine the extent of fretting wear in these devices; however, there is a lack of a fast, user-friendly and accurate computational approach reported in the literature (referenced in Table 2-3). Further, most studies that have tried to predict fretting wear computationally, in general, include many simplifications. For instance, the effect of changing the geometry due to material removal during the wear process has been commonly neglected.
- Wear coefficients are known to change during the wearing process based on the change in material surface properties and surface geometry. Accurate wear coefficients occurring at prosthesis taper junctions during the wear analysis have yet to be determined.

The overall aim of the research in this field is to develop the prosthetic devices which will last the life of the patients. Further, patients with implanted total hip or knee replacement are mostly advised to minimise any activity outside walking which is not satisfying for young active patients who wish to pursue an active life. This aim is achievable by further research and investigation to develop the design of the prosthetic devices to increase the longevity of them up to the natural end of a patient's life with better performance in service in terms of providing higher functionality.

Increasing the longevity of joint implants is also an economic benefit as the revision surgery is more costly than the primary one, less successful and not in the comfort zone of the patients. Reducing the number of revisions also helps to minimise the input of resources from the health authorities in terms of equipment and finance.

To increase the prosthetic devices life, being able to predict the extent of wear that could occur in the device over several years in service in the body is vital. This is the main aim of this study to introduce a new methodology to predict fretting wear between the head-stem of a modular hip prosthesis using FE analysis. In order to fulfil the requirements of minimal invasive surgery and for an attempt to bridge the above gaps, a comprehensive wear model is proposed in Chapter 3. This method is used in different studies in Chapter 4, 5 and 6 to investigate the long term performance of hip prosthetic implants in service considering different parameters affecting fretting wear. The following objectives are met in order to achieve this goal:

- The method proposed in Chapter 3 could consider the initial locking effect of impaction at assembly for modelling fretting wear.

- The method is user-friendly in order to be used in different parametric studies. Automation of the method has been performed with a graphical user interface (Python scripting) that allows using the method for different studies.
- The wear model is applicable to both axisymmetric and 3D FEA models. The FE analysis of axisymmetric models is much faster than 3D models with of course their limitations. This type of analysis would be useful for parametric studies such as the effect of mismatch angle.
- The wear algorithm is capable of considering different wear fractions for each material.
- The method is capable of considering varying wear coefficients during wear analysis, if this data is available from actual testing.

2.11 Conclusion

Firstly, this Chapter presented a comprehensive review of wear and its characteristics. Different wear mechanisms and theoretical approaches to calculate them were explained followed with an explanation on fretting wear which is the main focus of this study. Then the wear laws and their assessment using theoretical approaches were discussed. Secondly, the human hip joint and its possible disorders have been demonstrated followed by a detailed explanation on hip arthroplasty, the procedure of THRs, different designs and material combination of modular hip implants and reasons of failures in THRs. Thirdly, the fretting wear that could occur in THRs over time was discussed in detail. Fourthly, a review on the current experimental and computational methods to predict and investigate fretting wear proposed in literature was presented.

Finally, a discussion on the gaps in current research, overall aim of the present study and the considerations of the proposed methodology were presented. This study attempts to close these gaps by developing a wear model that is explained in Chapter 3 with illustration of three different studies following in Chapter 4, 5 and 6.

Chapter 3

Computational method of fretting wear prediction

3.1 Introduction

In this Chapter both Axisymmetric and 3D models of a commercial total hip prosthesis are used to demonstrate the method and to highlight key features of a bespoke wear algorithm. The models together with the wear algorithm can be used effectively to study certain aspects of taper junction design. The method presented in this chapter can subsequently be used to identify key factors leading to debris release at the taper junction so that appropriate prosthesis design and surgical procedural modifications can be made to mitigate against this damaging problem. The method proposed is also independent of model geometry and can be used for any FE models (not only prosthetic devices) to predict fretting wear. The method and the FE models that are to be explained in this Chapter will be, unless stated otherwise, the main analysis implementations for chapters that follow (4, 5 and 6).

3.2 Theoretical wear calculation

In what follows, the general wear equations to calculate volumetric and linear wear will be explained. The methodology described in this study allows for the implementation of either the ‘Archard’ or the ‘Dissipated Energy’ wear law for the prediction of fretting wear.

As discussed in section 2.8.1, the energy wear approach considers the interfacial shear work as the main parameter controlling wear modelling. There is evidence in literature that this approach is superior to the Archard’s wear law (Fouvry et al., 2001, Fouvry et al., 2003, Liskiewicz and Fouvry, 2005). However, it is not necessary to use the energy wear law over Archard (both can be used in the methodology presented here), mainly the energy wear approach is used in this study to present all the results. The main reason for using the Energy wear law in this study is that the fretting wear coefficients are better defined in the literature for this approach. In this section, the theoretical approach and the implementation of both laws to the FE analysis are described.

3.2.1 Dissipated Energy wear law

The energy wear law, Equation (3-1), bases the calculation of volumetric wear on the interfacial shear work being the predominant parameter determining wear. It shows that the total volumetric wear (W_v) is obtained from the product of the total local accumulated dissipated energy (E) and an energy wear coefficient α :

$$W_v = \alpha E \tag{3-1}$$

where

$$E = Qs \quad (3-2)$$

and Q is the shear traction and s the relative displacement between the contacting surfaces, giving:

$$W_v = \alpha Qs \quad (3-3)$$

By dividing both sides of Equation (3-3) by a contact area, the linear wear depth W_d can be calculated using Equation (3-4), where τ is the contact surface shear stress:

$$W_d = \alpha \tau s \quad (3-4)$$

For the numerical implementation of this wear law, the process used here is to first determine the wear depth at contacting surfaces generated by a single loading cycle on the components (such as the *in-vivo* loading applied on a hip for a single walking step); subsequently, as the components will typically be subject to millions of loading cycles during their lifetime, this single cycle wear depth is multiplied by a ‘wear scaling factor β ’ so as to make the execution of an analysis achievable in an acceptable period of time. The ‘wear scaling factor’ represents a specific number of loading cycles (e.g. 10^5) and its value depends on how accurately the evolution of wear is to be calculated, with a trade off against computer run time. After scaling the wear depth, the geometry of the contacting surfaces of the components is then modified to reflect the wear that would have occurred over the period of β cycles. The calculated wear can be applied to one component only, or to both in either equal or unequal amounts. The process is then repeated using the updated geometry until a specified number of cycles of loading have been applied or a pre-specified wear depth has been reached.

In order to model accurately the effect on wear of a time-variant load distribution during a loading cycle (such as occurs during walking) it is necessary to discretise the loading cycle into a number of time intervals n . As such, the wear depth for a single cycle of loading (the cyclic wear depth W_c) can be calculated using Equation (3-5), where τ_i and s_i are respectively the surface shear stress and relative displacement calculated at the end of a specific time interval i .

$$W_c = \sum_{i=1}^n \alpha \tau_i s_i \quad (3-5)$$

The cyclic wear depth W_c will be very small and if unmodified will have negligible influence on the evolving taper junction surface geometry due to wear. As such, ‘wear scaling factors β ’ are employed to increase W_c to a value which would have occurred over a much larger number of loading cycles. The total wear depth W_d that is generated over a specified total number of loading cycles N can be determined from Equation (3-6), where j represents a specific ‘analysis stage’ reflecting the evolution of wear:

$$W_d = \sum_{j=1}^{(N/\beta)} \beta \sum_{i=1}^n \alpha \tau_{i,j} s_{i,j} \quad (3-6)$$

The accuracy and efficiency of this approach is dependent on numerous factors, not least of which is the magnitude of the energy wear coefficient α used. In addition, the number of intervals i used to discretise the loading cycle, and the magnitude of the ‘wear scaling factor β ’ need careful consideration in terms of their influence on accuracy and analysis run times.

3.2.2 Archard's wear law

As discussed in section 2.4.1, according to Archard's wear model, volumetric wear W_v on the articulating surfaces can be described by,

$$W_v = KFs \quad (3-7)$$

where K is a dimensional Archard wear coefficient MPa^{-1} , F is the contact force and s is the relative slip. Linear wear depth can be calculated by dividing both sides of Equation (3-7) by an area,

$$W_d = KPs \quad (3-8)$$

where P represents the normal contact stress. Again similar to energy wear law, the cyclic wear depth W_d at any point of the surfaces in contact can be derived by discretising the whole load cycle for the load gait, given by,

$$W_c = \sum_{i=1}^n KP_i s_i \quad (3-9)$$

where P_i and s_i are respectively the surface contact pressure and relative displacement calculated at the end of a specific time interval i for the number of time intervals n .

Then, the total wear depth W_d that is generated over a specified total number of loading cycles N can be determined (as described in section 3.2.1) by Equation (3-10) to calculate the evolution of wear.

$$W_d = \sum_{j=1}^{(N/\beta)} \beta \sum_{i=1}^n KP_{i,j} s_{i,j} \quad (3-10)$$

The Archard's wear method is an option in the algorithm to be considered for the wear analysis by a graphical user interface (GUI) in ABAQUS which will be explained later in section 3.9.

3.3 Wear implementation

The energy or Archard wear law in the form of Equation (3-6) and (3-10) respectively can be used in conjunction with the FE analysis to calculate wear depth at the contacting surfaces of an FE model. The FE analysis can produce the nodal relative displacement and required nodal contact stresses to be used with an appropriate wear coefficient (Energy or Archard) to calculate wear depth.

The calculation of relative displacement at the contact interface is facilitated by creating sets of 'paired nodes' at the contacting surfaces (Figure 3-1 for axisymmetric model and Figure 3-2 for 3D models). This 'pairing' is achieved by determining which nodes on opposite mating surfaces are closest to each other geometrically prior to loading (at the start of the analysis and following a geometry update).

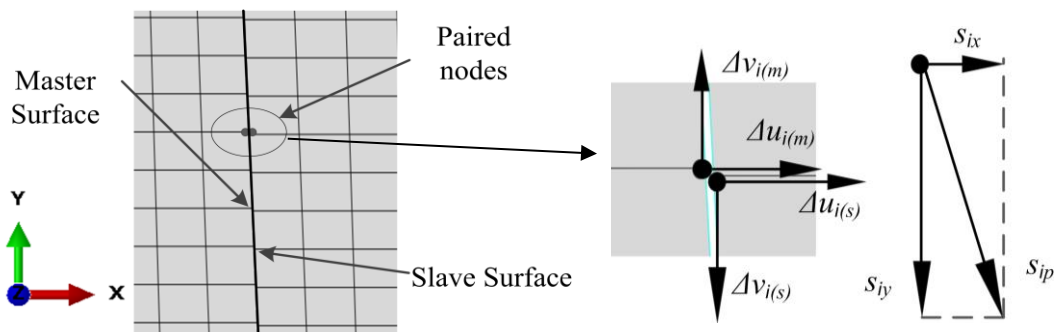


Figure 3-1: Nodal pairing and relative displacement of the paired node on axisymmetric models

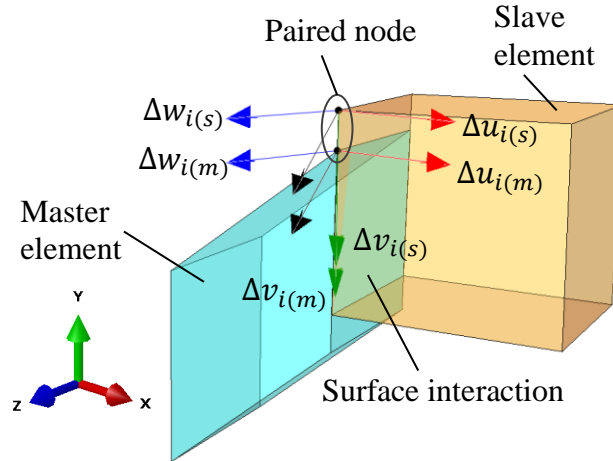


Figure 3-2 Nodal pairing and calculation of relative displacement on 3D models

The surface shear stress (or contact pressure) and displacements of all nodes which have been paired are extracted from the FE analysis at the end of each loading time interval i . These extracted values are then processed to provide values for use in the calculation of the wear depth.

As the paired nodes may not be exactly coincident (before and after loading) an average value of shear stress τ_{ip} or contact pressure is calculated for each nodal pairing as defined by Equation (3-11) and (3-12), where τ_{master} , τ_{slave} , P_{master} and P_{slave} are the surface shear stresses and contact pressures on the master and slave surface respectively for each set of paired nodes.

$$\tau_{ip} = \frac{|\tau_{master}| + |\tau_{slave}|}{2} \quad (3-11)$$

$$P_{ip} = \frac{P_{master} + P_{slave}}{2} \quad (3-12)$$

For the FE models, the relative displacement between paired nodes which has occurred during a time interval s_{ip} is calculated from the displacements of both the master and slave nodes in a pair at the end of the time interval i (see Figure 3-1 and

Figure 3-2). Specifically, for each set of paired nodes, s_{ip} is calculated from Equation (3-13),

$$s_{ip} = \sqrt{s_{ix}^2 + s_{iy}^2 + s_{iz}^2} \quad (3-13)$$

where s_{ix} , s_{iy} and s_{iz} are the Cartesian component relative displacements of the paired nodes in the x , y and z directions respectively (s_{iz} is zero for axisymmetric models) and can be determined from Equation (3-14),

$$\begin{aligned} s_{ix} &= \Delta u_{i(m)} - \Delta u_{i(s)} \\ s_{iy} &= \Delta v_{i(m)} - \Delta v_{i(s)} \\ s_{iz} &= \Delta w_{i(m)} - \Delta w_{i(s)} \end{aligned} \quad (3-14)$$

where $\Delta u_{i(m)}$, $\Delta u_{i(s)}$ are the nodal displacements that have occurred during time interval i in the x -direction for the paired master and slave nodes respectively, with $(\Delta v_{i(m)}, \Delta v_{i(s)})$ and $(\Delta w_{i(m)}, \Delta w_{i(s)})$ being the corresponding displacements in the y and z -direction (see Figure 3-1 and Figure 3-2). The nodal displacements in an interval are calculated using Equation (3-15) and are the difference in the total nodal displacement values u , v and w at the end of a time interval $i + 1$ and the start i (w is zero for axisymmetric models).

$$\begin{aligned} \Delta u_{i(m)} &= u_{i+1(m)} - u_{i(m)} \\ \Delta u_{i(s)} &= u_{i+1(s)} - u_{i(s)} \\ \Delta v_{i(m)} &= v_{i+1(m)} - v_{i(m)} \\ \Delta v_{i(s)} &= v_{i+1(s)} - v_{i(s)} \\ \Delta w_{i(m)} &= w_{i+1(m)} - w_{i(m)} \\ \Delta w_{i(s)} &= w_{i+1(s)} - w_{i(s)} \end{aligned} \quad (3-15)$$

Then, the total wear depth at the point locations of the paired nodes W_{dp} is found from Equation (3-16) and (3-17) respectively for Energy and Archard wear laws,

$$W_{dp} = \sum_{j=1}^{(N/\beta)} \beta \sum_{i=1}^n \alpha \tau_{ip,j} S_{ip,j} \quad (3-16)$$

$$W_{dp} = \sum_{j=1}^{(N/\beta)} \beta \sum_{i=1}^n K P_{ip,j} S_{ip,j} \quad (3-17)$$

3.4 Finite Element implementation

The geometry of a commercial THR (taper junction) was used in all studies illustrated in the chapters which follow to assess the algorithm's ability to predict the extent of fretting wear that could occur at the head-stem interface over a period of time *in-vivo* and to apply this wear to one component only or to both in either equal or unequal amounts. This section describes and highlights key aspects and considerations regarding the FE models and analysis used in the simulations.

3.4.1 Material properties and interaction behaviour

In this study fretting wear is modelled in a commercial THR consisting of a cobalt-chromium alloy femoral head and a titanium alloy stem. As discussed in section 2.6 the most common and widely used material for the stem of THRs is titanium. The advantage of the material properties of cobalt-chrome used in the femoral head have brought this combination together and it is widely used in most of the hip prosthetic devices. Therefore, in this study the material properties of cobalt-chrome and titanium as shown in Table 3-1 were assigned on the FE models of head and stem respectively and used in all analysis in chapters following. Both components were modelled as deformable and linearly elastic in ABAQUS.

Table 3-1: Material properties

Material	Young's Modulus (GPa)	Poisson's ratio	Density (kg/m ³)	Wear fraction
Co-28Cr-6Mo	210	0.3	7800	0.9
Ti-6Al-4V	119	0.29	4400	0.1

The contact interaction between the head and stem trunnion was modelled as ‘finite sliding’ using the ‘penalty’ contact formulation in ABAQUS. The friction force generated at the contact interface fixes the femoral head onto the trunnion at assembly. The associated friction coefficient is dependent on several factors such as material combination, surface finish and surface cleanliness. Values for the coefficient of friction μ at different total hip prosthesis modular taper junctions have been documented by Fessler and Fricker (1989). For the purposes of this study a constant isotropic coefficient of friction is defined on the FE models as shown in Table 3-2.

Table 3-2: Tribological material combination

Material Combination	Friction coefficient
Co-28Cr-6Mo / Ti-6Al-4V	0.21

The wear coefficient as discussed in detail in section 2.8.2 is experimentally determined and encompasses a variety of parameters affecting wear. The fretting wear coefficient used was taken from Zhang et al. (2013) (see Table 2-2) who used a pin on disk reciprocating sliding test for Co-28Cr-6Mo fretting on forged Ti-6Al-4V.

3.4.2 Wear fraction

The wear methodology can facilitate wearing of different trunnion-taper material combinations whereby the proportion of wear that is removed from each of the

contacting parts is specified by a ‘wear fraction’ (explained in section 2.8.3). As such, the wear depth removed from each part at the end of each analysis “stage” is calculated as the product of the parts’ “wear fraction” and the total wear depth determined for that particular “stage”.

The wear fractions associated with the cobalt chrome ‘head’ and titanium ‘stem’ in this work and the chapters that follow have been specified as 0.9 for the Co-28Cr-6Mo and 0.1 for the Ti-6Al-4V following work by Bone et al. (2015), Bishop et al. (2013), Moharrami et al. (2013) and Langton et al. (2012).

Bone et al. (2015) found a median wear volume of 0.14mm^3 from a retrieval study of 28 DePuy Corail titanium stem trunnions (23 of which were paired with metal femoral heads). Langton measured median wear volumes in excess of 2mm^3 (from a sample of 111 retrieved cobalt-chrome MoM femoral heads (all mated with either DePuy Corail or Summit titanium stems). The findings from their work indicate that the cobalt chrome head taper wears by around a factor of 10 more than the titanium alloy stem trunnion surface. This significant finding is supported further by work by Bishop et al. (2013) and has been explained by Moharrami et al. (2013) as occurring due to the preferential oxidation of titanium alloy over cobalt chrome thus increasing the hardness of the titanium trunnion which subsequently wears the un-oxidised CoCr head taper surface.

3.4.3 Finite element models

Axisymmetric and 3D FE models of the commercial THRs were modelled with the head taper and trunnion stem assembled as a perfect fit with a zero taper mismatch angle (see Figure 3-3).

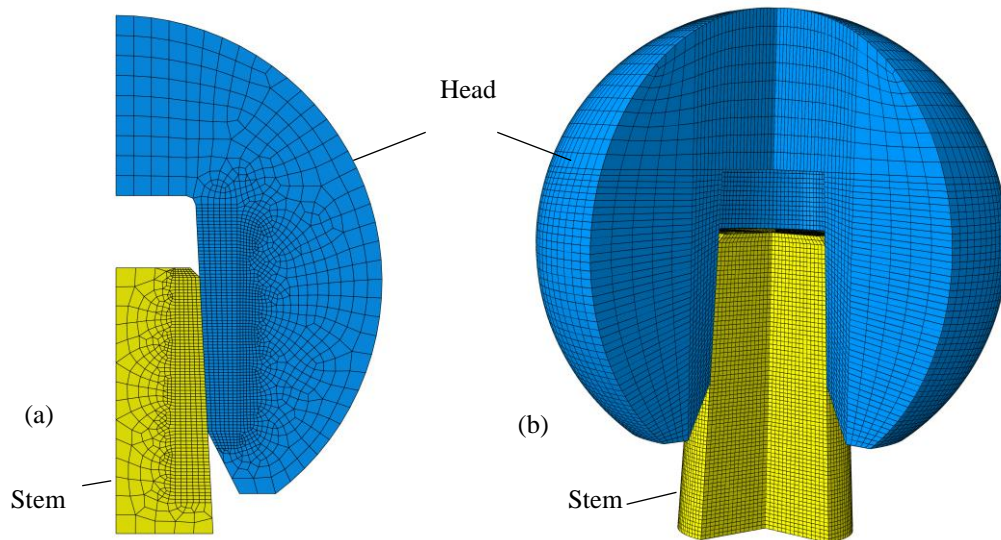


Figure 3-3: Mesh assigned on (a) axisymmetric model and (b) 3D model

The head and stem were assembled independently and then meshed in preparation for dynamic analysis in ABAQUS (version 6.13-1 ABAQUS Inc, Providence, Rhode Island) using eight-node linear brick, reduced integration hourglass controlled elements (C3D8R) for 3D models and four-node bilinear axisymmetric quadrilateral reduced integration elements (CAX4R) for axisymmetric models.

3.4.4 Impaction Load

As discussed in section 2.6.2 the head and stem of the THRs are assembled during surgery using impaction. The loading applied on the model included an initial impact to simulate the assembly of the head onto the stem and then time variant loading cycles to approximate hip loading during walking. The magnitude of the initial impaction force applied intra-operatively affects both the contact pressure and micromotion at the taper junction and ultimately the extent of any subsequent fretting wear.

In an attempt to simulate the impact event accurately a drop tower was used in this study to determine the impulse time associated with a particular impact (Figure 3-4).

Test samples were manufactured based on the dimensions of the commercial THR and a peak impact force from 2 to 6kN was applied by the drop mass to the test assembly (Heiney et al., 2009, Pennock et al., 2002, Rehmer et al., 2012, Lavernia et al., 2009).

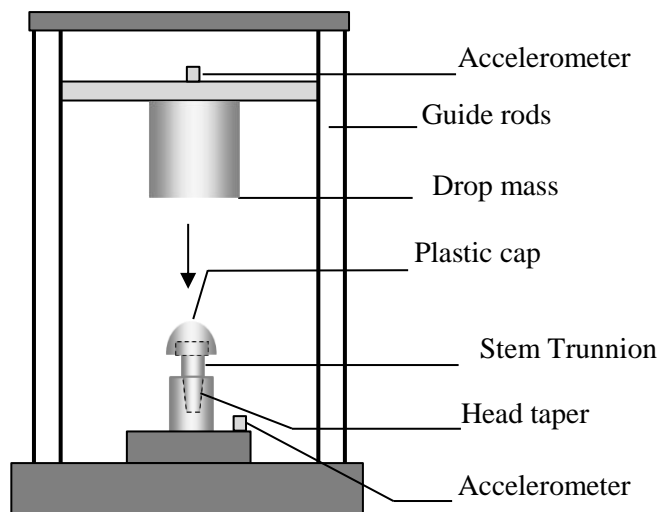


Figure 3-4: Drop rig to investigate impulse time and impact magnitude

The measured impact duration for a polymer tipped impactor with a metal “test” head was measured as 0.7ms. The load amplitude-time history obtained from the tests and the modified history used for the head-stem assembly event are shown in Figure 3-5. During this impactation the base of the stem trunnion is fixed in all degrees-of-freedom for both 3D and axisymmetric model.

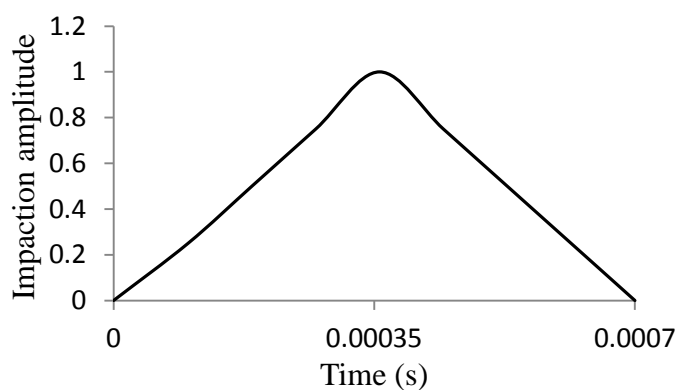


Figure 3-5: Impactation assembly load amplitude

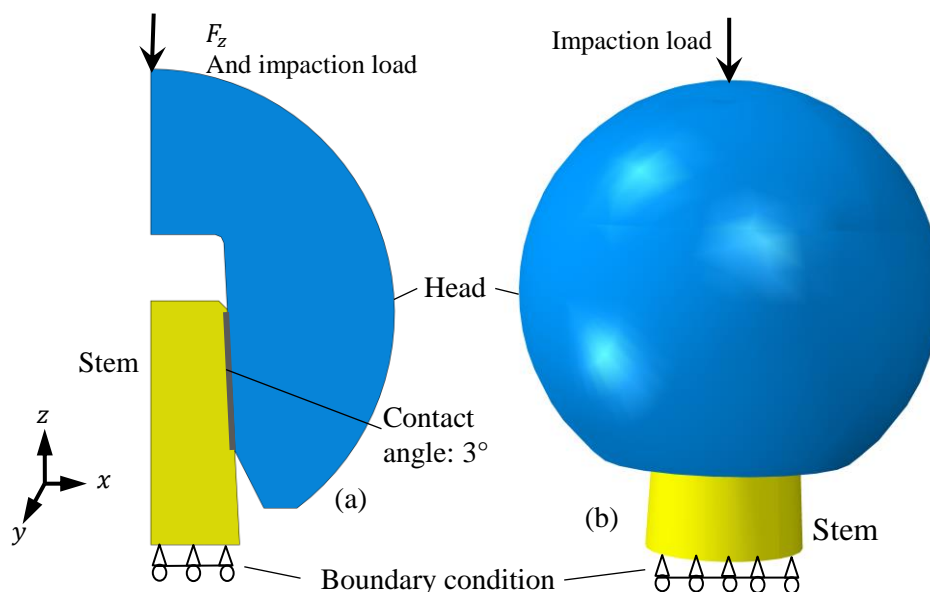


Figure 3-6: Boundary conditions and impaction loading assigned on (a) axisymmetric and (b) 3D model

3.4.5 Walking load and boundary conditions

For the most common activity of a human body, a physiological walking cycle, the *in-vivo* Superior-Inferior, Medial-Lateral and Anterior-Posterior hip loading (see Figure 3-7) with their respective Internal-External, Flexion-Extension and Adduction-Abduction rotations (see Figure 3-8) have been documented in literature (Bergmann et al., 2001, Bergmann et al., 1993, Elkins et al., 2014, Fialho et al., 2007, Liu et al., 2008, Mattei et al., 2011, Maxian et al., 1997, Zhang et al., 2013).

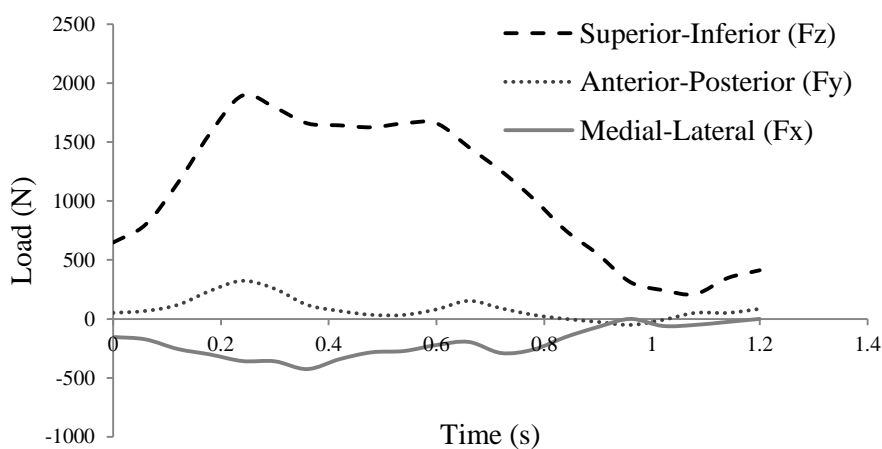


Figure 3-7: Hip loadings during a single walking cycle

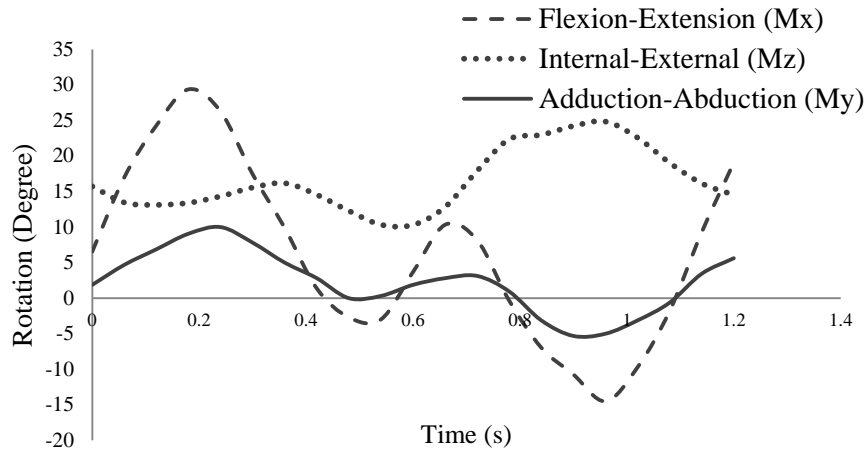


Figure 3-8: Hip rotations during a single walking cycle

The loading and boundary conditions prescribed to the 3D model during the walking cycle are shown in Figure 3-9. This includes both time variant rotations and loadings about the three global coordinate directions. The rotations are applied to a point located at the centre of the head, this point being coupled to the proximal end of the stem trunnion. In addition, the outer head surface is coupled with a second point located at the centre of the head which has all of its translational degrees of freedom restrained but is allowed to rotate. This constrains the outer head surface so that it can only rotate about this centre point and therefore locates the head virtually in the acetabular cup. The hip forces were applied to the model via a third remote point (located virtually in the femur) coupled to the distal end of the truncated stem component providing realistic load transfer to the prosthetic components. These loads and boundary conditions provide a realistic and efficient model with no requirement to model acetabular cup and femoral bone. The hip load history was applied to the model with a peak force of $2000N$ which is 2.5 times higher than body weight (assuming a patient has a weight of $800N$).

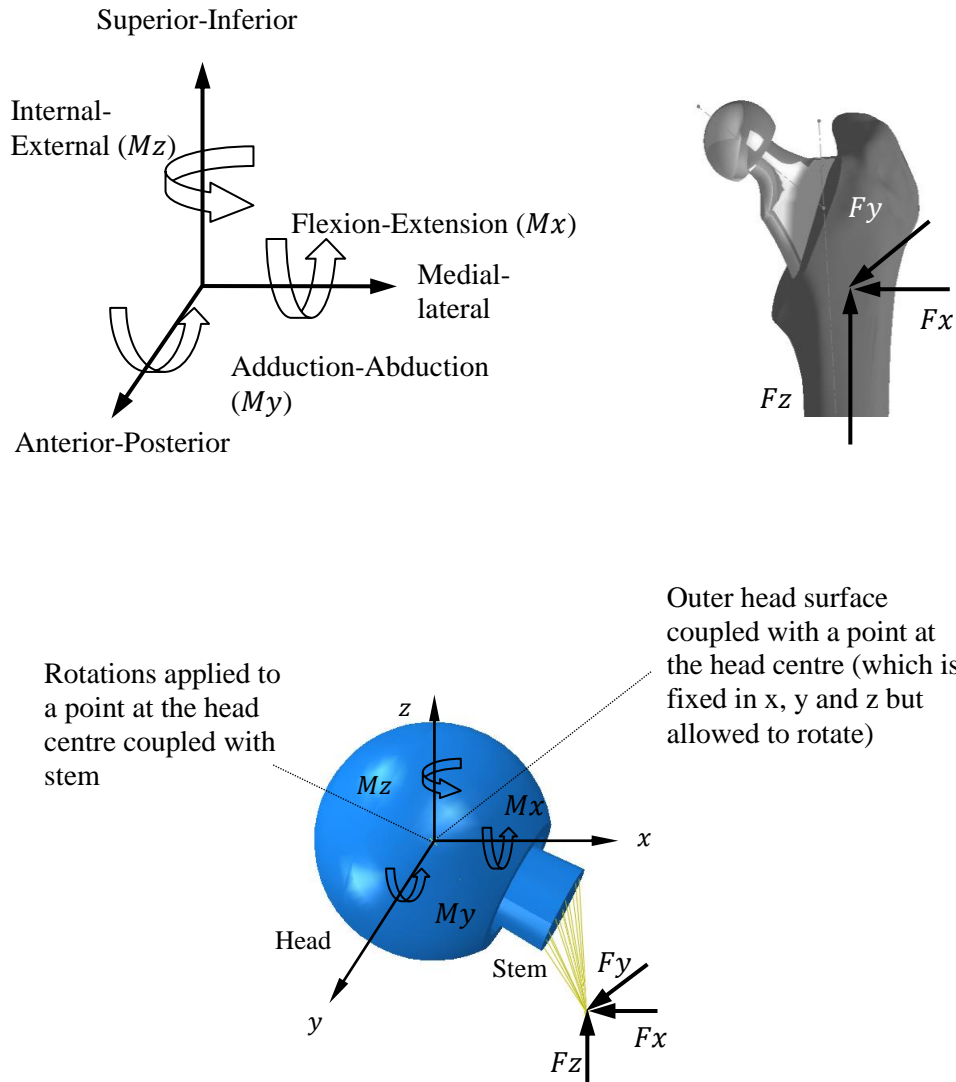


Figure 3-9: loading and boundary condition assigned on 3D FE model

For the axisymmetric models, only the Superior-Inferior load cycle (shown in Figure 3-7) was applied on the head of the model with a peak force of 2000N and the base of the stem trunnion was fixed in the y translational degree-of-freedom only (see Figure 3-6).

A quantitative assessment of walking activity in patients with various types of hip or knee joint replacements was published by Schmalzried et al. (1998). Electronic digital pedometers were used in the study of 111 patients which indicated that on average a patient would take 910,310 walking steps per year (the estimation being

very dependent on age, activity and gender). In this study an average of 1 million walking steps per year has been assumed based on the work by Schmalzried et al. (1998).

The walking cycle is discretised into 10 equal time intervals during the 1.2 second cycle time period. This number of time intervals is adequate to accurately simulate the load-history for this problem; other loading histories may require more or fewer intervals dependant on their detail and complexity.

The loading applied on the models for each study in the chapters to follow included an initial impact to simulate the assembly of the head onto the stem trunnion and then time variant loading cycles to approximate hip loading during walking.

3.5 Updating the geometry

The wear determined at each time interval is summed to provide a ‘cyclic’ wear depth which itself is then scaled by β to provide a sensible wear depth for updating purposes as described in section 3.3.

Then the contact surface normal directions at the positions of the paired nodes need to be obtained. The opposite direction of the normal direction for each paired node is extracted from its nodal contact normal force (CNORMF) which is available from the output database of ABAQUS. The CNORMF global Cartesian force components are divided by their magnitude to obtain the inner normal directions of the paired nodes (see Figure 3-10).

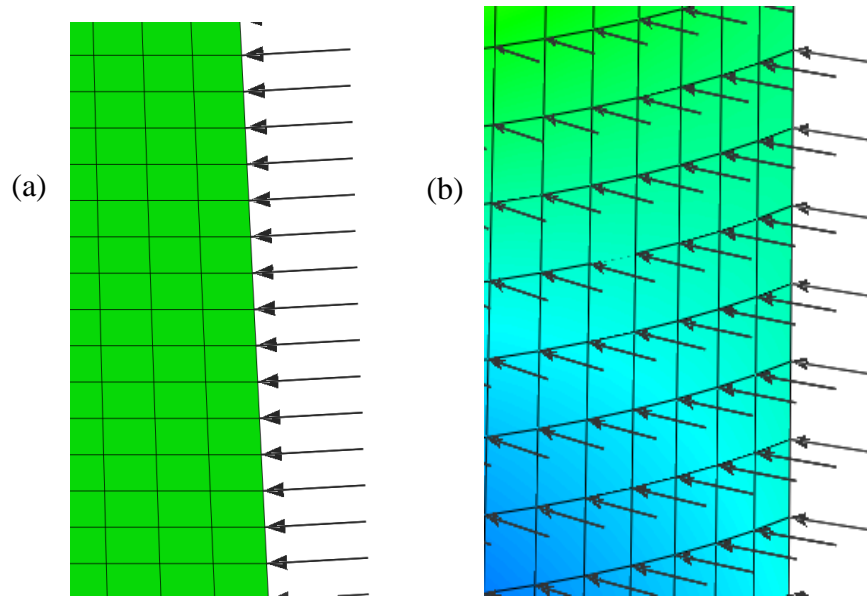


Figure 3-10: Opposite of nodal normals indicating the direction of wear evolution, (a) axisymmetric and (b) 3D model

Wear is then applied to the paired nodes (by updating their coordinate positions) inward to their nodal normals in order to create the new geometry for execution in the next ‘stage’ of the analysis. The normal directions need to be calculated following each geometry update as they will change due to the wearing process.

3.6 Computational framework

The method to predict wear contains three main phases which are necessary in order to accurately simulate the effect of impaction of the head onto the stem and the subsequent walking cycles.

In phase 1, a single dynamic impaction analysis is performed on the model with head and stem assembled just into contact. Then, as explained in section 3.8, the average displacement of the parts is extracted and imported into a new FE input file for use in phase 2 of the wear analysis method.

In phase 2, the method consists of two steps; in the first step the parts are assembled overlapped based on the displacements obtained from phase 1 which create

interference between the components at the contact interface (a general static analysis); in the second step, an implicit dynamic analysis is defined and the walking loads with relative rotations (explained in section 3.4.5) are applied on the 3D model (just a single superior-inferior load for axisymmetric model).

Using the results from the FE analysis, for nodal shear stress (or contact pressure) and displacement in the contact zone, and the wear law explained in section 2.4, the extent of fretting wear at the taper junction can be determined as a ‘wear depth’ for a single walking cycle. This ‘cyclic’ wear depth is then scaled up by β to provide a wear depth for the specified number of loading cycles (defined by β) and the part geometry updated as explained in section 3.5. This updating of part geometry will partially remove the initial overlap of the parts therefore gradually removing the effect of impaction. The updating of part geometry continues in this manner until the overlap has been entirely removed at which point the method continues into phase 3.

In phase 3, the static overlapped analysis step is removed and only a single implicit dynamic step (representing the walking loads) is maintained for the rest of the analysis until the specified number of cycles or wear depth for the study has been reached.

This method is illustrated in a flowchart shown in Figure 3-11.

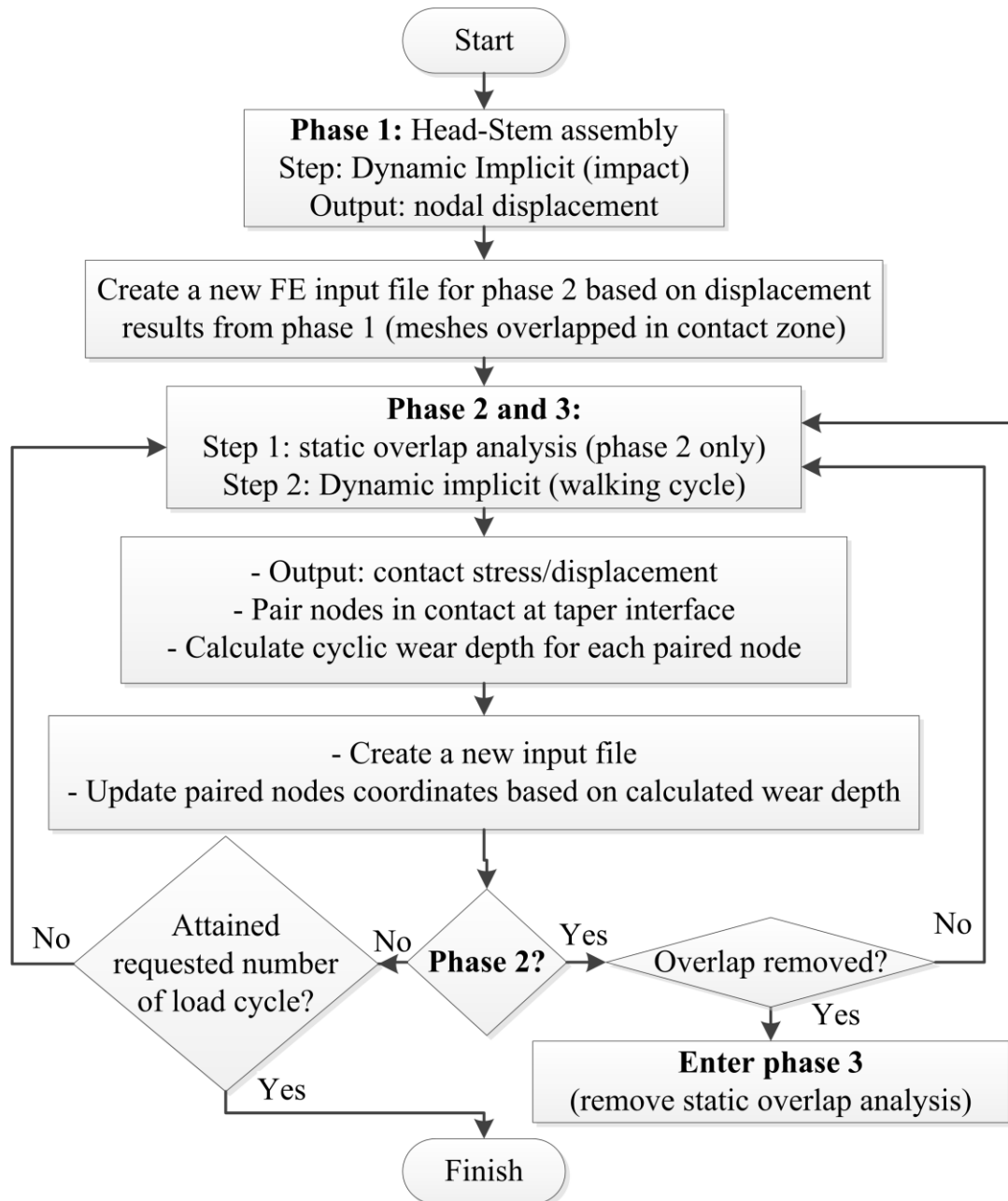


Figure 3-11: Quantitative procedure to predict fretting wear.

3.7 Initial assembly of components

The initial fixation (locking) of the femoral prosthetic head on the stem trunnion is generated by the surgeon impacting the head onto the stem intraoperatively. This is simulated here (in phase 1) by a single dynamic implicit analysis undertaken using the FE models described earlier and the load-time history shown in Figure 3-5. It has been postulated that the initial fixation of the prosthetic head on the stem trunnion is

reduced over time by fretting wear at their contacting surfaces. A key aspect of the wear methodology presented in this work is the use of an overlapped mesh at the taper interface with a static contact analysis step to model the weakening of this fixation (which is facilitated by the gradual removal of overlap with respect to time). As such, the contact conditions prevalent at the taper interface on completion of the dynamic analysis step (phase 1) need to be replicated at the start of step 2 in phase 2 by use of the static contact analysis step incorporating mesh overlap (step 1, phase 2).

The dynamic analysis undertaken in phase 1 provides part displacements that are used at the start of phase 2 to position the head and stem relative to one another so as to provide the necessary overlap for the static contact analysis step. Figure 3-12 shows contact pressure distributions along the stem trunnion interface at the completion of phase 1 and at the commencement of step 2 in phase 2 (following the static contact analysis step). The figures show that the contact pressures computed from the dynamic (phase 1) and static contact (phase 2 step 1) analyses are almost identical and that use of a static contact analysis step (with overlap) can facilitate accurate modelling of the effect of impaction on head-stem fixation.

Figure 3-12 shows a comparison of the contact pressure obtained from the dynamic impaction analysis and the corresponding overlap analysis. The pressure distribution is symmetrical which is due to the axisymmetric geometry and impaction force applied. The distributions along the taper interface for both an axisymmetric and 3D model are approximately the same. These results validate the use of the overlap analysis rather than the impaction analysis. The error shown in Figure 3-12 is less

than 10% and is due to creating the overlap model based on the average displacement of the parts from the impaction analysis.

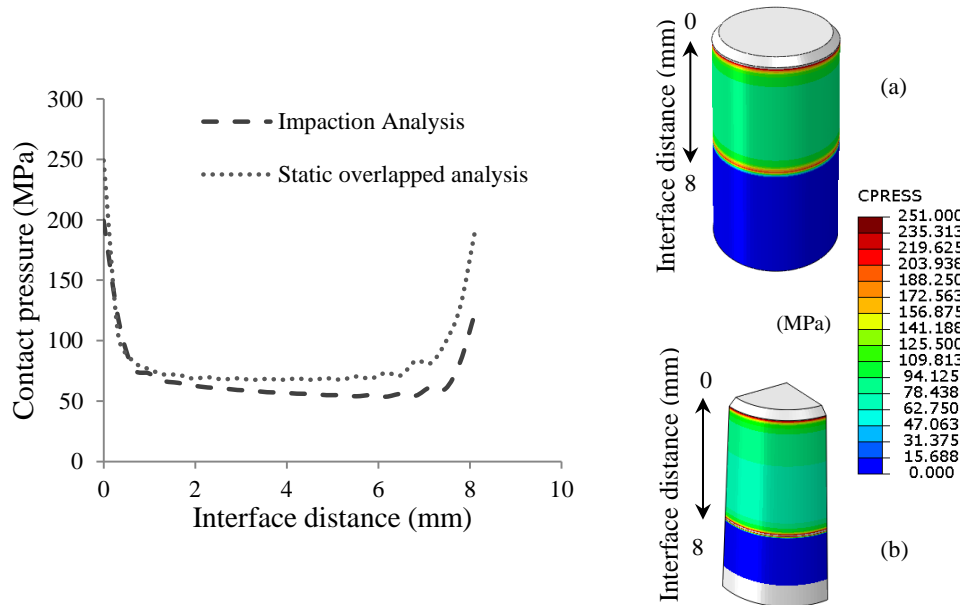


Figure 3-12: Contact pressure distribution along stem trunnion surface at the end of phase 1 and at the commencement of step 2 of phase 2, (a) 3D model and (b) axisymmetric model (swept by 80°)

3.8 Impaction and Overlapped analysis

To predict wear accurately, the model must be capable of accounting for the initial effect of impaction of the femoral head onto the stem trunnion in surgery with the prosthesis then subject to time variant loading cycles to approximate hip loading during walking.

The “locking” of the femoral head onto the stem trunnion intra-operatively is important regarding the stability of the assembly and the extent of any subsequent fretting wear occurring at the taper interface. This “locking” is achieved by the surgeon impacting the head onto the stem (a single event as already discussed). It has been postulated that the “locking effect” is diminished over time due to fretting wear at the taper interface. Consequently, the best approach to modelling this reduction in

the taper fixation over time was best facilitated by utilising a “static contact analysis incorporating mesh overlap in the contact zone”. The reasons why the initial impaction is handled in such a distinct manner (in comparison to the gait cycle) are best explained by considering other possible options/analyses for modelling this:

- a dynamic explicit step for the initial ‘impaction’ (short duration) would have to be followed by a dynamic explicit step for the ‘walking cycle’ (1.2 second duration) which would result in an inefficient analysis computationally.
- on completion of the walking cycle, a wear depth is calculated, scaled up and then removed from the taper interface surfaces (thus separating them using this approach). At this point therefore the ‘locking effect’ generated by the impaction will be removed completely. To rectify this, another impaction step would need to be undertaken, however, the required magnitude of this force will be unknown (it would need to be different to the initial impaction force to account for the wear that has taken place).
- a dynamic implicit step (for impaction) would need to be followed by a dynamic implicit step for the walking cycle. However, this “implicit” approach also suffers from not being able to enforce a reduction in the “locking effect” due to wear (for the same reasons as the ‘explicit’ approach explained above).

In this method, considering phase 1, a single, separate dynamic implicit analysis is used to model ‘impaction’. The displacement of the head onto the stem from this analysis is recorded and used to produce an initial “overlap” model for the subsequent wear analysis. This initial static contact analysis (phase 2, step 1) provides the same contact pressure distribution at the taper interface as the phase 1

dynamic implicit analysis (see Figure 3-12). The subsequent wear analysis (phase 2) consists of “stages”, with each ‘stage’ of the analysis consisting of a “static” contact analysis step to model the effect of impaction, a dynamic implicit step to model the walking cycle, calculation of wear for a specific number of cycles β , and a geometry update of the contacting surfaces). By using a contact analysis (with overlap) it is possible to model the reduction in the “locking effect” due to wear by removing the calculated wear depth for a particular “analysis stage” from the “overlap” value at the commencement of that particular “stage” (i.e. the geometry update).

It has been hypothesised therefore, the use of a static “contact” analysis (with overlap) to model the reduction in the locking effect of the head onto the stem seems to be the most efficient and plausible approach to adopt. The efficiency of the approaches is even more significant on extension to 3D and the multiple “stages” expected to return an accurate analysis.

3.9 Algorithms

Calculating wear for the paired nodes at the contact interface and updating their coordinate positions manually to reflect this, is time consuming and difficult. Consequently, the wearing process explained has been automated using a Python script⁴ linked within ABAQUS as a user plug-in. This helps to develop a generalized fretting wear algorithm that could be used for different studies and models.

The script is executed during phase 2 and 3 of the wear analysis. The script is runnable straight from ABAQUS CAE (as a plug-in) requesting initial input data from users. Figure 3-13 shows a graphical user interface of the algorithm written in the ABAQUS Python environment in order to request input data from a user. Different tabs of this window are shown in the appendix.

After obtaining the input data from the user, the script initially submits the FE input file to ABAQUS at which point the head and stem are assembled into contact (overlapped). The programme then pairs nodes in the contact zone by identifying which nodes on the two parts are closest to one another prior to application of the hip loading. On completion of each time interval i the script extracts the contact stress and displacements for all of the paired nodes. Using these values the script calculates the average contact stresses based on the requested wear law (τ_{ip} or P_{ip}) and relative displacement s_{ip} between paired nodes and subsequently the associated wear depth for a time interval. The wear depth calculated is then scaled up by the requested value of scaling factor (β). The script then obtains the contact surface normal directions at the positions of the paired nodes as described in section 3.5. Wear is

⁴ Around 2000-line script installable on ABAQUS

then applied to the paired nodes by updating their coordinate positions in the opposite direction to their nodal normals in order to create the new geometry for execution in the next “stage” of the analysis. The normal directions need to be calculated following each geometry update as they will change due to the wearing process.

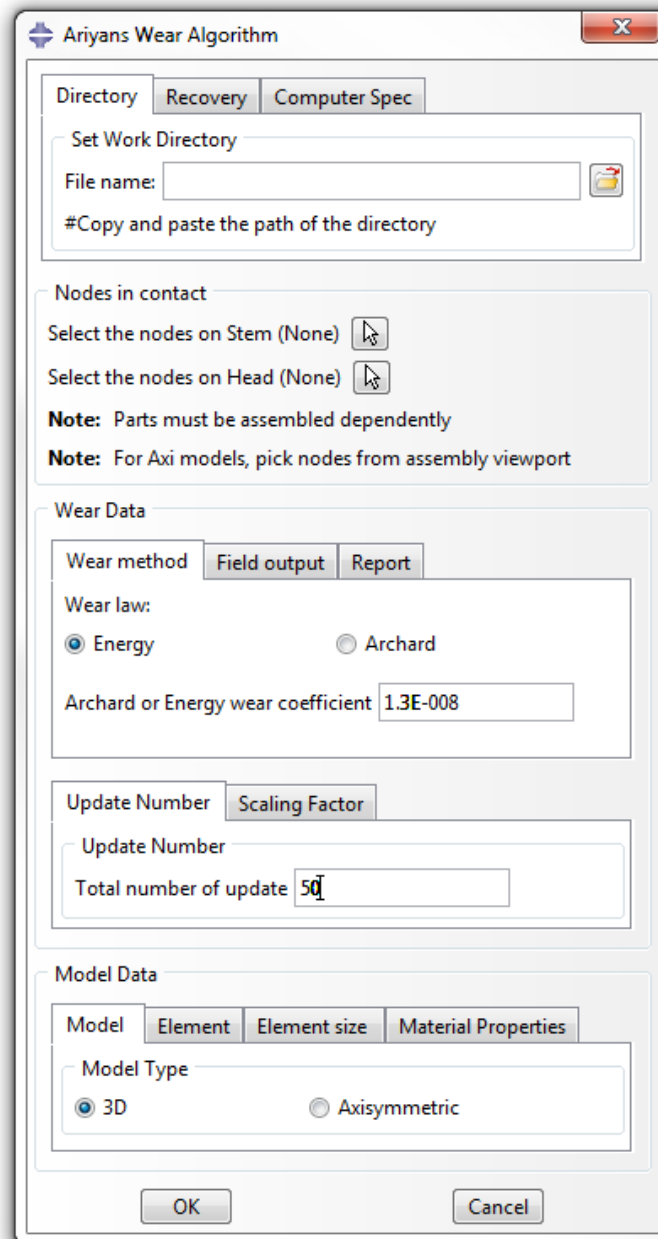


Figure 3-13: Graphical user interface of the wear algorithm, other tabs of this window are presented in the Appendix I

The Python script contains a numbers of script functions which are called by the “Kernel” in a main script. In this section, these functions are described in detail.

3.9.1 Input requested from user

In order to run the wear algorithm in ABAQUS, the user needs to assign initial data for wear modelling. This data can be provided in the graphical user interface window shown in Figure 3-13.

Algorithm 1: inputRequest

Input: ABAQUS dialog box builder

Output: Initial data from user

1. *Requested data:*
 2. *INP: Initial FE input file*
 3. *NS: Node set*
 4. *NS1: Node set in contact for part1*
 5. *NS2: Node set in contact for part2*
 6. *UN: Number of update required*
 7. *WM: Wear method*
 8. *Arc: Archard*
 9. *Enr: Energy*
 10. *SF: Starting scaling factor*
 11. *OR: wear depth, output request:*
 12. *Off;*
 13. *On: for specific spaced geometry update (SSGU)*
 14. *WC: Archard or Energy wear coefficient*
 15. *MT: Model type:*
 16. *Axi: Axisymmetric*
 17. *3D: Three dimension*
 18. *ET: Element type*
 19. *Lin: 4 or 8-node linear element*
 20. *Quad: 8 or 20-node quadratic element*
 21. *WF: Fraction of wear depth to be applied on parts*
 22. *WF1: Wear fraction for part 1*
 23. *WF2: Wear fraction for part 2*
-

An ABAQUS input file (*.inp file) of the model at the commencement of phase 2 is required to be browsed from the GUI. This file can be generated in ABAQUS CAE. Nodes in contact can be selected from the ABAQUS viewport in the mesh module. The number of geometry updates, wear method, scaling factor, model type, type of

elements used and the fraction of wear to be applied on the parts must also be assigned.

Furthermore, the user has an option to request the “nodal wear depth” results to be written in the output database (*.odb) of ABAQUS and/or as a report text file. These can be set for either all or specifically spaced geometry updates. Reducing the number of results requested can significantly reduce the computational time. There is also a recovery option embedded in the program that allows the user to restart from a crashed analysis. All the input data will be saved as variables shown in Algorithm 1.

3.9.2 Initial coordinates of the nodes in contact

From the node sets (*NS*) for both parts that have been assigned in section 3.9.1, node labels and initial coordinates are extracted from the model data bases (*MDB*) (see Algorithm 2).

Algorithm 2: nodeCoordinates

Input: NS
Output: NC

1. For each part:
2. For all nodes in *NS*:
3. *nodeLabel*, Extract node label
4. *nodeData*, Extract node coordinate
 Save the data extracted to *NC*

Where:

NC is an array containing all nodes label and relative coordinates
nodeLabel is a function that returns node label from *MDB*
nodeDat is a function that returns node coordinate from *MDB*

3.9.3 Extract data from input file

In order to read results from the ODB, the name of the parts and the name of the dynamic step defined by the user are required to be extracted from the initial ABAQUS input file. This data can be obtained and saved in variables shown in Algorithm 3.

Algorithm 3: dataFromInputFile

*Input: INP**Output: PN1, PN2 and SN*

1. Search in the whole INP file
2. Extract part names, PN1 and PN2
3. Extract step name, SN
4. Extract number of Frames in Dynamic step, FN

*Where:**PN1 and PN2 are the part names,**SN is the dynamic step name**FN is the number of frames in dynamic step*

3.9.4 Nodal normal direction

The wear depth needs to be removed in the nodal normal direction of the paired nodes. This nodal normal direction is an average of the normal direction of the elements attached to that node. Therefore, in the function shown in Algorithm 4, the normal direction of the nodes is extracted from the nodal contact normal force divided by its magnitude.

Algorithm 4: nodalNormalDirection

*Input: NC**Output: NND*

1. For each part:
2. For all nodes in NC:
3. Open ODB
4. If contact stress is not zero:
5. Read **CNORMF** from ODB for the relative node
6. Read **CNORMFmag** from ODB for the relative node
7. Divide the **CNORMF** components by **CNORMFmag**
8. Save the division vector with its node label in **NND**
9. Return **NND**

*Where:**NND is an arrays contains node label and their nodal normal directions,**CNORMF is the elements of nodal contact normal force in 3 direction**CNORMFmag is the magnitude of CNORMF*

3.9.5 Node deformed coordinate

The updated coordinates for the nodes at the last interval are required to pair the nodes at the contact interface. The relative displacement for the nodes in contact is

much smaller than the element size so that the paired nodes are not changing during the step time. Therefore, picking the updated coordinate at any time interval satisfies the pairing node function. The updated coordinates for nodes in contact can be obtained using the function shown in Algorithm 5.

Algorithm 5: nodeDefCoordinate

Input: NND
Output: NDC

1. *Open ODB for the last frame*
 2. *For each part:*
 3. *For all nodes in NND:*
 4. *Extract updated coordinate, **defCOORD** from ODB*
 5. *Save the data with relative node label in NDC*
 - 6.. *Return NDC*
-

Where:

NDC is an array contains node label and their updated coordinate at the last intervals
defCOORD is the deformed coordinate in ODB

3.9.6 Pairing nodes in contact

As explained in section 3.3 nodes in the contact area on one part need to be paired with the closest node on the other part. This is facilitated by calculating the distance between the nodes of the parts in contact. The function illustrated in Algorithm 6 returns an array which contains all pair nodes.

Algorithm 6: pairNode

Input: NDC for both parts
Output: PN

1. *Open ODB for the last frame*
 2. *For i in NDC1:*
 3. *For j in NDC2:*
 4. $x = NDC1[i]$
 5. $y = NDC2[j]$
 6. $dis = ||y - x ||$
 7. *if dis is smallest:*
 8. *Pair node x with b, **pairNode[i]***
 9. *Add pairNode[i] to PN array*
 10. *Return PN*
-

Where:

$||x - y||$ is the Euclidean distance between x and y,
NDC1 and NDC2 are sets for node updated coordinate for part 1 and 2 respectively
PN is an array contains arrays of paired nodes

3.9.7 Wear depth calculation

The wear depth at paired nodes can be calculated based on either Archard or the Energy wear law. Algorithm 7 calculates the total wear depth for a set of paired nodes.

Let:

- $\langle a_i, b_i \rangle$: paired nodes contained in PN
- $U_j^{a \text{ or } b}$: is the displacement vector for node a or b (e.g. for node a: $U_j^a = (u_1^a, u_2^a, u_3^a)$ at j^{th} time intervals)
- $D_{\delta j}^{a \text{ or } b}$ is the displacement between $(j+1)^{\text{th}}$ and j^{th} time intervals
- $S_{\delta j}^{ab}$ is the relative displacement for node a and b between $(j+1)^{\text{th}}$ and j^{th} time intervals
- $P_j^{a \text{ or } b}, \tau_j^{a \text{ or } b}$ are the contact pressure and shear stress for node a and b at j^{th} time interval
- $P_{\delta j}^{a \text{ or } b}, \tau_{\delta j}^{a \text{ or } b}$ is the average of the contact pressure and shear stress at consecutive time intervals for node a and b
- $w_{\delta j}^{ab}$ is the wear depth calculated at consecutive time intervals
- $W^{(a_i, b_i)}$ is the wear depth for the step time
- $W^{a_i b_i}$ is an array containing the scaled up wear depth

Algorithm 7. wearDepth

Input: PN, SF, WM, WC

 Output: $W^{(a_i, b_i)}$

1. Open ODB
2. Length (frame) = m
3. For $\langle a_i, b_i \rangle$ in PN:
4. For $j=0:(m-1)$
5. $U_j^a = \text{DisFromODB}(a_i, j)$
6. $U_{j+1}^a = \text{DisFromODB}(a_i, j+1)$
7. $U_j^b = \text{DisFromODB}(b_i, j)$
8. $U_{j+1}^b = \text{DisFromODB}(b_i, j+1)$
9. $D_{\delta j}^a = U_{j+1}^a - U_j^a$
10. $D_{\delta j}^b = U_{j+1}^b - U_j^b$
11. $S_{\delta j}^{ab} = \|D_{\delta j}^b - D_{\delta j}^a\|$
12. if WM is Archard:
13. $P_j^a = \text{CPRESSfromODB}(a_i, j)$
14. $P_{j+1}^a = \text{CPRESSfromODB}(a_i, j+1)$
15. $P_j^b = \text{CPRESSfromODB}(b_i, j)$
16. $P_{j+1}^b = \text{CPRESSfromODB}(b_i, j+1)$
17. $P_{\delta j}^a = \text{Avg}(P_j^a, P_{j+1}^a)$
18. $P_{\delta j}^b = \text{Avg}(P_j^b, P_{j+1}^b)$
19. $P_{\delta j}^{ab} = \text{Avg}(P_{\delta j}^a, P_{\delta j}^b)$
20. if WM is Energy:
21. $\tau_j^a = \text{CSHEARfromODB}(a_i, j)$
22. $\tau_{j+1}^a = \text{CSHEARfromODB}(a_i, j+1)$
23. $\tau_j^b = \text{CSHEARfromODB}(b_i, j)$
24. $\tau_{j+1}^b = \text{CSHEARfromODB}(b_i, j+1)$
25. $\tau_{\delta j}^a = \text{Avg}(\tau_j^a, \tau_{j+1}^a)$
26. $\tau_{\delta j}^b = \text{Avg}(\tau_j^b, \tau_{j+1}^b)$
27. $\tau_{\delta j}^{ab} = \text{Avg}(\tau_{\delta j}^a, \tau_{\delta j}^b)$
28. if WM is Archard:
29. $w_{\delta j}^{ab} [j] = WC_{Arc} \times P_{\delta j}^{ab} \times S_{\delta j}^{ab}$
30. if WM is Energy:
31. $w_{\delta j}^{ab} [j] = WC_{Eng} \times \tau_{\delta j}^{ab} \times S_{\delta j}^{ab}$
32. $W^{a_i b_i} = \text{sum}(w_{\delta j}^{ab} [j]) \times SF$
33. Return W^{ab}
34. Return W^{ab}

Where:

 $\|x - y\|$ is the Euclidean distance between x and y ,

 Avg(l, m) returns average of a and b ,

DisFromODB is a function that returns displacement from ODB,

CPRESSfromODB is a function that returns contact pressure from ODB,

CSHEARfromODB is a function that returns contact shear stresses, if model type is 3D, returns the resultant of contact shear stresses components, tangential to contact surface,

3.9.8 Geometry update

Section 3.5 described how the geometry of the parts needs to be updated. This procedure is facilitated by a function illustrated in Algorithm 8.

Algorithm 8: *geoUpdate*

Input: W^{ab} , PN , NND , INP

Output: $newINP$

1. Create a new input file, **newINP**, based on the old INP
 2. For $\langle a_i, b_i \rangle$ in PN :
 3. Find $NND[i]_a$ and $NND[i]_b$, normal directions for node a_i and b_i in NND
 4. Find $W^{a_i b_i}$, the wear depth for pair node $\langle a_i, b_i \rangle$ in W^{ab}
 5. In inputRequest find **WF1** and **WF2** for part 1 and 2
 6. Calculate wear Fraction, $W^{(a_i)}$ and $W^{(b_i)}$, by Multiplying $W^{a_i b_i}$ with **WF1** and **WF2** for node a_i and b_i respectively
 7. Calculate wear Array, **wArray1** and **wArray2**, by Multiplying $W^{(a_i)}$ and $W^{(b_i)}$ with $NND[i]_a$ and $NND[i]_b$ for node a_i and b_i respectively
 8. Reverse **wArray1** and **wArray2** to opposite side of their normal direction
 9. Search for **COOR** $[i]_a$ and **COOR** $[i]_b$, initial coordinates of node a_i and b_i for part 1 and 2 in the $newINP$
 10. Subtract **wArray1** and **wArray2** from **COOR** $[i]_a$ and **COOR** $[i]_b$ and save in $newINP$
 11. Return $newINP$
-

3.9.9 Results report (*.txt format)

A report on the results and data extracted can be requested to be written to a text file. Data such as the total number of load cycles, input data, paired node set and results such as the wear depth calculated for each paired node at each update and also in total. Algorithm 9 produces this report (A sample of the results is shown in Appendix II).

3.9.10 Writing results in output databases of ABAQUS (*.odb format)

At the end of each wear analysis the total wear depth can be requested to be written in the ABAQUS output databases. Algorithm 10 writes the results into the ABAQUS output database (A sample of the results is shown in Appendix III).

Algorithm 9: resultsReport

Input: inputRequest, PN, W^{ab} *Output: Results.txt*

1. *If UN is "1":*
 2. *Create an empty text file, **Results.txt***
 3. *Write inputRequest in the Results.txt*
 4. *At each update:*
 5. *Write update number in the Results.txt*
 6. *Write the pair node array for the current update, PN in the Results.txt*
 7. *For $\langle a_i, b_i \rangle$ in PN:*
 8. *Write $W^{a_i b_i}$ in the Results.txt*
 9. *Write PN1, node a_i and $W^{(a_i)}$ for part 1 in the Results.txt*
 10. *Write PN2, node b_i and $W^{(b_i)}$ for part 2 in the Results.txt*
- ... total wear depth*
- Write the number of load cycle, $SF \times UN$ in the Results.txt*
-

Algorithm 10: resultsODB

Input: inputRequest, PN, W^{ab} *Output: Abaqus output database*

1. *If OR is "on":*
 2. *Open ABAQUS *.ODB (not read only)*
 3. *For $\langle a_i, b_i \rangle$ in PN:*
 4. *Find the relative nodes in ODB*
 5. *Write PN1, node a_i and $W^{(a_i)}$ for part 1 in the ODB*
 6. *Write PN2, node b_i and $W^{(b_i)}$ for part 2 in the ODB*
 7. *Close the ODB file*
-

3.9.11 Error detection

The algorithm contains an error detection function to aid in the continual running of the program.

During the wear analysis, due to the removal of material from the model, in phase 3 of the analysis (when the overlap is removed completely), a gap is produced between parts on updating the geometry. If the gap is small, there is no difficulty to converge the FE analysis. Proceeding into phase 3, can lead to a relatively large gap between the parts and that creates either incorrect contact stresses or convergence problems. At this point the algorithm turns to the error detection section and firstly reassembles

the parts to remove the gap. The distance to reassemble the parts is calculated based on the last updated average wear depth. This brings the parts again into contact. If this does not help to converge the result for the next analysis, the script turns on the “contact stabilization” for the analysis in the input file.

The “contact stabilization” is found helpful to converge the results. Reducing the scaling factor is also helpful to have the FE analysis converge. In all analyses executed in this study, the error detection function allows continuous wear analysis without an FE convergence problem (see Algorithm 11).

Algorithm 11: errorDetection

Input: failedInputFile

Output: Try to continue mainAlgorithm

1. *If jobMessage is Job-Aborted:*
 2. *Open the failedInputFile which has not been converged*
 3. *Calculate an average of sum of all wear depth, sumWear, for all pair nodes*
 4. *Reassemble the new INP with the sumWearv /*to have the parts into contact*/*
 5. *Resubmit the newINP*
 6. *If jobMessage is Job-Aborted:*
 7. *Remove the over closure that might happen due to the reassembling the parts*
 8. *Resubmit the newINP*
 9. *If jobMessage is Job-Aborted:*
 10. *Turn on the “contact stabilization” in ABAQUS input file*
 11. *Resubmit the newINP*
 12. *If jobMessage is Aborted:*
 13. *Reduce the SF by half*
 14. *Resubmit the newINP*
 15. *If jobMessage is Job-Aborted:*
 16. *Write “The analysis cannot be converged further”*
 17. *Break from mainAlgorithm*
-

3.9.12 Main algorithm

All the functions explained in this section are called in a main algorithm in a “while” loop as shown in Algorithm 12. This main algorithm is called by the “Kernel” in ABAQUS.

Algorithm 12: mainAlgorithm

Input: inputRequest, nodeCoordinates, dataFromInputFile

Output:

1. **inputRequest**, request data from user
 2. **nodeCoordinates**, obtain node labels and their relative initial coordinates
 3. **dataFromInputFile**, extract initial data from first input file
 4. $update = 1$
 5. While $update < UN$:
 6. Create a FE job from INP[update], Job-[update]
 7. Submit the Job-[update] in ABAQUS
 8. From the model data bases read the message for job situation
 9. Open jobMessage from ODB
 10. If jobMessage is Job-Completed:
 11. Open ODB[update]
 12. **NodalNormalDirection**, obtain nodal normal direction
 13. **NodeDefCoordinate**, obtain the deformed coordinate for nodes at last frame
 14. **PairNode**, pair nodes in contact
 15. **WearDepth**, calculate wear depth for all pair nodes
 16. **geoUpdate**, write a new INP[update+1] and update the geometry
 17. **resultsReport**, write results as a report
 18. **resultsODB**
 19. $update += 1$
 - 20.
 21. Else:
 22. Return the input file which has been failed to converged, **failedInputFile**
 23. Run **errorDetection**
-

3.10 Computer specification and computational time

All analyses described in the chapters that follow were executed on a 64-bit Windows 7 professional operating system with twin dual six-core processor Intel Xeon central processing unit platforms at 2.60GHz configured with 128GB of random access memory.

The FE analysis and wear algorithm running time for each axisymmetric model (first geometry update) is around 5 minutes but increasing to around 6 hours for each single 3D model update.

3.11 Convergence

3.11.1 Finite element mesh study

Initially a uniform density mesh was generated and a mesh convergence study undertaken based on contact pressure in the model's femoral head. For the FE model used in this study an element size of approximately 1mm in the contact zone proved adequate in achieving converged results (Figure 3-14).

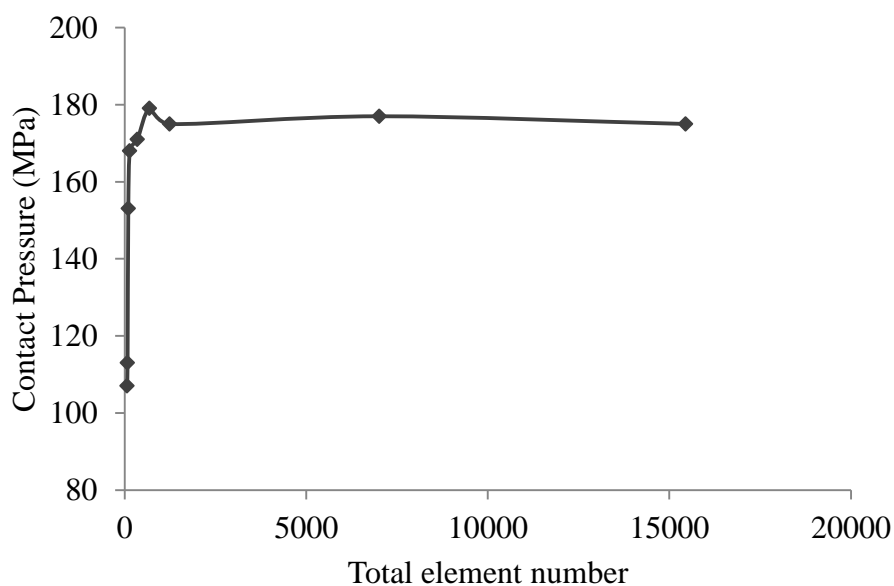


Figure 3-14: Mesh study

3.11.2 Mesh study for wear modelling

Wear depth is calculated at the paired nodes from the product of the Energy or Archard wear coefficient, relative displacement and average contact stress. As with any FE analysis model it is vital that a suitably refined mesh is generated in order to determine accurate results. It was found for both axisymmetric and 3D models when there is a large variation in contact stress across individual elements in the contact zone (due to a too coarse mesh) vastly different wear depths for adjacent paired nodes will be calculated (as $W_d = \alpha \tau s$ or $W_d = K \sigma s$). This generates an uneven worn surface and can lead to future solution convergence problems and the calculation of an inaccurate wear depth (see Figure 3-15).

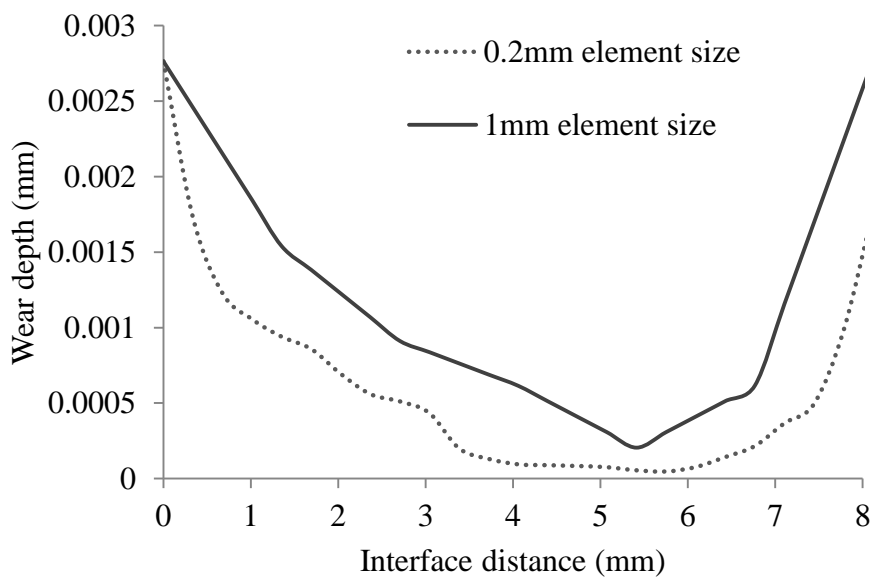


Figure 3-15: Wear evolution convergence. Interface distance is shown in Figure 3-12

It is therefore important that the mesh is further refined in the contact zone so that variations in contact stress values across an individual element are kept to a minimum. To model the wearing process accurately and efficiently an element size of 0.2mm (in the contact zone) was found appropriate which allowed a smooth wear pattern to develop on the model as the solution progressed. Figure 3-15 shows the

wear depth distribution for element sizes of 1mm and 0.2mm at the interface indicating a smooth wear pattern for the smaller element size.

3.11.3 Scaling factor (β)

The scaling factor β used in the analysis has a major impact on solution times, wear evolution and solution accuracy. A large scaling factor will facilitate a relatively quick analysis but may detrimentally affect the accuracy of the final calculated wear for a specified number of loading cycles. A comparatively small value for the scaling factor will increase solution times but should provide an accurate result and wear profile. This is demonstrated in Figure 3-16 which shows the average wear depth that has occurred on the stem trunnion surface over 2 million load cycles (2 years) when using scaling factors ranging from 50,000 to 2 million.

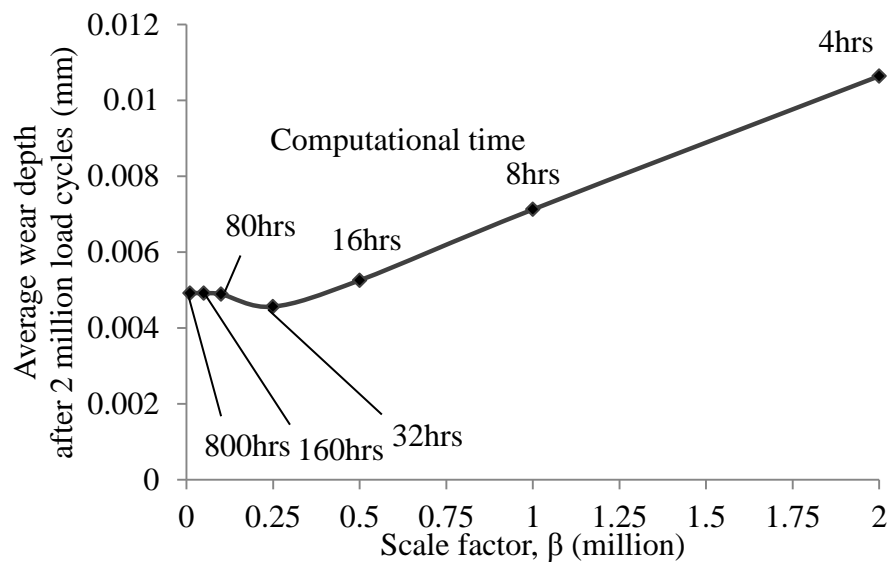


Figure 3-16: Effect of different scaling factor values.

A scaling factor of $\beta = 10^5$ was seen as necessary to produce the accuracy required for the wear depth (a scaling factor of 1 million developing around a 30% error, see Figure 3-16). The scaling factor in the algorithm can be varied (increased or decreased if there is any convergence problem in wear analysis stage) throughout

the analysis in order to optimise solution accuracy and run times. This needs consideration of the contact stress distribution and wear depth calculated during each analysis stage and the wear progress during the analysis. In the following studies $\beta = 10^5$ has been used for the start of the wear analysis as it shows a smooth and relatively uniform wear profile created on the models, and if necessary, can be reduced throughout the wear analysis.

3.12 Summary and Conclusion

The wear modelling presented in this thesis could be important in different aspects of engineering. The method has been developed by considering as many parameters as possible that affect an accurate prediction of fretting wear damage in engineering designs over time in service. A computational method, presented to predict the extent of fretting wear can be used in addition to testing (Elkins et al., 2014, Elkins et al., 2011, Liu et al., 2008, Uddin and Zhang, 2013, Zhang et al., 2013) to help reduce the wear damage in engineering designs.

The method has been automated using a Python script to extract the required results from the FE analysis and update the geometry to reflect the extent of wear that has occurred during the period analysed. The quantitative analysis of wear attempts to express linear wear rate, volumetric wear rate and also material removal which are all associated with wear surface damage or “wear pattern”.

The method has been applied to an axisymmetric and 3D FE model of a THR for a comprehensive illustration of the wear model. It has been successfully used to accurately predict the extent of fretting wear which can occur at the taper junction between the head and stem of a modular THR during its expected operational lifetime. The method could be used in design or applied to clinical practice to help

facilitate a reduction in wear. These models could be used to identify key factors leading to debris release at the taper junction so that appropriate prosthesis design and surgical procedural modifications can be made to mitigate against this damaging problem.

The method presented here can contribute to research in this area with the following advantages over the current methods proposed so far in the literature:

- The method is unique in that, it models the progressive weakening of the taper “fixation” due to the fretting wear process. This “reduction” in fixation is modelled using a static contact analysis incorporating mesh overlap at the taper interface. As wear occurs at the interface over time the overlap is removed accordingly by updating the contacting nodes positional coordinates. Simulating the reduction in the initial fixation strength of the head-stem assembly is seen as important to the accurate assessment of wear.
- As the wear coefficient changes during wear progression, assigning and changing the wear coefficient during the wear analysis is important. If the variation of the wear coefficient during the wear analysis is known by using controlled fretting wear tests, the method is capable of assigning this variation into the wear model.
- The method is user-friendly and generalized for any FE analysis with a graphical user interface. There is no complicated preparation needed to run the wear analysis.
- All the results can be requested (or results by specified spaced update) to be written to the output databases of ABAQUS. This helps to plot the predicted wear damage on the surfaces but also allows obtaining required results

straight from ABAQUS. Reducing the number of requested results (by requesting the results by a specified spaced update), though, will reduce the computational time. This part of the setting can be found on the graphical user interface window attached in appendix.

- The main algorithm contains an error detection function (see Algorithm 11) that can detect possible errors that may occur in the FE analysis due to convergence problems and resolve these problems without any further requirement and effort from the user.
- Due to the timing analysis, a recovery point has been considered in the algorithm. If the analysis fails due to any reason, the algorithm allows the users to recover the previous results and continue the analysis from that point. The recovery tab shown in the graphical user interface attached in the appendix.

As with any proposed method and hypothesis, there are possible shortcomings. The limitations of the proposed method are as follows:

- The assessment of wear in this study is solely based on mechanical wear (fretting) as being the primary mechanism causing damage.
- The method is highly dependent on the value of the fretting wear coefficient. In addition, the significance of the wear coefficient needs to be considered due to its effect on resulting wear depth calculated. This coefficient can only be obtained from controlled experiments.
- Accurate determination of wear of THR components in contact can only be realised by measurement from retrieved prostheses or from fretting wear tests

which may provide credible wear fractions for application in computational wear analysis.

- At this stage the role of oxide and other naturally occurring surface films will be avoided and the study concentrated on physical unlubricated wear process only.
- The boundary conditions used (although creating an efficient model by excluding the requirement to model the acetabular cup), create non-physiologic resisting moments at the centre of the head which need to be acknowledged when interpreting any results from an analysis. Further, the boundary conditions provide a restriction to the analysis of certain design / operational considerations which may be related to fretting wear such as head size and frictional torque. The analysis of these aspects of prosthesis design will require a modified model to that described here which by necessity will require the inclusion of the acetabular cup and an additional contact region thus increasing computational effort considerably.

In what follows in Chapter 4, 5 and 6, the results for different studies are presented with more detailed explanations of the aspects of present methodology.

Chapter 4

Prediction of fretting wear damage using an axisymmetric model of a total hip replacement

4.1 Introduction

An axisymmetric model of a commercial total hip prosthesis, as described in section 3.4, has been primarily used to develop the algorithm. This model has helped to investigate the principal parameters, with a wider sight on the subject, that are critical for predicting fretting wear accurately. Due to the long computational time of 3D FE analysis, this axisymmetric model could be useful for different parametric studies such as the effect of mismatch angle (manufacture tolerance) on fretting wear. This chapter describes key aspects and considerations regarding the axisymmetric model used in the simulations. The intention is to highlight the variation of contact stresses and relative micromotion with their relationship to fretting wear.

4.2 Wear analysis input

The input data shown in Table 4-1 was assigned for the wear analysis. In phase 1, the impaction force creates the necessary overlap for the wear analysis in phase 2.

Table 4-1: Input data for wear analysis of this study

	Input data
Model	Axisymmetric (Figure 3-6)
Material combination	Head: Cobalt-chrome Stem: Titanium (see Table 3-1)
Impaction force	4000N (Figure 3-5)
Walking load and boundary conditions	Superior-inferior (see Figure 3-7)
Wear law	Dissipated Energy
Wear coefficient	$5.35 \times 10^{-8} \text{ MPa}^{-1}$
Wear fraction	Cobalt-chrome: 0.9 Titanium: 0.1
Scaling factor	10^5
Number of load cycles	10^7

The time taken for each analysis “stage” was on average around 5 minutes on the system specification stated in section 3.10. Therefore, for an analysis of 10 million cycles (10 years), there would be 100 “stages” summing to a total run-time of around 8 hours.

4.3 Results

Although an energy wear law is used in this study which is based on shear traction, the results which follow are demonstrated based on contact pressure distribution for

clarity. For the axisymmetric model contact shear stress has a component tangential to the contact surface. This can be either positive or negative based on direction. As such, shear stress distributions are difficult to interpret in the context of wear and so contact pressure has been presented instead.

Values for relative displacement and contact pressure will be equal and opposite on the head and stem taper surfaces. The change in relative displacement (or “slip”), contact pressure and the wear pattern damage, in this chapter, are only demonstrated on the head taper. In this chapter, in order to enhance illustration of the results, the model is swept by 80 degrees. Therefore, although the results are shown in 3D, they are fundamentally axisymmetric.

4.3.1 Initial contact stress and slip variation

Figure 4-1 shows the variation of contact pressure and relative slip during the first analysis and for one walking cycle only. As discussed earlier, to predict wear accurately, the model must be capable of accounting for the initial effect of impaction of the femoral head onto the stem trunnion in surgery with the prosthesis then subject to time variant loading cycles to approximate hip loading during walking.

The first image in Figure 4-1 (at zero interval) shows the contact pressure at the end of static overlap analysis (step 1). Then the walking cycle discretised into 10 time intervals is subsequently shown. As expected, a symmetrical contact pressure and relative micromotion are visible.

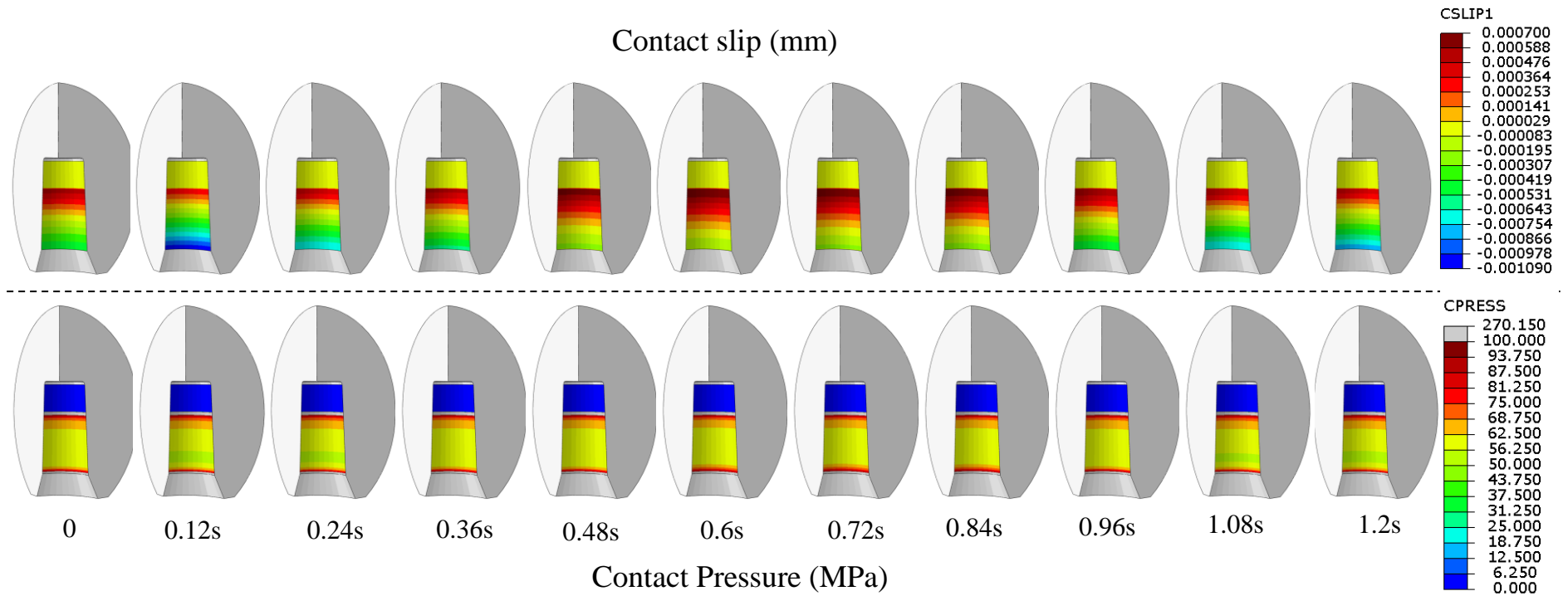


Figure 4-1: Contact pressure and slip distribution throughout a walking load discretised to 10 intervals during 1.2s

The very small slip (between -0.7 to $0.7\mu m$) is due to the high contact pressure along the interface with a peak value of around $270MPa$ at the edges of contact (see Figure 4-1). This indicates that a higher initial contact pressure results in very small relative micromotion between the mating surfaces. The majority of the contact surface, however, is subjected to a contact pressure of approximately $60MPa$.

For each analysis stage and at each time interval, the product of the contact stress, simultaneous contact slip and the wear coefficient value are used to calculate the interval wear depth. The sum of these interval wear depths provides the cyclic wear depth.

4.3.1 Variation in contact stress, slip and wear depth

Figure 4-2 shows the variation of contact pressure, slip and wear depth during phase 2 of the wear analysis at intervals of one million load cycles. It can be seen that during phase 2 of the analysis the value of contact pressure reduces resulting in an increase in micromotion. The value of contact pressure from the start of the analysis (approximately $65MPa$) reduces to around $30MPa$ (start of phase 3) for around half; however, the slip increases from around 0.7 to $1.7\mu m$ i.e. around 2.4 times. This leads to a relatively constant wear rate in phase 2 of the analysis (see Figure 4-7). The associated wear depth as shown in Figure 4-2 starts increasing at the edges initially due to the high contact stress and slip. A relatively smooth wear depth at the end of phase 2 from $1\mu m$ at centre to $2.4\mu m$ at edges of contact is visible.

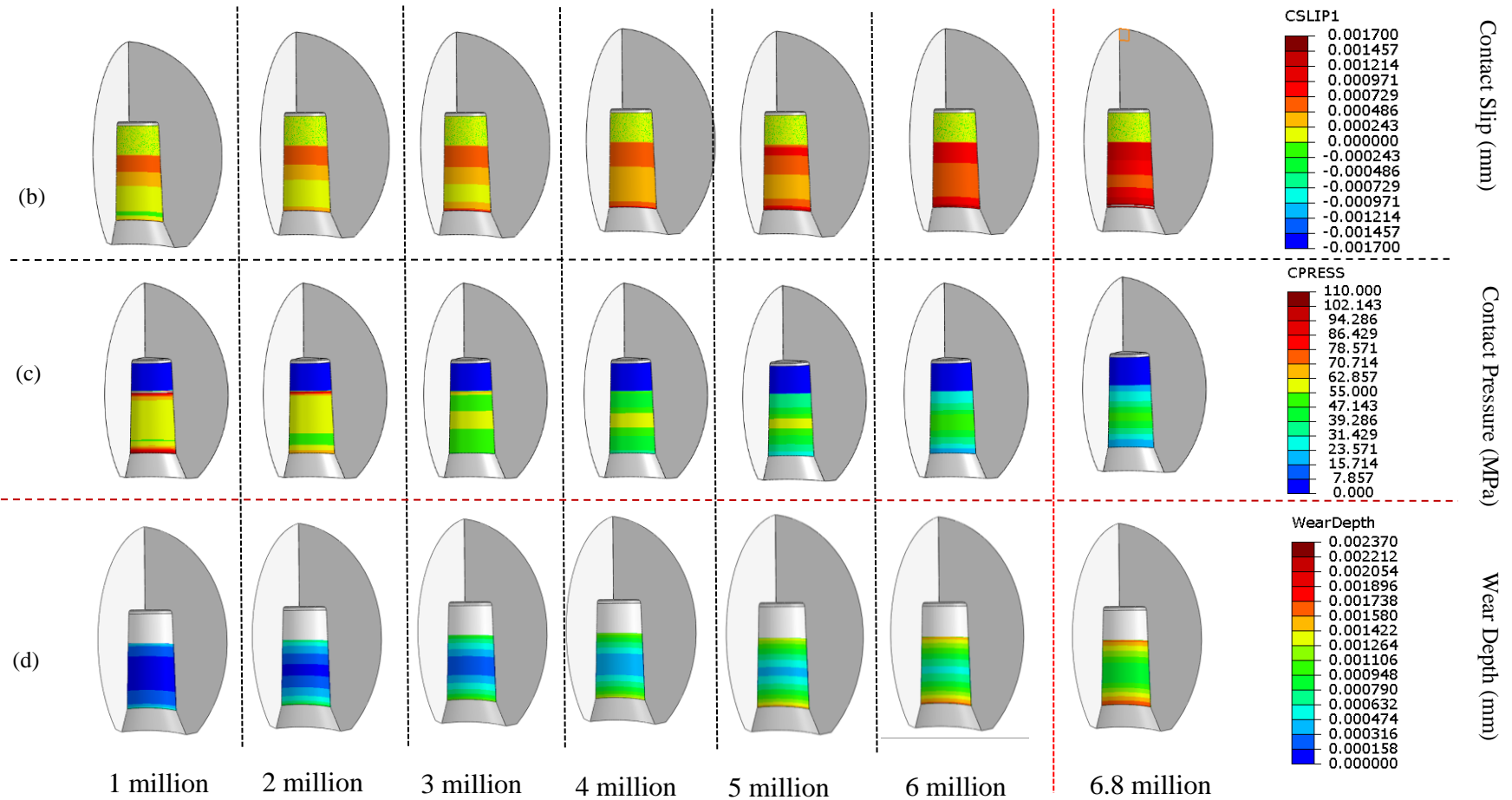


Figure 4-2: Contact pressure, slip and wear pattern evolution during phase 2 of the analysis (from 1 million to 6.8 million load cycles)

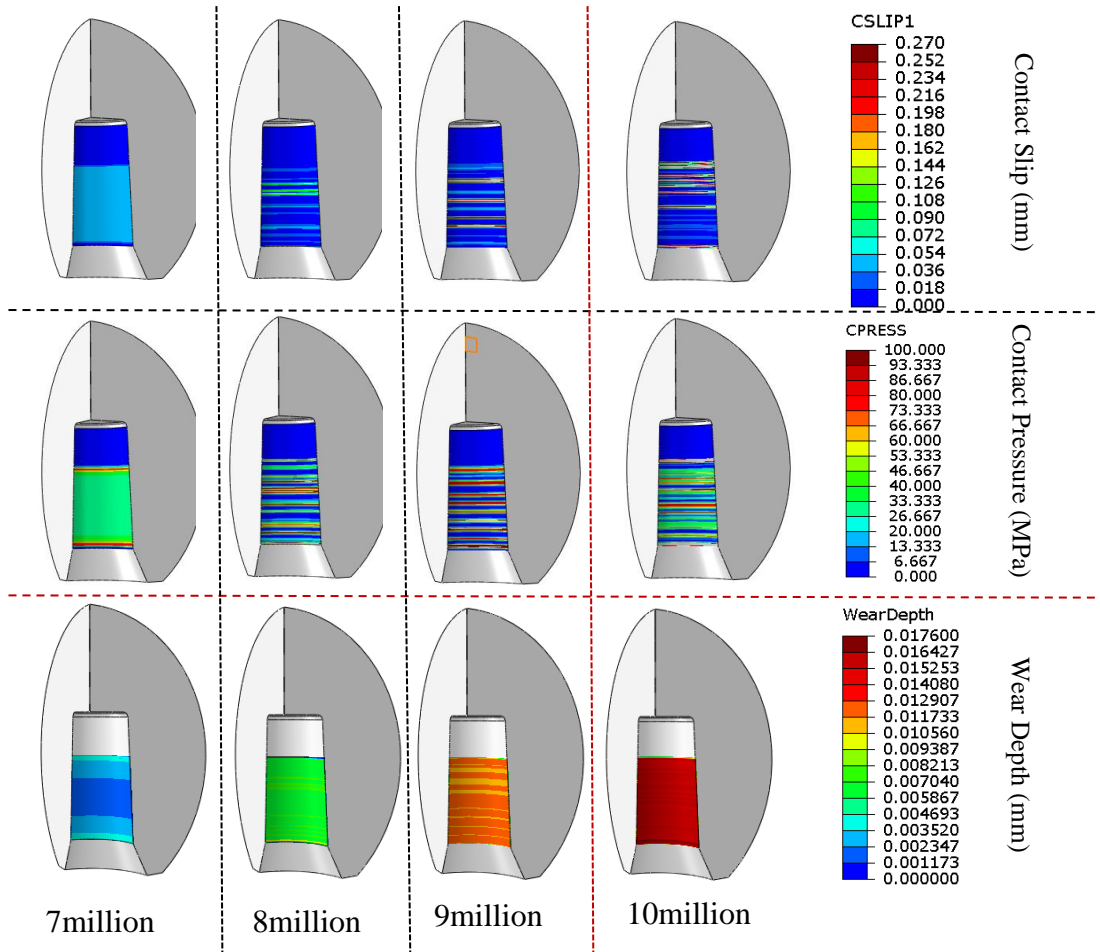


Figure 4-3: Contact pressure, slip and wear pattern evolution during phase 3 of the wear analysis (from 7 million to 10 million load cycles)

Figure 4-3 contains the variation of contact pressure, slip and wear depth during phase 3 of the analysis. The magnitude of the relative motion increases in phase 3 due to removal of the overlap from around $1.7\mu\text{m}$ (end of phase 2) to 0.2mm (end of phase 3). This slip follows a varying contact pressure between 25 to 100MPa . Due to the large increase in relative displacement, the magnitude of the wear rate jumps significantly in phase 3 of the analysis (see Figure 4-7).

Figure 4-4 and Figure 4-5 details the wear depth at the interface of the mating surfaces at the end of phase 2 and 3 of the wear analysis respectively. In phase 3, a relatively uniform wear is generated across the interface. A wear depth of $1.9\mu\text{m}$ can

be observed on the Titanium stem compared with $17\mu\text{m}$ wear depth on the cobalt chromium head.

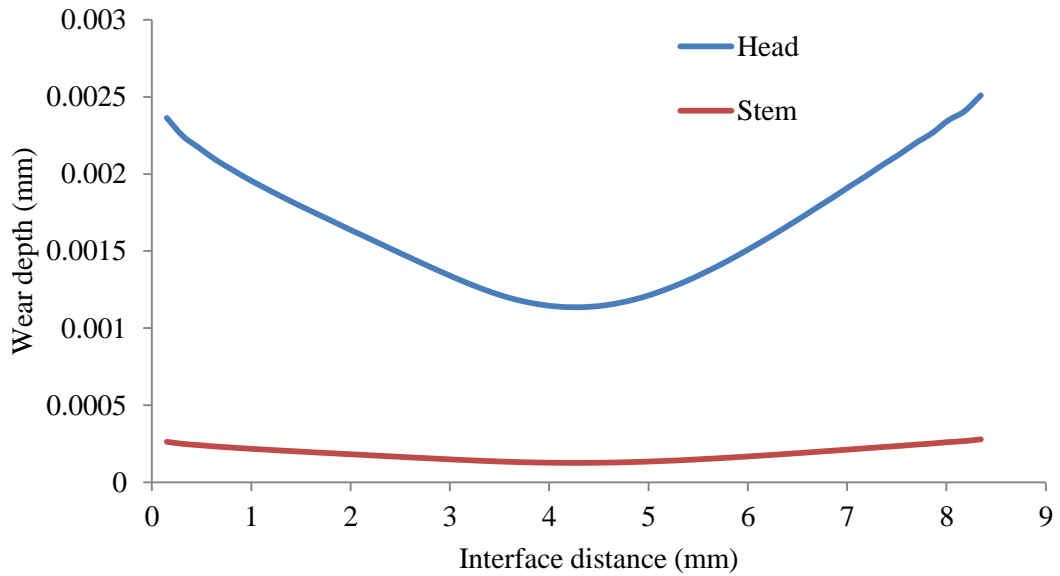


Figure 4-4: Wear depth along contact interface after 6.8 million load cycles (when initial overlap is removed),(contact interface shown in Figure 3-12)

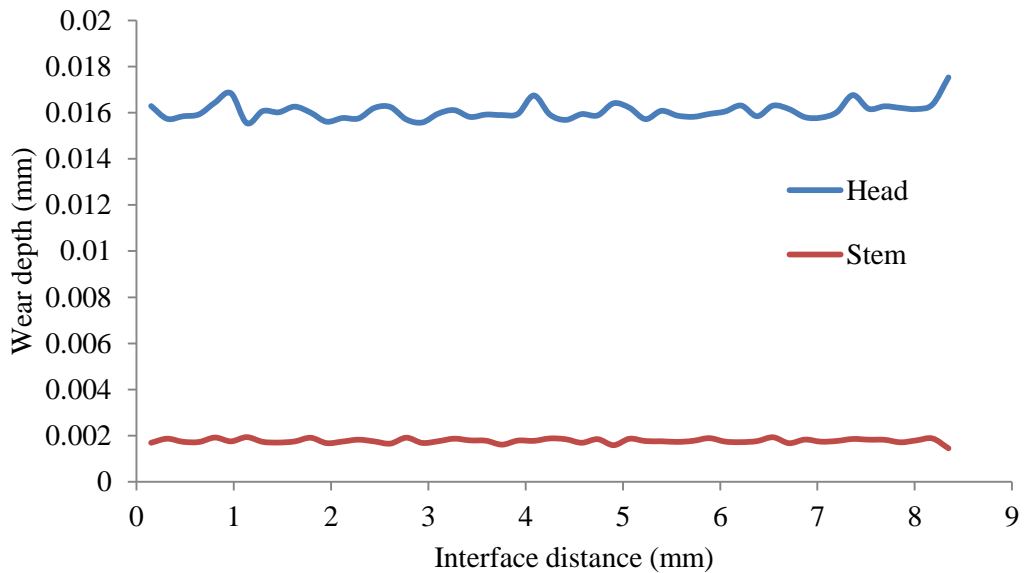


Figure 4-5: Wear depth along contact interface after 10 million load cycles (contact interface shown in Figure 3-12)

Figure 4-6 shows the evolution of the wear depth at specific times (millions of load cycles) during the wearing process. It can be seen that the wear is fairly uniform along the contacting surfaces throughout the analysis. In addition, the graphs show

that at the commencement of an analysis the wear rate is significantly less (demonstrated by the ‘closeness’ of the lines for the calculated wear depths) than that found for the rest of the analysis up until 10 million cycles of load (demonstrated by the “greater spacing” of wear depth lines).

There is a clear indication of the transition in the analysis from phase 2 to phase 3 and the anticipated increase in wear rate. The transition from phase 2 to phase 3 occurs at 6.8million walking cycles for this particular axisymmetric model. The transition points are clearly dependant on the wear coefficients used in the studies.

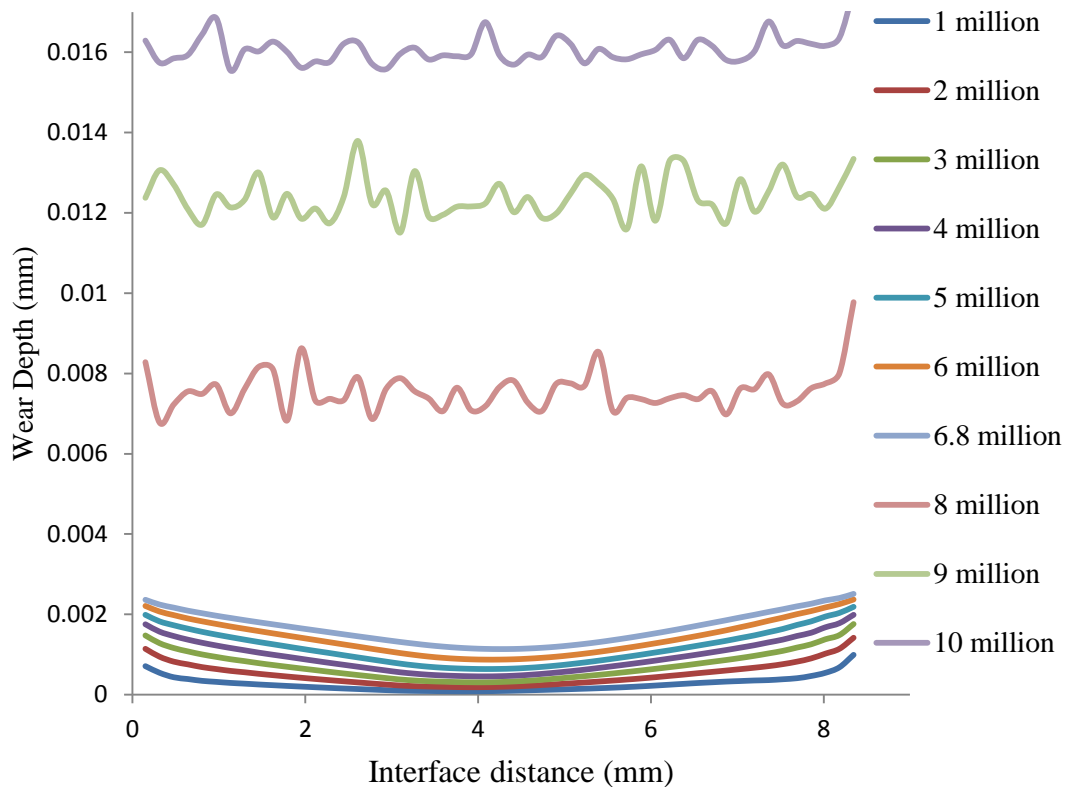


Figure 4-6: Wear depth evolution (from 1 to 10 million load cycles) along the head taper interface (contact interface shown in Figure 3-12)

4.3.2 Linear and volumetric wear rate

The average volumetric wear rate generated at the head taper, stem trunnion and in total during the wear analysis is shown in Figure 4-7. The transition points between

phase 2 and phase 3 can be clearly identified as a jump in the bars demonstrating the increase in wear rate that occurs in phase 3. This is due to the removal of the overlap and subsequent increase in relative displacement of the paired nodes in contact.

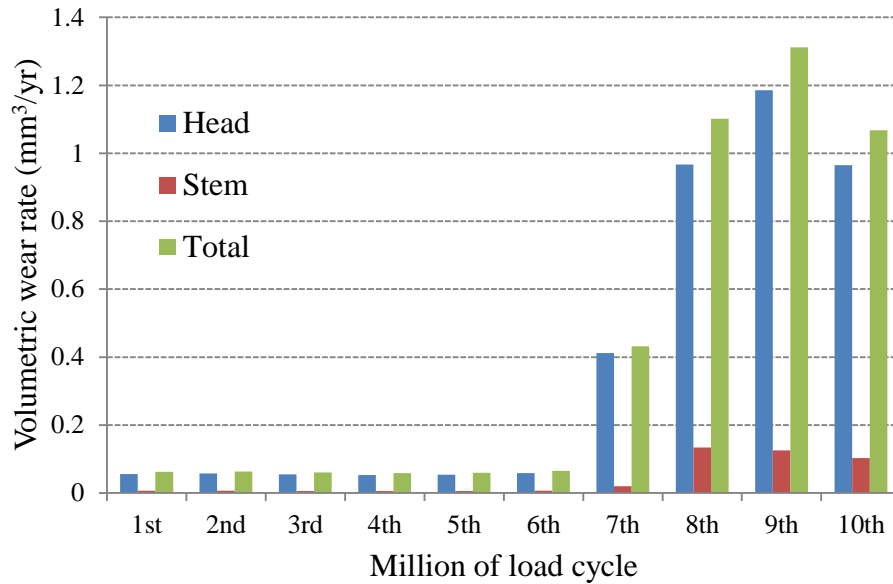


Figure 4-7: Variation in volumetric wear rate with respect to time

Table 4-2 compares the linear and volumetric wear rate. It can be clearly seen here that the wear rate in phase 3 is significantly larger than phase 2. The linear and volumetric wear rate, from phase 2 to phase 3, increases by a factor of around 15.5.

Table 4-2: Linear and volumetric wear rate of the head, stem and in total

	Head		Stem		Total (range)
	Phase 2	Phase 3	Phase 2	Phase 3	
Average linear wear rate ($\mu\text{m}/\text{yr}$)	0.237	3.650	0.026	0.405	1.781 (0.24-5.49)
Average volumetric wear rate (mm^3/yr)	0.055	0.882	0.006	0.095	0.428 (0.050-1.311)

4.4 Theoretical validation

When the overlap analysis is performed (namely a shrink-fit analysis) between the head and stem, a contact pressure will be generated. The model presented in this

study is fundamentally axisymmetric and the shrink-fit analysis is axisymmetric too. Therefore the analytical solution can be calculated based on Burr (1981). As shown in Figure 4-8 a taper and trunnion are overlapped by distance x to provide prestresses on the given surfaces.

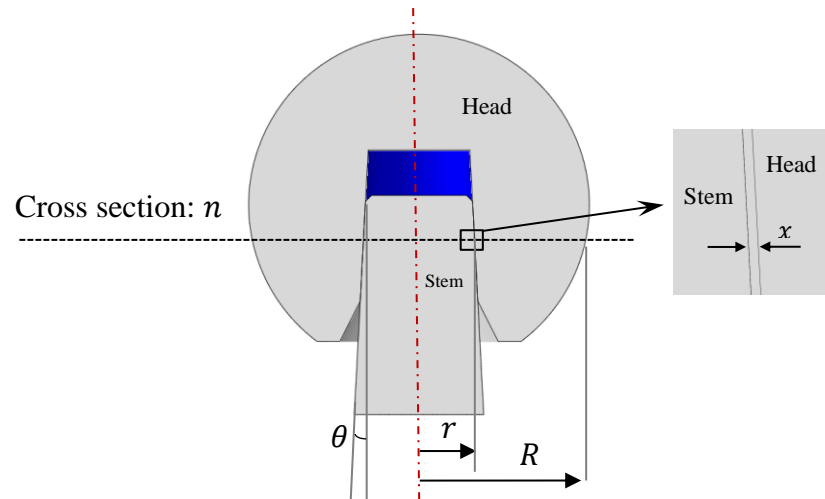


Figure 4-8: Overlap analysis (theoretical approach)

Contact pressure P is generated at the inner surface for each cross section n by shrink-fit procedure.

Let:

- R : radius of head at cross section;
- r : radius of stem at cross section;
- x : total overlap;
- P : contact pressure
- E_h, ν_h, E_s and ν_s are the Young's modulus and Poisson's ratio of the head and stem respectively defined based on Table 3-1

then, a relationship between total overlap (x) and contact pressure (P) can be expressed implicitly as:

$$\frac{x}{P} = r \left[\frac{r^2}{E_h(R^2 - r^2)} \left(1 - \vartheta_h + \frac{R^2}{r^2} (1 + \vartheta_h) \right) + \frac{1}{E_s} (1 - \vartheta_s) \right] \quad 4-1$$

Figure 4-9 shows a comparison of contact pressure between theoretical calculations (using Equation 4-1) and FE analysis. Differences are seen at the contact edges where the theoretical solution is not capable of calculating the singularity; otherwise a very good agreement is obtained for the random locations considered.

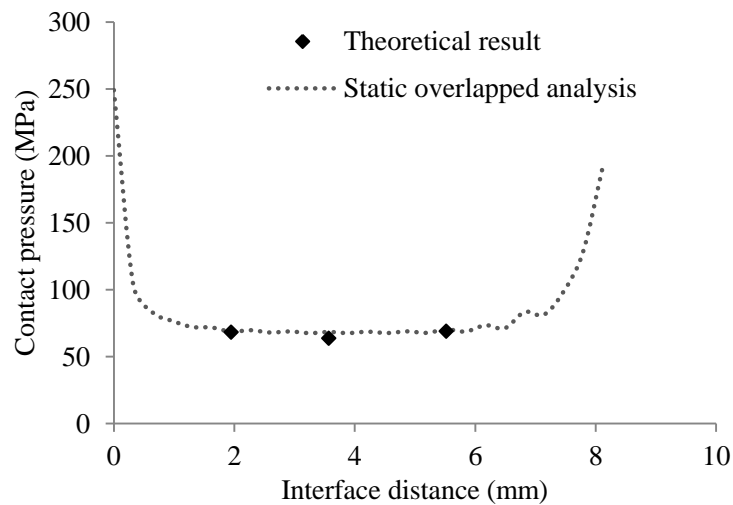


Figure 4-9 A comparison between theoretical and FE results

4.5 Discussion

As stated, the initial taper overlap enforced at the commencement of phase 2 is determined from the dynamic impaction analysis of phase 1 where the impulse applied to the femoral head is detailed in Figure 3-5.

The analysis undertaken in phase 1 is important as it models the actual assembly event of the surgeon impacting the head on to the stem during an operation. The subsequent displacements of the parts can be used at the start of phase 2 to position the head and stem relative to one another and provide the necessary overlap to generate the same contact conditions, pressures and stresses as seen at the end of phase 1.

At the start of phase 2 (prior to the application of the walking load cycle), the initial contact stresses generated by the overlap analysis create reaction forces on the parts that help to maintain the head on the stem trunnion without having to over constrain the model (see Figure 4-10). It is the initial normal contact forces at the taper junction (due to the static overlap analysis) and the specified coefficient of friction that provide the necessary friction forces tangential to the contacting surfaces that maintains the head on the stem. For this to occur, the magnitude of the friction force must be equal to or more than the resultant force created due to the stresses distributed on the head (see Figure 4-10). This fact is crucial for the wear analysis methodology as it can illustrate when the procedure needs to transfer to phase 3.

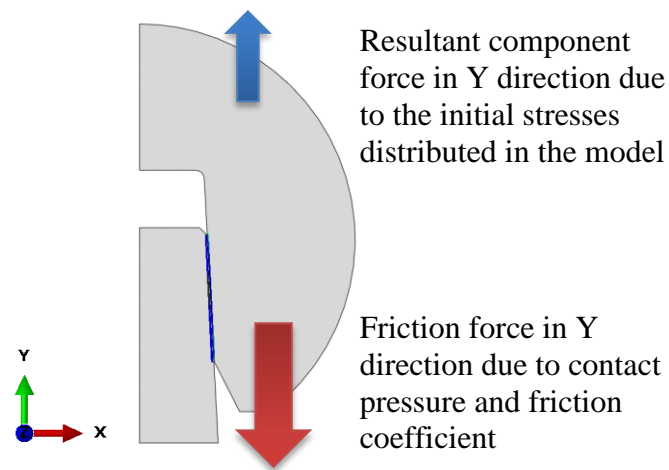


Figure 4-10: Reaction forces generated by overlap analysis

During phase 2 the progressive wear that occurs due to the application of the walking load cycles results in a reduction in the magnitude of the contact stresses at each geometry update. Eventually the wearing process reduces the overlap to such an extent that the associated normal contact forces produce lower friction forces than head reaction forces and at this point the head will lose its fixation to the stem. This loss of fixation generally occurs when the initial overlap is almost completely removed namely “limiting overlap” (although this is also dependant on the total

overlap and the value of the friction coefficient used). At this point it is necessary to move into phase 3 of the analysis.

In phase 3 of the analysis the overlap has been completely removed and only the walking load cycle is applied to the model. It is seen here that due to the removal of the overlap (and therefore loss of the effect of initial fixation), in comparison to phase 2, the contact stresses are reduced in magnitude but the relative displacements of paired nodes have increased by a greater proportion leading to a rise in the wear rate. The significant increase in relative displacements in phase 3 for some sets of paired nodes leads to large differences in wear depth calculations at discrete points across the contact interface leading to an uneven wear pattern. To mitigate against this occurring, the scaling factor is reduced automatically within the algorithm which effectively reduces the wear depth applied for a particular update encouraging the development of a smooth wear pattern. The scaling factor is modified during the wear analysis based on changes in stress and displacement from the previous update. Furthermore, the script is able to reassemble the model automatically if any gap occurs during phase 3 due to the wearing progression.

4.6 Conclusions

It has been demonstrated that the total dissipated energy wear law incorporated into the method can predict linear wear depth and subsequent volumetric wear rate effectively over a period of time when compared to a simple controlled experiments. The comparisons undertaken here showed considerable promise but are clearly dependent on the use of an appropriate wear coefficient and knowledge of the retrieved prostheses' loading history.

The accurate and smooth evolution of wear across the contact interface has been demonstrated with the guideline to refine the mesh in the contact zone to an element size of 0.2mm to avoid local ‘spikes’ in the contact stresses due to too larger element size.

The methodology and FE model incorporates the effect of initial head-stem assembly in surgery on the wearing process by modelling this effect as a static overlap analysis procedure. The work presented here shows that a static overlap analysis can model this effectively. The wear algorithm removes the effect of assembly impaction as the solution progresses by removing overlap in line with the calculated wear depth for a particular stage of the analysis. As the overlap is removed the contact pressure and shear stresses at the interface decrease, however, the relative displacements increase proportionally more, leading to a greatly increased wear rate.

The advantage of this analysis is the axisymmetric nature of the model. Although this inhibits the application of more realistic loading and boundary conditions (as the loads necessarily needs to be applied in three directions following three rotations), it reduces the computational time and is useful for comparative and parametric studies. As such, the following Chapter will demonstrate a 3D version of this wear model with realistic loading conditions.

Chapter 5

Fretting wear evaluation and evolution at taper junctions of total hip replacements

5.1 Introduction

In this chapter, the computational methodology presented in chapter 3 is used to predict fretting wear at the taper interface between the head and stem of THRs using a 3D FE model. The following sections are presented to demonstrate and discuss key features and functionality of the methodology and the findings from the THRs taper junction wear analysis on the 3D model with realistic loading conditions applied in three directions following three rotations.

5.2 Wear analysis input

The input data shown in Table 5-1 is used for the 3D wear analysis. The realistic gait cycle loading and rotation (as shown in Figure 3-7 and Figure 3-8) applied to the FE model over 1.2 second duration.

The wear analysis for this 3D model has been considered up to 5 million load cycles. This is because the instances of premature failure of these implants (<5 years) has been reported and attributed to aseptic loosening (Langton et al., 2011, Mattei et al., 2011). Based on the impaction analysis in phase 1, the overlapped model is prepared for the wear analysis in phase 2.

Table 5-1: Input data for 3D wear analysis

	Input data
Model	3D (see Figure 3-9)
Material combination	Head: Cobalt-chrome Stem: Titanium (see Table 3-1)
Impaction force	4000N (Figure 3-5)
Walking load and boundary conditions	Loads with relative rotations (see Figure 3-7 and Figure 3-8)
Wear law	Dissipated Energy
Wear coefficient	$2.97 \times 10^{-8} \text{ MPa}^{-1}$
Wear fraction	Cobalt-chrome: 0.9 Titanium: 0.1
Scaling factor	10^5
Number of load cycles	5×10^6

The time taken for each 3D analysis “stage” was on average around 6 hours (slightly longer in phase 3) on the system specification mentioned in section 3.10. Therefore, for an analysis of 5 million cycles (5 years), there would be 50 “stages” summing to a total run-time of 300 hours.

5.3 Results and discussion

Similar to what has been explained in Chapter 4, in this Chapter instead of presenting shear traction that was used to calculate the wear depth, all the results shown are based on contact pressure distribution for clarity. This is because in 3D models, contact shear stress has two components tangential to the contact surface and can be either positive or negative based on direction. Due to this fact, this has been found difficult to interpret in the context of wear and so contact pressure has been presented instead.

As values for relative displacement and contact pressure will be equal and opposite on the head and stem taper surfaces, the change in relative displacement (or ‘slip’) is shown on figures as distributed on the stem trunnion, whereas the variation in contact pressure is shown only on the head taper surface.

5.3.1 Variation in contact pressure and relative displacement during the walking cycle

In Figure 5-1 the distributions shown at time interval zero seconds are those determined from the initial static contact analysis (the contact conditions immediately after assembly of the head onto the stem). It can be seen that both the contact pressure and ‘slip’ distributions are symmetrical (as expected) and that maximum values occur at the edges of the taper contacts (both proximal and distal)

with values of around 350MPa and $9\mu\text{m}$. The majority of the taper surface is subject to a contact pressure of around 120MPa , whereas the relative displacements are seen to reduce in magnitude from the taper edges to the taper central contact.

Figure 3-7 in section 3.4.5 indicates that the largest loading on the hip occurs in the “superior-inferior” direction with the load increasing to its largest magnitudes between time intervals of 0.3s and 0.7s of the gait cycle (the same could “loosely” be said about loading in the “medial-lateral” and “anterior-posterior” directions too).

Without considering the edge contacts, it can be seen that during the gait cycle the distribution of contact pressure changes, such that the largest pressures occur at the centre of the taper “superior” surface (right hand side of taper plots), and the lowest values occur at the centre of the taper ‘inferior’ surface (left hand side).

The maximum value for contact pressures occur between 0.3 and 0.7 seconds (240MPa at 0.72s) in parallel with the applied loading. The relative displacements are seen to vary throughout the gait cycle with the largest values due to edge contact ($9\mu\text{m}$) occurring also during the time intervals when the loading is maximum (0.3 to 0.7s) and reducing nearer to the end of the cycle. It can be observed that the micromotion values are very small as these distributions are those occurring immediately after impaction.

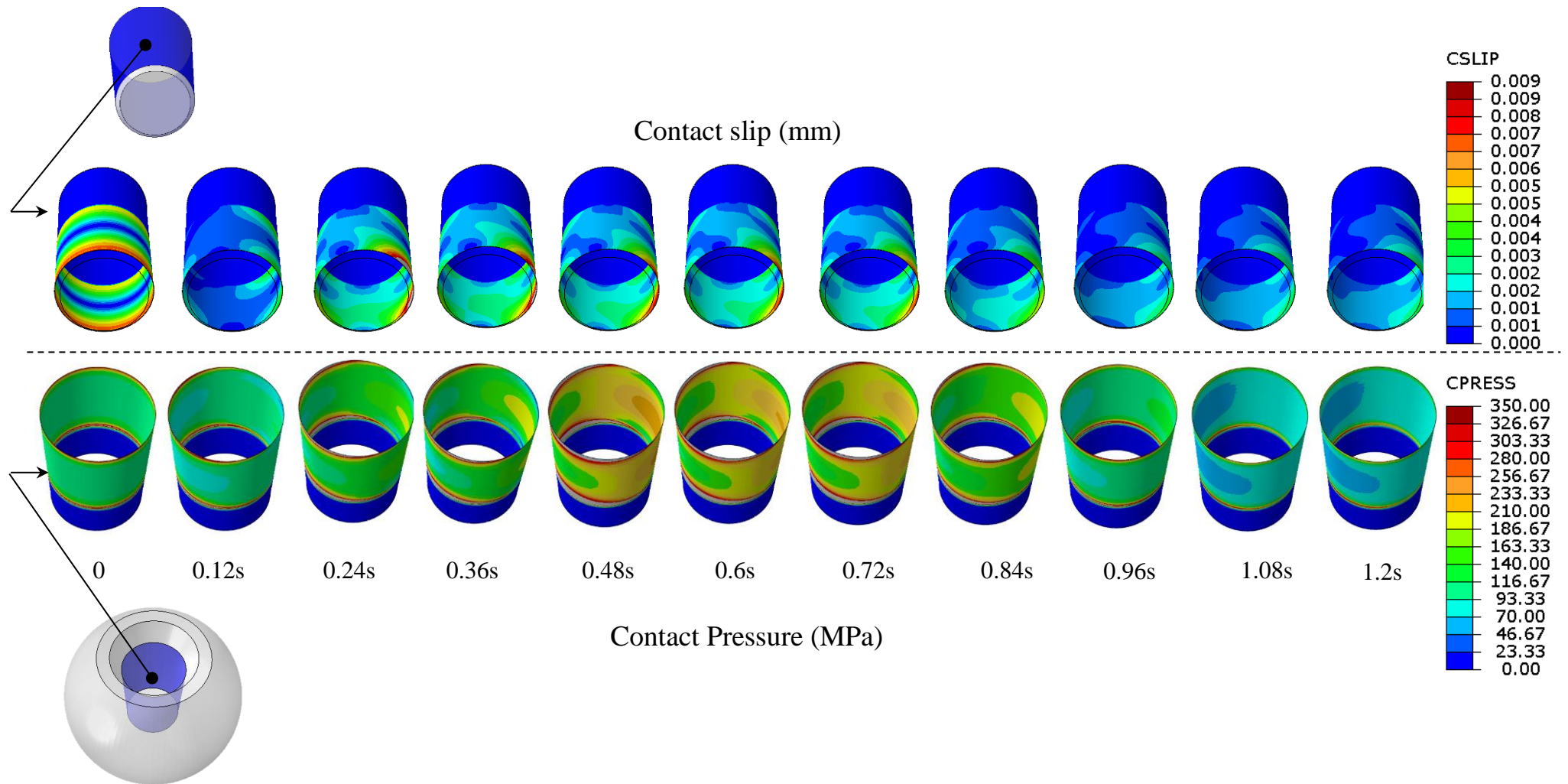


Figure 5-1: Variation in contact pressure and relative displacement during a walking cycle

5.3.2 Variation in taper wear over 5 year period

Figure 5-2 shows the variation of contact pressure and relative displacement as well as the evolution of taper wear over a five year period of time. During the first 2.6 million cycles of loading it can be seen that the contact pressure generally reduces from the initial uniform distribution of $120MPa$ following assembly (Figure 5-1) to a non-uniform distribution with the majority of the taper surface subject to contact pressure values of around $30MPa$ at the last time interval (Figure 5-2c). Conversely, the ‘bulk’ values of taper relative displacement (‘slip’) are seen to increase during the same time period from a value of around $2\mu m$ (Figure 5-1) at assembly to around $38\mu m$ at 2.6million cycles (Figure 5-2b). This reduction in contact pressure and increase in ‘slip’ is due to the gradual weakening of the taper fixation (modelled by a reduction in mesh overlap due to wear) with respect to time. At 2.6million cycles the initial overlap has been completely removed and the analysis moves from phase 2 to phase 3 of the methodology.

During the loading period 3 to 5million cycles the contact pressure distribution remains relatively constant with only a small reduction in contact pressure. During the same time period the relative displacements continue to increase on the inferior taper surface (left side) with values approaching $100\mu m$ in localised areas ; on the superior taper surface (right side) the values of ‘slip’ tended to decrease with localised areas indicating values of between 0 and $30\mu m$. The greater relative increase in ‘slip’ with minimal change to contact pressure in phase 3 creates an increase in wear rate in localised areas.

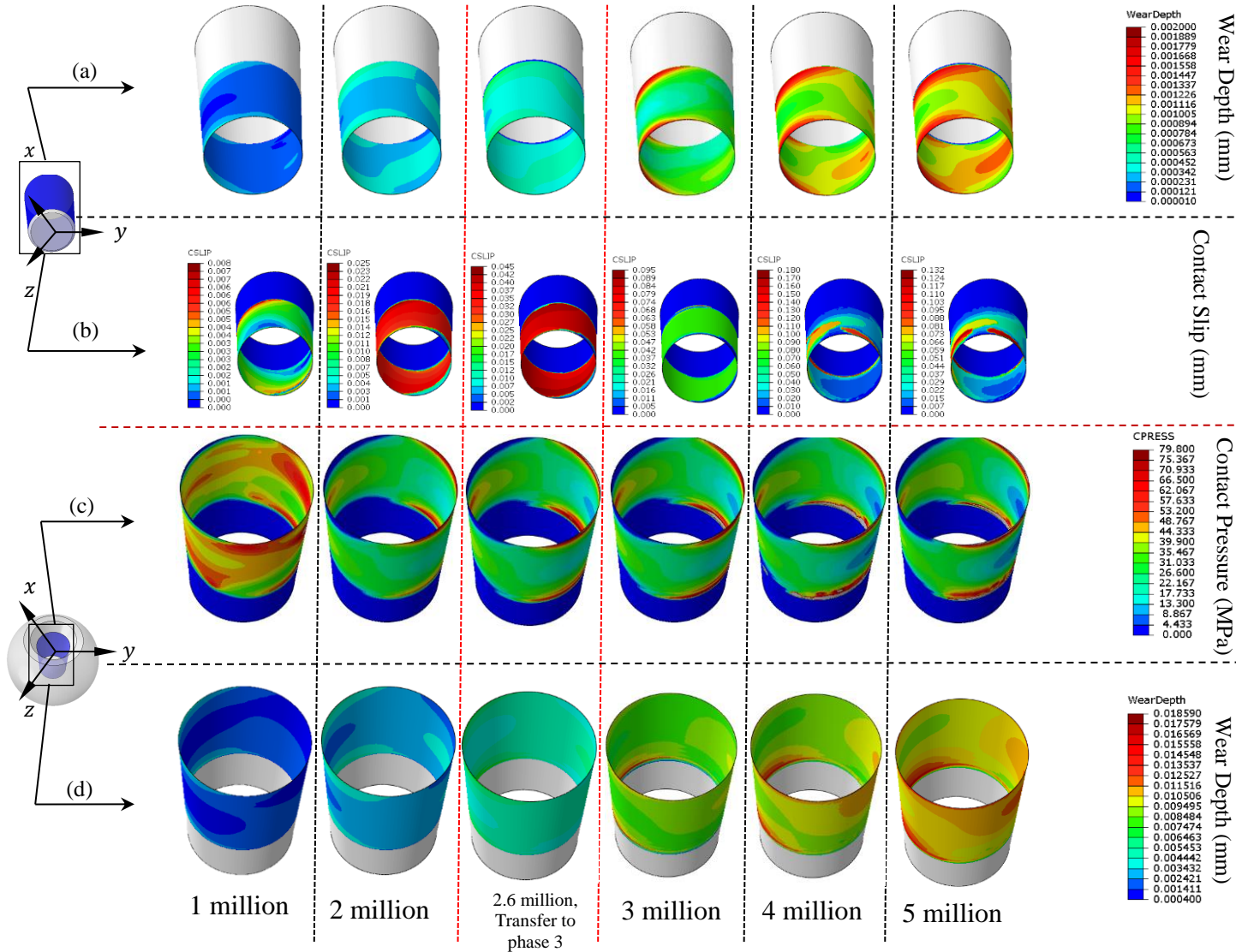


Figure 5-2: Evolution of contact pressure, slip and wear pattern during wear analysis, row (a) and (b) show the pattern of wear depth in mm and contact slip changes on the stem trunnion, row (c) and (d) show the contact pressure in MPa and the pattern of wear depth in mm on the head taper, results shown at the last time interval

It can be seen from Figure 5-2 that the wear depth on the titanium stem trunnion (Figure 5-2a) and in the cobalt chrome head taper (Figure 5-2d) at 5 million cycles are different by a factor of around 10 (as dictated by the ‘wear fractions’ associated with each part) at $2\mu\text{m}$ and $18.6\mu\text{m}$ respectively on the inferior surface taper edges (left hand side of plots). It is necessary in the wear analysis of metal head-stem taper junctions (and for MoM prostheses) to update the contact surface geometry of both parts of the prosthesis as this has an effect on the wear rate and wear pattern following each analysis “stage”. The wear pattern develops from a uniform zero wear pattern at the outset of the study to a non-uniform pattern with maximum wear occurring at the taper edges and on the superior surface of the taper, and minimum wear on the inferior surface at 5million cycles (5 years).

5.3.3 Volumetric and linear wear rate

The volumetric wear rate was determined based on the reduction of element volume for all elements in the contact zone. The volumetric wear rate was calculated following each 1million cycles as the solution progressed (Figure 5-3). It can be seen that the lowest wear rates occurred during the first 2 years (2million cycles) with total values of 0.4 and $0.36\text{mm}^3/\text{yr}$. Subsequently it can be seen that the wear rate increases to a value of $0.66\text{mm}^3/\text{yr}$ at 4 years. This is around a 50% increase in the wear rate and can be attributed to the removal of the initial taper locking effect and the subsequent increase in relative displacement at around 2.6million cycles.

The increase in wear rate can be linked to a “transition” point whereby the initial locking effect of the head-stem taper has been fully removed and increased micromotion occurs resulting in an increase in wear rate.

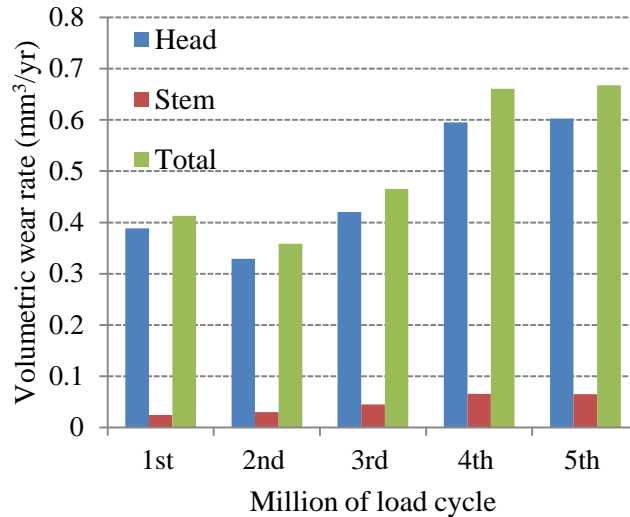


Figure 5-3: Variation in volumetric wear rate with respect to time

Table 5-2 details the average linear and volumetric wear rates over the 5 year period of study. The wear rates for the head were $1.917\mu\text{m}/\text{yr}$ and $0.467\text{mm}^3/\text{yr}$, whereas the stem wear rates were $0.213\mu\text{m}/\text{yr}$ and $0.0459\text{mm}^3/\text{yr}$.

Table 5-2: Average linear and volumetric wear rate on head taper and stem trunnion

	Head (Co-Cr)	Stem (Ti)	Total
Wear fraction	0.9	0.1	1
Average linear wear rate ($\mu\text{m}/\text{yr}$) (range)	1.917 (0.8 – 18.5)	0.213 (0.01-0.4)	N/A
Average volumetric wear rate (mm^3/yr) (range)	0.467 (0.329 – 0.603)	0.0459 (0.024 -0.065)	0.513

5.4 Validation

The results for taper wear (Figure 5-2) determined from the numerical wear analysis can be compared favourably with images and measurements from retrieved prostheses (retrieval prior to 5 years service). Figure 5-4 shows a comparison of the wear patterns associated with the numerical analysis and images of wear occurring on the head taper of a retrieved Birmingham XL femoral head. Several retrieved prostheses were available for inspection, all of which demonstrated similar wear damage as that shown in Figure 5-4.

It can be seen in Figure 5-2 that the wear pattern at any stage of phase 3 of the numerical analysis tends to be fairly constant and can be effectively compared against the wear observed in retrieved prostheses where common wear patterns tend to prevail too (as walking is overwhelmingly the most common activity in patients with a hip implant). Observation of Figure 5-4 shows that the extent of wear damage and patterns on the FE model are similar to the areas of wear shown on the images of the retrieved prosthesis.

The wear damage seen on the surface of the retrieved prosthesis has been categorised as severe, moderate and minor. In the areas of severe wear it is likely that initial adhesive wear due to fretting has developed into abrasive wear due to retained wear particles which have subsequently promoted corrosion. In the areas shown as having moderate damage it is possible that any wear particles have been able to exit the contact zone so exhibiting a less damaged surface likely generated by adhesive wear and corrosion.

The smooth surface highlighted as minor wear will be the result of adhesive wear only. It can be seen that the wear algorithm has identified accurately the areas of severe, moderate and minor wear damage based purely on the assumption of mechanical fretting wear. This is to be expected as any corrosion occurring on the taper surface will be due to Mechanically Assisted Crevice Corrosion (MACC) whereby fretting wear continually disrupts the protective surface oxide passivation layer of the taper junction materials exposing the metal and making it more susceptible to corrosion.

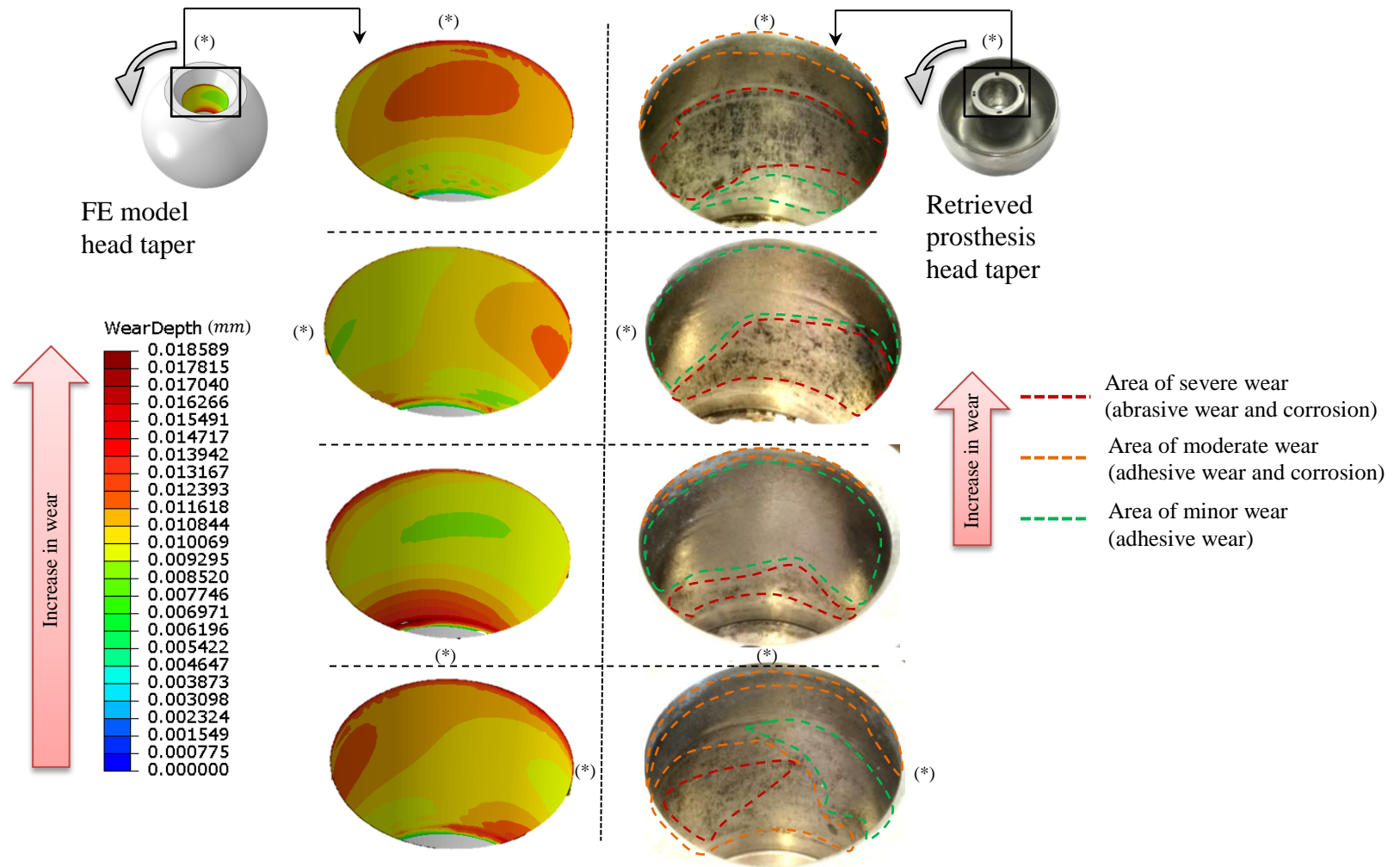


Figure 5-4: Validation against retrieved prostheses; figures are rotated anticlockwise based on a label shown as (*)

In addition to these observations, the wear pattern and wear rates determined in these studies are similar to those obtained by Langton et al. (2012) for measurements obtained for retrieved Articular Surface Replacement XL THRs (ASR; DePuy, Leeds, United Kingdom). Langton et al. (2012) used a highly accurate CMM (accuracy $0.8\mu\text{m}$) to measure linear and volumetric wear occurring at the head taper surface of retrieved large diameter MOM THRs (Articuleze (48 components) and ASR XL (63 components), Depuy). The median time *in vivo* for the Articuleze and ASR XL prostheses was approximately 1 to 5 years respectively with the mean volumetric wear rate for Articuleze being $0.127\text{mm}^3/\text{yr}$ (range 0.01 – 3.15) and the ASR XL measured at $0.44\text{mm}^3/\text{yr}$ (range 0.02 – 8.34). The small differences in volumetric wear rate determined in this study (see Table 5-2) in comparison to Langton et al. (2012) can be attributed to differences in the head-stem material combinations, wear coefficient, material loss due to corrosion and THR design. In addition, the effect of initial assembly of the head and stem is unclear and could be one of the reasons for the slight differences in wear rates too.

Malviya et al. (2011) also used the same CMM as Langton et al. (2012) and presented the wear pattern on the 2-year follow up of a retrieved Birmingham hip replacement . The investigation showed no material loss or corrosion on the articular bearing surfaces, but a wear depth of $6\mu\text{m}$ on the head taper. The wear pattern shown in Figure 5-2 at 2 million load cycles (2 years) on the head taper is within the same range of wear depth presented by Malviya et al. (2011). The results obtained are also comparable with the experimental results demonstrated by Hart et al. (2013) and Matthies et al. (2013).

Figure 5-5 shows a comparison between FE wear simulation and CMM measurement (after Langton et al. (2012)). The wear pattern damage obtained here compares favourably with the CMM measurement results. Figure 5-5a shows the FE fretting results after applying 3.9million walking load cycles. Figure 5-5b shows the CMM measurement on a retrieved prosthesis that had been in service for less than 5years⁵ (the exact loading history is not available).

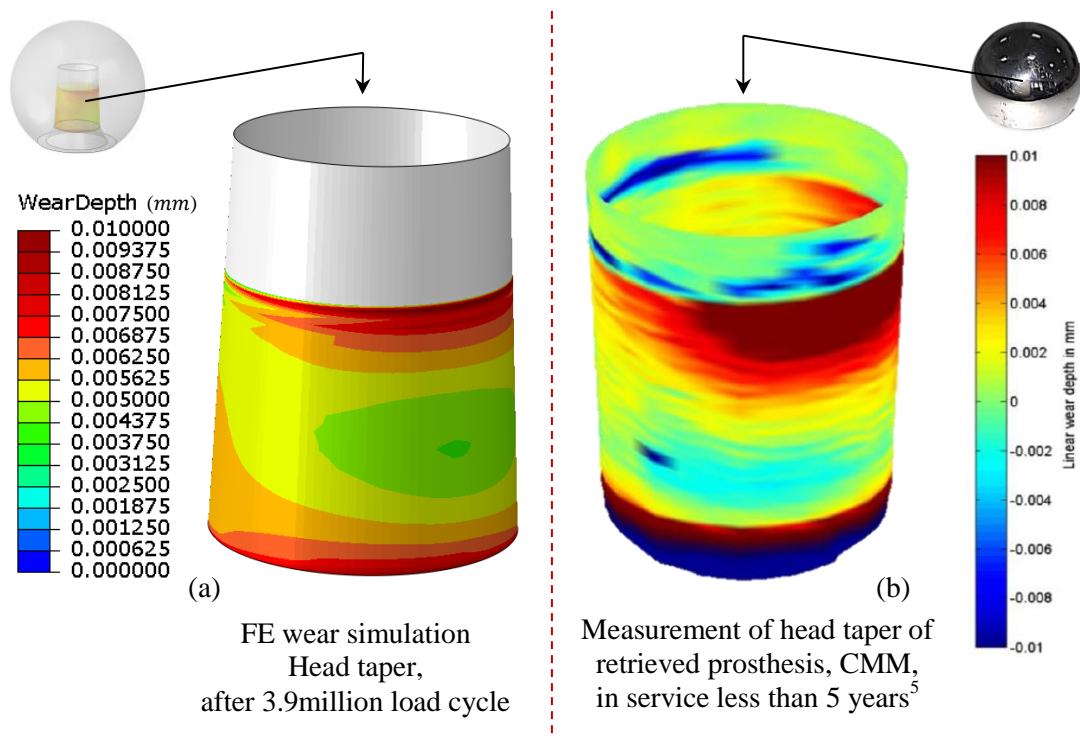


Figure 5-5: (a) wear modelling and (b⁵) coordinate measuring analysis of the retrieved head taper

The close similarities shown between the numerical analysis and the observed and measured wear damage of retrieved prostheses demonstrates the effectiveness of the 3D FE model, loading, boundary conditions and wear algorithm used.

⁵ Figure 5-5b was contributed by Prof Thomas Joyce and Mr David Langton, Newcastle University, Newcastle upon Tyne, UK, and it is reproduced here with permission.

5.5 Conclusions

A 3D FE model of a commercial THR is used to demonstrate the method and to highlight key features of the wear algorithm. The wear damage, depth, rate and patterns of wear are shown to be comparable with those found in the literature and from observation from available retrieved prostheses.

The methodology demonstrates that a static contact analysis incorporating mesh overlap can effectively model taper fixation (created during assembly of head and stem in surgery) and also the progressive weakening of this fixation due to the wearing process. This is achieved by removing overlap in line with calculated wear as the solution progresses and is seen as a novel aspect of the wear method described.

The total dissipated energy wear law and the 3D FE model described can predict linear wear depth and damage patterns effectively when compared to typical observed wear patterns and measured wear depths from retrieved prostheses. The comparisons undertaken show considerable promise but are clearly dependent on the use of an appropriate wear coefficient and knowledge of the retrieved prostheses loading history. Accurate determination of wear of individual THR components can be realised by measurement from retrieved prostheses or from fretting wear tests. These measurements can then provide accurate wear fractions for application in computational wear analysis.

In addition, it should be noted that the wear coefficient α is related to the component pair in contact and is used in the calculation of total wear, it does not differentiate as to the extent of wear occurring on each surface, as such, the use of component “wear fractions” is required.

The accurate and smooth evolution of wear across the contact interface has been demonstrated with the guideline to incorporate a highly refined mesh in the contact zone to avoid local “spikes” in the contact stresses due to a too large element size. Further, the wear scaling factor used in the analysis has a major effect on simulation run times and can affect the accuracy of the analysis results and the evolution of wear. A too large scaling factor can create an uneven wear profile across the contact interface due to cyclic wear “hot spots” being overtly increased. In contrast, a comparatively small scaling factor will facilitate an accurate and smooth development of wear but with the cost of a much increased run time. In this specific application, a scaling factor of 0.1million was appropriate.

Chapter 6

Effect of different taper fixation of the head and stem on the extent of fretting wear

6.1 Introduction

Non-standard assembly of the prosthesis femoral head onto the stem taper during surgery is known to have an effect on the stability of the fixation. As discussed in Chapter 2, the effect of variability of impaction forces on fretting wear is unclear and could be one of the reasons for higher initial wear rates (Wassef and Schmalzried, 2013). This chapter investigates and compares the effect of varying the initial head-stem assembly from a hand press force up to a high impaction force ($6kN$) on the extent of subsequent fretting wear. This chapter also describes key aspects and considerations regarding the impaction tests, pull off tests and the results obtained from the computational impaction and wear analysis that is described in Chapter 3, with regard to the effect of magnitude of assembly force on fretting wear. The results

obtained have been compared with observation and also measurement of fretting wear damage of available retrieved prostheses.

6.2 Experimental procedure

Several impaction tests were performed to determine typical impact magnitudes that could be applied during the surgeries. After impaction tests, pull off tests were performed to determine the stability of the fixations. As discussed in Chapter 2, in order to assemble a head to a particular stem, manufactures usually provide general and vague guidelines for surgeons with statements such as “slightly” or “firmly” impacted being the norm to describe the magnitude of any impaction force to be used. In fact, the magnitude of the force used to assemble the components is based on a surgeons’ preference, experience, the type of prosthetic femoral head, and the quality of the patients’ bone stock.

6.2.1 Impaction tests

Figure 6-1 shows a schematic of an impaction applied on the head of a total hip prosthesis. In order to investigate and quantify typical impaction cases, several primary and revision surgeries have been attended at Broadgreen Hospital, Liverpool, UK (2014-2015) to explore what could be a realistic impaction force applied during surgery. After replacing the modular stem and acetabular cup, trial heads are placed on the top of the femoral stem in order to check the size and adequacy of the hip motion. When the appropriate head size is found, the trunnion is being carefully cleaned and dried and the actual head is placed on the stem trunnion. Most of the surgeons normally apply two firm impactions in order to fix the head into the stem trunnion. Some surgeons check the stability of the fixation by hand-pulling the head slightly to be confident of the fixation condition.

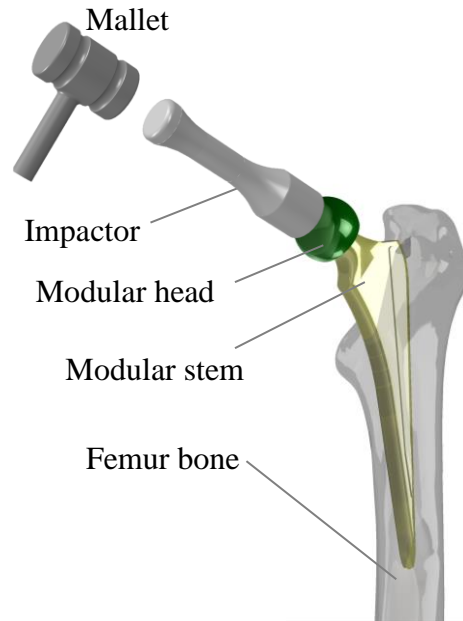


Figure 6-1: Total hip replacement in situ, impaction of the modular head onto the stem trunnion

In addition to the controlled drop test, explained in section 3.4.4, a more realistic experiment has been performed to further investigate the impaction of the head onto a THR stem. In this experiment, a simple model of a head and stem was assembled (just into contact) and placed and fixed on a single-pedestal load cell with a force and moment transducer. Four different scenarios were used to fix the components, namely “hand-press”, “low impaction”, “medium impaction” and “high impaction” (see Figure 6-2). The “low”, “medium” and “high” impactions have physically been assessed and applied based on the observation of the surgeon’s performance during the primary total hip replacements.

For all of the impaction cases, a mallet and impactor was used as shown in Figure 6-2. A hand press, although it is rare in clinical practice, was also performed in this experiment. For each scenario, the experiments have been performed several times to determine the approximate magnitude of the different assembly forces.

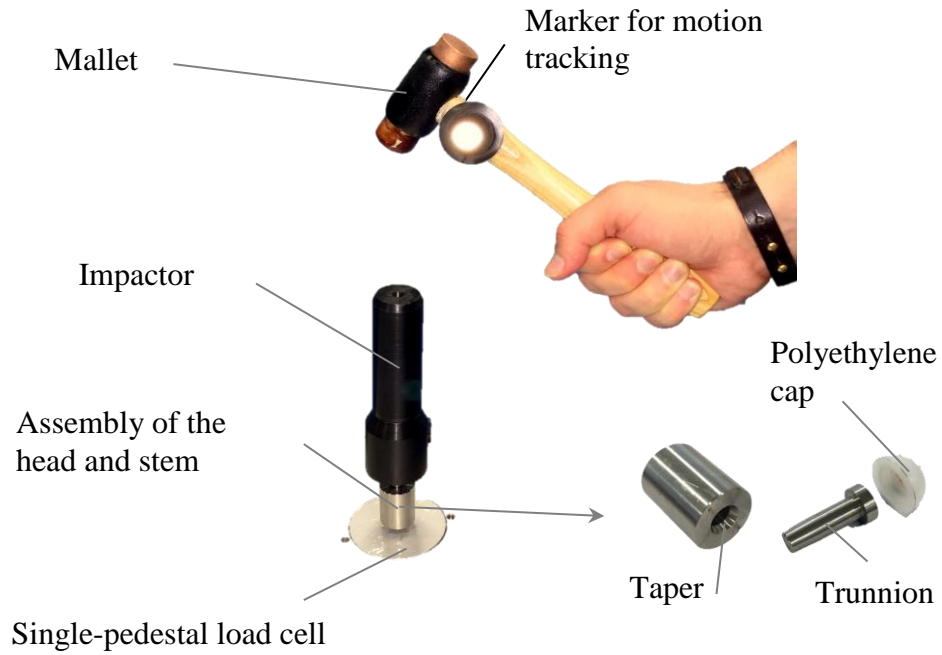


Figure 6-2: Impaction experiment on single-pedestal load cell

Considering the hand press assembly case, the loading duration was recorded for around 2 seconds. The amplitude of the force is shown in Figure 6-3 with the peak force being recorded as 160N.

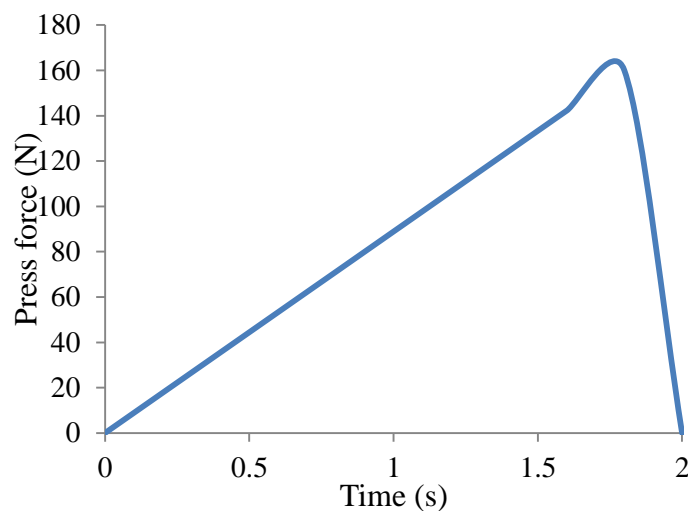


Figure 6-3: hand press load (press-fit) amplitude

For low impaction cases, peak forces between 1.6 to 2.2kN were recorded giving an approximate load amplitude as shown in Figure 6-4 with a maximum value of 2kN

(the curve has been modified to remove noise). Impaction forces between 3.5 to 4.4kN and 5.9 to 6.7kN were recorded for the medium and high impaction cases respectively. Therefore, impaction forces of 2, 3, 4 and 6kN have been defined for “low impaction”, “medium impaction” and “high impaction” respectively (see Figure 6-4).

On consideration of 6kN impaction force, it would seem prudent to apply as large an impact force at assembly as possible within the limits of safety for the patient and structural integrity of the prosthesis design.

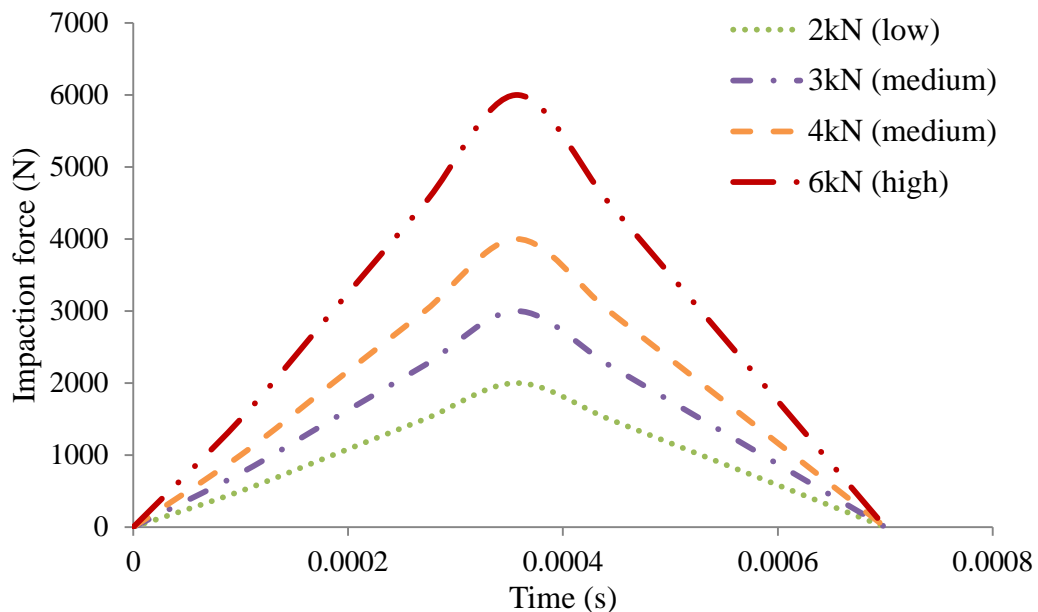


Figure 6-4: Approximate average impaction force from tests

6.2.2 Pull-off test

The effect of varying the assembly forces has an effect on the stability of the taper trunnion connection and has typically been assessed and based on the pull-off force after assembly in the literature (Heiney et al., 2009, Pennock et al., 2002, Rehmer et al., 2012, Lavernia et al., 2009) (section 2.6.2).

A Tinius Olsen tensile testing machine (H50K-S UTM Benchtop Tester) was used to determine the magnitude of pull-off forces for the assembly described in section 6.2.1 (see Figure 6-5). An average pull-off force around 40% to 47% of the impaction force was recorded for all of the different test assemblies.



Figure 6-5: Tinius Olsen, tensile testing machine

Based on this experiment, the greater impaction forces have indicated the greater pull-off forces and as such better stability and fixation between the head and stem; however, the effect of different assembly forces on the extent of fretting wear at the taper-trunnion interface has not been reported in the literature. This study investigates how increasing the assembly force could have an effect on the extent of fretting wear damage, wear rate and total volume loss during the wear process.

6.3 Finite element modelling of the initial forces (phase 1)

In phase 1 of the wear analysis, a single separate dynamic implicit impaction analysis is executed with the head and stem initially assembled just into contact. The load histories obtained from the experiments (see Figure 6-3 and Figure 6-4) are used for this analysis. Figure 6-6 shows the variation of contact pressure along the trunnion surface obtained from phase 1 of the wear analysis.

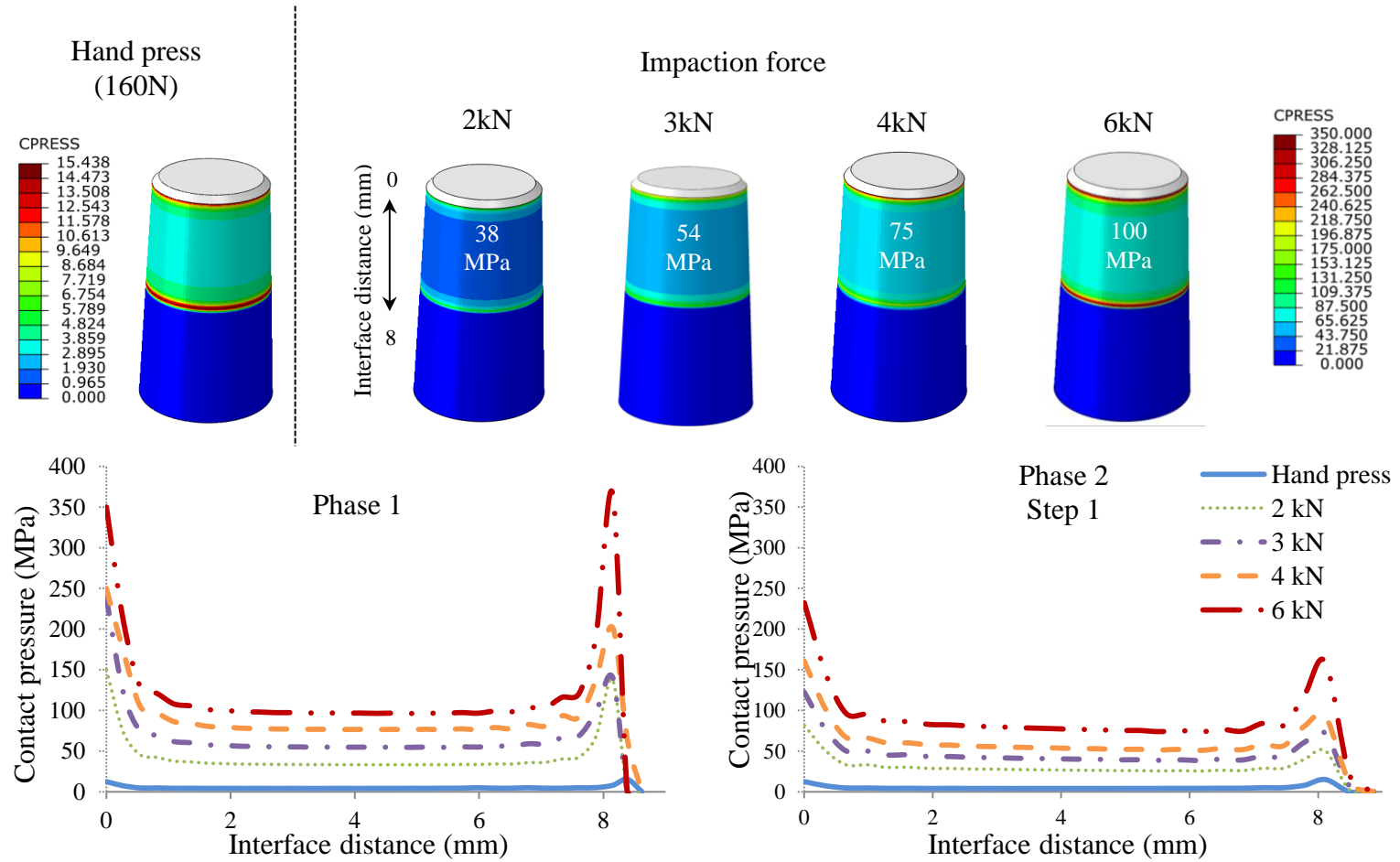


Figure 6-6: Variation of contact pressure for different assembly load (MPa)

The effect of increasing the assembly force from “hand press” (160N) to “high impaction” (6kN) increases the initial contact pressure at the taper-trunnion interface (see Figure 6-6). An increase in the impaction force also results in an increase in the axial displacement that is used to create the static overlap assembly model for phase 2 of the wear analysis.

Figure 6-7 shows the magnitude of the overlap used to start the wear analysis in phase 2. The contact pressures obtained from the impaction analysis are equivalent to those obtained at the end of step 1 (static overlap analysis) of phase 2 of the wear analysis for all specific cases (similar to Figure 3-12).

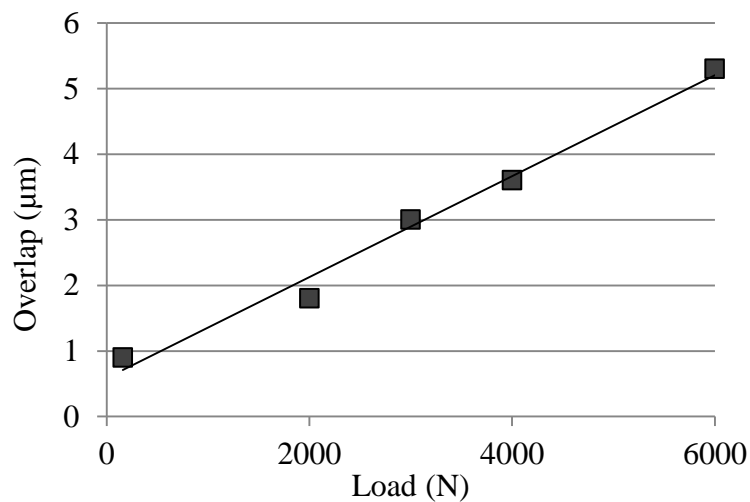


Figure 6-7: Initial overlap created for phase 2 of the wear analysis based on different assembly loads

6.4 Wear analysis input (phase 2 and 3)

The input data shown in Table 6-1 was used for the four different wear analyses, (hand press, 2, 4 and 6kN impaction force).

Each wear analysis took around 300 to 500 hours to simulate fretting wear over 5million load cycles using the computer specification specified in section 3.10.

Table 6-1: Input data for wear analysis

	Input data
Model	3D (see Figure 3-9)
Material combination	Head: Cobalt-chrome Stem: Titanium (see Table 3-1)
Assembly force	Hand-press (160N) (see Figure 6-3) 2000N, 4000N and 6000N (see Figure 6-4)
Walking load and boundary conditions	Loads with relative rotations (see Figure 3-7 and Figure 3-8)
Wear law	Dissipated Energy
Wear coefficient	$1.31 \times 10^{-8} \text{ MPa}^{-1}$
Wear fraction	Head, Cobalt-chrome: 0.9 Stem, Titanium: 0.1
Scaling factor	10^5
Number of load cycles	5×10^6

6.5 Results

Similar to Chapter 4 and 5, contact pressure is used to demonstrate the results rather than shear stress. The contact pressure and relative displacement are symmetrical and opposite on the head taper and stem trunnion, as such the results can be presented on either.

6.5.1 Transition point from phase 2 to 3 of the wear analysis

The transition point is defined as the time at which the wear analysis transfers from phase 2 to 3. This is the time at which the overlap is completely removed from the model and there is no requirement for a static overlap analysis in the further analysis.

At the transition point, it can be hypothesised that the effect of initial assembly has been removed from the model. The transition point is therefore very important as far as the production of wear debris is concerned and its implications to ASTR following arthroplasty.

Maintaining the locking effect due to impaction for as long as possible in phase 2 is the key to reduced wear rates. For assembly forces of “hand press” and impaction of 2, 3, 4 and 6kN, the transition points occur after approximately 0.8, 1.4, 3.1, 4.1 and 6.9 million load cycles respectively (see Figure 6-8).

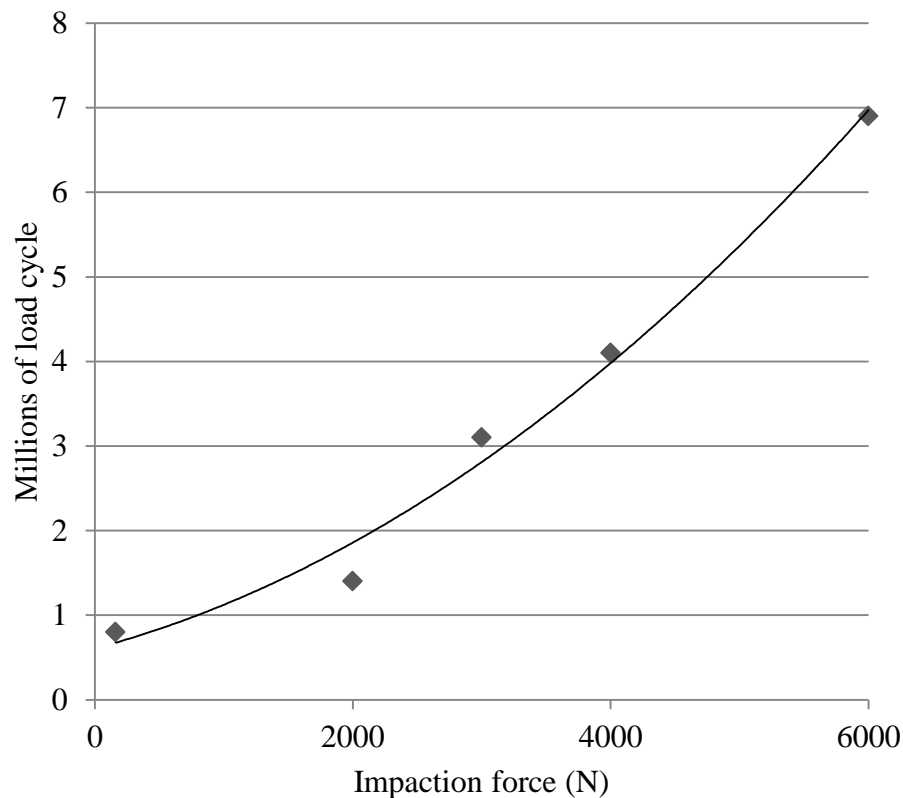


Figure 6-8: Transition point from phase 2 to 3 of the wear analysis

Figure 6-8 shows an early transition into phase 3 for the models assembled using “hand press” force and 2kN force. This subjects the prostheses to a much increased wear rate which could explain the early failure of some devices.

6.5.2 Evolution of wear pattern damage (phase 2 and 3)

Figure 6-9 details the evolution of wear along the head taper over a period associated with 5million load cycles (approximately 5 years of walking activity) following the application of varying head-stem initial assembly forces.

Figure 6-9a (“hand press”) shows that the evolution of wear along the head taper surface is of a fairly smooth wear pattern with a variation of around $1\mu m$ at each million of load cycles. After 5million load cycles, the majority of the head taper surface shows a wear depth of around $8.5\mu m$ (with a peak value of $16.3\mu m$ at the proximal edge of the taper inferior surface).

Figure 6-9b, c and d ($2kN$, $3kN$ and $4kN$ wear analyses) show a similar wear pattern distributed at the taper surface albeit with lower wear depths shown for the $4kN$ impaction analysis. The largest wear damage occurs at the proximal and distal edge of the taper inferior surface for both analyses; however, the edge wear is at its smallest at the distal edge of the taper superior surface for the $4kN$ impaction analysis.

Again, the largest wear depth is distributed at the distal and proximal edge of the taper inferior surface for the $6kN$ analysis (Figure 6-9e). Almost no wear damage occurs at the distal edge of the taper superior surface. This is due to the high contact pressure and very small relative displacement at this area during the time intervals and at each “stage” of the wear analysis.

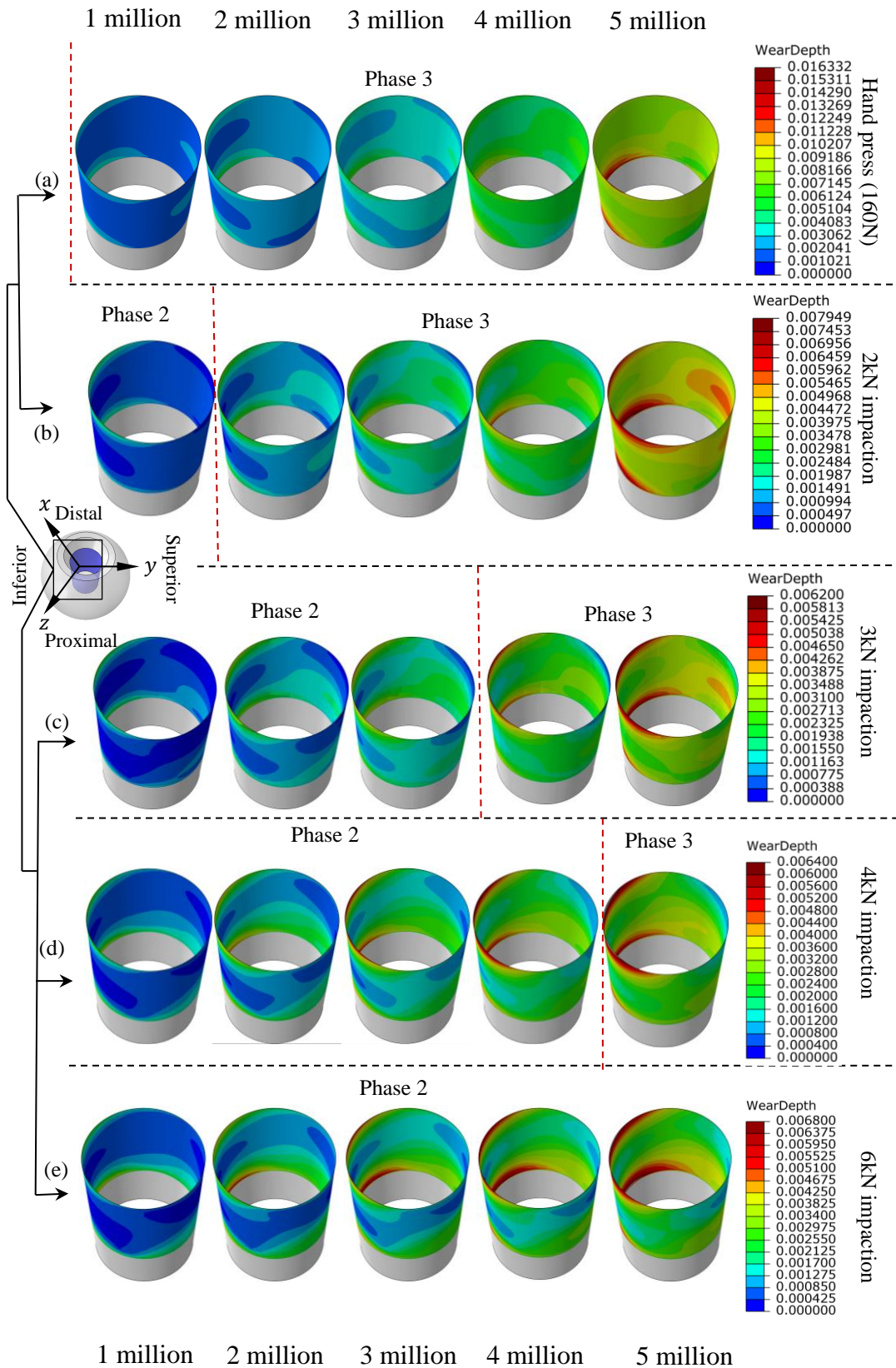


Figure 6-9: Evolution of wear pattern during wear analysis in mm; row (a) for hand press, (b), (c), (d) and (e) for different impaction force, results shown at the last time interval of cycle.

6.5.3 Variation of contact pressure and slip during the wear analysis (phase 2 and 3)

The contact pressure and slip are the key factors to assess the wear depth and rate.

- **Contact pressure**

Figure 6-10 details the contact pressure distribution along the head taper surface during phase 2 and 3 of the analysis. The results are shown at the last time interval of the loading cycle. Figure 6-6 showed that the average contact pressure increases with increasing assembly force (phase 1). This is also the case shown here with the magnitude of the contact pressure increasing with increasing impact force (Figure 6-10 (a) to (e)). Also, it can be seen in Figure 6-10c, d and e that during phase 2 the initial contact pressure reduces continuously until the overlap is removed from the model. In phase 3, the contact pressure distribution remains relatively constant over the contact interface for the remainder of the analysis (see Figure 6-10).

Figure 6-10a shows the variation of contact pressure for the hand press wear analysis. The model transfers to phase 3 at 0.8 million load cycles. The contact pressure, then, remains relatively constant over the taper surface.

Considering the 2kN impaction (Figure 6-10b), the average contact pressure reduces up to 1.4 million load cycles and then remains relatively constant throughout the remainder of the analysis. It can be seen that after 2 million load cycles the maximum contact pressure occurs at the distal and proximal edge of the taper superior surface with values around 91MPa. The majority of the taper surface is subject to a contact pressure of around 42MPa at each analysis stage.

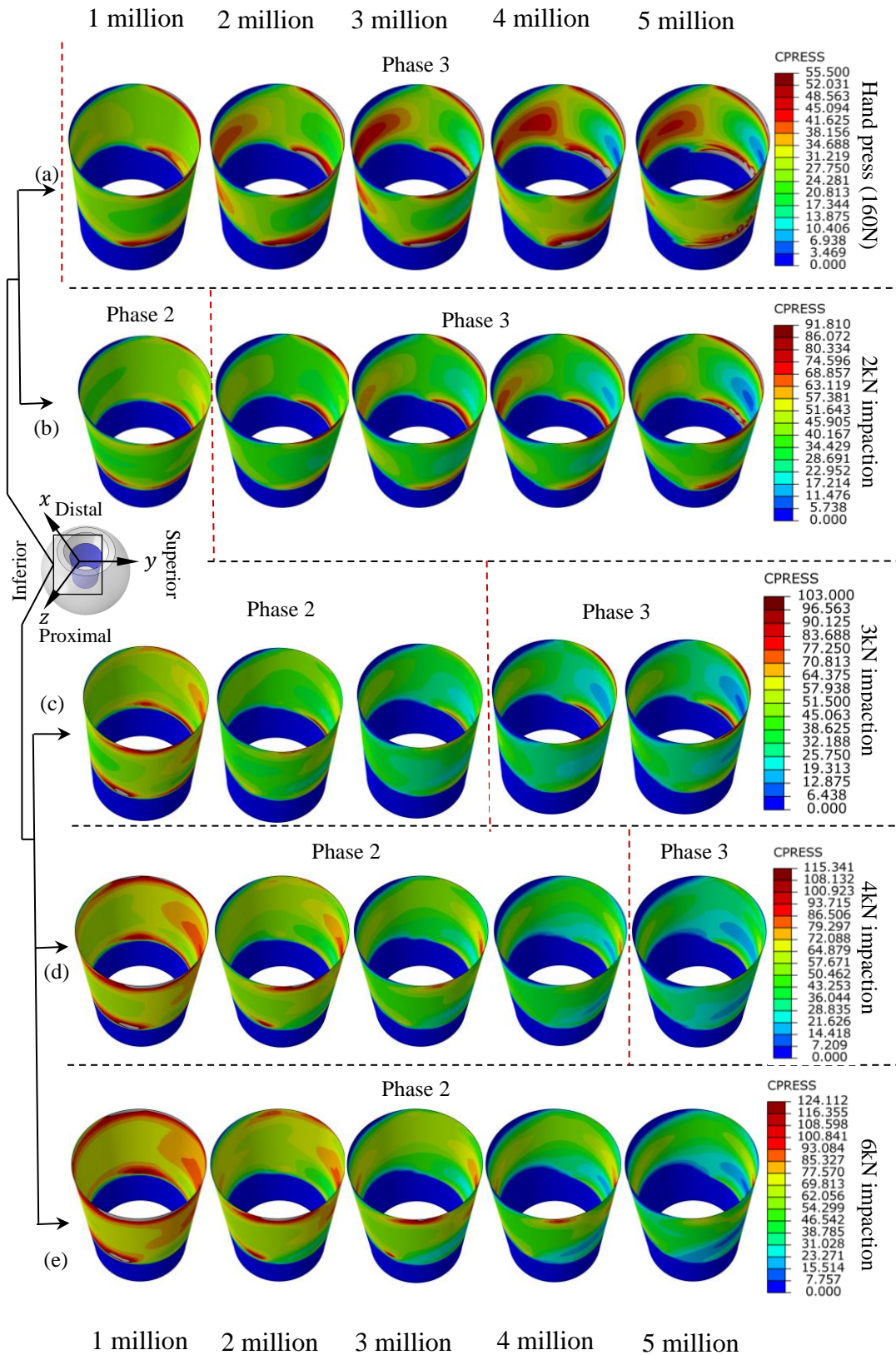


Figure 6-10: Variation of contact pressure during wear analysis in MPa, row (a) for hand press, (b), (c) and (d) for different impaction force, results shown at the last time interval of cycle.

In Figure 6-10 d and e, it can be seen that the average contact pressure reduces during the wear analysis. After applying one million load cycles, the majority of the taper surface is subject to contact pressure of $60MPa$ and $77MPa$ with maximum values of $115MPa$ and $124MPa$ at both proximal and distal edges for the $4kN$ and $6kN$ analyses respectively. The contact pressures then reduce over the duration of the analysis to approximately $36MPa$ and $46MPa$ for $4kN$ and $6kN$ impaction analysis respectively.

- **Contact slip**

Figure 6-11 shows the variation of resultant contact slip which occurs simultaneously with the contact pressure shown in Figure 6-10 (results shown at the last time interval of the loading cycle). Comparing the contact pressure and the slip in Figure 6-10 and Figure 6-11 shows that when the contact pressure is highest the contact slip is correspondingly low.

It can be seen here that as the impaction force increases, the “general” slip magnitude reduces (Figure 6-11 (a) to (e)). Furthermore, it can be seen in Figure 6-11 that, in general, for all cases, the slip increases during the wear analysis.

Figure 6-11a shows that the contact slip increases significantly with a peak value of $0.151mm$ localised at the distal and proximal edge of trunnion superior surface during the analysis.

The magnitude of slip is reduced to peak values of around $0.136mm$ at localised areas on the trunnion superior surface after 5 million load cycles for the $2kN$ impaction analysis. It is further significantly reduced to a fairly uniform value of $8\mu m$ for the $4kN$ wear analysis (see Figure 6-11 (b) to (d)).

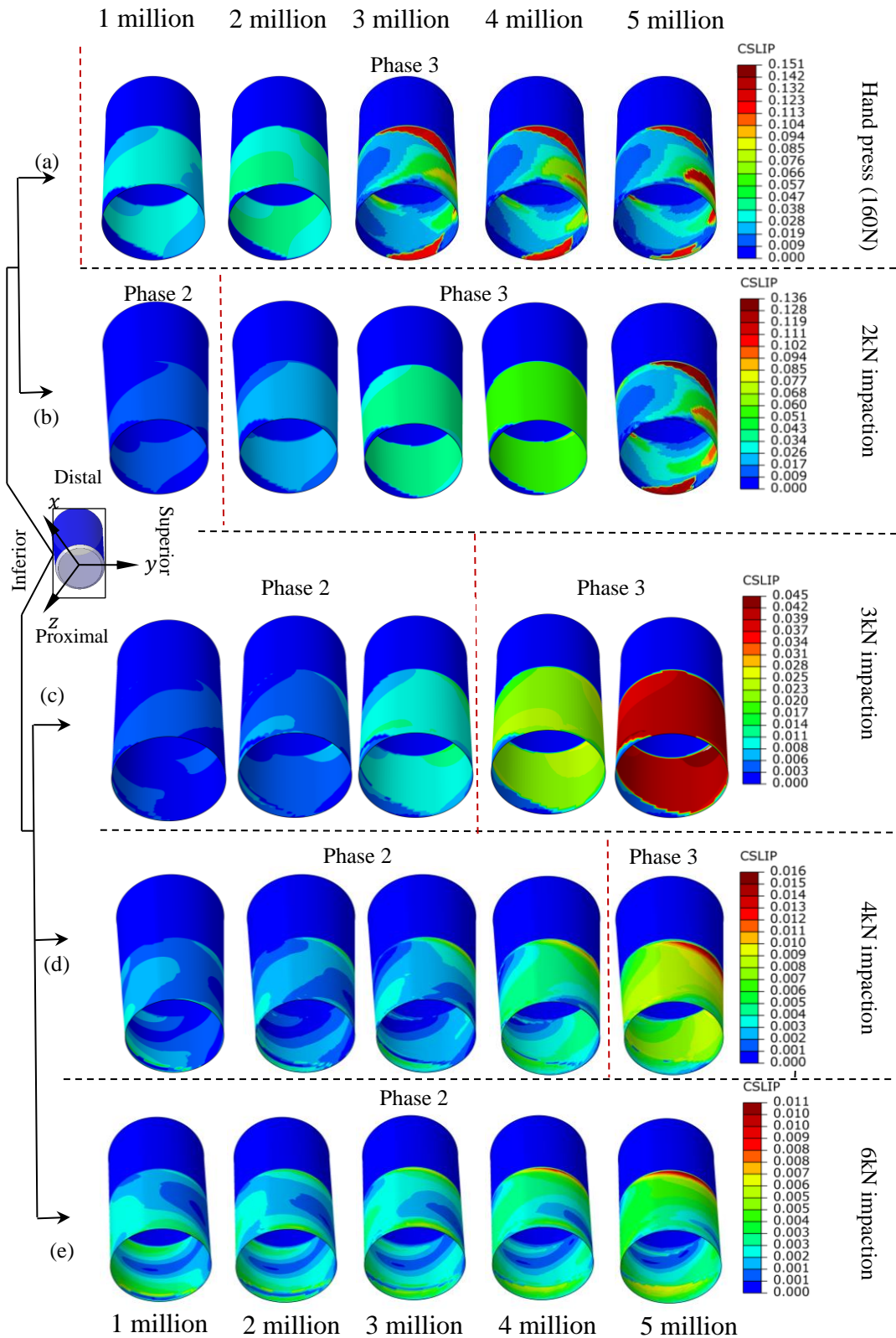


Figure 6-11: Variation of contact slip during wear analysis in mm, row (a) for hand press, (b), (c) and (d) for different impaction force, results shown at the last time interval of cycle.

Figure 6-11e again shows a lower and more uniform contact slip of around $3\mu m$ at the trunnion surface for the $6kN$ impaction analysis. This significant change is due to the early transition into phase 3 for the models assembled using “hand press” and $2kN$ impaction.

In general, it can be said that the contact pressure reduces in phase 2 due to the reduction in initial overlap and then remains relatively constant in phase 3; however, the magnitude of slip is low in phase 2 and then increases significantly in phase 3.

6.5.4 Volumetric wear rate for different impaction loads

Figure 6-12 shows the variation in volumetric wear rate over the period of 5 million load cycles for the different assembly models. In general, it can be seen that in phase 2 of the wear analysis the wear rate is relatively small in comparison to phase 3.

Monitoring the results in phase 2 of the wear analyses shows that increasing the assembly force leads to an increase in the initial contact stresses but a significant reduction in the magnitude of the slip. Progressing through phase 2 of the wear analysis leads to a gradual reduction of the contact stresses (due to the reduction in the initial overlap) and a slight increase in the contact slip. The proportional increase in slip is slightly less than the proportional reduction of contact stresses. For instance, there is 59% reduction in contact pressure (approximately $77MPa$ to $46MPa$) and a 50% increase in slip (2 to $4\mu m$) for the $6kN$ analysis over the duration of the analysis in phase 2. This leads to a continuous (small) reduction in volumetric wear rate in phase 2 of the analysis (see Figure 6-12 for $6kN$ impaction force).

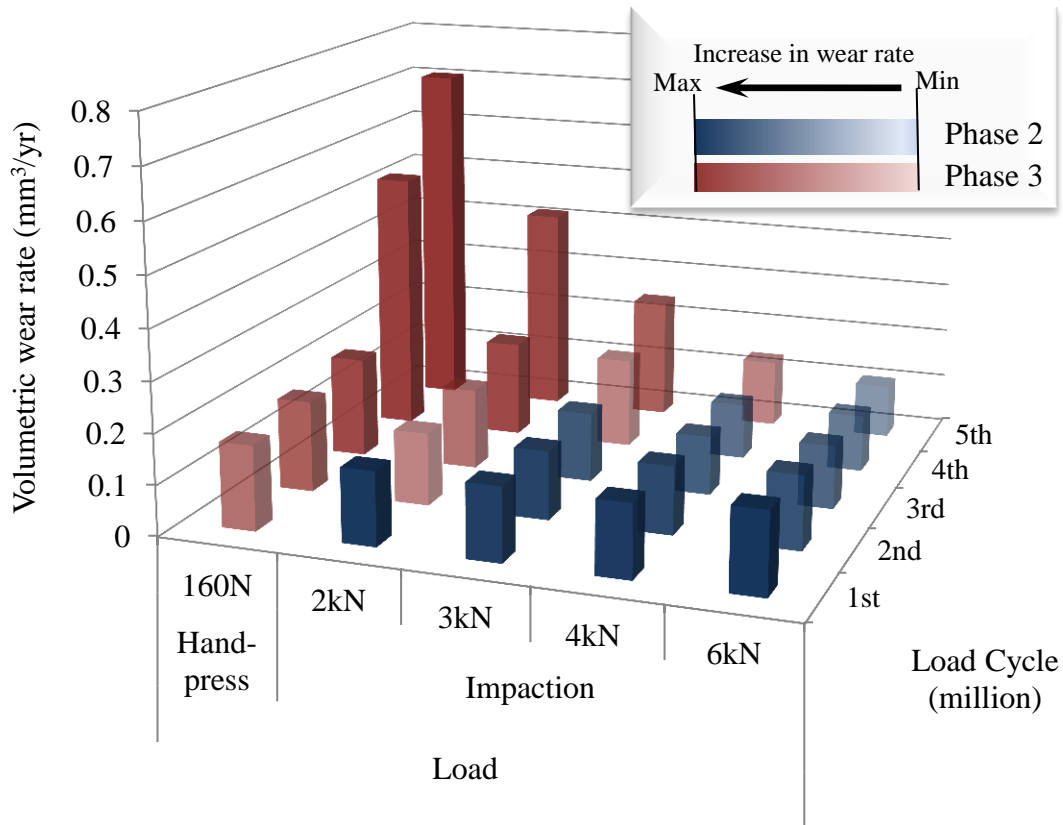


Figure 6-12: Total volumetric wear rate with respect to assembly load and over the wear analysis

Where the overlap is removed completely from the model, the magnitude of slip is increased. Therefore, the wear rate increases at the transition point. This is because the slip increases but the contact pressure stays relatively constant.

After transferring to phase 3 of the wear analysis, the magnitude of the contact stresses remain relatively constant; however, the slip increases significantly. This leads to dramatically increase in wear rate during phase 3 of the analysis (for instance, from the 3rd to 4th, or from the 4th to 5th million load cycles for hand press and 2kN wear analysis respectively, see Figure 6-12).

Comparing the magnitude of contact pressure after each 1 million load cycles, for different assembly forces indicates that from “hand press” to 4kN impaction the initial contact stress at the contact interface increases (see Figure 6-10). This increase

in contact pressure leads to a reduction in the magnitude of the contact slip (see Figure 6-11). The proportional increase in contact stress is lower than the proportional reduction in the magnitude of contact slip. This leads to a reduction in wear rate from “hand press” to 4kN impaction analysis. For instance, during the 3rd million load cycle the wear rate reduces from 0.2mm³/yr to 0.11mm³/yr from hand press to 4kN impaction. Comparatively, from 4kN to 6kN impaction, the contact pressure increases with no significant change in contact slip. This leads to a slightly higher wear rate for the 6kN model than for the 4kN model (0.12mm³/yr during the 3rd million load cycles for the 6kN wear analysis, see Figure 6-12). Further, the total initial overlap is higher for the 6kN analysis which causes the model to stay in phase 2 for a longer time. In phase 2 the wear rate keeps reducing and as such the model will take longer to transfer into phase 3 (the relationship for transferring to phase 3 is not linear as shown in Figure 6-8).

Table 6-2 details the average volumetric wear rates for different initial assembly over a 5-year period. The wear rates were 0.353mm³/yr and 0.213mm³/yr for the hand press and 2kN impaction. The average wear rate, though, is reduced to 0.170mm³/yr, 0.128mm³/yr and 0.132mm³/yr for the 3, 4 and 6kN impaction assembly respectively (slightly higher for 6kN due to the larger overlap and higher initial contact pressure).

Table 6-2: Average of total volumetric wear rate

	Hand press	2kN	3kN	4kN	6kN
Wear rate (mm ³ /yr)	0.353	0.213	0.170	0.128	0.132

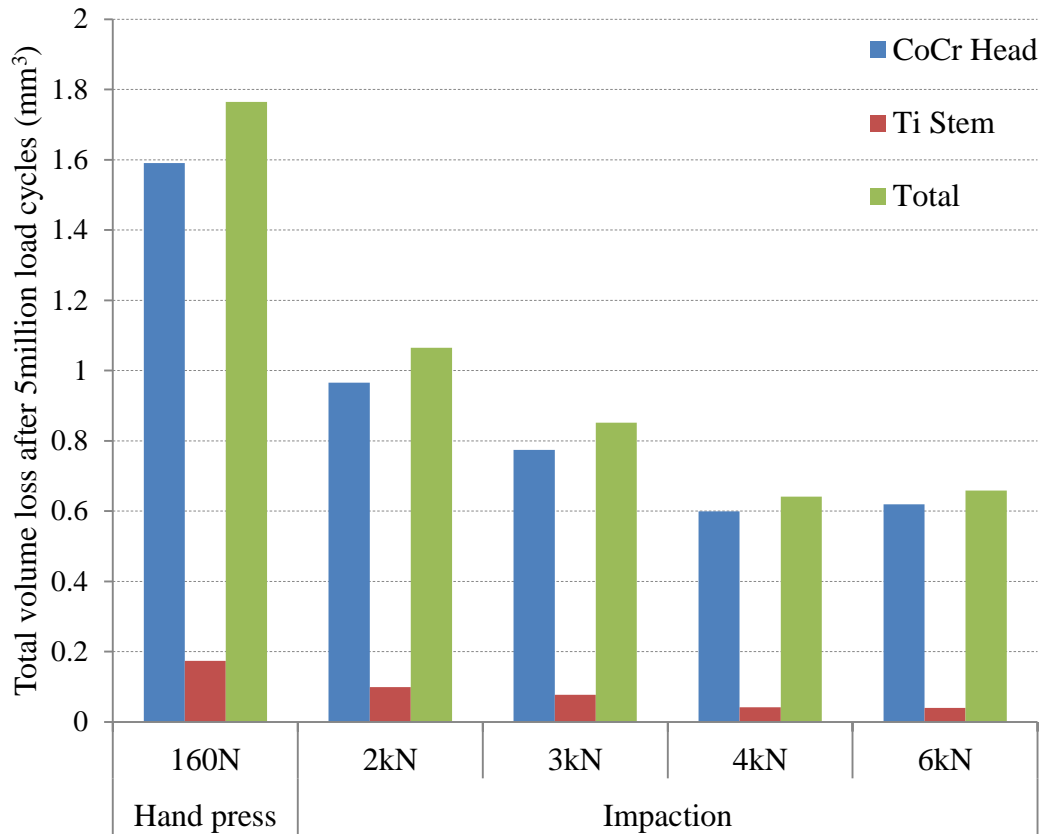


Figure 6-13: Total volume loss after 5million load cycles for different assembly forces

Figure 6-13 details the total volume loss after application of 5million load cycles for the different assembly forces from the cobalt chrome taper, titanium trunnion surface and in total. The highest material loss occurs for “hand press”, the material loss then reduces as the assembly force increases up to 4kN. Similar volume loss can be seen for the 4kN and 6kN impaction analysis.

6.6 Validation

The results for taper wear obtained in this study from the numerical wear model can be compared with observation and measurements of retrieved prostheses.

Sixteen retrieved prostheses have been scrutinised in order to determine the possible fretting wear damage that could occur on the taper surface. Twelve of those have

shown similar fretting wear damage as seen in Chapter 5 (see Figure 5-4). The observation of these twelve retrieved prostheses have shown high fretting wear damage on the taper inferior surface and comparatively lower wear damage on the taper superior surface. Circumferential edge wearing has also been observed on all of these twelve prostheses.

In this study, the fretting wear damage obtained from the 2kN to 4kN impaction wear analyses has shown fairly similar wear patterns to those observed on the 12 retrieved prostheses (similar to what has been shown in Chapter 5, Figure 5-4).

Nonetheless, the 2kN impaction wear analysis shows higher circumferential edge wear damage than the 4kN impaction analysis. Observation of five (out of 12) retrieved prostheses has shown similar edge wear which is higher on the taper inferior surface and slightly lower on the superior surface (see Figure 6-14).

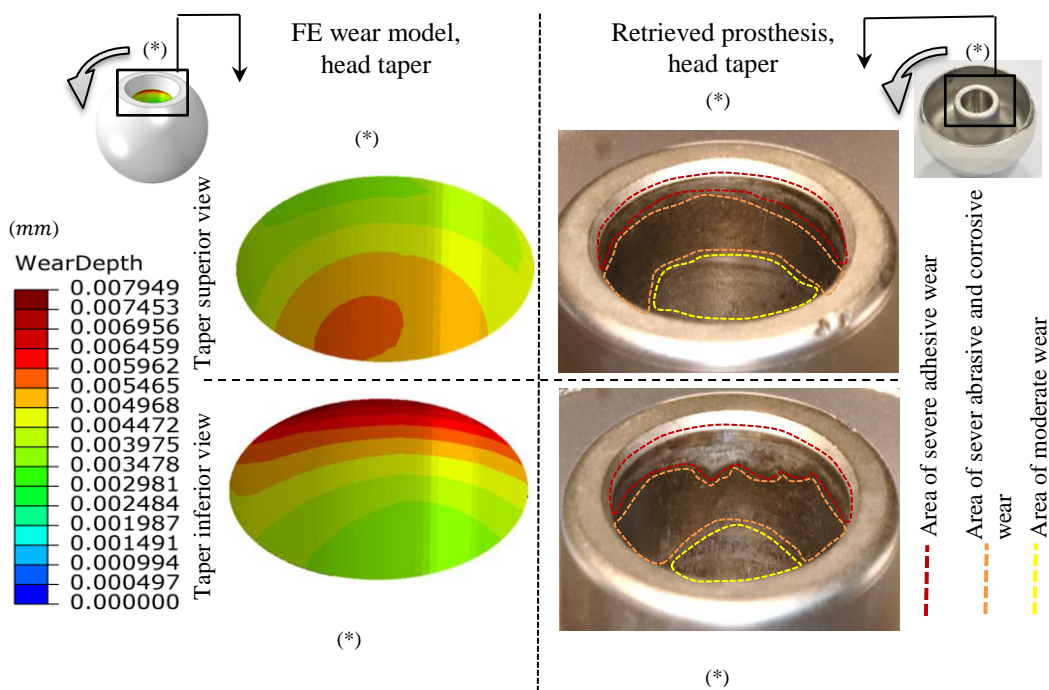


Figure 6-14: Comparison of fretting wear damage between FE wear model (2kN initial impaction) and a retrieved prosthesis; figures are rotated 180° based on a label shown as (*)

Figure 6-14 compares favourably the $2kN$ wear model with one of the retrieved prostheses. The differences in wear damage distribution specifically at the centre of the taper surfaces in the wear modelling in comparison to the retrieved prosthesis, could possibly be attributed to differences in the head-stem taper mismatch angle, wear coefficient, material loss due to corrosion and THR design. In addition, the load history of the retrieved prosthesis is unclear and could be one of the reasons for the slight differences in wear damage distribution too.

The wear analysis performed with the $6kN$ initial impaction has shown a different wear pattern compared to the other analyses. In this analysis, a significantly high wear distribution has been obtained at the distal and proximal edge of the taper inferior surface and very low wear distribution at the taper superior proximal edge with almost no wear damage at the taper superior distal edge. Figure 6-15 compares the wear analysis that has been performed with the $6kN$ initial impaction with a retrieved prosthesis. Similar wear damage has been observed in three more different retrieved prostheses.

One of the retrieved prostheses (out of 16) has shown a relatively high and smooth wear damage which is circumferentially distributed at the taper interface. Figure 6-16 shows high and smooth wear damage at the taper surface (both inferior and superior) of this prosthesis compared with the area which was not in contact. The extent of wear damage and pattern obtained from the wear analysis with the “hand press” assembly is similar to the areas of wear damage shown on the images of this particular retrieved prosthesis (see Figure 6-16).

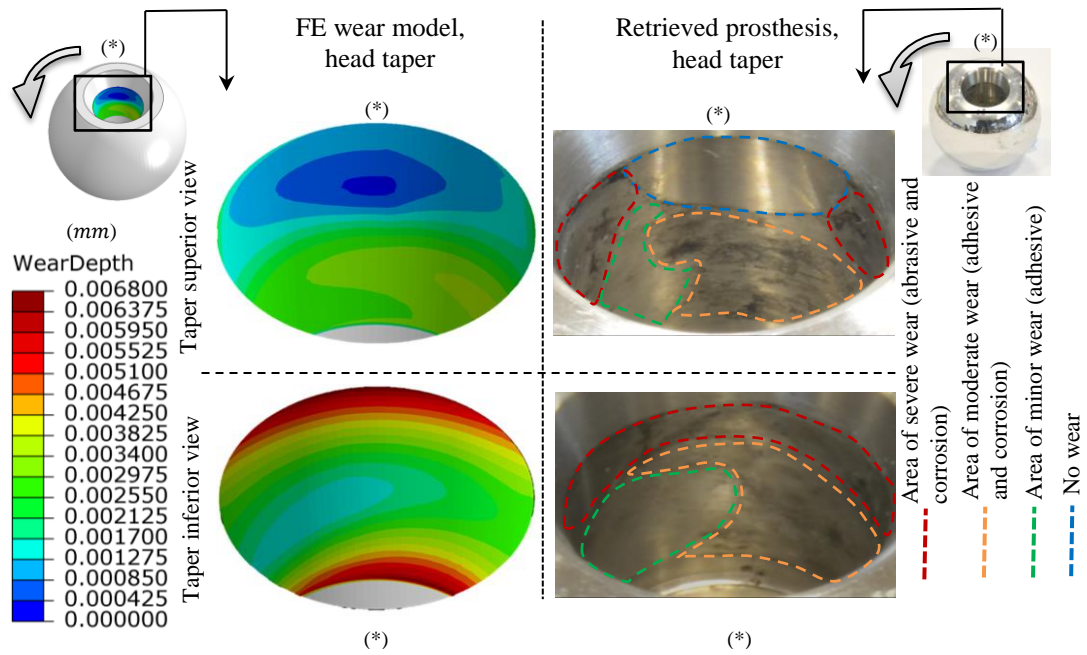


Figure 6-15: Comparison of fretting wear damage between FE wear model (6kN initial impaction) and a retrieved prosthesis; figures are rotated 180° based on a label shown as (*)

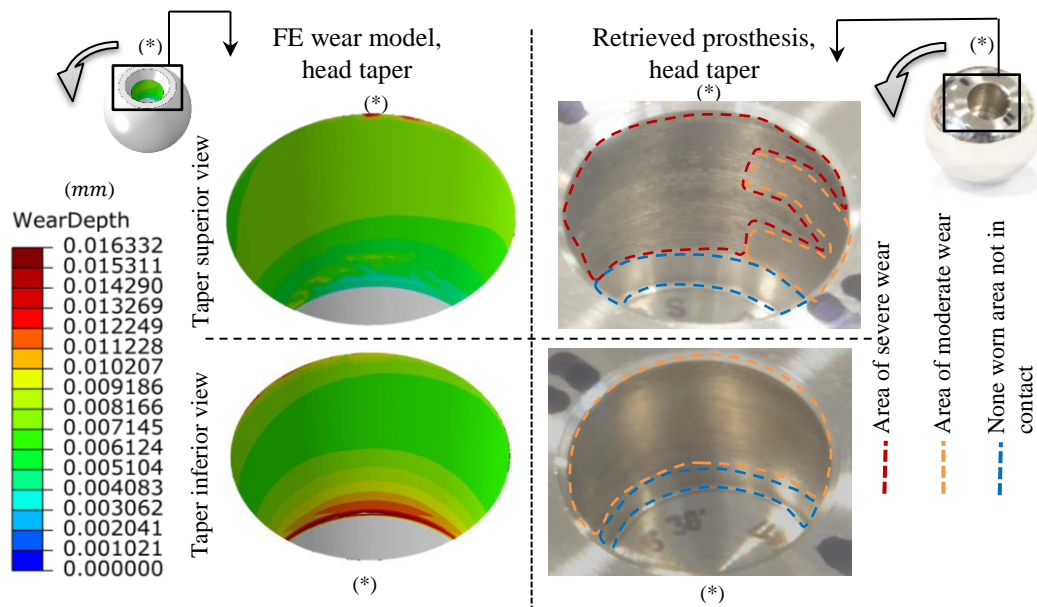


Figure 6-16: Comparison of fretting wear damage between FE wear model (hand press initial assembly) and a retrieved prosthesis; figures are rotated 180° based on a label shown as (*)

In addition to the observation of the retrieved prostheses, the average volumetric wear rates calculated here, as shown in Table 6-2 for different assembly forces, are in the range of the values obtained by Langton et al. (2012) for measurements obtained at the head taper for retrieved MOM THRs (0.127mm³/yr for Articuleze and

0.44mm³/yr for DePuy ASR XL at around 1 to 5 years in vivo). Differences can be attributed to differences in material combinations, THR design, as well as the loading history and the wear coefficient used in the numerical study.

It should be noted that although the wear distributions and wear rates for the different assembly models have been shown to be similar to that from retrieved prostheses, it has not been possible to prove how the retrieved prostheses were initially assembled or their loading history. As such, the retrieved prostheses used for the validation here have been assumed to have been assembled using a “light, medium and high” impaction based on their wear patterns and the comparison of the wear patterns from the wear models.

6.7 Discussion

The wear algorithm proposed calculates wear depth at the taper interface following a specified number of wearing cycles and then modifies the surface geometries gradually by removing the overlap based on the accumulated wear. Furthermore, the algorithm is able to consider the effect of initial fixation of the head-stem of the total hip replacements. The impaction force applied during assembly of the prosthetic femoral head to the stem intra-operatively is seen to have an effect on subsequent fretting wear at the taper junction of THRs. The gradual removal of overlap simulates the effect of wear on weakening the initial fixation which then has an effect on the magnitude of contact pressure and slip.

The greater the magnitude of the impaction force the longer the period of time the beneficial effects of fixation remain with the taper junction only subject to low wear rates. A transition point exists where the beneficial effects of fixation are completely removed and a significant increase in wear rate occurs.

It was found that increasing the impaction loads led to an increase in contact stresses but a significant reduction in slip resulting in a decrease in the initial wear rate. As the taper locking effect diminishes during the wear analysis due to the fretting wear process, it was observed that the slip increases leading to a significant increase in wear rate. The results demonstrate the relevance of the impaction force used intra-operatively by medical professionals to provide an optimum fixation to minimize wear due to fretting.

When the model is still in phase 2 of the analysis it can be hypothesised that the wear debris may remain trapped at the contact interface and only a small portion of the debris may be released into the body. When the model transfers to phase 3, debris can potentially escape from the taper junction, be released into the body and accumulate at the surrounding tissue which may lead to ASTR.

Design features such as taper angle and taper mismatch angle (see Figure 6-17) have been hypothesised to have a significant effect on the strength of the taper fixation and edge wearing (Hohman et al., 2011, Langton et al., 2012, Milošev et al., 2000, Pennock et al., 2002, Schmidt et al., 1997). In the opinion of Hohman et al. (2011) the head stem taper mismatch angle has a significant effect on the wear rate. Milošev et al. (2000) showed high edge wear damage in the taper junction of THRs and presumed that fretting wear accelerates due to the mismatch angle between the taper-trunnion interfaces. Langton et al. (2012) have shown taper wear damage more pronounced on one side than the other. They postulated that this might be due to the taper mismatch angle but this needs to be investigated by further analysis.

Although the taper mismatch angle is seen to have an effect on stability, strength and edge wearing of the taper-trunnion surfaces, this study has illustrated that even with a

zero mismatch angle there would be significant edge wearing and side wearing due to the initial assembly forces.

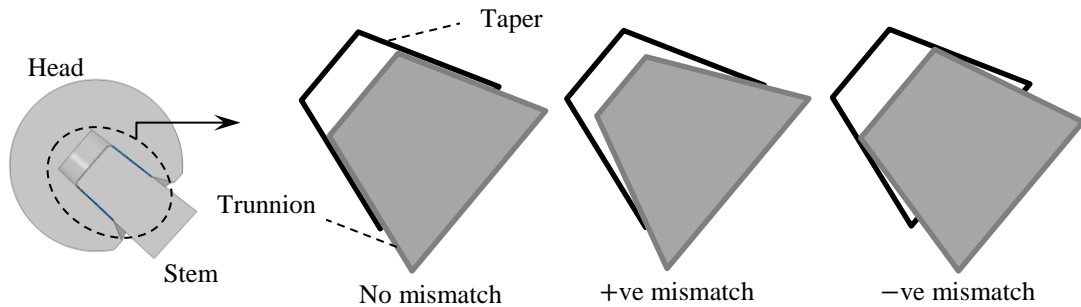


Figure 6-17: Zero, positive and negative mismatch angle

A study was performed using the same wear algorithm with an axisymmetric model of the same head and stem of THR used here. The results from this axisymmetric model with different impaction loads showed a linear relationship between the wear rate and increasing the impaction force. This wear analysis using the axisymmetric model indicated that increasing the initial impaction force reduces the wear rate significantly with a linear relationship. Furthermore, the impaction force and pull-off force has also showed to have a linear relationship where increasing the impaction force increases the pull off forces. These results were obtained due to the limitations of the axisymmetric models. This study showed that wear rate depends on many different factors. The initial contact stress, contact pressure distribution during a walking step and during the wear analysis and the contact slip variation under the accurate loading and boundary conditions all have an effect on the wear rate, depth and wear damage pattern. Therefore, it can be said that a simplified axisymmetric model cannot simulate this process accurately.

It has been suggested in the literature (Heiney et al., 2009, Pennock et al., 2002, Rehmer et al., 2012) that impaction forces of between 4000–5000N will maximize

taper strength whilst mitigating against damage to the femur. In this study, the total volume loss for $4kN$ and $6kN$ impaction analysis was almost equal; however, the analysis with $4kN$ impaction transferred to phase 3 after 4.1 million load cycles and from this transition point a higher wear rate can be expected (compared to $6kN$ impaction wear analysis). Furthermore, the wear analysis with $6kN$ initial impaction showed significantly high edge and side wear on the taper inferior surface with very low wear damage on the taper superior surface and also limits of safety for the patient and structural integrity of the prosthesis design needs to be considered while applying very high impact.

Maintaining “good fixation” for as long as possible is the key to reduced wear rates and as such the transition point should occur after the longest time *in vivo* as possible. As such, to minimize fretting wear, surgeons should apply a relatively large impaction force at assembly (ideally around $4kN$ and not less than $3kN$) whilst ensuring the integrity of the patient femur and prosthetic device.

The limitation of this study is again due to the magnitude of the wear coefficient used. Increasing the wear coefficient increases the wear rate and the transition point may occur earlier than has been predicted. As such, further investigation is required to obtain accurate fretting wear coefficients by controlled experiment. Another parameter that could affect the results is the magnitude of the friction coefficient. The friction coefficient could change the magnitude of slip and consequently wear rate. Further study is required to investigate the effect of the friction coefficient on the fretting wear damage.

Furthermore, as discussed in Chapter 2, some prosthetic devices have threaded trunnion surfaces (see Figure 2-9) in order to increase friction and improve fixation

of the components. The initial impaction assembly may plastically deform these threads. As such, further investigation is required to investigate the effect of threaded stems on the fixation of the components and also on the fretting wear occurred.

6.8 Conclusion

The wear algorithm and FE model presented here is able to model the effect the impaction forces (used to assemble the femoral prosthetic head to the stem trunnion) have on subsequent fretting wear at the taper junction in a THR. This is achieved by modelling the effect of assembly as a static overlap analysis procedure then simulating the development of wear by removing overlap in line with the calculated wear depth for a particular stage of the analysis.

Prior to the “transition” point, as the overlap is removed by wear, the contact pressure and contact stresses at the interface decrease whereas the relative displacements increase slightly. At the transition point (when the overlap is completely removed) a significant decrease in contact pressure occurs coinciding with a proportionally greater increase in relative displacement at the interface leading to a much increased wear rate. Subsequent to the transition point the contact pressure stays relatively constant with the magnitude of the relative displacement increasing gradually over several years resulting in increasing wear rates. It can be seen that in this application a reduction in the interface contact pressure results in an increase in relative displacement (slip); whereas an increase in contact pressure (due to increased initial impaction) results in reduced slip and fretting wear.

Chapter 7

Conclusion and future work

7.1 Conclusion

Research in tribology which is based on theories aided with computational capability and experiment can indeed complement each other in order to increase the longevity of mechanical devices in service. Furthermore, a theoretical approach with computational capability can be used to predict long term behaviour of these devices which otherwise require expensive and time consuming tests.

Experimental testing to determine wear that occurs in a prosthesis is time consuming, expensive and complicated. Therefore, computational wear modelling is an alternative method to predict wear. A computational method to determine fretting wear is a useful tool. It will allow speedy assessment of designs and its performance in service to determine functionality of the prosthetic device and to validate existing and new designs. It could also provide guidelines for clinical practice so as to perform surgical procedures more efficiently.

The aim of this research was to develop a computational methodology to predict fretting wear accurately at the taper interface between the head and stem of a THR.

Based on the wear model presented in this thesis, the main contributions of this research can be summarised as follows:

- The fretting wear method presented has been developed based on an axisymmetric model of a commercial total hip replacement. The axisymmetric model reduces the computational time and is useful for comparative and parametric studies.
- The uniqueness of the methodology is that the method is able to simulate the progressive weakening of the initial head-stem fixation due to the wearing process. Simulating the reduction in the initial fixation strength of the head-stem assembly is seen as important to the accurate assessment of wear and has not been reported in the literature before.
- The fretting wear method has been developed as a 3D model of the total hip prostheses with realistic loading and boundary conditions.
- The results obtained using the 3D model have been compared against observation of retrieved prostheses and from fretting wear measurements found in literature. From these comparisons, the results computed show considerable promise but are clearly dependant on the use of an appropriate wear coefficient.
- The fretting wear method presented has been generalized to be used for different design of THRs and also for other prosthetic devices such as knee and shoulder modular implants.

- The method has been used to investigate the effect of different taper fixation of the head and stem on the extent of fretting wear.
- The computational results from the different initial assembly forces were compared with different wear damage occurring at the taper surface of several retrieved total hip prostheses. This comparison showed that the side wearing and edge wearing that occur at the taper surface could be due to the different assembly forces used to fix these components.
- The method can consider different material combinations and specific wear fractions for different design of the THRs to predict fretting wear at the taper junction.
- The method is able to vary the wear coefficient during the analysis. This variation of the value of the wear coefficient can be obtained from a controlled fretting test.
- The method could be also used for any FE analysis subjected to oscillatory loads and micromotion.

It is hoped that the method and algorithm developed in this study can be used for further investigations in the future. These investigations could indeed help designers, physicians and surgeons to minimise the effects of fretting wear, give a good indication of the fretting wear pattern, surface damage and increase the longevity of the designs in operation.

7.2 Future work

Fretting wear is a very complex phenomenon to be predicted computationally. This research is a step to predict fretting wear between components that are in contact and under oscillatory loads. As discussed in Chapter 2, a review of literature has highlighted areas that need further investigations. The present study completed a computational approach to fretting wear prediction in total hip replacements which again warrants further investigations. Future research can be listed as below:

- It is apparent that further research is required to help inhibit the effects of corrosion; however, the work presented here focuses solely on fretting wear as being the primary mechanism causing damage at the head-stem taper junction in THRs.
- Accurate wear coefficients for this application have not yet been presented in the literature and as such this is an area for further investigation and testing. The wear coefficient will change during the wearing process and as such specific applications will benefit from knowledge of time dependant wear coefficients (in terms of loading cycles). A controlled fretting test could be carried out to obtain the variation of wear coefficient during the wear analysis.
- Friction plays a critical role in the wear process mainly due to the change in the magnitude of the slip. The effect of increasing the friction coefficient on fretting wear at taper junction of THRs could be an area to be investigated.
- The method can be developed for Adhesive, Abrasive wear with longer relative displacements, for instance, for the head-cup bearing.

References

- ABDELGAIED, A., LIU, F., BROCKETT, C., JENNINGS, L., FISHER, J. & JIN, Z. 2011. Computational wear prediction of artificial knee joints based on a new wear law and formulation. *Journal of biomechanics*, 44, 1108-1116.
- ABU-AMER, Y., DARWECH, I. & CLOHISY, J. C. 2007. Aseptic loosening of total joint replacements: mechanisms underlying osteolysis and potential therapies. *Arthritis Research and Therapy*, 9, S6.
- AJAYI, O. O. & LUDEMA, K. C. 1988. Surface damage of structural ceramics: implications for wear modeling. *Wear*, 124, 237-257.
- ALDINGER, P. R., THOMSEN, M., MAU, H., EWERBECK, V. & BREUSCH, S. J. 2003. Cementless Spotorno tapered titanium stems: excellent 10-15-year survival in 141 young patients. *Acta Orthopaedica*, 74, 253-258.
- ARCHARD, J. 1953. Contact and rubbing of flat surfaces. *Journal of Applied Physics*, 24, 981-988.
- BARTEL, D., BURSTEIN, A., TODA, M. & EDWARDS, D. 1985. The effect of conformity and plastic thickness on contact stresses in metal-backed plastic implants. *Journal of Biomechanical Engineering*, 107, 193-199.
- BERGMANN, G., DEURETZBACHER, G., HELLER, M., GRAICHEN, F., ROHLMANN, A., STRAUSS, J. & DUDA, G. 2001. Hip contact forces and gait patterns from routine activities. *Journal of biomechanics*, 34, 859-871.
- BERGMANN, G., GRAICHEN, F. & ROHLMANN, A. 1993. Hip joint loading during walking and running, measured in two patients. *Journal of Biomechanics*, 26, 969-990.
- BISHOP, N., WITT, F., POURZAL, R., FISCHER, A., RÜTSCHI, M., MICHEL, M. & MORLOCK, M. 2013. Wear patterns of taper connections in retrieved large diameter metal-on-metal bearings. *Journal of Orthopaedic Research*, 31, 1116-1122.
- BOLLAND, B., CULLIFORD, D., LANGTON, D., MILLINGTON, J., ARDEN, N. & LATHAM, J. 2011. High failure rates with a large-diameter hybrid metal-on-metal total hip replacement *Journal of Bone & Joint Surgery, British Volume*, 93, 608-615.
- BONE, M. C., SIDAGINAMALE, R. P., LORD, J. K., SCHOLLES, S. C., JOYCE, T. J., NARGOL, A. V. & LANGTON, D. J. 2015. Determining material loss from the femoral stem trunnion in hip arthroplasty using a coordinate measuring machine. *Proceedings of the Institution of Mechanical Engineers, Part H: Journal of Engineering in Medicine*, 229, 69-76.
- BROWN, L., ZHANG, H., BLUNT, L. & BARRANS, S. 2007. Reproduction of fretting wear at the stem—cement interface in total hip replacement. *Proceedings of the Institution of Mechanical Engineers, Part H: Journal of Engineering in Medicine*, 221, 963-971.
- BROWN, S. A. & LEMONS, J. E. 1996. *Medical applications of titanium and its alloys: the material and biological issues*, ASTM International.

- BULY, R. L., HUO, M. H., SALVATI, E., BRIEN, W. & BANSAL, M. 1992. Titanium wear debris in failed cemented total hip arthroplasty: an analysis of 71 cases. *The Journal of arthroplasty*, 7, 315-323.
- BURR, A. H. 1981. Mechanical analysis and design. *Elsevier North-Holland*, xxvi+ 640, 26 x 19 cm.
- CAWLEY, J., METCALF, J., JONES, A. H., BAND, T. & SKUPIEN, D. 2003. A tribological study of cobalt chromium molybdenum alloys used in metal-on-metal resurfacing hip arthroplasty. *Wear*, 255, 999-1006.
- CHAN, F. W., BOBYN, J. D., MEDLEY, J. B., KRYGIER, J. J. & TANZER, M. 1999. Wear and lubrication of metal-on-metal hip implants. *Clinical Orthopaedics and Related Research*, 369, 10-24.
- CHIBA, A., KUMAGAI, K., NOMURA, N. & MIYAKAWA, S. 2007. Pin-on-disk wear behavior in a like-on-like configuration in a biological environment of high carbon cast and low carbon forged Co-29Cr-6Mo alloys. *Acta Materialia*, 55, 1309-1318.
- CHOWDHURY, M., ALI, M. & HELALI, M. 2010. The effect of natural frequency of the experimental set-up on the friction coefficient. *Industrial Lubrication and Tribology*, 62, 78-82.
- COHEN, D. 2012. How safe are metal-on-metal hip implants? *BMJ: British Medical Journal*, 344.
- COOK, S. D., BARRACK, R. L. & CLEWOW, A. 1994. Corrosion and wear at the modular interface of uncemented femoral stems. *Journal of Bone & Joint Surgery, British Volume*, 76, 68-72.
- DANIEL M ESTOK, I. & HARRIS, W. H. 1994. Long-term results of cemented femoral revision surgery using second-generation techniques: an average 11.7-year follow-up evaluation. *Clinical orthopaedics and related research*, 299, 190-202.
- DING, J., LEEN, S. & MCCOLL, I. 2004. The effect of slip regime on fretting wear-induced stress evolution. *International journal of fatigue*, 26, 521-531.
- DONALDSON, F. E., COBURN, J. C. & SIEGEL, K. L. 2014. Total hip arthroplasty head-neck contact mechanics: A stochastic investigation of key parameters. *Journal of biomechanics*, 47, 1634-1641.
- DUISABEAU, L., COMBRADE, P. & FOREST, B. 2004. Environmental effect on fretting of metallic materials for orthopaedic implants. *Wear*, 256, 805-816.
- ELKINS, J. M., CALLAGHAN, J. J. & BROWN, T. D. 2014. Stability and Trunnion Wear Potential in Large-diameter Metal-on-Metal Total Hips: A Finite Element Analysis. *Clinical Orthopaedics and Related Research*, 472, 529-542.
- ELKINS, J. M., O'BRIEN, M. K., STROUD, N. J., PEDERSEN, D. R., CALLAGHAN, J. J. & BROWN, T. D. 2011. Hard-on-hard total hip impingement causes extreme contact stress concentrations. *Clinical Orthopaedics and Related Research*, 469, 454-463.
- ELTOBGY, M., NG, E. & ELBESTAWI, M. 2005. Finite element modeling of erosive wear. *International Journal of Machine Tools and Manufacture*, 45, 1337-1346.

- ENGEL, L. & KLINGELE, H. 1981. *An atlas of metal damage: surface examination by scanning electron microscope*, Prentice-Hall.
- ENGLISH, R., ASHKANFAR, A. & ROTHWELL, G. 2015. A computational approach to fretting wear prediction at the head–stem taper junction of total hip replacements. *Wear*, 338, 210-220.
- FESSLER, H. & FRICKER, D. 1989. Friction in femoral prosthesis and photoelastic model cone taper joints. *Proceedings of the Institution of Mechanical Engineers, Part H: Journal of Engineering in Medicine*, 203, 1-14.
- FIALHO, J. C., FERNANDES, P. R., ECCA, L. & FOLGADO, J. 2007. Computational hip joint simulator for wear and heat generation. *Journal of Biomechanics*, 40, 2358-2366.
- FOUVRY, S., KAPSA, P. & VINCENT, L. 2001. An elastic-plastic shakedown analysis of fretting wear. *Wear*, 247, 41-54.
- FOUVRY, S., LISKIEWICZ, T., KAPSA, P., HANNEL, S. & SAUGER, E. 2003. An energy description of wear mechanisms and its applications to oscillating sliding contacts. *Wear*, 255, 287-298.
- FRIDRICI, V., FOUVRY, S. & KAPSA, P. 2001. Effect of shot peening on the fretting wear of Ti–6Al–4V. *Wear*, 250, 642-649.
- GILBERT, J. L., BUCKLEY, C. A. & JACOBS, J. J. 1993. In vivo corrosion of modular hip prosthesis components in mixed and similar metal combinations. The effect of crevice, stress, motion, and alloy coupling. *Journal of Biomedical Materials Research*, 27, 1533-1544.
- GOLDBERG, J. R., GILBERT, J. L., JACOBS, J. J., BAUER, T. W., PAPROSKY, W. & LEURGANS, S. 2002. A multicenter retrieval study of the taper interfaces of modular hip prostheses. *Clinical Orthopaedics and Related Research*, 401, 149-161.
- HAILER, N. P., GARELLICK, G. & KÄRRHOLM, J. 2010. Uncemented and cemented primary total hip arthroplasty in the Swedish Hip Arthroplasty Register: evaluation of 170,413 operations. *Acta orthopaedica*, 81, 34-41.
- HALLAB, N. J., MESSINA, C., SKIPOR, A. & JACOBS, J. J. 2004. Differences in the fretting corrosion of metal–metal and ceramic–metal modular junctions of total hip replacements. *Journal of Orthopaedic Research*, 22, 250-259.
- HANNEL, S., FOUVRY, S., KAPSA, P. & VINCENT, L. 2001. The fretting sliding transition as a criterion for electrical contact performance. *Wear*, 249, 761-770.
- HART, A., MATTHIES, A., RACASAN, R., BILLS, P., PANAGIOTIDOU, A., BLUNT, L., BLUNN, G. & SKINNER, J. 2013. Taper wear contributes only a third of the total volumetric material loss in large head metal on metal hip replacement. *Bone & Joint Journal Orthopaedic Proceedings Supplement*, 95, 14-14.
- HEAD, W. C., BAUK, D. J. & EMERSON JR, R. H. 1995. Titanium as the material of choice for cementless femoral components in total hip arthroplasty. *Clinical orthopaedics and related research*, 311, 85-90.
- HEINEY, J. P., BATTULA, S., VRABEC, G. A., PARIKH, A., BLICE, R., SCHOENFELD, A. J. & NJUS, G. O. 2009. Impact magnitudes applied by surgeons

- and their importance when applying the femoral head onto the Morse taper for total hip arthroplasty. *Archives of Orthopaedic and Trauma Surgery*, 129, 793-796.
- HOHMAN, D., AFFONSO, J. & ANDERS, M. 2011. Ceramic-on-ceramic failure secondary to head-neck taper mismatch. *Am J Orthop*, 40, 571-573.
- HOLM, R. 1951. *Electric Contacts*, 1946. *Stockholm, Sweden*.
- HOSSEINZADEH, H. R. S., SHAHI, A. S. & EAJAZI, A. 2012. *The Bearing Surfaces in Total Hip Arthroplasty-Options, Material Characteristics and Selection*, INTECH Open Access Publisher.
- HUTCHINGS, I. M. 1992. *Tribology: friction and wear of engineering materials*.
- JEFFERS, J. R., ROQUES, A., TAYLOR, A. & TUKE, M. A. 2009. The problem with large diameter metal-on-metal acetabular cup inclination. *Bulletin of the NYU hospital for joint diseases*, 67, 189.
- JIN, Z., HENG, S., NG, H. & AUGER, D. 1999. An axisymmetric contact model of ultra high molecular weight polyethylene cups against metallic femoral heads for artificial hip joint replacements. *Proceedings of the Institution of Mechanical Engineers, Part H: Journal of Engineering in Medicine*, 213, 317-327.
- JOHNSON, K. 1995. Contact mechanics and the wear of metals. *Wear*, 190, 162-170.
- KAPOOR, A. 1997. Wear by plastic ratchetting. *Wear*, 212, 119-130.
- KARMAKAR, S., RAO, U. & SETHURAMIAH, A. 1996. An approach towards fatigue wear modelling. *Wear*, 198, 242-250.
- KUSABA, A. & KUROKI, Y. 1997. Femoral component wear in retrieved hip prostheses. *Journal of Bone & Joint Surgery, British Volume*, 79, 331-336.
- LANGTON, D., JAMESON, S., JOYCE, T., GANDHI, J., SIDAGINAMALE, R., MEREDDY, P., LORD, J. & NARGOL, A. 2011. Accelerating failure rate of the ASR total hip replacement. *Journal of Bone & Joint Surgery, British Volume*, 93, 1011-1016.
- LANGTON, D., SIDAGINAMALE, R., LORD, J., NARGOL, A. & JOYCE, T. 2012. Taper junction failure in large-diameter metal-on-metal bearings. *Bone and Joint Research*, 1, 56-63.
- LAVERNIA, C. J., BAERGA, L., BARRACK, R. L., TOZAKOGLU, E., COOK, S. D., LATA, L. & ROSSI, M. D. 2009. The effects of blood and fat on Morse taper disassembly forces. *Am J Orthop (Belle Mead NJ)*, 38, 187-90.
- LESLIE, I., WILLIAMS, S., BROWN, C., ISAAC, G., JIN, Z., INGHAM, E. & FISHER, J. 2008. Effect of bearing size on the long-term wear, wear debris, and ion levels of large diameter metal-on-metal hip replacements—An in vitro study. *Journal of Biomedical Materials Research Part B: Applied Biomaterials*, 87, 163-172.
- LISKIEWICZ, T. & FOUVRY, S. 2005. Development of a friction energy capacity approach to predict the surface coating endurance under complex oscillating sliding conditions. *Tribology international*, 38, 69-79.

- LIU, F., LESLIE, I., WILLIAMS, S., FISHER, J. & JIN, Z. 2008. Development of computational wear simulation of metal-on-metal hip resurfacing replacements. *Journal of Biomechanics*, 41, 686-694.
- MADGE, J., LEEN, S., MCCOLL, I. & SHIPWAY, P. 2007a. Contact-evolution based prediction of fretting fatigue life: effect of slip amplitude. *Wear*, 262, 1159-1170.
- MADGE, J., LEEN, S. & SHIPWAY, P. 2007b. The critical role of fretting wear in the analysis of fretting fatigue. *Wear*, 263, 542-551.
- MADGE, J., LEEN, S. & SHIPWAY, P. 2008. A combined wear and crack nucleation-propagation methodology for fretting fatigue prediction. *International Journal of Fatigue*, 30, 1509-1528.
- MAGAZINER, R., JAIN, V. & MALL, S. 2008. Wear characterization of Ti-6Al-4V under fretting-reciprocating sliding conditions. *Wear*, 264, 1002-1014.
- MAI, K., VERIOTI, C., EZZET, K. A., COPP, S. N., WALKER, R. H. & COLWELL JR, C. W. 2010. Incidence of 'squeaking' after ceramic-on-ceramic total hip arthroplasty. *Clinical Orthopaedics and Related Research*, 468, 413-417.
- MALONEY, W. J., SMITH, R. L., SCHMALZRIED, T. P., CHIBA, J., HUENE, D. & RUBASH, H. 1995. Isolation and characterization of wear particles generated in patients who have had failure of a hip arthroplasty without cement. *The Journal of Bone & Joint Surgery*, 77, 1301-1310.
- MALVIYA, A., RAMASKANDHAN, J., BOWMAN, R., HASHMI, M., HOLLAND, J., KOMETA, S. & LINGARD, E. 2011. What advantage is there to be gained using large modular metal-on-metal bearings in routine primary hip replacement? A preliminary report of a prospective randomised controlled trial. *Journal of Bone & Joint Surgery, British Volume*, 93, 1602-1609.
- MAO, X., TAY, G. H., GODBOLT, D. B. & CRAWFORD, R. W. 2012. Pseudotumor in a well-fixed metal-on-polyethylene uncemented hip arthroplasty. *The Journal of Arthroplasty*, 27, 493-e13.
- MATTEI, L., DI PUCCIO, F., PICCIGALLO, B. & CIULLI, E. 2011. Lubrication and wear modelling of artificial hip joints: A review. *Tribology International*, 44, 532-549.
- MATTHIES, A. K., RACASAN, R., BILLS, P., BLUNT, L., CRO, S., PANAGIOTIDOU, A., BLUNN, G., SKINNER, J. & HART, A. J. 2013. Material loss at the taper junction of retrieved large head metal-on-metal total hip replacements. *Journal of Orthopaedic Research*, 31, 1677-1685.
- MAXIAN, T. A., BROWN, T. D., PEDERSEN, D. R. & CALLAGHAN, J. J. 1996a. 3-Dimensional sliding/contact computational simulation of total hip wear. *Clinical Orthopaedics and Related Research*, 333, 41-50.
- MAXIAN, T. A., BROWN, T. D., PEDERSEN, D. R. & CALLAGHAN, J. J. 1996b. A sliding-distance-coupled finite element formulation for polyethylene wear in total hip arthroplasty. *Journal of Biomechanics*, 29, 687-692.
- MAXIAN, T. A., BROWN, T. D., PEDERSEN, D. R., MCKELLOP, H. A., LU, B. & CALLAGHAN, J. J. 1997. Finite element analysis of acetabular wear: validation,

- and backing and fixation effects. *Clinical Orthopaedics and Related Research*, 344, 111-117.
- MCCARTHY, J. C., BONO, J. V. & O'DONNELL, P. J. 1997. Custom and modular components in primary total hip replacement. *Clinical orthopaedics and related research*, 344, 162-171.
- MCCOLL, I., DING, J. & LEEN, S. 2004. Finite element simulation and experimental validation of fretting wear. *Wear*, 256, 1114-1127.
- MEARS, D. 1975. The use of dissimilar metals in surgery. *Journal of biomedical materials research*, 9, 133-148.
- MERCHANT, S. M., MISRA, S., ROY, P. K. & VAIDYA, H. M. 2002. Polishing fluid, polishing method, semiconductor device and semiconductor device fabrication method. Google Patents.
- MILOŠEV, L., ANTOLIČ, V., MINOVIČ, A., CÖR, A., HERMAN, S., PAVLOVČIČ, V. & CAMPBELL, P. 2000. Extensive metallosis and necrosis in failed prostheses with cemented titanium-alloy stems and ceramic heads. *Journal of Bone & Joint Surgery, British Volume*, 82, 352-357.
- MINAKAWA, H., STONE, M., WROBLEWSKI, B., LANCASTER, J., INGHAM, E. & FISHER, J. 1998. Quantification of third-body damage and its effect on UHMWPE wear with different types of femoral head. *Journal of Bone & Joint Surgery, British Volume*, 80, 894-899.
- MOHARRAMI, N., LANGTON, D., SAYGINER, O. & BULL, S. 2013. Why does titanium alloy wear cobalt chrome alloy despite lower bulk hardness: A nanoindentation study? *Thin Solid Films*, 549, 79-86.
- MORSHED, S., BOZIC, K. J., RIES, M. D., MALCHAU, H. & COLFORD JR, J. M. 2007. Comparison of cemented and uncemented fixation in total hip replacement: a meta-analysis. *Acta orthopaedica*, 78, 315-326.
- MROCZKOWSKI, M. L., HERTZLER, J. S., HUMPHREY, S. M., JOHNSON, T. & BLANCHARD, C. R. 2006. Effect of impact assembly on the fretting corrosion of modular hip tapers. *Journal of orthopaedic research*, 24, 271-279.
- OHASHI, K., ROMERO, A., MCGOWAN, P., MALONEY, W. & DAUSKARDT, R. 1998. Adhesion and reliability of interfaces in cemented total joint arthroplasties. *Journal of orthopaedic research*, 16, 705-714.
- PANDIT, H., GLYN-JONES, S. & MCLARDY-SMITH, P. 2008. Pseudotumours associated with metal-on metal hip resurfacings. *J Bone Joint Surg [Br]*, 847-851.
- PATIL, S., BERGULA, A., CHEN, P. C., COLWELLJR, C. W. & D'LIMA, D. D. 2003. Polyethylene wear and acetabular component orientation. *The Journal of Bone & Joint Surgery*, 85, 56-63.
- PENNOCK, A. T., SCHMIDT, A. H. & BOURGEOULT, C. A. 2002. Morse-type tapers: factors that may influence taper strength during total hip arthroplasty. *The Journal of arthroplasty*, 17, 773-778.
- RAIMONDI, M., SANTAMBROGIO, C., PIETRABISSA, R., RAFFELINI, F. & MOLFETTA, L. 2001. Improved mathematical model of the wear of the cup

- articular surface in hip joint prostheses and comparison with retrieved components. *Proceedings of the Institution of Mechanical Engineers, Part H: Journal of Engineering in Medicine*, 215, 377-390.
- REHMER, A., BISHOP, N. E. & MORLOCK, M. M. 2012. Influence of assembly procedure and material combination on the strength of the taper connection at the head–neck junction of modular hip endoprotheses. *Clinical Biomechanics*, 27, 77-83.
- SCHAAFF, P., DALMIGLIO, M. & HOLZWARTH, U. 2006. Frequency effect in fretting wear of Co-28Cr-6Mo versus Ti-6Al-4V implant alloys. *Journal of Biomedical Materials Research Part B: Applied Biomaterials*, 77, 79-88.
- SCHMALZRIED, T. P., SZUSZCZEWICZ, E. S., NORTHFIELD, M. R., AKIZUKI, K. H., FRANKEL, R. E., BELCHER, G. & AMSTUTZ, H. C. 1998. Quantitative Assessment of Walking Activity after Total Hip or Knee Replacement*. *The Journal of Bone & Joint Surgery*, 80, 54-9.
- SCHMIDT, A. H., LOCH, D. A., BECHTOLD, J. E. & KYLE, R. F. 1997. Assessing Morse taper function: the relationship between impaction force, disassembly force, and design variables. *Modularity of Orthopedic Implants*, 1301, 114.
- SHAHGALDI, B., HEATLEY, F., DEWAR, A. & CORRIN, B. 1995. In vivo corrosion of cobalt-chromium and titanium wear particles. *Journal of Bone & Joint Surgery, British Volume*, 77, 962-966.
- SMITH, A. J., DIEPPE, P., PORTER, M. & BLOM, A. W. 2012. Risk of cancer in first seven years after metal-on-metal hip replacement compared with other bearings and general population: linkage study between the National Joint Registry of England and Wales and hospital episode statistics. *BMJ: British Medical Journal*, 344, 125-127.
- SMITH, S., DOWSON, D. & GOLDSMITH, A. 2001. The lubrication of metal-on-metal total hip joints: a slide down the Stribeck curve. *Proceedings of the Institution of Mechanical Engineers, Part J: Journal of Engineering Tribology*, 215, 483-493.
- SPOERER, S. M. & CHALMERS, P. N. 2012. Cutaneous manifestation of metallosis in a Metal-on-Metal total hip arthroplasty after acetabular liner dissociation. *The Journal of Arthroplasty*, 27, 1580-e13.
- SRINIVASAN, A., JUNG, E. & LEVINE, B. R. 2012. Modularity of the femoral component in total hip arthroplasty. *Journal of the American Academy of Orthopaedic Surgeons*, 20, 214-222.
- STACK, M. & JANA, B. 2004. Modelling particulate erosion–corrosion in aqueous slurries: some views on the construction of erosion–corrosion maps for a range of pure metals. *Wear*, 256, 986-1004.
- STOWERS, I. F. & RABINOWICZ, E. 1973. The mechanism of fretting wear. *Journal of Tribology*, 95, 65-70.
- TELOKEN, M. A., BISSETT, G., HOZACK, W. J., SHARKEY, P. F. & ROTHMAN, R. H. 2002. Ten to fifteen-year follow-up after total hip arthroplasty with a tapered cobalt-chromium femoral component (tri-lock) inserted without cement. *The Journal of Bone & Joint Surgery*, 84, 2140-2144.

- TEOH, S., CHAN, W. & THAMPURAN, R. 2002. An elasto-plastic finite element model for polyethylene wear in total hip arthroplasty. *Journal of Biomechanics*, 35, 323-330.
- TOBI, A. M., DING, J., BANDAK, G., LEEN, S. & SHIPWAY, P. 2009. A study on the interaction between fretting wear and cyclic plasticity for Ti-6Al-4V. *Wear*, 267, 270-282.
- UDDIN, M. & ZHANG, L. 2013. Predicting the wear of hard-on-hard hip joint prostheses. *Wear*, 301, 192-200.
- VAN, K. D. & MAITOURNAM, M. 1994. *Elasto-plastic calculations of the mechanical state in reciprocating moving contacts: application to fretting fatigue*. *Fretting fatigue, ESIS 18* [Online]. Mechanical Engineering Publications, London.
- VARENBERG, M., HALPERIN, G. & ETSION, I. 2002. Different aspects of the role of wear debris in fretting wear. *Wear*, 252, 902-910.
- VINGSBO, O. & SÖDERBERG, S. 1988. On fretting maps. *Wear*, 126, 131-147.
- WANG, A., ESSNER, A. & KLEIN, R. 2001. Effect of contact stress on friction and wear of ultra-high molecular weight polyethylene in total hip replacement. *Proceedings of the Institution of Mechanical Engineers, Part H: Journal of Engineering in Medicine*, 215, 133-139.
- WASSEF, A. & SCHMALZRIED, T. 2013. Femoral taperosis an accident waiting to happen? *Bone & Joint Journal*, 95, 3-6.
- WU, J. S. S., HUNG, J. P., SHU, C. S. & CHEN, J. H. 2003. The computer simulation of wear behavior appearing in total hip prosthesis. *Computer Methods and Programs in Biomedicine*, 70, 81-91.
- YANG, L. 2003. The transient and steady wear coefficients of A6061 aluminium alloy reinforced with alumina particles. *Composites science and technology*, 63, 575-583.
- YANG, L. 2005. A test methodology for the determination of wear coefficient. *Wear*, 259, 1453-1461.
- YOUNG, S., LOTITO, M. & KELLER, T. 1998. Friction reduction in total joint arthroplasty. *Wear*, 222, 29-37.
- ZHANG, H., BLUNT, L., JIANG, X., BROWN, L., BARRANS, S. & ZHAO, Y. 2008a. Femoral stem wear in cemented total hip replacement. *Proceedings of the Institution of Mechanical Engineers, Part H: Journal of Engineering in Medicine*, 222, 583-592.
- ZHANG, H., BROWN, L., BLUNT, L. & BARRANS, S. 2008b. Influence of femoral stem surface finish on the apparent static shear strength at the stem-cement interface. *Journal of the mechanical behavior of biomedical materials*, 1, 96-104.
- ZHANG, T., HARRISON, N., MCDONNELL, P., MCHUGH, P. & LEEN, S. 2013. A finite element methodology for wear-fatigue analysis for modular hip implants. *Tribology International*, 65, 113-127.

- ZHANG, T., HARRISON, N. M., MCDONNELL, P. F., MCHUGH, P. E. & LEEN, S. B. 2014. Micro-macro wear-fatigue of modular hip implant taper-lock coupling. *The Journal of Strain Analysis for Engineering Design*, 49, 2-18.
- ZHANG, T., MCHUGH, P. & LEEN, S. 2011. Computational study on the effect of contact geometry on fretting behaviour. *Wear*, 271, 1462-1480.
- ZUM GAHR, K. 1988. Modelling of two-body abrasive wear. *Wear*, 124, 87-103.

Appendices

List of Appendix

Appendix I: graphical user interface of the wear algorithm

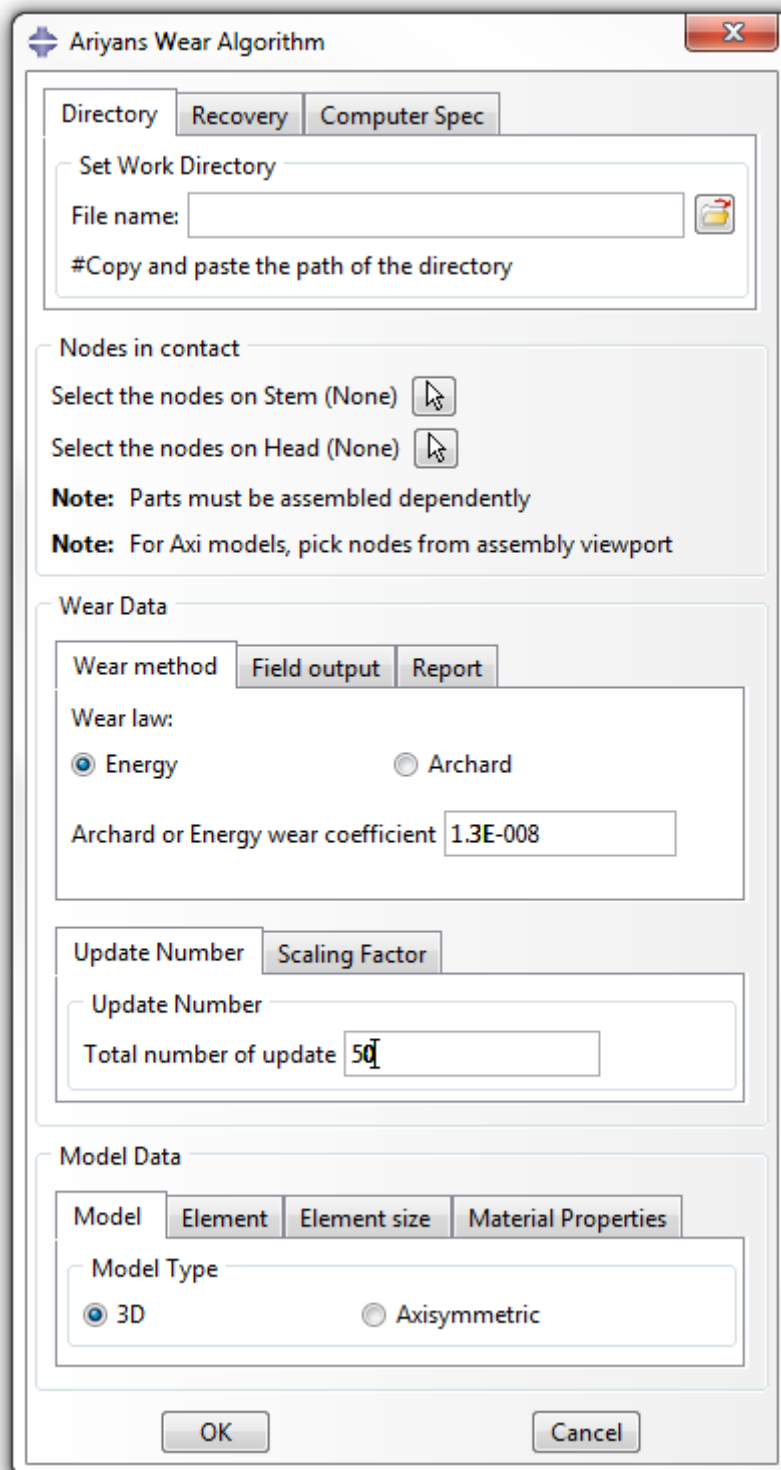
Appendix II: An example of output request, text format (*.txt)

Appendix III: An example of output request, from ABAQUS Field Output database (*.ODB)

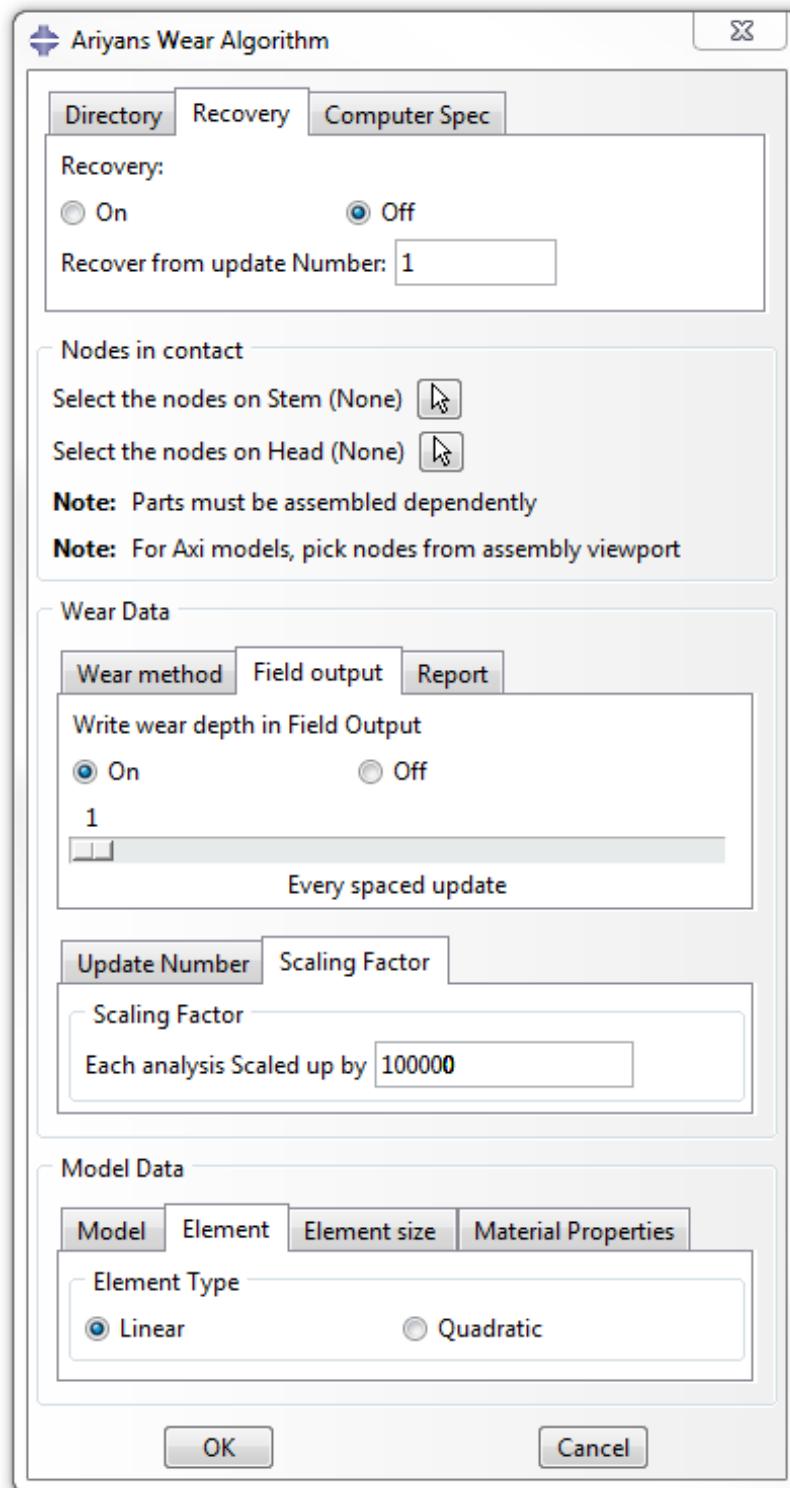
Appendix IV: Publications

Appendix V: Poster presentations

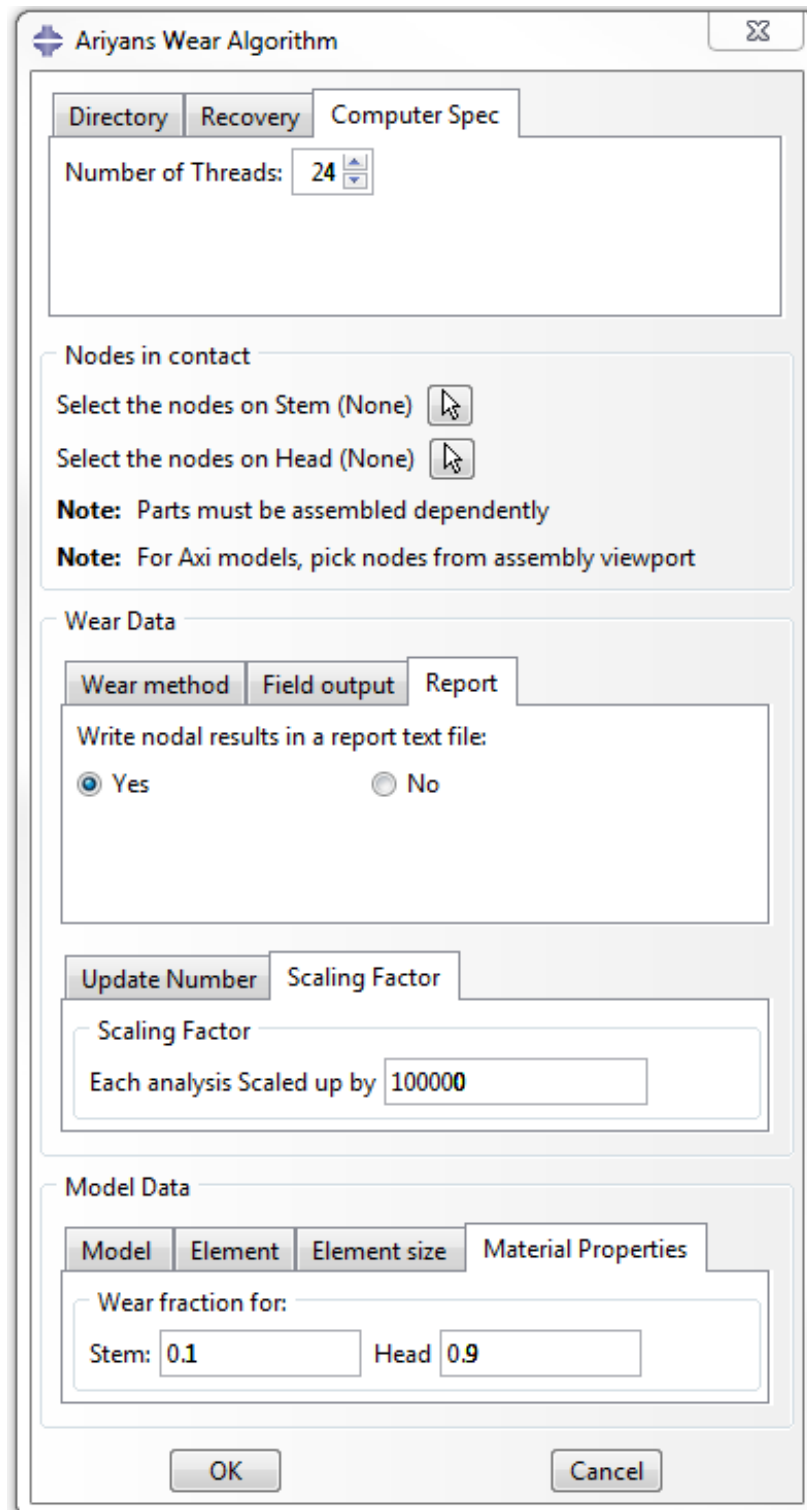
Appendix I: Graphical user interface of the wear algorithm



Graphical user interface of the wear algorithm (1st tabs)



Graphical user interface of the wear algorithm (2nd tabs)



Graphical user interface of the wear algorithm (3rd and 4th tabs)

Appendix II: An example of output request, text format (*.txt); Axisymmetric model

#####

The following parameters have been submitted for the wear analysis:

Input file and work directory: D: \ * \ Job-1.inp

Total load cycles: 15000000

Wear method chosen is Energy

Scaling factor is: 100000

Energy wear Coefficient is: 5.75e-08

Model is Axisymmetric

Elements are Linear

Approximate element size: 0.08

Wear fraction for the Stem: 0.1

Wear fraction for the Head: 0.9

#####

Update Number: 1

#####

Paired Nodes:

[[3, 4], [6, 1], [31, 140], [32, 139], [33, 138], [34, 137], [35, 136], [36, 135], [37, 134], [38, 133], [39, 132], [40, 131], [41, 130], [42, 129], [43, 128], [44, 127], [45, 126], [46, 125], [47, 124], [48, 123], [49, 122], [50, 121], [51, 120], [52, 119], [53, 118], [54, 117], [55, 116], [56, 115], [57, 114], [58, 113], [59, 112], [60, 111], [61, 110], [62, 109], [63, 108], [64, 107], [65, 106], [66, 105], [67, 104], [68, 103], [69, 102], [70, 101], [71, 100], [72, 99], [73, 98], [74, 97], [75, 96], [76, 95], [77, 94], [78, 93], [79, 92]]

#####

Wear depth, for paired nodes:

Wear depth, paired node No: 3-4 = 0.000106920437805

Wear depth, paired node No: 6-1 = 0.000176679257303

Wear depth, paired node No: 31-140 = 8.95696756702e-05

Wear depth, paired node No: 32-139 = 5.34792177971e-05

Wear depth, paired node No: 33-138 = 4.9755629996e-05

Wear depth, paired node No: 34-137 = 4.37857901799e-05

Wear depth, paired node No: 35-136 = 4.3385366419e-05

Wear depth, paired node No: 36-135 = 4.09283949178e-05

Wear depth, paired node No: 37-134 = 4.1065003234e-05

Wear depth, paired node No: 38-133 = 3.98432674453e-05

Wear depth, paired node No: 39-132 = 3.97773780692e-05

Wear depth, paired node No: 40-131 = 3.71853742114e-05

Wear depth, paired node No: 41-130 = 3.44526546335e-05

Wear depth, paired node No: 42-129 = 3.13630973387e-05

Wear depth, paired node No: 43-128 = 2.88436992342e-05

Wear depth, paired node No: 44-127 = 2.62088672693e-05

Wear depth, paired node No: 45-126 = 2.38356877073e-05

Wear depth, paired node No: 46-125 = 2.1589010518e-05

Wear depth, paired node No: 47-124 = 1.95367795943e-05

Wear depth, paired node No: 48-123 = 1.76223446098e-05

Wear depth, paired node No: 49-122 = 1.62769660811e-05
 Wear depth, paired node No: 50-121 = 1.50753420008e-05
 Wear depth, paired node No: 51-120 = 1.39930521899e-05
 Wear depth, paired node No: 52-119 = 1.29137126909e-05
 Wear depth, paired node No: 53-118 = 1.18814587366e-05
 Wear depth, paired node No: 54-117 = 1.08690391276e-05
 Wear depth, paired node No: 55-116 = 9.90218112351e-06
 Wear depth, paired node No: 56-115 = 9.06097257701e-06
 Wear depth, paired node No: 57-114 = 8.76553975768e-06
 Wear depth, paired node No: 58-113 = 8.49008428891e-06
 Wear depth, paired node No: 59-112 = 8.815645237e-06
 Wear depth, paired node No: 60-111 = 9.20351089621e-06
 Wear depth, paired node No: 61-110 = 9.59619393682e-06
 Wear depth, paired node No: 62-109 = 1.01920402996e-05
 Wear depth, paired node No: 63-108 = 1.12839941697e-05
 Wear depth, paired node No: 64-107 = 1.28152137132e-05
 Wear depth, paired node No: 65-106 = 1.43456794671e-05
 Wear depth, paired node No: 66-105 = 1.59070948136e-05
 Wear depth, paired node No: 67-104 = 1.74704407685e-05
 Wear depth, paired node No: 68-103 = 1.92595597966e-05
 Wear depth, paired node No: 69-102 = 2.10927866895e-05
 Wear depth, paired node No: 70-101 = 2.29729495003e-05
 Wear depth, paired node No: 71-100 = 2.49099994721e-05
 Wear depth, paired node No: 72-99 = 2.68367734789e-05
 Wear depth, paired node No: 73-98 = 2.91264146577e-05
 Wear depth, paired node No: 74-97 = 3.11607899686e-05
 Wear depth, paired node No: 75-96 = 3.41929586369e-05
 Wear depth, paired node No: 76-95 = 3.66605432559e-05
 Wear depth, paired node No: 77-94 = 4.20367861935e-05
 Wear depth, paired node No: 78-93 = 4.66107638941e-05
 Wear depth, paired node No: 79-92 = 7.06182494067e-05

#####

Total Wear, Stem

Total wear depth after 1st updates on Stem node No 3: 1.069e-05
 Total wear depth after 1st updates on Stem node No 6: 1.767e-05
 Total wear depth after 1st updates on Stem node No 31: 8.96e-06
 Total wear depth after 1st updates on Stem node No 32: 5.35e-06
 Total wear depth after 1st updates on Stem node No 33: 4.98e-06
 Total wear depth after 1st updates on Stem node No 34: 4.38e-06
 Total wear depth after 1st updates on Stem node No 35: 4.34e-06
 Total wear depth after 1st updates on Stem node No 36: 4.09e-06
 Total wear depth after 1st updates on Stem node No 37: 4.11e-06
 Total wear depth after 1st updates on Stem node No 38: 3.98e-06
 Total wear depth after 1st updates on Stem node No 39: 3.98e-06
 Total wear depth after 1st updates on Stem node No 40: 3.72e-06
 Total wear depth after 1st updates on Stem node No 41: 3.45e-06
 Total wear depth after 1st updates on Stem node No 42: 3.14e-06
 Total wear depth after 1st updates on Stem node No 43: 2.88e-06
 Total wear depth after 1st updates on Stem node No 44: 2.62e-06
 Total wear depth after 1st updates on Stem node No 45: 2.38e-06
 Total wear depth after 1st updates on Stem node No 46: 2.16e-06
 Total wear depth after 1st updates on Stem node No 47: 1.95e-06

Total wear depth after 1st updates on Stem node No 48: 1.76e-06
Total wear depth after 1st updates on Stem node No 49: 1.63e-06
Total wear depth after 1st updates on Stem node No 50: 1.51e-06
Total wear depth after 1st updates on Stem node No 51: 1.4e-06
Total wear depth after 1st updates on Stem node No 52: 1.29e-06
Total wear depth after 1st updates on Stem node No 53: 1.19e-06
Total wear depth after 1st updates on Stem node No 54: 1.09e-06
Total wear depth after 1st updates on Stem node No 55: 9.9e-07
Total wear depth after 1st updates on Stem node No 56: 9.1e-07
Total wear depth after 1st updates on Stem node No 57: 8.8e-07
Total wear depth after 1st updates on Stem node No 58: 8.5e-07
Total wear depth after 1st updates on Stem node No 59: 8.8e-07
Total wear depth after 1st updates on Stem node No 60: 9.2e-07
Total wear depth after 1st updates on Stem node No 61: 9.6e-07
Total wear depth after 1st updates on Stem node No 62: 1.02e-06
Total wear depth after 1st updates on Stem node No 63: 1.13e-06
Total wear depth after 1st updates on Stem node No 64: 1.28e-06
Total wear depth after 1st updates on Stem node No 65: 1.43e-06
Total wear depth after 1st updates on Stem node No 66: 1.59e-06
Total wear depth after 1st updates on Stem node No 67: 1.75e-06
Total wear depth after 1st updates on Stem node No 68: 1.93e-06
Total wear depth after 1st updates on Stem node No 69: 2.11e-06
Total wear depth after 1st updates on Stem node No 70: 2.3e-06
Total wear depth after 1st updates on Stem node No 71: 2.49e-06
Total wear depth after 1st updates on Stem node No 72: 2.68e-06
Total wear depth after 1st updates on Stem node No 73: 2.91e-06
Total wear depth after 1st updates on Stem node No 74: 3.12e-06
Total wear depth after 1st updates on Stem node No 75: 3.42e-06
Total wear depth after 1st updates on Stem node No 76: 3.67e-06
Total wear depth after 1st updates on Stem node No 77: 4.2e-06
Total wear depth after 1st updates on Stem node No 78: 4.66e-06
Total wear depth after 1st updates on Stem node No 79: 7.06e-06

#####

Total Wear, Head

Total wear depth after 1st updates on Head node No 4: 9.623e-05
Total wear depth after 1st updates on Head node No 1: 0.00015901
Total wear depth after 1st updates on Head node No 140: 8.061e-05
Total wear depth after 1st updates on Head node No 139: 4.813e-05
Total wear depth after 1st updates on Head node No 138: 4.478e-05
Total wear depth after 1st updates on Head node No 137: 3.941e-05
Total wear depth after 1st updates on Head node No 136: 3.905e-05
Total wear depth after 1st updates on Head node No 135: 3.684e-05
Total wear depth after 1st updates on Head node No 134: 3.696e-05
Total wear depth after 1st updates on Head node No 133: 3.586e-05
Total wear depth after 1st updates on Head node No 132: 3.58e-05
Total wear depth after 1st updates on Head node No 131: 3.347e-05
Total wear depth after 1st updates on Head node No 130: 3.101e-05
Total wear depth after 1st updates on Head node No 129: 2.823e-05
Total wear depth after 1st updates on Head node No 128: 2.596e-05
Total wear depth after 1st updates on Head node No 127: 2.359e-05
Total wear depth after 1st updates on Head node No 126: 2.145e-05
Total wear depth after 1st updates on Head node No 125: 1.943e-05

Total wear depth after 1st updates on Head node No 124: 1.758e-05
Total wear depth after 1st updates on Head node No 123: 1.586e-05
Total wear depth after 1st updates on Head node No 122: 1.465e-05
Total wear depth after 1st updates on Head node No 121: 1.357e-05
Total wear depth after 1st updates on Head node No 120: 1.259e-05
Total wear depth after 1st updates on Head node No 119: 1.162e-05
Total wear depth after 1st updates on Head node No 118: 1.069e-05
Total wear depth after 1st updates on Head node No 117: 9.78e-06
Total wear depth after 1st updates on Head node No 116: 8.91e-06
Total wear depth after 1st updates on Head node No 115: 8.15e-06
Total wear depth after 1st updates on Head node No 114: 7.89e-06
Total wear depth after 1st updates on Head node No 113: 7.64e-06
Total wear depth after 1st updates on Head node No 112: 7.93e-06
Total wear depth after 1st updates on Head node No 111: 8.28e-06
Total wear depth after 1st updates on Head node No 110: 8.64e-06
Total wear depth after 1st updates on Head node No 109: 9.17e-06
Total wear depth after 1st updates on Head node No 108: 1.016e-05
Total wear depth after 1st updates on Head node No 107: 1.153e-05
Total wear depth after 1st updates on Head node No 106: 1.291e-05
Total wear depth after 1st updates on Head node No 105: 1.432e-05
Total wear depth after 1st updates on Head node No 104: 1.572e-05
Total wear depth after 1st updates on Head node No 103: 1.733e-05
Total wear depth after 1st updates on Head node No 102: 1.898e-05
Total wear depth after 1st updates on Head node No 101: 2.068e-05
Total wear depth after 1st updates on Head node No 100: 2.242e-05
Total wear depth after 1st updates on Head node No 99: 2.415e-05
Total wear depth after 1st updates on Head node No 98: 2.621e-05
Total wear depth after 1st updates on Head node No 97: 2.804e-05
Total wear depth after 1st updates on Head node No 96: 3.077e-05
Total wear depth after 1st updates on Head node No 95: 3.299e-05
Total wear depth after 1st updates on Head node No 94: 3.783e-05
Total wear depth after 1st updates on Head node No 93: 4.195e-05
Total wear depth after 1st updates on Head node No 92: 6.356e-05
#####

Total No of load cycle is 100000

#####

Update Number: 2

#####

Paired Nodes

[[3, 4], [6, 1], [31, 140], [32, 139], [33, 138], [34, 137], [35, 136], [36, 135], [37, 134], [38, 133], [39, 132], [40, 131], [41, 130], [42, 129], [43, 128], [44, 127], [45, 126], [46, 125], [47, 124], [48, 123], [49, 122], [50, 121], [51, 120], [52, 119], [53, 118], [54, 117], [55, 116], [56, 115], [57, 114], [58, 113], [59, 112], [60, 111], [61, 110], [62, 109], [63, 108], [64, 107], [65, 106], [66, 105], [67, 104], [68, 103], [69, 102], [70, 101], [71, 100], [72, 99], [73, 98], [74, 97], [75, 96], [76, 95], [77, 94], [78, 93], [79, 92]]

#####

Wear depth, for paired nodes:

Wear depth, paired node No: 3-4 = 0.000102829952488

Wear depth, paired node No: 6-1 = 0.000157613616695

Wear depth, paired node No: 31-140 = 8.62276321532e-05

Wear depth, paired node No: 32-139 = 5.6820338098e-05

... and so on up to:

#####

Update Number: 153

#####

Paired Nodes

[[3, 175], [6, 137], [31, 136], [32, 135], [33, 134], [34, 133], [35, 132], [36, 131], [37, 130], [38, 129], [39, 128], [40, 127], [41, 126], [42, 125], [43, 124], [44, 123], [45, 122], [47, 120], [48, 119], [49, 118], [50, 117], [54, 113], [55, 112], [56, 111], [57, 110], [58, 109], [59, 108], [79, 176], [199, 1], [200, 140]]

#####

Wear depth, for paired nodes:

Wear depth, paired node No: 3-175=0.00037085212738

Wear depth, paired node No: 6-137=0.00058901912849

Wear depth, paired node No: 31-136=1.10227527029e-05

Wear depth, paired node No: 32-135=0.000113908290225

Wear depth, paired node No: 33-134=9.3301333299e-05

Wear depth, paired node No: 34-133=0.000285674751725

Wear depth, paired node No: 35-132=0.000207459581091

Wear depth, paired node No: 36-131=5.07588150853e-05

Wear depth, paired node No: 37-130=0.00010663823987

Wear depth, paired node No: 38-129=7.35394502589e-05

Wear depth, paired node No: 39-128=9.04853831394e-05

Wear depth, paired node No: 40-127=3.98880606902e-05

Wear depth, paired node No: 41-126=9.37404410961e-05

Wear depth, paired node No: 42-125=6.66798222269e-05

Wear depth, paired node No: 43-124=0.000328204563419

Wear depth, paired node No: 44-123=0.00029646901692

Wear depth, paired node No: 45-122=6.67196957019e-05

Wear depth, paired node No: 47-120=7.06586537356e-05

Wear depth, paired node No: 48-119=0.000731150787109

Wear depth, paired node No: 49-118=0.000447425021158

Wear depth, paired node No: 50-117=5.30217862197e-05

Wear depth, paired node No: 54-113=0.000122520909333

Wear depth, paired node No: 55-112=0.00135313136862

Wear depth, paired node No: 56-111=0.00192006356796

Wear depth, paired node No: 57-110=0.000858041218831

Wear depth, paired node No: 58-109=0.000371850426631

Wear depth, paired node No: 59-108=0.00131849908208
Wear depth, paired node No: 79-176=4.96583022221e-05
Wear depth, paired node No: 199-1=5.83227863443e-05
Wear depth, paired node No: 200-140=0.000338778904776

#####

Total Wear, Stem

Total wear depth after 153 updates on Stem node No3: 0.01062128
Total wear depth after 153 updates on Stem node No 6: 0.0037176
Total wear depth after 153 updates on Stem node No 31: 0.00330802
Total wear depth after 153 updates on Stem node No 32: 0.00337916
Total wear depth after 153 updates on Stem node No 33: 0.00340185
Total wear depth after 153 updates on Stem node No 34: 0.00335303
Total wear depth after 153 updates on Stem node No 35: 0.00330533
Total wear depth after 153 updates on Stem node No 36: 0.00342166
Total wear depth after 153 updates on Stem node No 37: 0.00351946
Total wear depth after 153 updates on Stem node No 38: 0.00330615
Total wear depth after 153 updates on Stem node No 39: 0.00328778
Total wear depth after 153 updates on Stem node No 40: 0.00353012
Total wear depth after 153 updates on Stem node No 41: 0.00335119
Total wear depth after 153 updates on Stem node No 42: 0.00329491
Total wear depth after 153 updates on Stem node No 43: 0.00338817
Total wear depth after 153 updates on Stem node No 44: 0.00340746
Total wear depth after 153 updates on Stem node No 45: 0.00339765
Total wear depth after 153 updates on Stem node No 46: 0.00349141
Total wear depth after 153 updates on Stem node No 47: 0.00336716
Total wear depth after 153 updates on Stem node No 48: 0.00340137
Total wear depth after 153 updates on Stem node No 49: 0.00340226
Total wear depth after 153 updates on Stem node No 50: 0.00326029
Total wear depth after 153 updates on Stem node No 51: 0.00334663
Total wear depth after 153 updates on Stem node No 52: 0.00342553
Total wear depth after 153 updates on Stem node No 53: 0.00340296
Total wear depth after 153 updates on Stem node No 54: 0.00334831
Total wear depth after 153 updates on Stem node No 55: 0.00343209
Total wear depth after 153 updates on Stem node No 56: 0.00336561
Total wear depth after 153 updates on Stem node No 57: 0.0033625
Total wear depth after 153 updates on Stem node No 58: 0.00327721
Total wear depth after 153 updates on Stem node No 59: 0.00339932
Total wear depth after 153 updates on Stem node No 60: 0.0034075
Total wear depth after 153 updates on Stem node No 61: 0.00322452
Total wear depth after 153 updates on Stem node No 62: 0.00324147
Total wear depth after 153 updates on Stem node No 63: 0.00328411
Total wear depth after 153 updates on Stem node No 64: 0.00317278
Total wear depth after 153 updates on Stem node No 65: 0.00329568
Total wear depth after 153 updates on Stem node No 66: 0.00340147
Total wear depth after 153 updates on Stem node No 67: 0.0032128
Total wear depth after 153 updates on Stem node No 68: 0.00322062
Total wear depth after 153 updates on Stem node No 69: 0.00339012
Total wear depth after 153 updates on Stem node No 70: 0.00318755
Total wear depth after 153 updates on Stem node No 71: 0.00328931
Total wear depth after 153 updates on Stem node No 72: 0.00326759
Total wear depth after 153 updates on Stem node No 73: 0.00330292
Total wear depth after 153 updates on Stem node No 74: 0.00328102

Total wear depth after 153 updates on Stem node No 75: 0.0034053
Total wear depth after 153 updates on Stem node No 76: 0.0031567
Total wear depth after 153 updates on Stem node No 77: 0.00362169
Total wear depth after 153 updates on Stem node No 78: 0.0035986
Total wear depth after 153 updates on Stem node No 79: 0.00314197
Total wear depth after 153 updates on Stem node No 201: 0.00328025
Total wear depth after 153 updates on Stem node No 200: 0.00201367
Total wear depth after 153 updates on Stem node No 199: 0.00084378

Total Wear, Head

Total wear depth after 153 updates on Head node No 4: 0.03108249
Total wear depth after 153 updates on Head node No 1: 0.03327276
Total wear depth after 153 updates on Head node No 140: 0.03259467
Total wear depth after 153 updates on Head node No 139: 0.0305635
Total wear depth after 153 updates on Head node No 138: 0.02923528
Total wear depth after 153 updates on Head node No 137: 0.03307427
Total wear depth after 153 updates on Head node No 136: 0.03033169
Total wear depth after 153 updates on Head node No 135: 0.03045535
Total wear depth after 153 updates on Head node No 134: 0.03042903
Total wear depth after 153 updates on Head node No 133: 0.03065642
Total wear depth after 153 updates on Head node No 132: 0.03055048
Total wear depth after 153 updates on Head node No 131: 0.03036886
Total wear depth after 153 updates on Head node No 130: 0.03037759
Total wear depth after 153 updates on Head node No 129: 0.03061305
Total wear depth after 153 updates on Head node No 128: 0.03045112
Total wear depth after 153 updates on Head node No 127: 0.0304696
Total wear depth after 153 updates on Head node No 126: 0.03047995
Total wear depth after 153 updates on Head node No 125: 0.03048722
Total wear depth after 153 updates on Head node No 124: 0.0305234
Total wear depth after 153 updates on Head node No 123: 0.03044921
Total wear depth after 153 updates on Head node No 122: 0.03057558
Total wear depth after 153 updates on Head node No 121: 0.03124722
Total wear depth after 153 updates on Head node No 120: 0.03056599
Total wear depth after 153 updates on Head node No 119: 0.03059766
Total wear depth after 153 updates on Head node No 118: 0.03050126
Total wear depth after 153 updates on Head node No 117: 0.03034412
Total wear depth after 153 updates on Head node No 116: 0.03033095
Total wear depth after 153 updates on Head node No 115: 0.03049722
Total wear depth after 153 updates on Head node No 114: 0.03041046
Total wear depth after 153 updates on Head node No 113: 0.03023158
Total wear depth after 153 updates on Head node No 112: 0.03066356
Total wear depth after 153 updates on Head node No 111: 0.03121623
Total wear depth after 153 updates on Head node No 110: 0.03027695
Total wear depth after 153 updates on Head node No 109: 0.02989742
Total wear depth after 153 updates on Head node No 108: 0.03045828
Total wear depth after 153 updates on Head node No 107: 0.02936342
Total wear depth after 153 updates on Head node No 106: 0.02939366
Total wear depth after 153 updates on Head node No 105: 0.0294623
Total wear depth after 153 updates on Head node No 104: 0.02938912
Total wear depth after 153 updates on Head node No 103: 0.02989556
Total wear depth after 153 updates on Head node No 102: 0.0294816
Total wear depth after 153 updates on Head node No 101: 0.02941148
Total wear depth after 153 updates on Head node No 100: 0.02960983
Total wear depth after 153 updates on Head node No 99: 0.02962093

Total wear depth after 153 updates on Head node No 98: 0.02939543
Total wear depth after 153 updates on Head node No 97: 0.02955586
Total wear depth after 153 updates on Head node No 96: 0.02957698
Total wear depth after 153 updates on Head node No 95: 0.02960646
Total wear depth after 153 updates on Head node No 94: 0.0297007
Total wear depth after 153 updates on Head node No 93: 0.02955171
Total wear depth after 153 updates on Head node No 92: 0.02938088
Total wear depth after 153 updates on Head node No 178: 0.02934043
Total wear depth after 153 updates on Head node No 177: 0.0333092
Total wear depth after 153 updates on Head node No 176: 0.02960112
Total wear depth after 153 updates on Head node No 175: 0.02170698

#####

Total No of load cycle is 15,000,000

#####

The wear analysis reaches to 15,000,000 load cycles

End of the wear analysis

**Appendix III: An example of output request, from ABAQUS Field Output database
(*.ODB); Axisymmetric model**

First update

Field Output Report,

Source 1

ODB: D:/ * /Job-1.odb
Step: Step-2-DI
Frame: Increment 10: Step Time = 1.250

Loc 1 : Nodal values from source 1

Output sorted by column "Node Label".

Field Output reported at nodes for part: HEAD-1

Node Label	WearDepth @Loc 1
1	159.011E-06
4	96.2284E-06
92	63.5564E-06
93	41.9497E-06
94	37.8331E-06
95	32.9945E-06
96	30.7737E-06
97	28.0447E-06
98	26.2138E-06
99	24.1531E-06
100	22.4190E-06
101	20.6757E-06
102	18.9835E-06
103	17.3336E-06
104	15.7234E-06
105	14.3164E-06
106	12.9111E-06
107	11.5337E-06
108	10.1556E-06
109	9.17284E-06
110	8.63657E-06
111	8.28316E-06
112	7.93408E-06
113	7.64108E-06
114	7.88899E-06
115	8.15488E-06
116	8.91196E-06

117	9.78213E-06
118	10.6933E-06
119	11.6223E-06
120	12.5937E-06
121	13.5678E-06
122	14.6493E-06
123	15.8601E-06
124	17.5831E-06
125	19.4301E-06
126	21.4521E-06
127	23.5880E-06
128	25.9593E-06
129	28.2268E-06
130	31.0074E-06
131	33.4668E-06
132	35.7996E-06
133	35.8589E-06
134	36.9585E-06
135	36.8356E-06
136	39.0468E-06
137	39.4072E-06
138	44.7801E-06
139	48.1313E-06
140	80.6127E-06

Minimum 7.64108E-06
At Node 113

Maximum 159.011E-06
At Node 1

Total 1.43835E-03

Field Output reported at nodes for part: STEM-1

Node Label	WearDepth @Loc 1
3	10.6920E-06
6	17.6679E-06
31	8.95697E-06
32	5.34792E-06
33	4.97556E-06
34	4.37858E-06
35	4.33854E-06
36	4.09284E-06
37	4.10650E-06
38	3.98433E-06
39	3.97774E-06
40	3.71854E-06
41	3.44527E-06
42	3.13631E-06
43	2.88437E-06

44	2.62089E-06
45	2.38357E-06
46	2.15890E-06
47	1.95368E-06
48	1.76223E-06
49	1.62770E-06
50	1.50753E-06
51	1.39931E-06
52	1.29137E-06
53	1.18815E-06
54	1.08690E-06
55	990.218E-09
56	906.097E-09
57	876.554E-09
58	849.008E-09
59	881.565E-09
60	920.351E-09
61	959.619E-09
62	1.01920E-06
63	1.12840E-06
64	1.28152E-06
65	1.43457E-06
66	1.59071E-06
67	1.74704E-06
68	1.92596E-06
69	2.10928E-06
70	2.29729E-06
71	2.49100E-06
72	2.68368E-06
73	2.91264E-06
74	3.11608E-06
75	3.41930E-06
76	3.66605E-06
77	4.20368E-06
78	4.66108E-06
79	7.06182E-06

Minimum	849.008E-09
At Node	58

Maximum	17.6679E-06
At Node	6

Total	159.816E-06
-------	-------------

After 1500000 load cycles

Field Output Report,

Source 1

ODB: D:/ * /Job-153.odb
 Step: Step-2-DI
 Frame: Increment 21: Step Time = 1.250

Loc 1 : Nodal values from source 1

Output sorted by column "Node Label".

Field Output reported at nodes for part: HEAD-1

Node Label	WearDepth @Loc 1

1	33.2728E-03
4	31.0825E-03
92	29.3809E-03
93	29.5517E-03
94	29.7007E-03
95	29.6065E-03
96	29.5770E-03
97	29.5559E-03
98	29.3954E-03
99	29.6209E-03
100	29.6098E-03
101	29.4115E-03
102	29.4816E-03
103	29.8956E-03
104	29.3891E-03
105	29.4623E-03
106	29.3937E-03
107	29.3634E-03
108	30.4583E-03
109	29.8974E-03
110	30.2769E-03
111	31.2162E-03
112	30.6636E-03
113	30.2316E-03
114	30.4105E-03
115	30.4972E-03
116	30.3309E-03
117	30.3441E-03
118	30.5013E-03
119	30.5977E-03
120	30.5660E-03
121	31.2472E-03
122	30.5756E-03

123	30.4492E-03
124	30.5234E-03
125	30.4872E-03
126	30.4799E-03
127	30.4696E-03
128	30.4511E-03
129	30.6130E-03
130	30.3776E-03
131	30.3689E-03
132	30.5505E-03
133	30.6564E-03
134	30.4290E-03
135	30.4553E-03
136	30.3317E-03
137	33.0743E-03
138	29.2353E-03
139	30.5635E-03
140	32.5947E-03
175	21.7070E-03
176	29.6011E-03
177	33.3092E-03
178	29.3404E-03

Minimum	21.7070E-03
At Node	175

Maximum	33.3092E-03
At Node	177

Total	1.66063
-------	---------

Field Output reported at nodes for part: STEM-1

Node Label	WearDepth @Loc 1
3	10.6213E-03
6	3.71760E-03
31	3.30802E-03
32	3.37916E-03
33	3.40185E-03
34	3.35303E-03
35	3.30533E-03
36	3.42166E-03
37	3.51946E-03
38	3.30615E-03
39	3.28778E-03
40	3.53012E-03
41	3.35119E-03
42	3.29491E-03
43	3.38818E-03
44	3.40746E-03
45	3.39765E-03

46	3.49141E-03
47	3.36716E-03
48	3.40137E-03
49	3.40226E-03
50	3.26029E-03
51	3.34663E-03
52	3.42553E-03
53	3.40296E-03
54	3.34831E-03
55	3.43209E-03
56	3.36561E-03
57	3.36250E-03
58	3.27721E-03
59	3.39932E-03
60	3.40750E-03
61	3.22452E-03
62	3.24147E-03
63	3.28411E-03
64	3.17278E-03
65	3.29568E-03
66	3.40147E-03
67	3.21280E-03
68	3.22062E-03
69	3.39012E-03
70	3.18755E-03
71	3.28931E-03
72	3.26759E-03
73	3.30292E-03
74	3.28102E-03
75	3.40530E-03
76	3.15670E-03
77	3.62169E-03
78	3.59860E-03
79	3.14197E-03
199	843.781E-06
200	2.01367E-03
201	3.28025E-03

Minimum	843.781E-06
At Node	199

Maximum	10.6213E-03
At Node	3

Total	184.515E-03
-------	-------------

Appendix IV: Publications

Journal of Wear, 2015

Available online: <http://www.sciencedirect.com/science/article/pii/S0043164815003488>

*LJMU research conference, 2015
Awarded the best research impact*

A computational approach to fretting wear prediction in Total Hip Replacements

A Ashkanfar^{1,2}, R English^{1,3} and G Rothwell^{1,4}

¹ Mechanical Engineering and Materials Research Centre, School of Engineering, Technology and Maritime Operation, Liverpool John Moores University, Byrom Street, L3 3AF, UK

² Corresponding author; E-mail: a.ashkanfar@2012.ljmu.ac.uk, Tel.: +44 151 7213662

E-mail: ³ r.english@ljmu.ac.uk, ⁴ g.rothwell@ljmu.ac.uk

Abstract. A challenge in engineering coupling design is the understanding of performance of contact geometry for a given application. “Wear” is one of a number of mechanical failures that can occur in mechanical coupling design. Fretting has been observed in many mechanical coupling and known as a reason of failure of the designs. Recent evidence suggests that fretting wear that occurs at the taper junction of modular total hip replacement leads to failure of the implants. The present study proposes a computational methodology utilising an energy wear law and a 3D finite element model to predict fretting wear at the taper junction of total hip replacements. The proposed method is used to determine surface wear damage, linear and volumetric wear rates that could occur at taper junction of total hip replacements over time. The results obtained are consistent with those found from observation and measurement of retrieved prostheses. The method presented could be used to consider the effect of design changes and clinical technique on subsequent fretting wear in total hip replacements.

Keywords. Wear, Fretting, Finite Element Analysis

1. Introduction

Wear is one of a number of mechanical failures. It is known as an inevitable phenomenon occurring when surfaces of mechanical components are mated together while subjected to load and sliding or rolling. During the wear process, material removes from the surfaces as particles. Fretting is observed in many mechanical assemblies such as shrink fitted coupling, pressure armour layer, keyway-shaft couplings and the specific example which has motivated this research, the taper junction of total hip prosthesis.

Total hip replacement (THR) is a common arthroplasty performed worldwide as a key and successful solution to improve a patient’s lifestyle who is suffering from hip joint diseases or joint fracture. Modern THRs are a major clinical success with expected lifetimes of 10 to 15 years which is a relative success[1, 2].

Traditionally the debris released at the head stem interface has been assumed negligible compared to the wear occurring at bearing surfaces. The determination of wear in THRs up until recently has mainly focused on the articulating surfaces between the head and (plastic) acetabular cup [3-5]; however, fretting and its resulting damage at the taper junction causes failure in many types of prosthetic devices. Corrosion occurs due to fretting which not only leads to implant failure but also causes serious problem such as adverse soft tissue reaction.

This study tries to develop a computational methodology to predict “fretting wear” that could occur in THRs. The study proposes a methodology to predict the wear depth, volumetric wear loss and also the surface damage associated with wear which could occur in a hip prosthesis over time in service.

2. Method

In this study fretting wear is modelled in a commercial THR consisting of a cobalt chromium alloy femoral head and a titanium alloy stem. The material properties of cobalt-chrome and titanium as shown in table 1 were assigned on the FE model of head and stem respectively. Both components were modelled as deformable and linearly elastic in ABAQUS. For the purposes of this study a constant isotropic coefficient of friction is defined for the FE models as shown in table 1 [6].

Table 1: material and interaction properties

Material	Young's Modulus (GPa)	Poisson's ratio	Density (kg/m^3)	Wear fraction	Wear coefficient (MPa^{-1})	Friction coefficient
Co-28Cr-6Mo	210	0.3	7800	0.9	$2.97e-8$	0.21
Ti-6Al-4V	119	0.29	4400	0.1		

The energy wear law bases the calculation of wear depth on the interfacial shear work being the predominant parameter determining wear. It shows that the total wear is obtained from the product of the total local accumulated dissipated energy and an energy wear coefficient α . The total wear depth W_d that is generated over a specified total number of loading cycles N can be determined by equation 1 to calculate the evolution of wear,

$$W_d = \sum_{j=1}^{(N/\beta)} \beta \sum_{i=1}^n \alpha \tau_i s_i \quad (1)$$

where τ_i and s_i are respectively the surface contact shear stress and relative displacement calculated at the end of a specific time interval i for the number of time intervals n and β is a wear scaling factor. The fretting wear coefficient used (table 1) was taken from Zhang, et al. [7] who used a pin on disk reciprocating sliding test for Co-28Cr-6Mo fretting on forged Ti-6Al-4V.

The loading and boundary conditions prescribed to the 3D model during the walking cycle are shown in figure 1. This includes both time variant rotations and loadings about the three global coordinate directions.

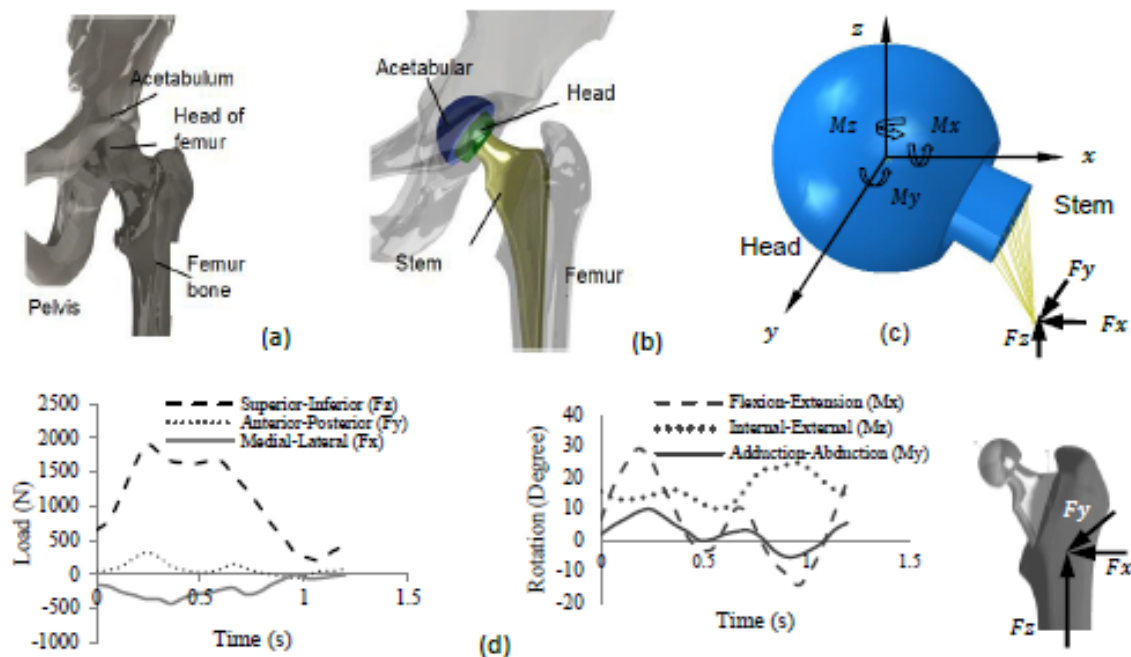


Figure 1: (a) hip joint, (b) hip arthroplasty, (c) finite element model of head and stem of commercial total hip replacement and (d) load and rotation during one step of walking cycle.

The method to predict wear contains three main phases. This method has previously been developed and illustrated by English, et al. [8] and used in this study. The method is summarised in figure 2.

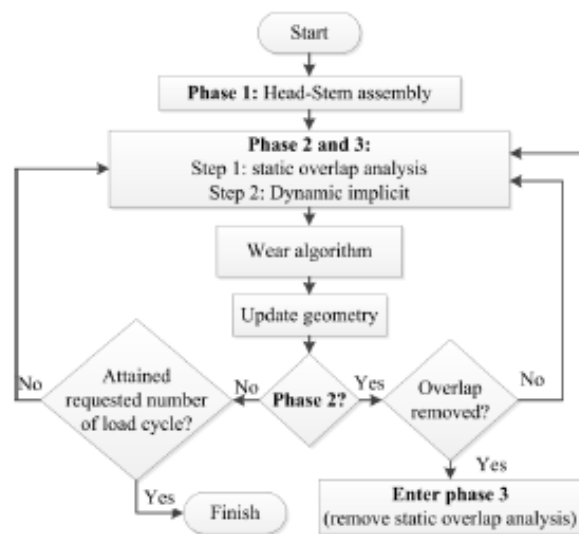


Figure 2: computational wear algorithm [8]

3. Results

Figure 3 shows the contact pressure and slip as well as the wear pattern after applying 5 million walking load cycles. It can be seen that the wear depth on the titanium stem trunnion and in the cobalt chrome head taper at 5 million cycles are different by a factor of around 10 (as dictated by the 'wear fractions' associated with each part) at $2\mu\text{m}$ and $18.6\mu\text{m}$ respectively on the inferior surface taper edges.

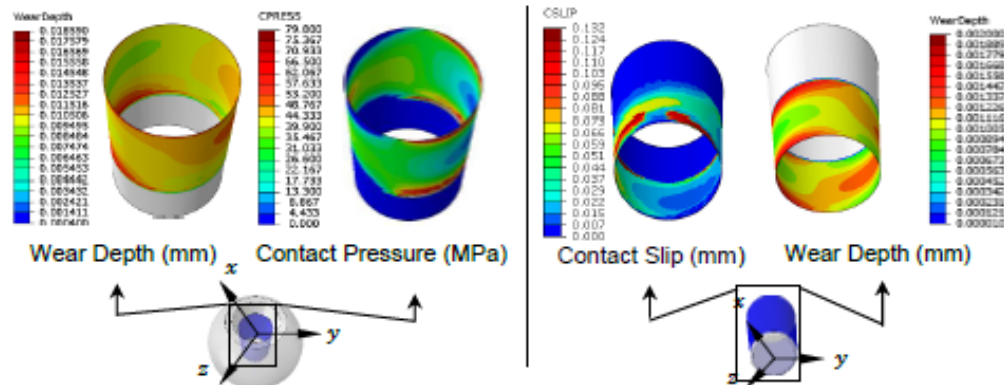


Figure 3: contact pressure, slip and wear depth distribution on the taper and trunnion of the THR

3.1 Validation

The wear pattern and wear rates determined in these studies are similar to those obtained by Langton, et al. [9] for measurements obtained for retrieved THRs. Figure 4 shows a comparison between FE wear simulation and CMM measurement. The wear pattern damage obtained here compare favourably with the CMM measurement results. Figure 4(a) shows the FE fretting results after applying 3.9 million walking load cycle. Figure 4(b) shows the CMM measurement on a retrieved prosthesis that had been in service for less than 5 years.

4. Conclusion

The wear damage pattern, depth and rate are shown to be comparable with those found in the literature and from observation from available retrieved prostheses.

The total dissipated energy wear law and the 3D FE model described can predict linear wear depth and damage patterns effectively when compared to typical observed wear patterns and measured wear depths from retrieved prostheses. The comparisons undertaken show considerable promise but are clearly dependent on the use of an appropriate wear coefficient and knowledge of the retrieved prostheses loading history.

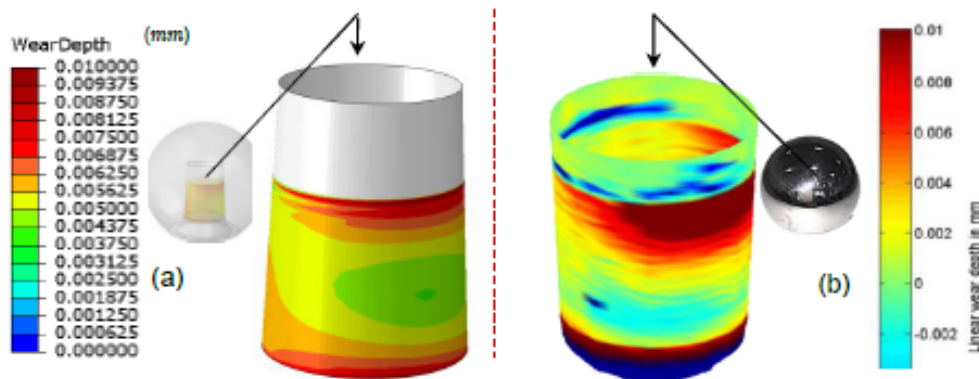


Figure 4: (a) FE wear simulation, head taper, 3.9 million load cycle and (b) Measurement of head taper of retrieved prosthesis, in service less than 5 years, after Langton, et al. [9]

Acknowledgments

This work is funded by the School of Engineering, Technology and Maritime Operations, LJMU.

References

- [1] P. R. Aldinger, M. Thomsen, H. Mau, V. Ewerbeck, and S. J. Breusch, "Cementless Spotorno tapered titanium stems: excellent 10-15-year survival in 141 young patients," *Acta Orthopaedica*, vol. 74, pp. 253-258, 2003.
- [2] M. A. Teloken, G. Bissett, W. J. Hozack, P. F. Sharkey, and R. H. Rothman, "Ten to fifteen-year follow-up after total hip arthroplasty with a tapered cobalt-chromium femoral component (tri-lock) inserted without cement," *The Journal of Bone & Joint Surgery*, vol. 84, pp. 2140-2144, 2002.
- [3] J. C. Fialho, P. R. Fernandes, L. Ecça, and J. Folgado, "Computational hip joint simulator for wear and heat generation," *Journal of Biomechanics*, vol. 40, pp. 2358-2366, 2007.
- [4] S. Patil, A. Bergula, P. C. Chen, C. W. Colwell Jr, and D. D. D'Lima, "Polyethylene wear and acetabular component orientation," *The Journal of Bone & Joint Surgery*, vol. 85, pp. 56-63, 2003.
- [5] J. S. S. Wu, J. P. Hung, C. S. Shu, and J. H. Chen, "The computer simulation of wear behavior appearing in total hip prosthesis," *Computer Methods and Programs in Biomedicine*, vol. 70, pp. 81-91, 2003.
- [6] H. Fessler and D. Fricker, "Friction in femoral prosthesis and photoelastic model cone taper joints," *Proceedings of the Institution of Mechanical Engineers, Part H: Journal of Engineering in Medicine*, vol. 203, pp. 1-14, 1989.
- [7] T. Zhang, N. Harrison, P. McDonnell, P. McHugh, and S. Leen, "A finite element methodology for wear-fatigue analysis for modular hip implants," *Tribology International*, vol. 65, pp. 113-127, 2013.
- [8] R. English, A. Ashkanfar, and G. Rothwell, "A computational approach to fretting wear prediction at the head-stem taper junction of total hip replacements," *Wear*, pp. submitted IH-96712014, 2014.
- [9] D. Langton, R. Sidaginamale, J. Lord, A. Nargol, and T. Joyce, "Taper junction failure in large-diameter metal-on-metal bearings," *Bone and Joint Research*, vol. 1, pp. 56-63, 2012.

Symposium on Modularity and Tapers in Total Joint Replacement Devices, New Orleans, USA, 2014

Symposium on Modularity and Tapers in Total Joint Replacement Devices

Effect of impaction force at assembly on fretting wear at the taper junction of total hip prosthesis

Authors: Russell English¹, Ariyan Ashkanfar^{1,2} and Glynn Rothwell¹

Running Title: EFFECT OF IMPACT ASSEMBLY ON FRETTING WEAR IN THR

Abstract: In the past two decades, changes to hip prosthesis design and surgical technique have led to reports of wear debris release from taper junctions. It is believed that this occurs partly due to fretting which can lead to adverse soft-tissue reaction and subsequent revision surgery. The non-standard assembly of the prosthesis femoral head onto the stem taper at surgery is known to have an effect on the stability of the fixation. However, the effect of variability of impaction forces on fretting wear is unclear. This study investigates the effect of varying the initial impact assembly forces on the extent of any subsequent fretting wear using an axisymmetric finite element model with an algorithm based on the dissipated energy wear law. Impulse data for the finite element simulations were extracted from controlled drop tests with an initial impaction analysis undertaken to provide part displacements for use in subsequent wear analyses. The wear analysis consists of a series of shrink-fit simulations to model the diminishing effect of impaction during the wearing process. It was found that increasing the impaction loads led to an increase in contact stresses but a reduction in micromotion resulting in a decrease in the initial wear rate. As the taper locking effect diminishes during the analysis due to the fretting wear process, it was observed that the micromotion increased leading to a significant increase in wear rate. The results demonstrate the relevance of the impaction force used intra-operatively by medical professionals to provide an optimum fixation to minimize wear due to fretting. Linear wear rates presented in this study are comparable to those found in literature but are dependent on the use of an accurate wear coefficient for specific simulations.

Keywords: wear modeling, fretting, wear, finite element modeling, total hip replacements, prosthesis, energy wear law

Introduction

Modern Total Hip Replacements (THR) are a major clinical success with expected lifetimes of 10 – 15 years. There are approximately 80,000 hip replacement operations each year in the UK (tenth annual report of NJR for England, Wales and Northern Ireland, 2013) and 285,000 in the USA (National Hospital Discharge Survey, USA, 2010) with this number expected to rise with an ageing population. In addition, as these devices are becoming more common place,

¹ School of Engineering, Technology and Maritime Operations, Liverpool John Moores University, Byrom Street, Liverpool, L3 3AF, UK

² Corresponding author Tel: +44 151 231 2028 and +44 759 198 0781. E-mail address: a.ashkanfar@2012.ljmu.ac.uk and ariyan.ashkanfar@gmail.com (A. Ashkanfar).

2 EFFECT OF IMPACT ASSEMBLY ON FRETTING WEAR IN THR

younger patients are adopting this solution too and as such there is a need to improve existing designs further to accommodate their more active lifestyle and to extend the prostheses life.

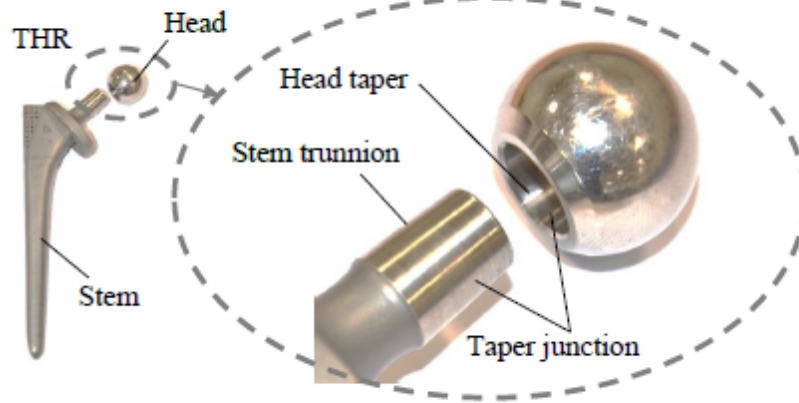


Fig. 1. A commercial THR

THRs normally comprise of three components, an acetabular cup, femoral head and stem. The modularity of the THR allows flexibility intra-operatively to facilitate optimum prosthetic functionality and anatomical fit for the patient. The acetabular cup is fitted into the pelvis and the bearing surface is typically manufactured from Ultra-High-Molecular-Weight Polyethylene (UHMWPE), highly cross-linked polyethylene (HXLPE), ceramic or to a lesser extent recently a cobalt chrome alloy. Prosthetic femoral heads are normally made from either a cobalt chrome alloy, ceramic or stainless steel. The acetabular cup and femoral head provide a smooth articulating bearing surface to allow necessary hip movement and to minimize wear. The stem is made from either titanium alloy, a cobalt chrome alloy, or stainless steel and is fitted into the medullary cavity of the femur. The femoral head is assembled to the stem by means of a Morse taper fixation (Fig. 1).

As well as the benefits associated with modularity there are inherent difficulties associated with the release of wear debris at both the acetabular cup-head articulating surface and the head taper-stem trunnion junction which has led to adverse soft-tissue reactions (ASTR) in recipients [1, 2]. The determination of wear in THRs up until recently has mainly focused on the articulating surfaces between the head and (plastic) acetabular cup [3-10]. Modern large diameter metal-on-metal (MoM) THRs were introduced around 1997 [11] with the promise of much reduced wear rates at the metal cup-head articulation in comparison to the UHMWPE cups. However, it has been reported [1, 11-14] that under certain circumstances metal wear debris can be generated at these articulating surfaces which can lead to Metallosis and immobility in patients [15]. Due to this serious problem large diameter MoM THRs are no longer used for arthroplasty.

Importantly, there have also been reports of ASTR due to metallic wear debris produced from the head – trunnion taper junction for both metal-on-plastic (MoP) [15] and MoM prostheses [1, 12]. Langton et al. [13] presented Scanning Electron Microscope (SEM) images of taper junction surface damage in large diameter MOM THRs. It was hypothesized that the material loss was primarily due to mechanical fretting wear and not corrosion, contrary to the opinion of Malviya et al. [16], Goldberg et al. [17], and Gilbert et al. [18].

3 EFFECT OF IMPACT ASSEMBLY ON FRETTING WEAR IN THR

Femoral head and stem assembly

The assembly of the femoral head onto the stem trunnion at surgery is achieved by impaction by the surgeon using a mallet and polymer tipped impactor. It is known that the magnitude of this impaction force affects the initial taper strength and it has been postulated that attaining maximum fixation is crucial in minimizing problems associated with these tapers such as corrosion, fretting, micromotion and unintended disassembly. A number of experimental studies have investigated parameters that affect taper fixation [19-22] with taper 'pull-off' force being used as the measure to assess taper strength. All of these studies involved (at least) the simulation of the assembly and disassembly of cobalt chrome alloy heads with titanium alloy stem trunnions.

The magnitude of the impaction forces used in the studies were determined initially using tests in [19], [20], and [22] where surgeons were required to apply an impact typical of that used intra-operatively to assemble the head to the stem. The average of the measured forces from the three studies were approximately 5000N (1 surgeon \times 11 impacts) [20]; 1633N, Standard Deviation 422N (8 surgeons \times 5 impacts each) [22]; and 4409N (10 surgeons \times 1 impact) [19]. Rehmer et al. [21] used impact forces of 2000N, 3000N and 4000N (to cover the typical range of force applied by surgeons) describing them as light, medium and firm hammer blows for seating the femoral head on to the stem.

A linear relationship was found by [19], [20], and [21] such that increased impaction resulted in increased pull-off forces (with the ratio between pull-off and impaction being around 0.4 [20] and 0.48 [19]). Lavernia et al. [22] found much reduced pull-off forces where biological debris (blood, fat) existed on the taper during assembly. Pennock et al. [20] and Rehmer et al. [21] stated multiple impacts did not increase taper strength, whereas Heiney et al. [19] advised two firm blows would attain maximum fixation. Pennock et al. [20] suggested that surgeons should apply an in-line maximum impaction but Heiney et al. [19] and Rehmer et al. [21] recommended a firm blow (4000N) so as not to risk damage to the femur. However, Mroczkowski et al. [23] used an impact load of 6700N and hand assembly to represent the 'extremes of what may be seen clinically' in an experimental study into the effect of impact assembly on fretting corrosion of hip tapers.

These studies highlight the non-standard nature of the surgical assembly process for the prosthetic femoral head and stem with evidence of significant variation by surgeons with regard to impaction force and technique used. This variation occurs due to a surgeons differing experience; the type of head (metal or ceramic); and crucially, the quality of the bone stock of the patient. In addition, manufacturers guidelines are vague, with statements such as 'slightly' or 'firmly' impacted the norm to describe the magnitude of any impaction force to be used. There is evidence that the magnitude of the impaction force affects taper fixation [19-21], further, [19-21, 23] suggest that the extent of taper fixation may have an effect on corrosion, micromotion and fretting wear. However, the effect of variability of impaction forces on fretting wear at the taper junction is still unclear [24]. As such, this study investigates the effect of varying the initial impact assembly forces (2000–7000N) on the extent of any subsequent fretting wear at the taper junction over a period of 15 years using an axisymmetric finite element (FE) model with a wear algorithm based on the dissipated energy wear law [25]. The assessment of wear in this study is

4 EFFECT OF IMPACT ASSEMBLY ON FRETTING WEAR IN THR

solely based on mechanical wear (fretting) as being the primary mechanism causing damage at the head-trunnion taper junction.

Wear

The dissipated energy wear law implemented in this study bases the calculation of volumetric wear on the interfacial shear work being the predominant parameter determining wear. Based on this, for axisymmetric analysis, the linear wear depth at the taper junction W_d can be obtained using Eq 1

$$W_d = \alpha \tau s \quad (1)$$

where:

α = energy wear coefficient, MPa^{-1} (determined experimentally),

τ = contact surface shear stress, MPa, (determined using FE analysis), and

s = relative displacement between contacting surfaces, mm (determined using FE analysis).

In order to calculate wear at the taper junction numerically, the method used here is to first calculate the wear depth that would occur during one loading cycle (such as the superior-inferior hip loading during walking). Due to the complex load-time history involved, this is facilitated by discretizing the loading cycle into a number of time intervals n and calculating (then summing) the contribution to the wear depth of each specific time interval i over the cycle. As such, the wear depth for a single cycle of loading (the cyclic wear depth W_c) can be calculated using Eq 2

$$W_c = \sum_{i=1}^n \alpha \tau_i s_i \quad (2)$$

where:

τ_i = surface shear stress, MPa, and

s_i = relative displacement, mm, both calculated at the end of a specific time interval i .

The cyclic wear depth W_c will be very small and if unmodified will have negligible influence on the evolving taper junction surface geometry due to wear. As such, 'wear scaling factors β ' are employed to increase W_c to a value which would have occurred over a much larger number of loading cycles (e.g. 10^5). The total wear depth W_d that is generated over a specified total number of loading cycles N can be determined from Eq 3

$$W_d = \sum_{j=1}^{(N/\beta)} \beta \sum_{i=1}^n \alpha \tau_i s_i \quad (3)$$

where:

j = a specific 'analysis stage' reflecting the evolution of wear

N = total number of loading cycles

β = wear scaling factor

5 EFFECT OF IMPACT ASSEMBLY ON FRETTING WEAR IN THR

It should be noted that the accuracy and efficiency of this approach is dependent on the magnitude of the energy wear coefficient α used, the number of time intervals i used to discretise the loading cycle, and the magnitude of the 'wear scaling factor β '. The approach is described and illustrated in detail in [25].

The energy wear coefficient α encompasses a variety of parameters affecting wear and in addition it is known to change during the wearing process. To the authors knowledge accurate wear coefficients occurring at prosthesis taper junctions have yet to be determined. However, there has been a limited number of *in-vitro* studies considering MoM interactions for both cup and head wear (hip simulators/pin-on-disk) and to consider taper junction wear due to fretting (by means of fretting test rigs) [26-30]. The wear coefficient used in this study ($\alpha=5.75 \times 10^{-8} \text{MPa}^{-1}$) was the average of the two values obtained by Zhang et al. [30] for Co-28Cr-6Mo / forged Ti-6Al-4V from wear measurements taken using SEM and profilometry. Zhang et al. [30] used a pin on disk apparatus with linear reciprocating motion ($\pm 2\text{mm}$) to determine α for application to fretting at THR taper junctions.

Finite Element Model

Geometry and Material

The taper junction geometry of a commercial THR shown in Fig. 1 was used to assess the effect of variability in the magnitude of the impact force used at assembly of the head to the stem trunnion in surgery on the extent of fretting wear that could occur at the taper junction over a period of time *in-vivo*. To predict wear accurately, the model accounts for the initial effect of impaction of the femoral head onto the stem trunnion in surgery with the prosthesis then subject to time variant loading cycles to approximate hip loading during walking.

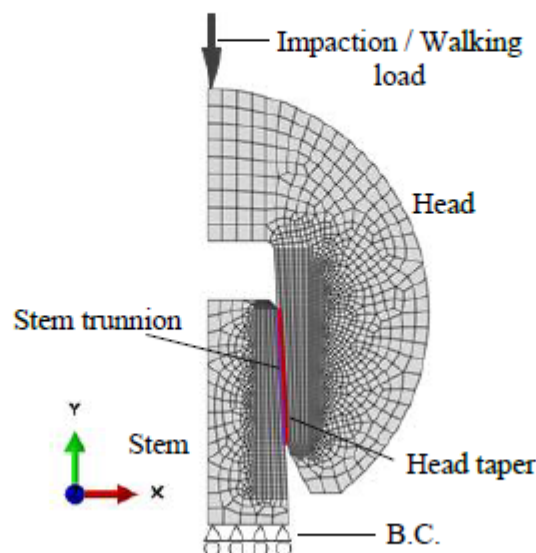


Fig. 2. An axisymmetric FE model of the THR shown in Fig. 1

6 EFFECT OF IMPACT ASSEMBLY ON FRETTING WEAR IN THR

An axisymmetric FE model was used with the head and trunnion tapers modeled as a perfect fit with a zero taper mismatch angle (see Fig. 2). The head and stem trunnion were assembled independently and then meshed in preparation for dynamic analysis in ABAQUS 6.13-1 using four-node bilinear axisymmetric quadrilateral reduced integration elements (CAX4R).

The cobalt chrome alloy head and titanium alloy stem trunnion of the prosthesis were modeled as deformable, linearly elastic and assigned material properties as shown in Table 1. The base of the stem trunnion was fixed in the y translational degree-of-freedom only (see Fig. 2). The contact interaction between the head and stem trunnion was modeled as 'finite sliding' using the 'penalty' contact formulation in ABAQUS, a constant isotropic coefficient of friction of 0.21 was used [31].

Table 1. Material properties of THR components

	Material	Young's Modulus (GPa)	Poisson's ratio	Density (kg/m ³)
Head	Co-28Cr-6Mo	210	0.3	7800
Stem	Ti-6Al-4V	119	0.29	4400

Loading Conditions

The loading applied on the model for each study included an initial impact to simulate the assembly of the head onto the stem trunnion and then time variant loading cycles to approximate hip loading during walking.

Impaction Load

The magnitude of the initial impaction force applied intra-operatively affects both the contact pressure and micromotion at the taper junction and ultimately the extent of any subsequent fretting wear. Manufacturers only provide vague guidelines for the assembly of the head and stem, in reality, the magnitude of the impact used is based on a surgeons experience, the type of prosthetic femoral head, and the quality of the patients bone stock.

In an attempt to simulate the impact event accurately a drop tower was used in this study to determine the impulse time associated with a particular impact (Fig. 3). Test samples were manufactured based on the dimensions of a commercial THR and a peak impact force of 4kN was applied by the drop mass to the test assembly.

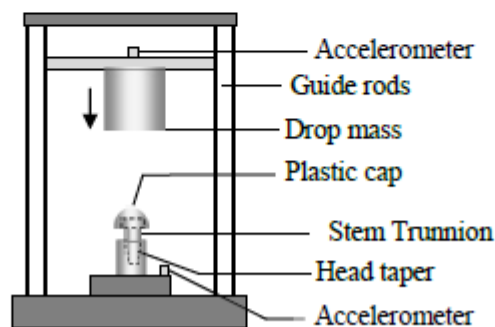


Fig. 3. Drop rig to investigate impulse time and impact magnitude

7 EFFECT OF IMPACT ASSEMBLY ON FRETTING WEAR IN THR

The measured impact duration for a polymer tipped impactor with a metal ‘test’ head was measured as 0.7ms. The load amplitude-time history obtained from the tests and the modified history used for the head-stem assembly event in this study are shown in Fig. 4. The impactation forces investigated during the wear analysis simulation ranged from 2000N to 7000N [19-22].

Walking Load

The in-vivo superior-inferior hip loading during walking was applied on the models as shown in Fig. 5 [32]. The load was applied on the head of the model with a peak force of 2500N with the walking cycle discretized into 20 equal time intervals during the 1.2 second cycle time period. A quantitative assessment of walking activity in patients with various types of hip or knee joint replacements was published by Schmalzried et al. [33], based on this work, in this study, an average of 1 million walking steps per year has been assumed.

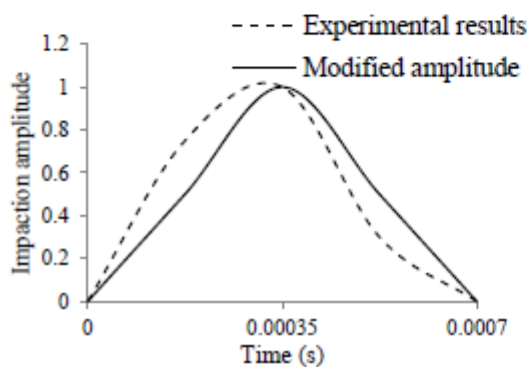


Fig. 4. Impactation assembly load amplitude

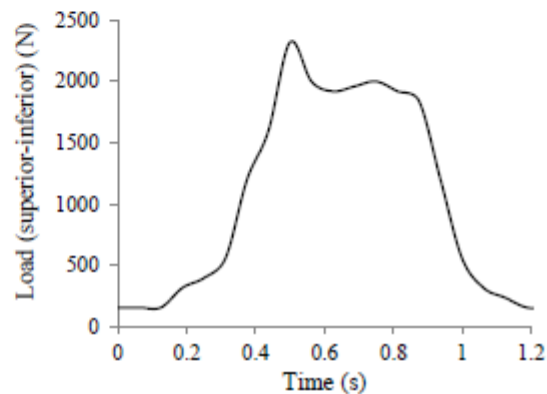


Fig. 5. Superior-inferior load amplitude of a walking cycle applied on the hip.

Wear algorithm and methodology

The FE method incorporating the previously developed wear algorithm [25] is implemented as a user plug-in for ABAQUS and contains three phases to determine the wear depth at the THR taper junction. In phase 1 the impactation load is applied to the top of the head to simulate the process of assembly of the head onto the stem in surgery. The displacements of the parts from this initial analysis are extracted for use in phase 2. In phase 2 the parts are assembled as a shrink-fit based on the displacements obtained from phase 1 which create interference between the components at the contact interface; subsequently, a dynamic analysis is defined and the walking load is applied to the top of the head. The advantage of using a shrink-fit analysis rather than an actual impactation analysis here is that the impactation effect can be diminished gradually from the model during the wearing process by removing the overlap based on accumulated wear. Using the results from the FEA and the energy wear law as defined by Eq. 3, the extent of fretting wear at the taper junction can be determined as a ‘wear depth’ for β walking cycles and the part geometries updated as appropriate. This updating of geometry will partially remove the initial overlap of the parts therefore gradually removing the effect of impactation. For this study, wear is only removed from the titanium alloy stem, although the method can accommodate removal of material from both components dependent on a specified relative wear fraction. The

8 EFFECT OF IMPACT ASSEMBLY ON FRETTING WEAR IN THR

updating of part geometry continues in this manner until the shrink-fit overlap has been almost entirely removed at which point the method continues into phase 3. In phase 3, the shrink-fit analysis step is removed and only a single dynamic step (representing the walking load) is maintained for the rest of the analysis until the specified number of cycles or wear depth for the study has been reached. The method is summarized in Fig. 6.

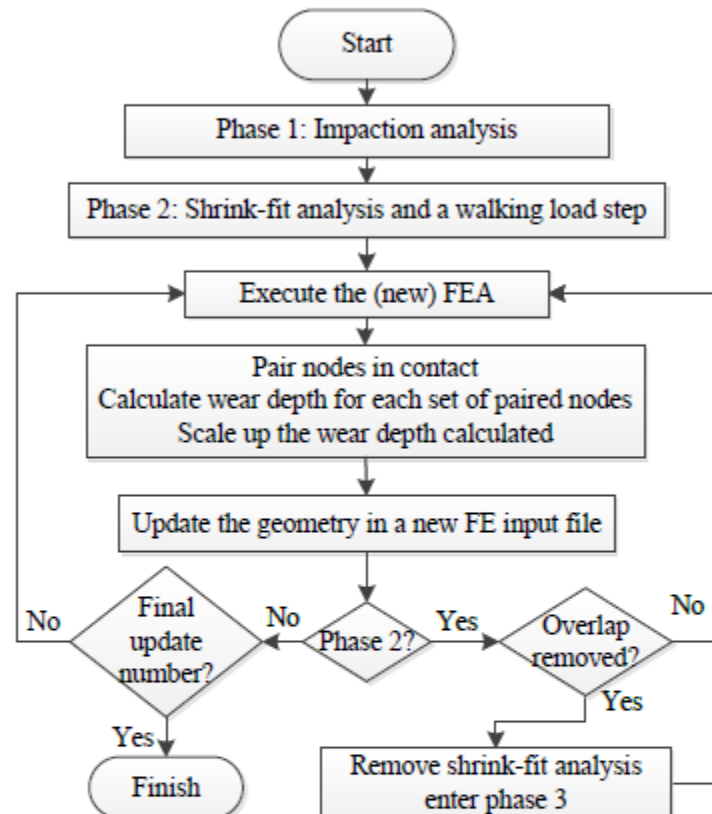


Fig. 6. Computational approach to predict fretting wear considering the initial impact assembly

Convergence

In order to achieve accurate results for wear, three convergence criteria must be met [25]. It was found that an element size of 0.15mm (in the contact area) was appropriate to model a smooth wear pattern on the model. The scaling factor β used in the analysis has a major impact on solution times, wear evolution and solution accuracy. A large scaling factor will facilitate a relatively quick analysis but may detrimentally affect the accuracy of the final calculated wear for a specified number of loading cycles. A comparatively small value for the scaling factor will increase solution times but should provide an accurate result and wear profile. The scaling factor in this study is varied throughout the analysis in order to optimise solution accuracy and run times. This is achieved by consideration of the shear stress distribution and wear depth calculated during each analysis stage. Here the value of β starts from 1 million in phase 2 and reduces to 0.1 million in phase 3 of the analysis.

9 EFFECT OF IMPACT ASSEMBLY ON FRETTING WEAR IN THR

Results and Discussion

The following section details the results from the wear simulations regarding the effect of magnitude of impaction force on fretting wear.

Femoral head and stem assembly

The effect of increasing the assembly impact force on the contact pressure and displacement (in the Y-direction) of an interface node on the femoral head at end of phase 1 of the wear analysis is shown in Fig. 7. It can be seen that an increase in the impaction force results in a linear increase in both the Y-displacement and contact pressure. The displacements (in the Y-direction) for all nodes on the head are almost identical and as such this displacement is used to create the overlap assembly model for the shrink-fit analysis in phase 2.

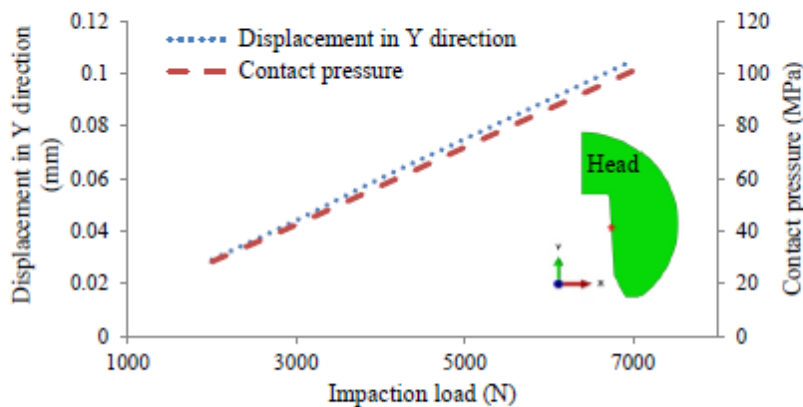


Fig. 7. The effect of increasing the assembly impact force on the contact pressure and displacement (in the Y-direction) of an interface node at end of phase 1 of the wear analysis

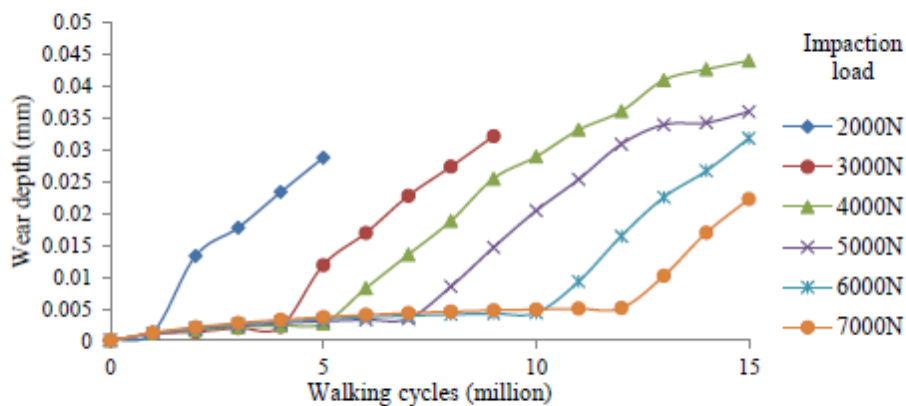


Fig. 8. Wear depth evolution with varying head-stem assembly impaction force

Evolution of wear

Fig. 8 details the evolution of wear along the stem trunnion over a period associated with 15 years of walking activity (15 million load cycles) following the application of varying head-stem

10 EFFECT OF IMPACT ASSEMBLY ON FRETTING WEAR IN THR

assembly impaction forces. The ‘knee’ that can be observed in each curve is the transition point in the wear analysis from phase 2 to phase 3 and can be explained as the point where the ‘locking’ effect caused by the assembly impaction has been fully removed due to the wearing process.

The ‘linear wear rate’ is categorized as the gradient of the curves and is seen to be fairly constant both in phase 2 and 3 for all studies but with a significant increase in wear rate following the transition point (Fig.8). The transition point is therefore very important as far as the production of wear debris is concerned and its implications to early ASTR following arthroplasty. In general, it can be said that a larger impact force at assembly will initially result in higher contact pressures but reduced micromotion at the taper junction. The larger impact forces result in a greater head movement onto the stem and as such a greater taper overlap for the associated shrink-fit analysis. The wear algorithm calculates wear depth at the taper interface following a specified number of wearing cycles and then modifies the surface geometries gradually by removing the overlap based on the accumulated wear. The gradual removal of overlap simulates the effect of wearing and this has an effect on the magnitudes of contact pressure and micromotion. It can be seen that impact forces of 2000N and 3000N result in transition occurring after only 1 and 4 years respectively before significantly greater wear rates commence. On consideration of Fig. 8 it would seem prudent to apply as large an impact force at assembly as possible within the limits of safety for the patient and structural integrity of the prosthesis design. Maintaining the effect of impaction for as long as possible (in phase two) is key to reduced wear rates. For impaction forces of 4000, 5000, 6000 and 7000N, the transition points occur after approximately 5, 7, 10 and 12 years respectively with associated wear depths after 15 years of 43 μ m, 36 μ m, 32 μ m and 22 μ m. Fig. 9 shows an approximately linear relationship between the impaction force and the transition point line (for an impaction force interval from 2000N to 7000N).

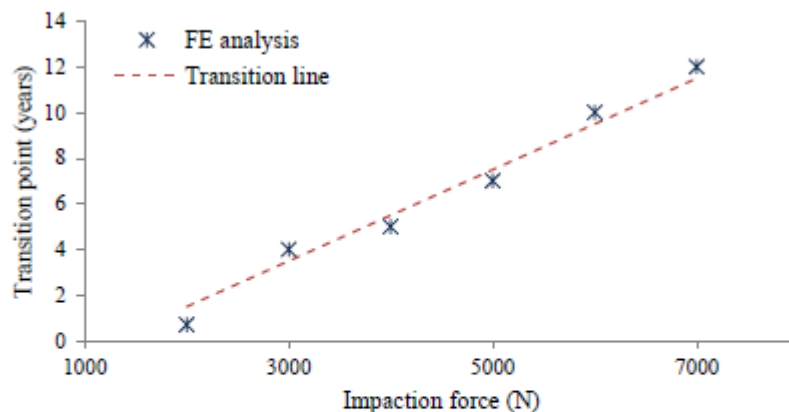


Fig. 9. Variation in transition point (in years) with head-stem assembly impaction force

Fig. 10a, b, c and d detail the wear occurring along the stem taper after different periods of time (1, 5, 10 and 15 years). In general it can be seen that the evolution of wear along the stem trunnion surface is of a fairly uniform depth indicating a smooth wearing out as would be expected for the conforming contacts throughout the time period analyzed.

Fig. 10a and b show the early transition into phase 3 for the models assembled using a 2000N and 3000N impact force. It can be seen that the wear depths along the interface are significantly greater at 1 and 5 million cycles than that for models impacted with a force greater

11 EFFECT OF IMPACT ASSEMBLY ON FRETTING WEAR IN THR

than 4000N (all of which remain in phase 2 until at least 5 million cycles (5 years)). Fig. 8 shows that the 2000N and 3000N impaction models enter phase 3 of the analysis after less than 1 million cycles and 4 million cycles respectively. This subjects the prostheses to a much increased wear rate which could be attributed to the early failure of these devices. In terms of the simulation, the early high wear rates and subsequent wear depths cause convergence problems for the FE analysis at around 10 million load cycles and as such these results have not been included in Fig. 10c and d. It has been suggested [19-21] that impaction forces of between 4000–5000N will maximize taper strength whilst mitigating against damage to the femur. Fig. 8 shows that the 4000N impaction model enters phase 3 (and the much increased wear rate) after approximately 5 million cycles (5 years); whereas the 5000N impaction model enters phase 3 after around 7 million cycles (7 years). The models associated with impaction forces of 6000N and 7000N are maintained in phase 2 up until 10 million cycles (Fig. 10). The 6000N impaction model enters phase 3 at 10 million cycles whereas the 7000N impaction model enters at 12 million cycles. This late entry into phase 3 would indicate minimal wear debris generation over 10 to 12 years *in vivo*.

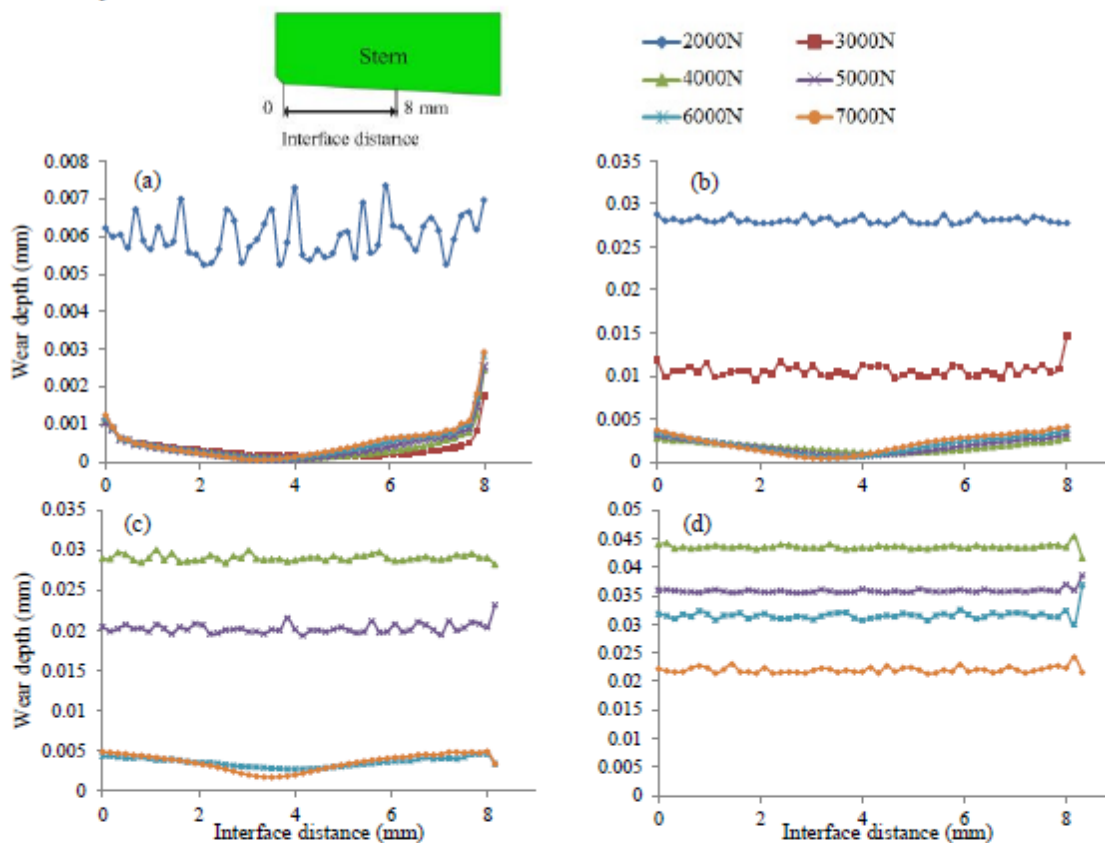


Fig. 10. Wear profile evolution along stem trunnion after (a) 1, (b) 5, (c) 10, and (d) 15 million load cycles

12 EFFECT OF IMPACT ASSEMBLY ON FRETTING WEAR IN THR

Wear rate

Fig. 11 shows the variation in wear rate over a period of 15 million cycles for the different assembly impaction models. It can be seen that in phase 2 the wear rate is relatively small (in comparison to phase 3) with values of around $0.4\mu\text{m}/\text{year}$ for all models. It is clear that there is a significant increase in wear rate at the transition points for each model with a wear rate just after this point of around $6.2\mu\text{m}/\text{year}$ for all models. The severity of the transition is considered to be a numerical effect caused by a remaining small residual overlap term at the transition between phase 2 and 3, in practice, this transition is likely to be less severe. In phase 3 it can be seen that the wear rate reduces over time but is still much greater than that occurring in phase 2 (10 to 15 times greater).

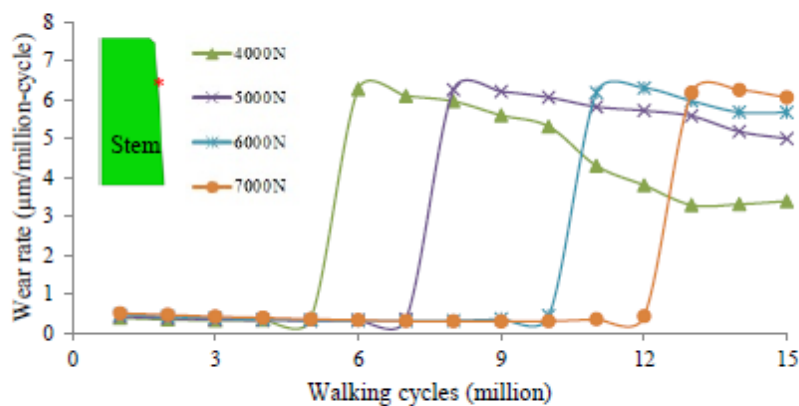


Fig. 11. Linear wear rate during the wearing process for different impaction assembly forces

From Fig. 11 it can be seen that the mean wear rates in phase 3 for the 4000N, 5000N, 6000N and 7000N impaction models are approximately 4.83 , 5.63 , 5.92 and $6.15\mu\text{m}/\text{year}$ respectively. The lower mean wear rate at the lower impactions is due to their earlier entry into phase 3. The mean wear rates calculated here compare favorably (in phase 3) with values obtained by Langton et al. [13] for measurements obtained at the head taper for retrieved large diameter MOM THRs ($5.92\mu\text{m}/\text{yr}$ for DePuy ASR XL at around 3.5 years in vivo). Differences can be attributed to differences in material combinations, THR design, head-stem assembly, loading history as well as the idealized FE model and the wear coefficient used in the numerical study.

The area under the curves shown in Fig. 11 are the product of wear rate and the number of loading cycles considered (in this case 15 million cycles). As such, the areas under the curve represent the average linear wear depths after 15 million load cycles and are shown in Table 2.

Table 2. Average linear wear depth after 15 million load cycles for different initial impaction assembly forces

Impaction force (N)	4000	5000	6000	7000
Average linear wear depth after 15 million load cycle (μm)	43.71	35.46	31.14	21.93

13 EFFECT OF IMPACT ASSEMBLY ON FRETTING WEAR IN THR

Variation in contact pressure and relative displacement

Fig. 12 details changes in wear rate and wear depth occurring at an interface node on the model stem with respect to contact pressure and relative displacement over a period of 15 years for the 4000N impaction model. The nodal contact pressure initially has a value of 60MPa at the commencement of phase 2 with this gradually reducing in value during the first 5 million loading cycles as the interface wears. At the transition point the contact pressure has a value of 48MPa before it reduces significantly to a value of 22MPa at the start of phase 3. The contact pressure reduces only slightly during phase 3 maintaining a value of around 17MPa throughout. During phase 2 the relative displacement occurring at the taper junction is only around 2 μm . At the transition point this increases rapidly to 32 μm at 5–6 million cycles. However, unlike the contact pressure which stays fairly constant, the relative displacement reduces in phase 3 to a value of 12 μm at 15 million cycles. It can be seen that the wear rate is mainly affected by changes in the relative displacement over the time period considered. As mentioned previously, the wear rate increases from a value of around 0.4 $\mu\text{m}/\text{yr}$ in phase 2 to a value of 6.4 $\mu\text{m}/\text{yr}$ immediately following the transition point. During phase 3 the wear rate is heavily influenced by the reducing relative displacement (rather than the more constant contact pressure) attaining a value at 15 million cycles of 3.4 $\mu\text{m}/\text{yr}$. The wear depth does not increase much during phase 2, however it increases fairly uniformly between 5 and 9 million cycles reaching a depth of 26 μm . From this point onwards the wear depth still increases but at a lesser rate due to the reducing wear rate and relative displacement.

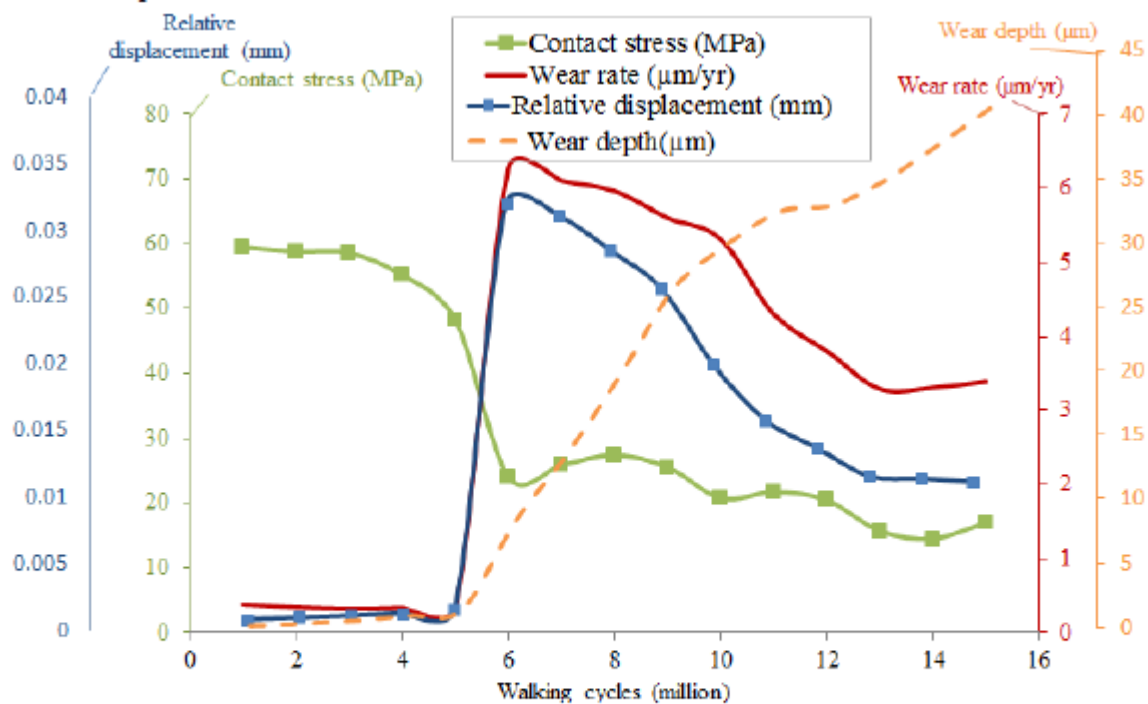


Fig. 12. The evolution of wear rate and wear depth with respect to contact stress and relative displacement over 15 years (results for 4000N impaction force), values have been averaged for each set of a million cycles

14 EFFECT OF IMPACT ASSEMBLY ON FRETTING WEAR IN THR

Conclusions*Clinical*

The impaction force applied during assembly of the prosthetic femoral head to the stem intra-operatively has an effect on subsequent fretting wear at the taper junction of THRs

The greater the magnitude of the impaction force the longer the period of time the beneficial effects of fixation remain with the taper junction only subject to very low wear rates.

A 'transition' point exists where the beneficial effects of fixation are completely removed and a significant increase in wear rate occurs.

Maintaining 'good fixation' for as long as possible is key to reduced wear rates and as such the transition point should occur after the longest time *in vivo* as possible. As such, to minimize fretting wear, surgeons should apply as large an impaction force as possible at assembly (ideally greater than 4kN) whilst ensuring the integrity of the patient femur and prosthetic device.

Numerical

The wear algorithm and FE model presented here is able to model the effect the impaction forces (used to assemble the femoral prosthetic head to the stem trunnion) have on subsequent fretting wear at the taper junction in a THR. This is achieved by modeling the effect of assembly as a shrink-fit procedure then simulating the development of wear by removing overlap in line with the calculated wear depth for a particular stage of the analysis.

Prior to the 'transition' point, as the overlap is removed by wear, the contact pressure and contact stresses at the interface decrease whereas the relative displacements increase slightly. At the transition point (when the overlap is completely removed) a significant decrease in contact pressure occurs coinciding with a proportionally greater increase in relative displacement at the interface leading to a much increased wear rate. Subsequent to the transition point the contact pressure stays relatively constant with the magnitude of the relative displacement reducing gradually over several years resulting in reducing wear rates. It can be seen that in this application a reduction in the interface contact pressure results in an increase in relative displacement (micromotion) ; whereas an increase in contact pressure (due to increased impaction) results in reduced micromotion and fretting wear.

Limitations of the method and FE model are the axisymmetric nature of the model and the assumption that the wear coefficient is a constant over the wearing process. These limitations are currently being addressed by the authors with the development and extension of the existing methodology to 3D and the determination of more realistic and accurate wear coefficients for typical THR head-stem material combinations from controlled experiments.

Acknowledgment

This work is funded by the School of Engineering, Technology and Maritime Operations, Liverpool John Moores University, Liverpool, UK. The authors would like to acknowledge the contribution of Professor Thomas Joyce from Newcastle University, Newcastle, UK. We would

15 EFFECT OF IMPACT ASSEMBLY ON FRETTING WEAR IN THR

also like to thank Mr Viju Peter, Mr Alasdair Santini, and Mr Andrew Phillipson orthopedic surgeons from Broadgreen Hospital, Liverpool, UK, for their advice and cooperation.

References

- [1] Langton, D., Jameson, S., Joyce, T., Gandhi, J., Sidaginamale, R., Mereddy, P., Lord, J. and Nargol, A., "Accelerating Failure Rate of the Asr Total Hip Replacement", *Journal of Bone & Joint Surgery, British Volume*, Vol. 93, 2011, pp. 1011-1016.
- [2] Mattei, L., Di Puccio, F., Piccigallo, B. and Ciulli, E., "Lubrication and Wear Modelling of Artificial Hip Joints: A Review", *Tribology International*, Vol. 44, 2011, pp. 532-549.
- [3] Fialho, J. C., Fernandes, P. R., Eccia, L. and Folgado, J., "Computational Hip Joint Simulator for Wear and Heat Generation", *Journal of Biomechanics*, Vol. 40, 2007, pp. 2358-2366.
- [4] Maxian, T. A., Brown, T. D., Pedersen, D. R. and Callaghan, J. J., "3-Dimensional Sliding/Contact Computational Simulation of Total Hip Wear", *Clinical Orthopaedics and Related Research*, Vol. 333, 1996, pp. 41-50.
- [5] Maxian, T. A., Brown, T. D., Pedersen, D. R. and Callaghan, J. J., "A Sliding-Distance-Coupled Finite Element Formulation for Polyethylene Wear in Total Hip Arthroplasty", *Journal of Biomechanics*, Vol. 29, 1996, pp. 687-692.
- [6] Maxian, T. A., Brown, T. D., Pedersen, D. R., McKellop, H. A., Lu, B. and Callaghan, J. J., "Finite Element Analysis of Acetabular Wear: Validation, and Backing and Fixation Effects", *Clinical Orthopaedics and Related Research*, Vol. 344, 1997, pp. 111-117.
- [7] Patil, S., Bergula, A., Chen, P. C., Colwell Jr, C. W. and D'Lima, D. D., "Polyethylene Wear and Acetabular Component Orientation", *The Journal of Bone & Joint Surgery*, Vol. 85, 2003, pp. 56-63.
- [8] Raimondi, M., Santambrogio, C., Pietrabissa, R., Raffelini, F. and Molfetta, L., "Improved Mathematical Model of the Wear of the Cup Articular Surface in Hip Joint Prostheses and Comparison with Retrieved Components", *Proceedings of the Institution of Mechanical Engineers, Part H: Journal of Engineering in Medicine*, Vol. 215, 2001, pp. 377-390.
- [9] Teoh, S., Chan, W. and Thampuran, R., "An Elasto-Plastic Finite Element Model for Polyethylene Wear in Total Hip Arthroplasty", *Journal of Biomechanics*, Vol. 35, 2002, pp. 323-330.
- [10] Wu, J. S. S., Hung, J. P., Shu, C. S. and Chen, J. H., "The Computer Simulation of Wear Behavior Appearing in Total Hip Prosthesis", *Computer Methods and Programs in Biomedicine*, Vol. 70, 2003, pp. 81-91.
- [11] Cohen, D., "How Safe Are Metal-on-Metal Hip Implants?", *BMJ: British Medical Journal*, Vol. 344, 2012,
- [12] Bolland, B., Culliford, D., Langton, D., Millington, J., Arden, N. and Latham, J., "High Failure Rates with a Large-Diameter Hybrid Metal-on-Metal Total Hip Replacement", *Journal of Bone & Joint Surgery, British Volume*, Vol. 93, 2011, pp. 608-615.
- [13] Langton, D., Sidaginamale, R., Lord, J., Nargol, A. and Joyce, T., "Taper Junction Failure in Large-Diameter Metal-on-Metal Bearings", *Bone and Joint Research*, Vol. 1, 2012, pp. 56-63.

16 EFFECT OF IMPACT ASSEMBLY ON FRETTING WEAR IN THR

- [14] Sporer, S. M. and Chalmers, P. N., "Cutaneous Manifestation of Metallosis in a Metal-on-Metal Total Hip Arthroplasty after Acetabular Liner Dissociation", *The Journal of Arthroplasty*, Vol. 27, 2012, pp. 1580-e13.
- [15] Mao, X., Tay, G. H., Godbolt, D. B. and Crawford, R. W., "Pseudotumor in a Well-Fixed Metal-on-Polyethylene Uncemented Hip Arthroplasty", *The Journal of Arthroplasty*, Vol. 27, 2012, pp. 493-e13.
- [16] Malviya, A., Ramaskandhan, J., Bowman, R., Hashmi, M., Holland, J., Kometa, S. and Lingard, E., "What Advantage Is There to Be Gained Using Large Modular Metal-on-Metal Bearings in Routine Primary Hip Replacement? A Preliminary Report of a Prospective Randomised Controlled Trial", *Journal of Bone & Joint Surgery, British Volume*, Vol. 93, 2011, pp. 1602-1609.
- [17] Goldberg, J. R., Gilbert, J. L., Jacobs, J. J., Bauer, T. W., Paprosky, W. and Leurgans, S., "A Multicenter Retrieval Study of the Taper Interfaces of Modular Hip Prostheses", *Clinical Orthopaedics and Related Research*, Vol. 401, 2002, pp. 149-161.
- [18] Gilbert, J. L., Buckley, C. A. and Jacobs, J. J., "In Vivo Corrosion of Modular Hip Prosthesis Components in Mixed and Similar Metal Combinations. The Effect of Crevice, Stress, Motion, and Alloy Coupling", *Journal of Biomedical Materials Research*, Vol. 27, 1993, pp. 1533-1544.
- [19] Heiney, J. P., Battula, S., Vrabec, G. A., Parikh, A., Blice, R., Schoenfeld, A. J. and Njus, G. O., "Impact Magnitudes Applied by Surgeons and Their Importance When Applying the Femoral Head onto the Morse Taper for Total Hip Arthroplasty", *Archives of Orthopaedic and Trauma Surgery*, Vol. 129, 2009, pp. 793-796.
- [20] Pennock, A. T., Schmidt, A. H. and Bourgeault, C. A., "Morse-Type Tapers: Factors That May Influence Taper Strength During Total Hip Arthroplasty", *The Journal of arthroplasty*, Vol. 17, 2002, pp. 773-778.
- [21] Rehmer, A., Bishop, N. E. and Morlock, M. M., "Influence of Assembly Procedure and Material Combination on the Strength of the Taper Connection at the Head-Neck Junction of Modular Hip Endoprostheses", *Clinical Biomechanics*, Vol. 27, 2012, pp. 77-83.
- [22] Lavemia, C. J., Baerga, L., Barrack, R. L., Tozakoglou, E., Cook, S. D., Lata, L. and Rossi, M. D., "The Effects of Blood and Fat on Morse Taper Disassembly Forces", *Am J Orthop (Belle Mead NJ)*, Vol. 38, 2009, pp. 187-90.
- [23] Mroczkowski, M. L., Hertzler, J. S., Humphrey, S. M., Johnson, T. and Blanchard, C. R., "Effect of Impact Assembly on the Fretting Corrosion of Modular Hip Tapers", *Journal of orthopaedic research*, Vol. 24, 2006, pp. 271-279.
- [24] Wassef, A. and Schmalzried, T., "Femoral Taperosis an Accident Waiting to Happen?", *Bone & Joint Journal*, Vol. 95, 2013, pp. 3-6.
- [25] English, R., Ashkanfar, A. and Rothwell, G., "A Computational Approach to Fretting Wear Prediction at the Head-Stem Taper Junction of Total Hip Replacements ", *Submitted for Publication*, 2014,

17 EFFECT OF IMPACT ASSEMBLY ON FRETTING WEAR IN THR

- [26] Chiba, A., Kumagai, K., Nomura, N. and Miyakawa, S., "Pin-on-Disk Wear Behavior in a Like-on-Like Configuration in a Biological Environment of High Carbon Cast and Low Carbon Forged Co-29cr-6mo Alloys", *Acta Materialia*, Vol. 55, 2007, pp. 1309-1318.
- [27] Fridrici, V., Fouvry, S. and Kapsa, P., "Effect of Shot Peening on the Fretting Wear of Ti-6al-4v", *Wear*, Vol. 250, 2001, pp. 642-649.
- [28] Liu, F., Leslie, I., Williams, S., Fisher, J. and Jin, Z., "Development of Computational Wear Simulation of Metal-on-Metal Hip Resurfacing Replacements", *Journal of Biomechanics*, Vol. 41, 2008, pp. 686-694.
- [29] Magaziner, R., Jain, V. and Mall, S., "Wear Characterization of Ti-6al-4v under Fretting-Reciprocating Sliding Conditions", *Wear*, Vol. 264, 2008, pp. 1002-1014.
- [30] Zhang, T., Harrison, N., McDonnell, P., McHugh, P. and Leen, S., "A Finite Element Methodology for Wear-Fatigue Analysis for Modular Hip Implants", *Tribology International*, Vol. 65, 2013, pp. 113-127.
- [31] Fessler, H. and Fricker, D., "Friction in Femoral Prosthesis and Photoelastic Model Cone Taper Joints", *Proceedings of the Institution of Mechanical Engineers, Part H: Journal of Engineering in Medicine*, Vol. 203, 1989, pp. 1-14.
- [32] Bergmann, G., Graichen, F. and Rohlmann, A., "Hip Joint Loading During Walking and Running, Measured in Two Patients", *Journal of Biomechanics*, Vol. 26, 1993, pp. 969-990.
- [33] Schmalzried, T. P., Szuszczewicz, E. S., Northfield, M. R., Akizuki, K. H., Frankel, R. E., Belcher, G. and Amstutz, H. C., "Quantitative Assessment of Walking Activity after Total Hip or Knee Replacement*", *The Journal of Bone & Joint Surgery*, Vol. 80, 1998, pp. 54-9.

Finite Element Models for quantitative analysis of wear damage in Metal-on-Metal modular hip prosthesis

A Ashkanfar^{1,2}, R English² and G Rothwell².

Mechanical Engineering and Materials Research Centre,

Liverpool John Moores University, Byrom Street, L3 3AF, UK

E-mail: a.ashkanfar@2012.ljmu.ac.uk, r.english@ljmu.ac.uk, g.rothwell@ljmu.ac.uk

Abstract. Wear is known as one of the main reasons for failure of modular medical implants such as metal-on-metal (MoM) Total Hip Replacements (THR) which are subject to oscillatory loads. Wear debris from MoM THR is currently a major issue. The wear debris produced from these devices occurs from the acetabular cup and head articulating surface and the head-stem taper connection. Fretting wear occurs between the fixed parts of modular prosthesis (head and stem) and has been neglected in investigations so far. Fretting wear can remove the effect of impaction, which is used to fix these parts together. Moreover, the fine wear debris released due to the fretting can lead to adverse side effects such as metallosis. To increase the prosthetic devices life, being able to predict the extent of wear that could occur in the device over several years in service in the body is vital. Experimental testing to determine wear that occurs in the prostheses is time consuming, expensive and complicated. Therefore, computational wear modelling is an alternative method to predict wear. The aim of this study is to introduce a methodology to predict fretting wear between the head and stem of a modular MoM prosthesis using finite element analysis (FEA). The method has been automated using a Python script to extract the required results from the FEA and update the prosthesis geometry to reflect the extent of wear that has occurred during the period analysed. The method considers the initial locking effect of impaction at assembly. The method has been applied successfully to both axisymmetric and 3-d FEA models. Currently, the results have been compared against those found in the literature. From these comparisons, the results computed, show considerable promise but are clearly dependant on the use of an appropriate wear coefficient and accurate loading history.

1. Introduction

A hip joint can allow a wide range of movement and transmit high dynamic loads. Its performance to carry loads and provide this mobility is remarkable; however, it is vulnerable and can lose its functionality due to disease such as osteoarthritis or bone fracture. At the final stage of severe hip pathologies, arthroplasty is a key solution for patients. Sir John Charnley carried out the first hip arthroplasty in November 1962. He developed a method to replace the total hip joint by an artificial one and established a surgical technique for implantation. Implants and surgical techniques have advanced since then but they use the same foundation proposed by Charnley. The aim of the surgery is to accommodate an active lifestyle for patients. In general, a hip prosthesis consists of a head, stem

¹ Corresponding author; Tel.: +44 151 7213662

² Mechanical Engineering and Material Research Centre, School of Engineering, Technology and Maritime Operation, Liverpool John Moores University, Byrom Street, Liverpool, United Kingdom, L3 3AF

and cup (Figure 1). There are two main types available for selection by a surgeon dependant on the age, activity and biological condition of individual patients, these are; total hip replacements (THR) and hip resurfacing replacements (HRRs). THR consists of a femoral head, tapered stem and cup; HRR are based on a spigotted hollow head (which references the surgically prepared head of the femur bone) and an acetabular cup component. The femoral stem primarily carries the body load and replaces a considerable portion of the bone.

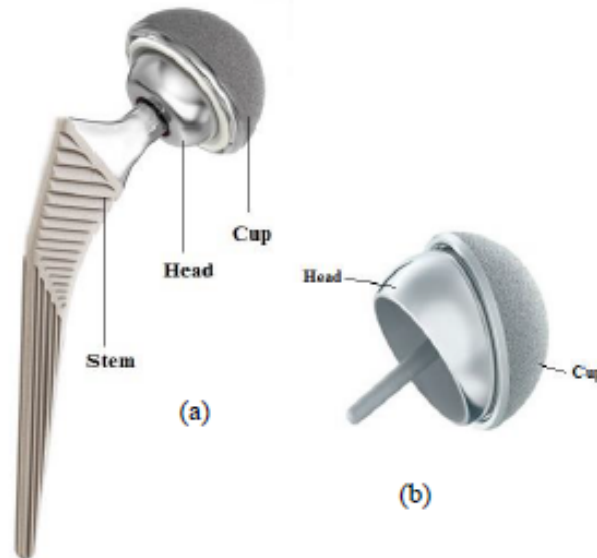


Figure 1. (a) Corail THR, (b) ASR HRR (DePuy, United Kingdom)

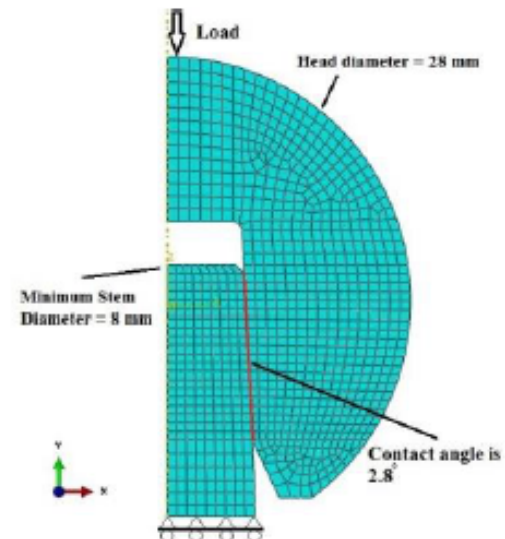


Figure 2. Axisymmetric FE model of DePuy Elite 9/10 prosthesis

Current data from the National Joint Registry (NJR) indicates that around 80,000 hip operations per year are performed in the UK using arthroplasty [4]. It has been recorded that a large number of implants fail at either an early stage after surgery due to dislocation of parts or disassembly, or later due to adverse biological reaction to wear debris [5]. The failure rates vary with the brand of the prosthesis. For Articular Surface Replacement (ASR; DePuy, United Kingdom) the NJR announced more than 29% failure between 2008 and 2011 [4]. The failure rate at 7 years is around 11.8% for MoM HRRs and 13.6% for MoM THRs. This compares with 3.3% to 4.9% failure rate for those made of other materials. It is clear therefore that a large percentage of MoM prostheses have failed recently and it can be claimed that the implants are not a complete success and still require further development. A significant increase in the number of young active patients using hip prosthesis has led to much research to raise the longevity of the prosthetic device. These investigations include improvement in design, use of alternative bearing surfaces, materials and surgical techniques [6-9].

It is known that wear is one of the main characteristics that causes implant failure [3, 10]. Thus, one of the main mechanical requirements of an improved prosthetic device design would be to minimize wear to increase device longevity. Experimental testing to determine wear that occurs in a prosthesis is time consuming, expensive and complicated. Therefore, computational wear modelling is an alternative method to predict wear. It can be used to highlight the reasons for failure after arthroplasty and can help to improve prosthesis design for individual patients to increase the prosthetic devices functional life.

Current artificial hip joints may typically last 10 to 15 years with around 10% of patients requiring revision surgery. A Cobalt Chrome head on Polyethylene cup (Metal-on-plastic MoP) produces 10 times more wear debris each year than a Cobalt Chrome head on a Crossfire Polyethylene cup

combination [11]. MoP modular prosthesis combinations can have a short life in service and lead to revision surgery. A ceramic head on ceramic cup (CoC) produces the least wear debris of all the material combinations used, 200 times less than Cobalt Chrome on Polyethylene. Using CoC also guarantees less risk of any side effects but they are brittle and not suitable for young active patients. The MoM hip prosthesis was developed to decrease failure rates and increase the longevity of the prosthesis. Current MoM prostheses have a much reduced wear rate in comparison to MoP and are the most popular prostheses for young active patients [12]. Scientifically, MoM THR's are supposed to provide less wear debris, less risk of dislocation, greatest strength and longer life [4]. However, as well as the numerous benefits of the MoM prostheses, there is a unique risk in using them that can lead to other serious problems and possible increased failure rates. The metal debris may cause damage to the bones or soft tissues around the implants and metal ions released into the body may enter blood vessels and move to other parts of the body that may lead to the presence of cancerous metal ions. Nonetheless, Smith et al. claimed that there is no evidence of the risk of cancer in the first seven years after MoM implants [13] but this debris increases the risk of metallosis (Figure 3) and infection that cause immobility in patients [14].



Figure 3: Metallosis [14]

Wear does not only occur between parts sliding with what could be considered long relative displacement (the head and cup), but fretting wear can occur between those parts that are fixed together and faced with oscillatory load in pressured contact (the head and tapered stem trunnion³). In fact, a small amount of wear produced by fretting at this interface could be significant after millions of load cycles and could cause loosening or failure of the prosthesis. This method of assembly of head and stem can produce a considerable amount of very fine wear debris over many years which is thought to be more damaging than the wear produced at the head-cup articulation [1]. The worn tapered surfaces could lead to implant disassembly and the fine metal debris may lead to adverse side effects such as metallosis (Figure 3). Many recent recalls of MoM hip prostheses have been due to unexpected pain and adverse soft tissue reactions [15].

The aim of this research is to develop a computational capability to quantify the extent of wear damage occurring between head and stem of MoM hip prosthesis and identify factors leading to debris release, so that appropriate design and procedural modifications can be made to increase the life of the prosthetic device. The research primarily focusses on the development of an accurate axisymmetric FE model of a hip prosthesis. This process is automated by a dedicated Python script in order to extract contact pressures and relative displacements to calculate wear and update the geometry for subsequent loading cycles. Future research will then develop the method to 3-d models with more realistic loading conditions and therefore more accurate results for wear. The FE models can be easily used in parametric studies to investigate the effect of geometric design, such as manufacturing tolerances,

³ Terminology; male and female tapers are called 'trunnion' and taper respectively.

femoral head size, stem angles, trunnion dimensions, trunnion surface (friction model) and frictional torque.

2. Methodology

Modular THRs allow a surgeon to choose different prosthesis components for individual patients dependent on their anatomy, age and level of activity. The prosthesis head in THR is assembled to the stem using a morse taper. The head is fixed onto the trunnion stem during surgery by impaction loads which can vary between 3500 to 7500 N dependant on the surgeon [16]. Some prostheses have threaded taper surfaces which increase friction and makes for an improved fixation. A method to predict wear must be capable of accounting for the initial effect of impaction. From a mechanical point of view, it makes sense that after applying millions of walking cycles on parts with this kind of fixation, they will become loose and will need reassembling or replacing. The method proposed here can predict fretting wear by considering the initial impact, with the effect being diminished gradually during the geometry updates. The method involves three main phases, impaction, shrink fit/walking and walking only.

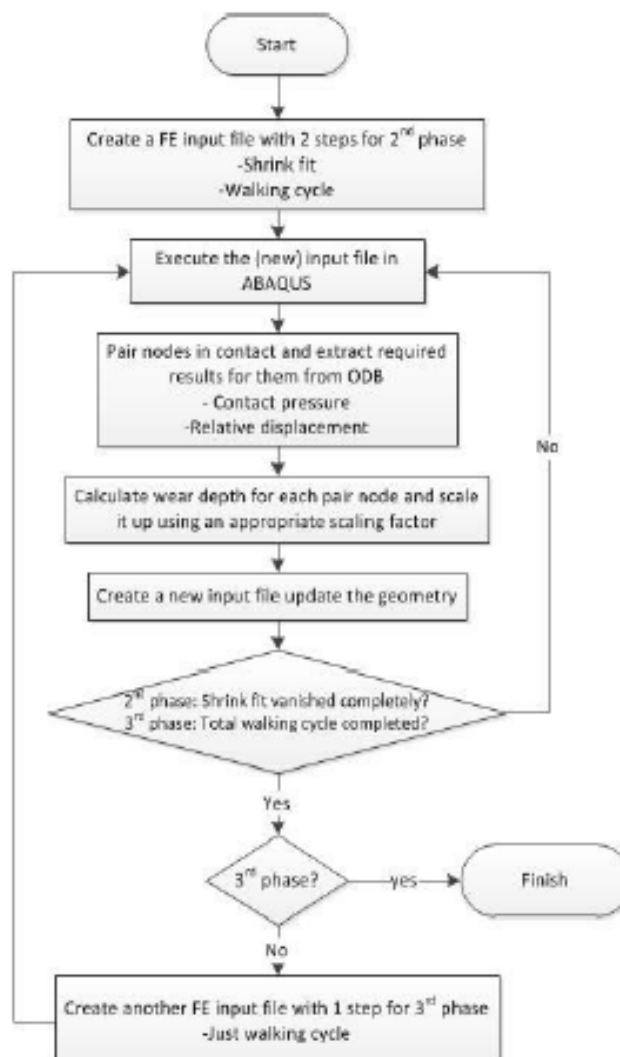


Figure 5. Quantitative procedure to predict wear

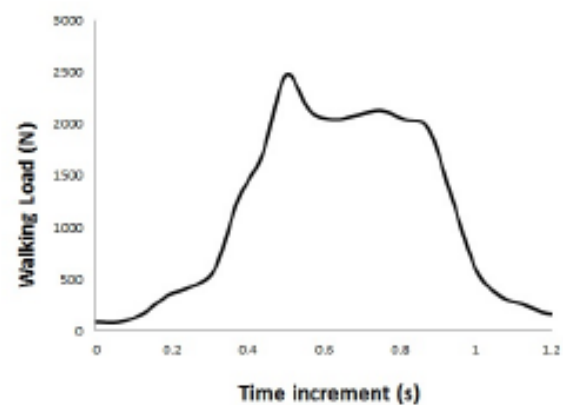


Figure 4. The load amplitude of walking cycle applied on hip [2]

Table 1. Material properties of CoCr [3]

Material properties of Co-Cr		
Young modulus	E	210 GPa
Poisson's ratio	ν	0.3
Density	ρ	7800 kg/m ³

2.1 Wear law

According to Archard's wear law (equation 1), the wear depth W is proportional to the wear coefficient K , contact pressure P and relative displacement S . This law assumes a small sliding velocity and negligible surface heating [17].

$$W = K P S \quad (1)$$

2.2 Finite Element Model

An axisymmetric FE model of a DePuy Elite 9/10 prosthesis was created in ABAQUS 6.11-1 (Figure 2). The head and stem trunnion were assembled independently and then meshed using axisymmetric linear elements (CAX4). A mesh study was performed which produced converged results at an element size of 0.7mm (Figure 2).

2.3 Material, boundary conditions and Interaction Behavior

Material properties of CoCr were assigned to the FE model as shown in Table 1. The wear coefficient was defined to be $1.13 \times 10^{-8} \text{ mm}^3/\text{Nm}$ and was kept constant [18]. An isotropic coefficient of friction of 0.13 was assumed using a penalty contact formulation within ABAQUS. The stem is fixed in the Y-direction only (see Figure 2). In the impaction step, a pressure load representing 7500N force (the maximum and critical load) was applied on the top of the head for a duration of 0.003s. For the walking step, a walking load distribution with a peak of 2500N, as shown in Figure 4, was applied on the head.

In summary, the method contains three main phases. In the first phase, the head and stem are assembled so that they just come into contact. Next, an impaction load is applied on the top of the head (as a dynamic explicit analysis). The results from this initial analysis are extracted and imported to a new FE input file. In the second phase of the methodology, the parts are assembled as a shrink fit (a general static step) based on the interference results obtained from the first phase. A new dynamic step is then defined and the walking load is applied on the top of the head. When the shrink fit overlap has been removed completely, the method continues to a third phase. In this phase the static shrink fit step is removed from the analysis and only one dynamic step of walking load is maintained for the rest of the analyses (Figure 5).

2.4 Algorithm and Computational Framework

Calculating wear for the many paired nodes at the contact interface and updating their positions manually is difficult and time consuming; consequently, the method has been automated using a Python script linked with ABAQUS. This script is executed during the 2nd and 3rd analysis phases. The program submits the FE input file, identifies the nodes in contact to pair them, extracts contact pressure and relative displacement for each set of paired nodes, calculates the wear depth and updates the position of the nodes to create the new geometry. The wear depth calculated in one walking cycle is negligible and running millions of FE analyses to represent every walking cycle a person may make is unrealistic; therefore, a suitable wear depth scaling factor is used to make the procedure computationally sensible. In this study, a scaling factor of 100,000 has been used to scale up the wear depth. This procedure is illustrated in Figure 5.

3. Results and Conclusions

Figure 6 shows contours of hoop stress after impaction, the maximum displacement after impaction is equal to -0.24 mm in the Y-direction. This displacement is used to create the overlap assembly model for the shrink fit analysis in the 2nd phase. Using a static shrink fit analysis instead of a dynamic impaction step allows modelling of the diminishing effect of impaction by removing the overlap gradually. Figure 7 shows the top three paired nodes in the model before and after the analysis. Table 2 shows the wear depth during the 2nd and 3rd phase for the paired nodes. At the end of the 2nd phase

all initial interference has been removed by wear. At the end of the 3rd analysis phase the wear depth for all paired nodes is almost equal. This is due to the use of an axisymmetric model, however in reality, loads are not applied axisymmetrically; hence, this shows the need for further 3-d analyses.

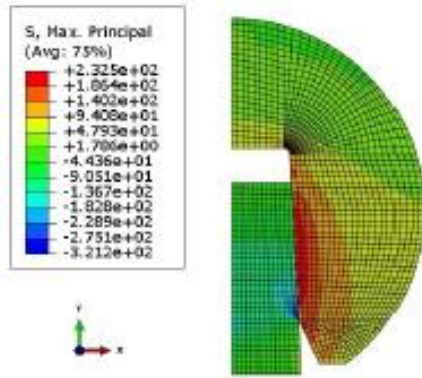


Figure 6. Hoop stress distribution at the end of the first phase of the analysis (impaction), a pressure load representing 7500N force is applied on the top of the head during 0.003 s using a dynamic explicit step (results are in MPa)

Table 2. Results for 2nd and 3rd phase of the method

Node No.		Wear depth (mm)				
Stem	Head	Total wear depth after 12 updates	Wear occurring during 13 th update only	Total wear depth at the end of 2nd phase	Total wear occurring between 2 nd and 3 rd phase (16 updates)	Total wear depth at the end of analysis (28 updates)
2	2	0.001144376	0.0000015	0.001145876	0.017974837	0.019119213
130	30	0.019939613	0.006128486	0.026068099	0.000669654	0.026737753
129	31	0.018829064	0.005559257	0.024388321	0.0000626	0.024450921
⋮	⋮	⋮	⋮	⋮	⋮	⋮
Min value of 20 pair nodes		0.008720527		0.012565481		0.018597381
Average of 20 pair nodes		0.011333245		0.015349786		0.018967105

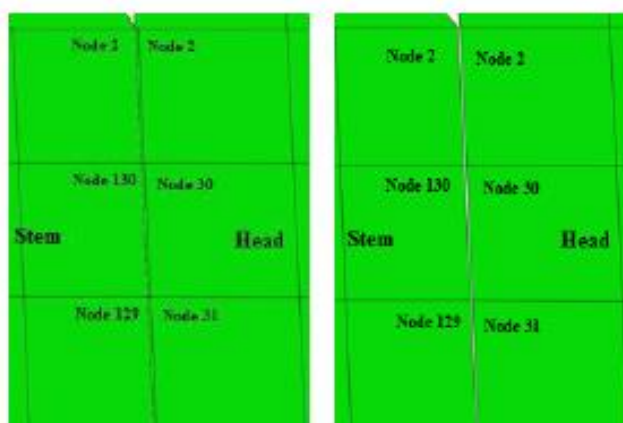


Figure 7. Top 3 pair nodes of the model (a) before analysis (overlap) and (b) after analysis

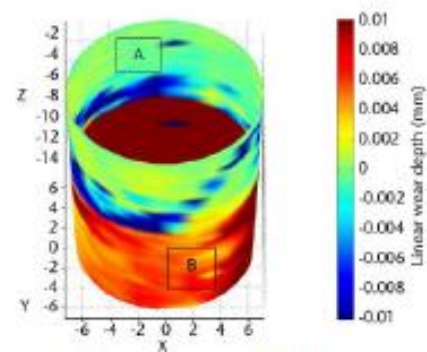


Figure 8. Linear wear depth measured from retrieved prosthesis [1]

The wear depth obtained can be compared against those found in literature. In 2012, Langton et al. used a highly accurate coordinate measuring to calculate volumetric and linear rates of wear on retrieved prosthesis. A maximum wear depth of 0.01 mm (Figure 8) was measured which is comparable with the results obtained in this study shown in Table 2 [1]. This comparison shows considerable promise but is clearly dependent on the use of an appropriate wear coefficient and accurate loading history. The results described here modelled the total removal of the effect of impaction and then further until surface wear became negligible.

4. Further Work

The present study has proposed a methodology for a computational capability to predict the fretting wear depth between the head and stem of prosthesis considering the initial effect of impaction. The algorithm has been applied to an axisymmetric model. By applying this scheme to a 3-d model and considering the load in correct directions, the results would be more accurate and consequently would provide a reliable virtual wear modelling capability. This model then will help to develop the prosthesis design, improve the material combinations and change surgical techniques in order to increase the longevity of the hip implants. Furthermore, the method will be capable of application to the head and acetabular cup. The wear methodology can be utilised generically in the analysis of other prosthetic devices such as knee and shoulder modular implants.

Acknowledgment


This work is funded by the school of Engineering, Technology and Maritime Operations, Liverpool John Moores University (2012-2015). The authors would like to acknowledge the contribution of Professor Tom Joyce from Newcastle University, UK.

References

- [1] Langton, D.J., R. Sidaginamale, J.K. Lord, A.V.F. Nargol, and T.J. Joyce, *Taper junction failure in large-diameter metal-on-metal bearings*. British Editorial Society of Bone and Joint Surgery, 2012. 1: p. 56-63.
- [2] Bergmann, G., F. Graichen, and A. Rohlmann, *HIP-JOINT LOADING DURING WALKING AND RUNNING, MEASURED IN 2 PATIENTS*. Journal of Biomechanics, 1993. 26(8): p. 969-990.
- [3] Mattei, L., F. Di Puccio, B. Piccigallo, and E. Ciulli. *Lubrication and wear modelling of artificial hip joints: A review*. Tribology International 2011 May [cited 44 5]; 532-549]. Available from: <Go to ISI>://WOS:000289398900005.
- [4] NJR. *National Joint Registry for England and Wales*: . 2013 [cited Date last accessed 20 Jan 2013; Available from: <http://www.njrcentre.org.uk/>]
- [5] DoITPoMS. *Structure of bone and implant materials*. 2012; Available from: <http://www.doitpoms.ac.uk/>.
- [6] Li, X., D. Li, Q. Lian, H. Guo, and Z. Jin, *The effect of stem structure on stress distribution of a custom-made hip prosthesis*. Proceedings of the Institution of Mechanical Engineers Part H-Journal of Engineering in Medicine, 2010. 224(H11): p. 1275-1284.
- [7] Smith, S.L., D. Dowson, and A.A.J. Goldsmith, *The effect of femoral head diameter upon lubrication and wear of metal-on-metal total hip replacements*. Proceedings of the Institution of Mechanical Engineers Part H-Journal of Engineering in Medicine, 2001. 215(H2): p. 161-170.
- [8] Liu, F., I.J. Udofia, Z.M. Jin, F. Hirt, C. Rieker, P. Roberts, and P. Grigoris, *Comparison of contact mechanics between a total hip replacement and a hip resurfacing with a metal-on-metal articulation*. Proceedings of the Institution of Mechanical Engineers Part C-Journal of Mechanical Engineering Science, 2005. 219(7): p. 727-732.
- [9] Gao, L.M., Q.E. Meng, F. Liu, J. Fisher, and Z.M. Jin, *The effect of aspherical geometry and surface texturing on the elastohydrodynamic lubrication of metal-on-metal hip prostheses*

- under physiological loading and motions*. Proceedings of the Institution of Mechanical Engineers Part C-Journal of Mechanical Engineering Science, 2010. 224(C12): p. 2627-2636.
- [10] Soderberg, A. and S. Andersson, *Simulation of wear and contact pressure distribution at the pad-to-rotor interface in a disc brake using general purpose finite element analysis software*. Wear, 2009. 267(12): p. 2243-2251.
- [11] Biomet, *The Stanmore Hip Replacement System*, B.U. Ltd, Editor 2010: South Wales.
- [12] Anissian, H.L., A. Stark, A. Gustafson, V. Good, and I.C. Clarke, *Metal-on-metal bearing in hip prosthesis generates 100-fold less wear debris than metal-on-polyethylene*. Acta Orthopaedica Scandinavica, 1999. 70(6): p. 578-582.
- [13] Smith, J.A., P. Dieppe, M. Porter, and W.A. Blom, *Risk of cancer in first seven years after metal-on-metal hip replacement compared with other bearings and general population: linkage study between the National Joint Registry of England and Wales and hospital episode statistics*. BMJ 2012;344:e2383 doi: 10.1136/bmj.e2383 2012: p. 11.
- [14] Sporer, S.M. and P.N. Chalmers, *Cutaneous manifestation of metallosis in a metal-on-metal total hip arthroplasty after acetabular liner dissociation*. The Journal of arthroplasty, 2012. 27(8): p. 1580.e13-6.
- [15] Pandit, H., S. Glyn-Jones, and P. McLardy-Smith, *Pseudotumours associated with metal-on-metal hip resurfacings*. J Bone Joint Surg [Br], 2008(90-B): p. 847-851.
- [16] Pennock, A.T., A.H. Schmidt, and C.A. Bourgeault, *Morse-type tapers - Factors that may influence taper strength during total hip arthroplasty*. Journal of Arthroplasty, 2002. 17(6): p. 773-778.
- [17] Liu, F., I. Leslie, S. Williams, J. Fisher, and Z. Jin, *Development of computational wear simulation of metal-on-metal hip resurfacing replacements*. Journal of Biomechanics, 2008. 41(3): p. 686-694.
- [18] Goreham-Voss, C.M., P.J. Hyde, R.M. Hall, J. Fisher, and T.D. Brown, *Cross-shear implementation in sliding-distance-coupled finite element analysis of wear in metal-on-polyethylene total joint arthroplasty: Intervertebral total disc replacement as an illustrative application*. Journal of Biomechanics, 2010. 43(9): p. 1674-1681.

Appendix V: Poster presentations




Faculty of Technology and Environment

A Computational Approach to Fretting Wear Modelling in Total Hip Replacements

Ariyan Ashkanfar, Russell English and Glynn Rothwell
 School of Engineering, Technology and Maritime Operations
 Byrom Street, Liverpool, L3 3AF, UK
 This project has been funded by the School of Engineering, Technology and Maritime Operations, LJMU, Liverpool, UK

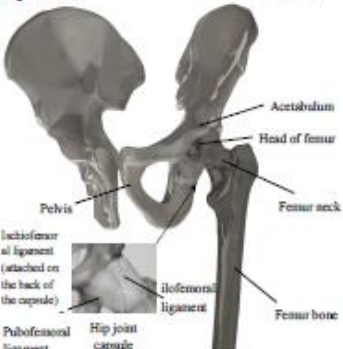
Abstract . . . A challenge in engineering coupling design is the understanding of performance of contact geometry for a given application. "Wear" is one of a number of mechanical failures that can occur in mechanical coupling design. Fretting has been observed in many mechanical coupling and known as a reason of failure of the design. Recent evidence suggests that fretting wear that occurs at the taper junction of modular total hip replacement leads to failure of the implants. The present study proposes a computational methodology utilising an energy wear law and a 3D finite element model to predict fretting wear at the taper junction of total hip replacements over time. The results obtained are consistent with those found from observation and measurement of retrieved prostheses. The method presented could be used to consider the effect of design changes and clinical technique on subsequent fretting wear in total hip replacements.

Introduction
 - At the final stage of severe hip pathologies, arthroplasty is a key solution for patients.
 - Sir John Charnley carried out the first hip arthroplasty in Nov 1962.
 - The aim of the surgery is to accommodate an active lifestyle for patients




Sir John Charnley, Lancashire, UK (RBC)

Hip Joint




Acetabulum
 Head of femur
 Femur neck
 Pelvis
 Femur bone
 Iliofemoral ligament (attached on the back of the capsule)
 Iliopsoas ligament
 Hip joint capsule
 Pubofemoral ligament

Hip Arthroplasty
 Expected life time: 10-15 years
 Number of operations: UK: 80,000/USA: 285,000 per year
 THRs comprise of:
 Flexibility intraoperatively
 Advantage of modularity:
 Acetabular cup: UHMWPE
 Femoral head: CoCr - Ceramic - Steel
 Stem: CoCr - Titanium - Steel



Acetabular cup
 Head
 Pelvis
 Head of femur bone cut
 Femur bone
 Stem

Taper junction problems
 Fretting, corrosion, micro-motion and unintended disassembly.
 Adverse soft tissue reaction due to metal debris released in body such as metallosis.

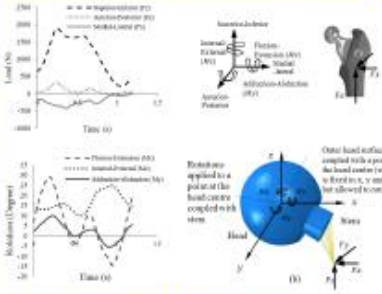


Metallosis

Aim
 To develop a computational wear model using FEA to quantify and predict the extent of wear damage occurring at the head-stem taper junction.
 Improve the wear characteristics of prosthetic design.
 Identify factors leading to debris released.
 Minimise wear.

Methodology

Finite Element Model, load and boundary condition




Wear implementation

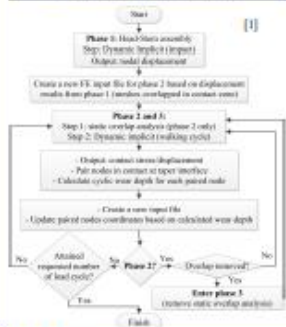
$$W_d = \sum_{j=1}^{(N/\beta)} \beta \sum_{i=1}^n \alpha \tau_i \varepsilon_i$$

W_d = linear wear depth
 α = relative displacement
 τ = contact shear stress
 ε = energy wear coefficient
 β = wear scaling factor

Head-stem assembly

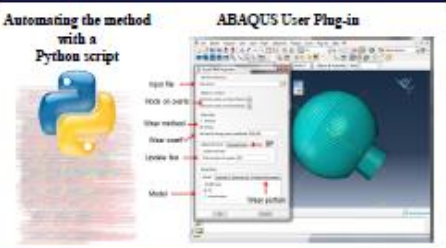


Computational framework



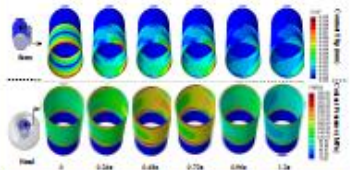
Wear algorithm

Automating the method with a Python script

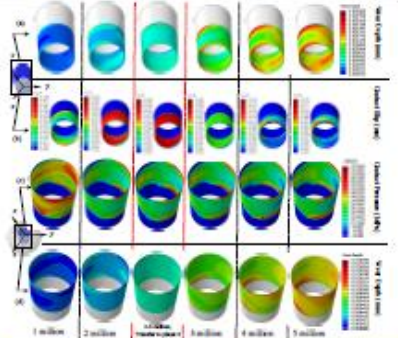


Results

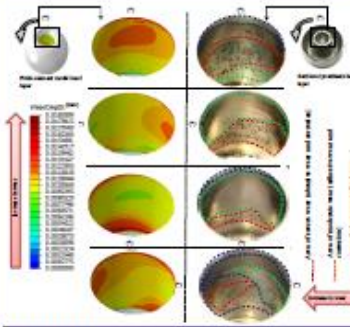
Variation in contact pressure and slip during a walking cycle



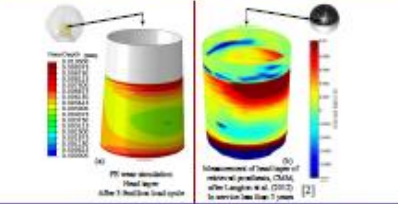
Evolution of contact pressure, slip and wear during wear analysis



Validation against observation of retrieved prostheses



Validation against CMM measurement



References

[1] R. English, A. Ashkanfar, and G. Rothwell, "A computational approach to fretting wear prediction at the head stem taper junction of total hip replacement," *Proc. Inst. Mech. Engrs.*, 2015.

[2] D. Langton, S. Jansen, T. Joyce, J. Dudley, R. Shingadia, P. Mundy, et al., "Accelerating failure rate of the ASB total hip replacement," *Journal of Bone & Joint Surgery*, British Volume, vol. 93, pp. 1011-1016, 2011.

A. Ashkanfar, June 2015
a.ashkanfar@2012.ljmu.ac.uk

Poster presented, LJMU Research conference, Liverpool, UK, 2015; Awarded the best research impact



Effect of Impaction Force at Assembly on Fretting Wear at the Taper Junction of Total Hip Prosthesis

Ariyan Ashkanfar¹, Russell English², Glynn Rothwell³

School of Engineering, Technology and Maritime Operations Liverpool John Moores University, Liverpool, UK
Symposium on Modularity and Tapers in Total Joint Replacement Devices, ASTM International, New Orleans, USA



The project has been funded by the School of Engineering, Technology and Maritime Operations Liverpool John Moores University, Liverpool, UK

Contact:
1. a.ashkanfar@2012.ljmu.ac.uk
2. r.english@ljmu.ac.uk
3. g.rothwell@ljmu.ac.uk

Introduction

At the final stage of severe hip pathologies, arthroplasty is a key solution for patients. Sir John Charnley carried out the first hip arthroplasty in November 1962. The aim of the surgery is to accommodate an active lifestyle for patients.

Modular Total Hip Replacement (THR)

- Expected life time: 10-15 years
- Number of operations: UK 30,000 / USA 285,000 per year
- THR's comprise of: Acetabular cup – Femoral head – Stem
- Advantage of modularity: Flexibility intraoperatively to optimise prosthetic functionality and anatomical fit
- Materials: Acetabular cup: UHMWPE
Femoral head: Cobalt-Chrome – Ceramic – Stainless Steel
Stem: Cobalt-Chrome – Titanium – Stainless Steel
Acetabular cup: Pebax; Press-fit
Stem / Femoral base: Cemented – Uncemented
Femoral head / Stem : Morse taper fixation (using a mallet and polymer tipped impactor)

Assembly:

- 2000-7000N
- A linear relationship was found by [1-3] ratio of 0.4-0.48
- Multiple impacts did not increase taper strength [3]
- Heinay et al. [1] advised 2 firm blows
- Pennock et al. advised in-line maximum impact [2]
- Taper 'pull-off' force used as the measure to assess taper strength
- Magnitude of impaction force at assembly affects the taper strength

Methodology

Finite Element Model

Asymmetric finite element model

Impaction / Walking load

Superior-inferior walking load

Drop rig experiment

Stem Transition Head taper Acceleometer Head taper Acceleometer

Material properties:

Material	Young's Modulus (GPa)	Poisson's ratio	Density (kg/m ³)
Co-28Cr-6Mo	210	0.3	7800
Ti-6Al-4V	119	0.29	4400

Disipated Energy Wear Law

Energy Wear Law: $W_v = \alpha E$, $W_c = \beta Q s$, $W_d = \alpha Q s$

where: W_v = volumetric wear, W_c = linear wear depth, W_d = cyclic wear depth, E = accumulated dissipated energy, Q = shear traction, α = energy wear coefficient, A = area, s = relative displacement, τ = contact shear stress, β = wear scaling factor

Wear Algorithm

3 main phases of the algorithm:

- Phase 1: Head/stem assembled just into contact. Single dynamic impaction FE analysis. Displacement of the parts.
- Phase 2: Head/stem assembled as shrink-fit analysis (based on results from phase 1). 2 step dynamic analysis: Shrink-fit, Walking cycle.
- Phase 3: Shrink-fit analysis removed from FEA. 1 step dynamic analysis: Walking cycle.

Quantitative procedure to predict fretting wear:

```

Start
Phase 1: Impaction analysis
Phase 2: Shrink-fit analysis and a walking load step
Execute the (new) FEA
Calculate wear depth for each pair nodes
Scale up the wear depth calculated
Update the geometry in a new FEA input file
Final update number?
No -> Phase 2
Yes -> Overlap removed?
Yes -> Remove shrink-fit analysis; enter phase 3
No -> Finish
    
```

Automating the method with a Python script

More than 1k lines python script written to automate the procedure

ABAQUS User Plug-in

Script has been developed as a user plug-in with user interface options for ABAQUS

Results

Reaction force generated by shrink-fit procedure

Resultant component force in Y direction due to the initial stresses distributed in the model

Friction force in Y direction due to contact pressure and friction coefficient

Displacement vs Pressure

The effect of increasing the assembly impact force on the contact pressure and displacement (in the Y-direction) of an interface node at end of phase 1 of the wear analysis

Wear depth vs Walking cycles

Wear depth evolution with varying load-stem assembly impaction force

Transition point (Phase 2 to Phase 3)

Variation in transition point (in years) with head-stem assembly impaction force

Wear profile evolution along stem transition

1 million, 5 million, 10 million, 15 million

Average linear wear depth after 15 million load cycles

Impaction Force (kN)	4000	4500	5000	5500
Average linear wear depth after 15 million load cycles (mm)	48.71	55.66	61.54	67.89

Linear wear rate vs walking cycles

Linear wear rate during the wearing process for different impaction assembly forces

Wear rate, wear depth vs Displacement, Stress

The evolution of wear rate and wear depth with respect to contact stress and relative displacement over 15 years (results for 4000N impaction force); values have been averaged for each set of a million cycles

Taper Junction Problems

Fretting, Corrosion, Micro-motion and Unintended Disassembly

- Debris released due to fretting: Adverse soft-tissue reactions (Metallosis)
- Surgical assembly process (Stem/Head): There is no standard (manufacturers guidelines are vague)
- Impaction force and technique at assembly: There is a significant variation by surgeons
- Reasons for variation: Surgeons differing experience, Type of head (metal or ceramic), Quality of the bone stock

Attaining maximum fixation is crucial in minimizing problems associated with taper junction problems

Aim

To develop a computational wear model using FEA to quantify and predict the extent of wear damage occurring at the head-stem taper junction.

The assessment of wear in this study is solely based on mechanical wear (fretting)

This method incorporate: An asymmetric finite element model, A wear algorithm based on the dissipated energy wear law

To investigate: The effect of varying the initial impact assembly forces (2000-7000N) on the extent of any subsequent fretting wear at the taper junction (over 15 years)

In order to: Provide advice for surgeons to better assemble the parts during surgery, Provide advice on design and procedural modifications, Improve the wear characteristics of prosthetic designs, Identify factors leading to debris released, Minimize wear

Increase prosthetic device longevity

Conclusion and Further Work

Conclusion

- The impaction force applied during assembly of THRs has an effect on subsequent fretting wear at the taper junction.
- The greater the magnitude of the impaction force the longer the period of the time the beneficial effect of fixation remains.
- A 'transition' point exists where the beneficial effects of fixation are completely removed and a significant increase in wear rate occurs.
- Maintaining 'good fixation' for as long as possible is key to reduced wear rates and as such the transition point should occur after the longest time in vivo as possible.
- To minimize fretting wear, surgeons should apply as large an impaction force as possible at assembly (ideally greater than 4kN) whilst ensuring the integrity of the patient femur and prosthetic device.

Further work

- Develop a 3D FE model to simulate hip loading more accurate.
- Develop the algorithm for 3D models
- Generalize methodology for application to other prosthetic devices
- Determine accurate wear coefficient
- Develop the method for head and acetabular cup articulation

Test rig to determine wear coefficient using Instron

Poster presented in American Society for Testing Material (ASTM) conference, New Orleans USA 2014



Finite Element Models for quantitative analysis of wear damage in modular hip prosthesis

Ariyan Ashkanfar¹, Russell English², Glynn Rothwell³
 School of Engineering, Technology and Maritime Operations, Liverpool John Moores University, Liverpool, UK



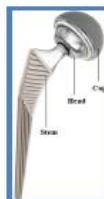
The project has been funded by the School of Engineering, Technology and Maritime Operations Liverpool John Moores University.
 Contact:
 1. a.ashkanfar@2012.ljmu.ac.uk
 2. r.english@ljmu.ac.uk
 3. g.rothwell@ljmu.ac.uk

Introduction:

A hip joint can allow a wide range of movement and transmit high dynamic loads. Its performance to carry loads and provide this mobility is remarkable; however, it is vulnerable and can lose its functionality due to disease such as osteoarthritis or bone fracture. At the final stage of severe hip pathologies, arthroplasty is a key solution for patients.

Sir John Charnley carried out the first hip arthroplasty in November 1962. He developed a method to replace the total hip joint by an artificial one and established a surgical technique for implantation. Implants and surgical techniques have advanced since then but they use the same foundation proposed by Charnley. The aim of the surgery is to accommodate an active lifestyle for patients.

In general, a hip prosthesis consists of a head, stem and cup:



Material combinations:

- Metal-on-Polyethylene THR's (fail due to wear)
- Ceramic-on-ceramic (least wear rate with no side effects, but is brittle and expensive)
- Metal-on-metal (for young active patients fail due to infection or metallosis)

Problem:

Around 80,000 hip operations per year are performed in the UK. Current artificial hip joints may typically last 10 to 15 years with around 10% of patients requiring revision surgery.



Reasons for revision surgery:

- Mainly **PAIN**
- Adverse reaction to metal debris
- Loosening of the femoral component
- Loosening of the acetabular component

The main characteristic of implants failure is **Wear**

Thus, one of the main mechanical requirements of an improved prosthetic device design would be to minimize wear to increase device longevity.

Aims

- Develop a **computational capability** to quantify the extent of wear
- Identify factors leading to **debris release**
- Provide advice on design and procedural modifications

to
Increase the life of prosthetic device

Methodology:

Modular THR's allow a surgeon to choose different prosthesis components for individual patients. The prosthesis head is assembled to the stem using a Morse taper. The head is fixed onto the trunnion stem during surgery by impact loads. The method proposed here predicts fretting wear by considering the initial impact with the effect being diminished gradually over time. The method involves three main phases, impact, shrink fit/walking and walking only.

- Archard's Wear Law

$$W = KPS$$

W: Wear coefficient, P: Contact Pressure, S: Relative displacement

- Model Databases

- Material Properties
- Contact properties
- Load
- Boundary Conditions
- Assembly
- Mesh

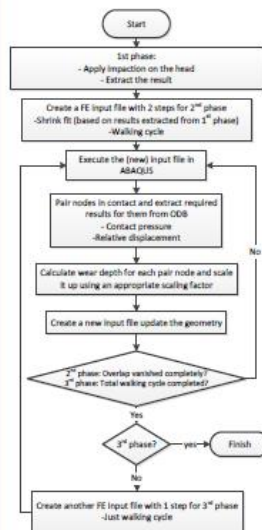
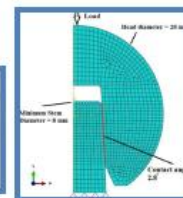
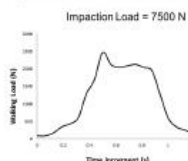
- Output Databases

- Contact Pressure
- Displacement

Material properties of Co-Cr	
Young modulus	210 GPa
Poisson's ratio	0.3
Density	7800 kg/m ³

$$K = 1.13 \times 10^{-8} \text{ mm}^3/\text{Nm}$$

$$\mu = 0.13$$



- **Impaction (1st phase):**
 - Assembled just into contact
 - Impact load applied on the top of the head
 - Bottom of the stem constrained

- **Shrink-fit/Walking (2nd phase):**
 - There are 2 steps
 - Shrink fit (static)
 - Walking cycle (dynamic) 1.25 s

- **Walking (3rd phase):**
 - Just a walking cycle step

Calculating wear for the many paired nodes at the contact interface and updating their positions manually is difficult and time consuming; consequently, the method has been automated using a Python script linked with ABAQUS.

This script is executed during the 2nd and 3rd analysis phases. A 1200-line-program submits the FE input file, identifies the nodes in contact to pair them, extracts contact pressure and relative displacement for each set of paired nodes, calculates the wear depth and updates the position of the nodes to create the new geometry.

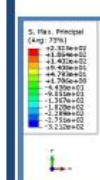
Python script:



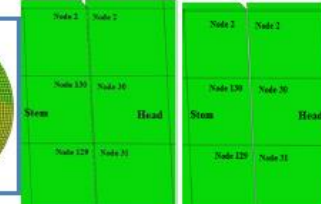
```

# Python script for wear analysis
# This script is executed during the 2nd and 3rd analysis phases
# It submits the FE input file, identifies the nodes in contact
# to pair them, extracts contact pressure and relative displacement
# for each set of paired nodes, calculates the wear depth and
# updates the position of the nodes to create the new geometry.
# ... (rest of the script code)
  
```

Results:

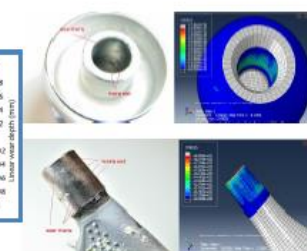
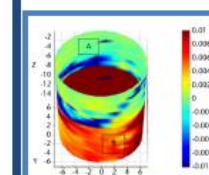


Before analysis: After analysis:



Node No.	Wear depth (mm)					
Stress	Head	Total wear depth after 12 updates	Wear occurring during 2 nd update only	Total wear depth: the end of 2 nd phase	Total wear occurring between 2 nd and 3 rd phase (18 updates)	Total wear depth: the end of analysis (18 updates)
3	3	0.001164876	0.0000016	0.011564476	0.017914827	0.019119213
130	30	0.019099613	0.006126486	0.021068099	0.000669554	0.026757753
129	31	0.018619064	0.005559357	0.024888021	0.0000626	0.024450921
Min value of 20 pair nodes:		0.008700507		0.011595481		0.016377801
Average of 20 pair nodes:		0.011553245		0.015549786		0.018967103

Validation:



Further work:

- Develop an accurate 3D model
 - Apply locomotion in appropriate directions
 - Apply the algorithm on a 3D model
- Investigate the most effective wear coefficient / scaling factor
- Develop the method for head and acetabular cup that has a greater relative displacement
- The wear methodology can be utilised generically in the analysis of other prosthetic devices (such as knee and shoulder modular implants).

May 2014

Poster presented in Simulia conference Crew UK 2013; Awarded the best poster presentation

